UNIVERSITY OF NAPLES "FEDERICO II"

DEPARTMENT OF PHARMACY

PhD in "SCIENZA DEL FARMACO"

XXXII CYCLE 2017/2020

Exploitation of natural products in the search of drug-like molecules and leads: a fascinating resource

SUPERVISOR

Dr. Concetta Imperatore

COORDINATOR

Prof. M.V. D'Auria

CANDIDATE

Dr. Marcello Casertano

“Be less curious about people and

more curious about ideas"

Marie Skłodowska-Curie

Index

ABSTRACT

Natural compounds are characterized by a considerable chemical and structural diversity alongside to be considered as the most valuable and prolific source of new drugs up to now. Not surprisingly, nature remains a key inspirational factor in the search for new therapeutic agents. In this frame, marine environment holds a central role furnishing a wealth number of secondary metabolites which possess peculiar functionality groups on their backbone and a wide ranging of biological activities. Despite this promising potential, the main disadvantage of marine-derived compounds is represented by their limited availability. Therefore, always more frequently marine metabolites are useful not only as effective drugs but also as inspiration for countless synthetic drugs. During the PhD activity, the whole of my work was managed in two different topics:

a) Structural and pharmacological characterization of novel secondary metabolites isolated from marine organisms.

This task implied the extensive application of most spectroscopic (mainly NMR) and spectrometric techniques, often assisted by computational studies, as well as the development of efficient method for stereochemical assignments, including chemical derivatization and synthesis.

The whole of these studies led to the isolation of two novel alkaloids, polyaurine A and B, from the Caribbean ascidian *Polycarpa aurata* featuring unusual and unique structural moieties. Polyaurine A with its peculiar *N*-methylguanidine group resulted in the impairment of the development of eggs-laid by the blood-dwelling *Schistosoma mansoni*.

The chemical investigation of the "sesquiterpenoid quinones/hydroquinones-rich" sponge *Dysidea avara* afforded the isolation of its two main secondary metabolites, avarone and avarol. According to the substantiated redox properties of different quinones against *Plasmodium* and the similarities in physio-pathological processes of that protozoon and the blood fluke *Schistosoma*, these derivatives were included into pharmacological screening against malaria and some neglected tropical diseases (i.e. schistosomiasis and leishmaniasis) since there is an urgent need of new therapeutic alternatives to keep up with the widespread parasite resistance. Moreover, my PhD activity was also focused in completing the configurational assignment of phosphoeleganin, an acyclic phosphorylated polyketide with inhibitory activity against protein tyrosine phosphatase 1B. The univocal stereochemical elucidation required combined approaches with the synthesis of the 8,9-*anti* stereoisomers of the tetradecan-5,8,9-triol as suitable diastereoisomeric model compounds directed to the application of UDB concept. Accordingly, the interesting biological activity and the widening of NMR database as useful support for stereostructural elucidation has encouraged the synthesis of several polyoxy and polyacetoxy simplified analogues of the marine metabolite.

b) Design and chemical synthesis of quinone molecules inspired by bioactive marine natural products and creation of synthetic chemical libraries for antiparasitic and cytotoxicity screenings, including SAR studies.

Taking into account the antiplasmodial effects of a group of marine secondary compounds endowed with the thiazinoquinone bicyclic moiety and also the antischistosomal properties of several effective antimalarials, a rationalized chemical library of thiazinoquinones has been designed and synthesised inspired by the marine cytotoxic aplidinone A. The adopted synthetic scheme reflected the compelling priority

of an efficient and inexpensive procedure for neglected diseases. Additionally, in order to further explore the role of the thiazinoquinone scaffold as antiparasitic agent, the quinone avarone has been converted into the novel semisynthetic thiazinoquinone derivative, named thiazoavarone, which showed interesting properties on the above-mentioned parasites. Some requirements appeared crucial for the antiparasitic activity: a specific regiochemistry of the thiazinoquinone heterocyclic system strongly affected the antiparasitic potency whereas the nature of the side-chain substituents on the quinone moiety could address the selective toxicity against mammalian cells or parasites as well as specific developmental stages of parasites. Furthermore, computational studies provided useful insights on putative mechanism of action exerted by thiazinoquinones supporting the one-electron reduction bioactivation step with subsequent formation of a toxic semiquinone radical species. Overall these data clearly point out the thiazinoquinone scaffold as potential new lead structure for neglected disease drugs discovery.

To further exploit the versatility of the synthetic protocol, a small series of prenylated quinones and related thiazinoquinones has been prepared in order to broaden the knowledge on the antiproliferative effects of these compounds. Among these, a geranylquinone derivative exerted a cytostatic activity through G0/G1 cell-cycle arrest in BxPC-3 cells.

PUBLICATIONS

1. Imperatore, C.; Gimmelli, R.; Persico, M.; Casertano, M.; Guidi, A.; Saccoccia, F.; Ruberti, G.; Luciano, P.; Aiello, A.; Parapini, S.; Avunduk, S.; Basilico, N.; Fattorusso, C.; Menna, M. Investigating the antiparasitic potential of the marine sesquiterpene avarone, its reduced form avarol, and the novel semisynthetic thiazinoquinone analogue thiazoavarone. *Mar. Drugs* **2020**, *18*, 112.

2. Imperatore, C.; Valadan, M.; Tartaglione, L.; Persico, M.; Ramunno, A.; Menna, M.; Casertano, M.; Dell'Aversano, C.; Singh, M.; d'Aulisio Garigliota, M. L.; Bajardi, F.; Morelli, E.; Fattorusso, C.; Altucci, C.; Varra, M. Exploring the photodynamic properties of two antiproliferative benzodiazopyrrole derivatives. *Int. J. Mol. Sci.* **2020**, *21*, 1246.

3. Gimmelli, R.; Persico, M.; Imperatore, C.; Saccoccia, F.; Guidi, A.; Casertano, M.; Luciano, P.; Pietrantoni, A.; Bertuccini, L.; Paladino, A.; Papoff, G.; Menna, M.; Fattorusso, C.; Ruberti, G. Thiazinoquinones as new promising multistage schistosomicidal compounds impacting *Schistosoma mansoni* and egg viability. *ACS Infect. Dis.* **2020**, *6*, 124-137.

4. Imperatore, C.; Della Sala, G.; Casertano, M.; Luciano, P.; Aiello. A.; Laurenzana, I.; Piccoli, P.; Menna, M. *In vitro* antiproliferative evaluation of synthetic meroterpenes inspired by marine natural products. *Mar. Drugs* **2019**, *17*, 684.

5. Casertano, M.; Imperatore, C.; Luciano, P.; Aiello, A.; Putra, M.Y.; Gimmelli, R.; Ruberti, G.; Menna, M. Chemical investigation of the Indonesian tunicate *Polycarpa aurata* and evaluation of the effects against *Schistosoma Mansoni* of the novel alkaloids polyaurines A and B. *Mar. Drugs* **2019**, *17*, 278.

6. Casertano, M.; Avunduk, S.; Kacar, A.; Omuzbuken, B.; Menna, M.; Luciano, P.; Aiello, A.; Imperatore, C. Analysis of anti-biofilm activities of extracts from marine invertebrate collected from İzmir Bay (Eastern Aegean Sea). *Biomed. J. Sci. & Tech. Res.* **2019**, *20*, 15023-15028.

7. Imperatore, C.; Persico, M.; Senese, M.; Aiello, A.; Casertano, M.; Luciano, P.; Basilico, N., Parapini, S.; Paladino, A.; Fattorusso, C.; Menna, M. Exploring the antimalarial potential of the methoxy-thiazinoquinone scaffold: identification of a new lead candidate. *Bioorg. Chem*. **2019**, *85*, 240–252.

8. Luciano, P.; Imperatore, C.; Senese, M.; Aiello, A.; Casertano, M.; Guo, Y.; Menna, M. Assignment of the absolute configuration of phosphoeleganin via synthesis of model compounds. *J. Nat. Prod.* **2017**, *80*, 2118-2123.

Poster presentation:

- "Marine environment to fight multiparasitism: new leads in the treatment of neglected diseases"; (III International Summer School on Natural Products, Naples, July 2019).
- "Identification of new multi-stage thiazinoquinone compounds with activity against *Schistosoma mansoni"* (Workshop on malaria and neglected parasitic diseases: core science and perspectives, Bologna, March 2018).
- "The absolute stereochemistry of phosphoeleganin: A hard challenge in natural products chemistry"; (II International Summer School on Natural Products, Naples, July 2017).

Oral communications:

- "Development and synthesis of simplified analogs of a bioactive natural polyketide"; (XXXIX National conference SCI-Divisione di Chimica Organica, Turin, September 2019).
- "The thiazinoquinone scaffold as chemical starting point for the design and synthesis of antiparasitic drugs"; (XXXVIII National conference SCI-Divisione di Chimica Organica, Milan, September 2018).

Doctorate training:

Institute of Nanoscience and Nanotechnology- NCSR Demokritos, Athens (Greece) under the supervision of Dr. Anastasia Hiskia.

LIST OF ABBREVIATIONS

ROVs, remotely operated vehicles; FDA, Food and Drug Administration; EMA, European Medicines Agency; PKSs, polyketide synthetases; NRPSs, non-ribosomal peptide synthetases; NTDs, neglected tropical diseases; WHO, World Health Organisation; STHs, soil-transmitted helminths; ROS, reactive oxygen species; NIH-3T3, mouse embryonic fibroblasts; inosine monophosphate dehydrogenase, IMPDH; MPLC, medium pressure liquid chromatography; DFT, density functional theory; GIAO, gauge including atomic orbitals; MAE, mean absolute errors; CMAE, correct mean absolute errors; SEM, standard error of the mean; t_R, retention time; *m/z*, mass-to-charge ratio; HMEC-1, human microvascular endothelial cells; THP-1, acute monocytic leukaemia cells; FPP, farnesyl pyrophosphate; SAR, structure activity relationship; CQ, chloroquine; CQ-S, chloroquine-sensitive; CQ-R, chloroquine-resistant; SI, selectivity index; QM, quantum mechanical; GM, global minimum; MM, molecular mechanic; C-PCM, conductor-like polarizable continuum model; HOMO, highest occupied molecular orbital; LUMO, lowest unoccupied molecular orbital; IP, ionization potential; E°, standard redox potential; ΔG°, standard Gibbs free energy; SOMO, single occupied molecular orbital; pLDH, parasite lactate dehydrogenase activity; NAG, *N*-acetylglucosamine; MTT, 3-(4,5-dimethylthiazol-2-yl)-2,5-diphenyltetrazolium bromide; SDS, sodium dodecyl sulfate; PMA, phorbol myristate acetate; NBO, natural bond orbital; THF, tetrahydrofuran; CAN, cerium ammonium nitrate; TES, triethylsilane; RBCs, red blood cells; NAC, *N*-Acetylcysteine; GSH, glutathione; PZQ, praziquantel; MCF-7, breast adenocarcinoma cells; BxPC-3, pancreas adenocarcinoma cells; MG-63, bone osteosarcoma cells; RTCA, real-time cell analyser; NCI, normalized cell index; SD, standard deviation; UDB, universal NMR

database; PTP, protein tyrosine phosphatase; CDAs, chiral derivatizing agents; MPA, α-methoxyphenylacetic acid; 9-AMA, 9-anthrylmethoxyacetic acid; BPG, boc-phenylglycine; MTPA, α-methoxy-α-(trifluoromethyl)phenylacetic acid; PTKs, protein tyrosine kinases.

CHAPTER 1

Natural products for human health

1.1 Introduction

Natural products from living organisms, such as terrestrial plants, marine organisms, and microorganisms, as fungi and/or bacteria, have been considered as the most valuable and prolific source of new drugs up to now. The fascinating and significant wealth of different chemical entities isolated and structurally fully characterized from natural sources served humankind as drug leads to treat a wide range of diseases for more than thousands of years. Several life-saving drugs and biomedical tools take great advantage from the chemical diversity of nature developing new beneficial therapeutic agents. Indeed, over 70% of bioactive compounds for infectious diseases treatment and over 77% of small molecules for cancer treatment traced their origin back to natural products [1-2]. Approximatively, one-third of top-selling drugs are/or derived from natural products.

However, the percentage of novel natural compounds provided of medical interest is expected to increase every year mainly as result of the evolution processes occurred over a billion years, and due to the environmental pressure. The wide variety of natural products outputs from the coexistence of a huge number of organisms, both terrestrial and marine, which interact with each other in several ways and with the environment showing a strong adaptability to their habitat. Interestingly, unique and complex chemical entities have been shaped by the evolution as a defensive system against other predatory or competing organisms or parasites enhancing the survival and

competitiveness of living species [3-4]. In this view, chemistry plays a crucial role; in fact, all the organisms share almost the same biochemical pathways necessary for living cells, but in addition they have developed a great diversity of so-called secondary metabolites involved into the interaction with other species. It is not surprising that the countless possible interactions among the organisms and the existence of millions of diverse terrestrial and marine species worldwide allowed to produce a wide number of secondary metabolites with unusual structures and endowed with interesting biological potency. For this reason, the wider chemical space occupied by natural products represents an authentic example of how combinatorial chemistry has been performed by the nature from thousands of years giving a real arsenal of bioactive compounds more attractive as drugs leads and more drug-like than the compounds synthesised by combinatorial chemistry processes [5-7]. Therefore, nowadays the increasing of novel biological targets, discovered by the researchers, requires a constant search of new elements in drug-like lead compounds, and so the availability of chemical libraries is an essential requirement.

Despite a huge number of compounds and related bioactivity having been discovered, a greater number of natural compounds and their varied uses are yet to be determined, hence this resource has been barely scratched and nature is considered the most fascinating way to realize drug discovery up to now. In fact, it is estimated that only the 6% of terrestrial flora has been pharmacologically investigated whereas, phytochemically, only the 15% of these species have been investigated [8-10]. On the other hand, the presence of the ocean on more than 70% of planet surface, providing to a variety of animal species, plants, and microorganisms interacting with each other led to consider this marine ecosystem certainly as a rich source of secondary metabolites.

In this view, marine habitat as source of novel bioactive compounds is still virtually unexplored and restricted, primarily, at first to tropical and subtropical regions while nowadays is being expanded to colder region of the planet [11]. Most of the bioactive natural products from sea have been isolated from marine invertebrates: sponges are the most prolific source of new compounds (almost 47%), followed by corals (34%) and then smaller amount (~ 18%) is extracted from echinoderms and tunicates [12-14]. Generally, the peculiar production of a great number of secondary metabolites is mainly due to the evolution of marine species since these organisms have been associated to symbiotic microorganisms, fungi and/or bacteria, that are involved in the synthesis of these metabolites playing a key role.

The therapeutic areas of oncology, anti-inflammatory, cardiovascular, antiparasitic and many others have greatly brought out benefits from the marine natural products which potential bioactivity has been applied to eradicate several illnesses. The incidence of biological activity in marine-derived compounds is very high, especially regarding the cytotoxicity, so much that the efficacy of marine extracts overcomes that of terrestrial origin. In fact, an additional reason which feeds the interest towards the analysis of marine compounds lies in the possibility of those products to show a remarkable activity in many cases at extremely low concentration.

Biogenetically, marine invertebrates exhibit the major biosynthetic pathways involved also into synthesis of terrestrial metabolites. Nevertheless, these organisms often are characterized by recurring features on the carbon skeleton of their metabolites; indeed, it is quite common discover atypical functionality groups which are considered of predominantly marine origin. For example, the recurred presence of halogen atoms, primarily chlorine and bromine, depends upon the relative abundance of halogens in

marine environment as well as groups like isonitrile, isothiocyanate, thiocyanate and formamide are further features essentially found in marine natural metabolites [15-18].

Until today, the endless research of secondary metabolites from marine invertebrates allowed the finding and full characterization of more than 300,000 novel compounds and shed light on multitude of biological properties [19]. However, the complexity of the screening procedures necessary to isolate the pure bioactive metabolites, with the risk to have altered biological responses, the time-consuming efforts, the costs and often the scarce availability of the biological starting material, are some of the principal problems connected to the pharmaceutical application of marine natural products.

Therefore, in last century, natural products have not only served as effective drugs but have been also served as inspiration for countless synthetic drugs and drug leads built around the pharmacophores of natural products [20]. This interesting potential has been widely explored during my PhD activity under the supervision of Dr. Concetta Imperatore at the Department of Pharmacy of University of Naples "Federico II". The performed studies join a multidisciplinary work in which national and foreign research groups have been involved, too.

Indeed, the active collaborations with the research groups of:

- Prof. Caterina Fattorusso (Department of Pharmacy, University of Naples Federico II) for computational studies;
- Prof. Nicoletta Basilico (Department of Biomedical, Surgical and Dental Science of University of Milan) for *in vitro* antiplasmodial, antileishmanial and cytotoxicity studies;

- Dr. Giovina Ruberti (Institute of Cell Biology and Neurobiology of the National Research Council in Monterotondo, Rome) for antischistosomal and cytotoxicity studies;
- Dr. Sibel Avunduk (Department of Vocational School of Medicinal Health Services at Mugla University, Turkey) for the collection of biological material;
- Prof. Yue-Wei Guo (Shanghai Institute of Materia Medica at Chinese Academy of Sciences) for PTP1B activity evaluation

gave a key contribution to the achieved results that are in depth described in this thesis.

1.2 The promising effects of marine natural products

More than 50 years ago, the analysis of the metabolic content of marine species may have been underestimated due to the difficult methods for the collection of organisms and, in fact, this investigation was limited due to the latter collected only by skin diving. Subsequently, beginning in the mid-1970s, the systematic investigation of marine environment as fascinating source of bioactive therapeutic agents has been increasingly explored after the development of reliable scuba diving techniques. Thanks to these latter, depths from around 3 meters to 40 meters became routinely attainable, and thus it was possible to increase the availability of living material. Moreover, techniques as dredging or trawling have been involved in the deep-water collections too; nevertheless, these methods may provoke serious damages to marine environment and a nonselective collection of sampling; it needed resorting to manned submersibles or remotely operated vehicles (ROVs) which increased the costs of these collection operations precluding the possibility of their routine use.

Notable examples of active marine compounds have been approved for medical application including anticancer, antibacterial, antiviral, antidiabetics and treatment of many other diseases [11,21]. Although the main focus of the medical research has been the discovery of novel potential anticancer compounds, the first marine compound able to gain approval as drug was the powerful analgesic drug zicotonide, marketed with the name of Prialt® [22]. Zicotonide is a peptide isolated from the venom of the fish-eating marine snails, *Conus magus*, which are able to release this venom to stun their prey [23]. This peptidic drug is approved for the treatment of chronic pain and exerts its activity through a selectivity block of *N*-type calcium channels thereby interrupting the pain signalling at level of spinal cord. The limited application of zicotonide is ascribable to its lowered capability to cross the blood-brain barrier needing intrathecal administration to achieve optimal analgesic efficacy and few side effects [24].

Ecteinascidin 743 (Yondelis®, **1**) extracted from the colonial tunicate *Ecteinascidia turbinata*, as well as dehydrodidemnin B, (Aplidin®, **2**) isolated instead for the first time from the ascidian *Aplidium albicans*, are two marine-derived compounds that have received the orphan drug status in 2007 and 2017, respectively (Figure 1) [25-27]. The alkaloid ecteinascidin (**1**) is an FDA approved compound for treatment of soft tissue sarcomas that in 2009 has been approved by EMA for ovarian cancer along with doxorubicin, too. Currently, compound **1** is additionally involved in several clinical trials of multiple countries for prostate, breast and paediatric sarcomas. Nowadays, a semisynthetic route has been developed to increase the quantity of ecteinascidin (**1**) at disposal for above cited clinical trials and this semisynthetic scheme expects to start from cyanosafracin B (**3**, Figure 1), a microbial product which may solve the issue

related to the lower availability of natural products after isolation and purification procedures [28].

Similarly to compound **1**, dehydrodidemnin B (**2**) is another orphan drug marketed by PharmaMar (Madrid, Spain) with the name of Aplidin® and originated from the marine environment. Its structure highlighted the presence of a pyruvyl substitution which replaced a lactyl group and so it may be regarded as a derivative of didemnin B (**4**) as depicted in Figure 1. Aplidin® was granted the orphan drug status for multiple myeloma since its clinical trials are in advanced for several malignancy cancer [27]. Further examples of marine compounds with therapeutic application, mainly as anticancer agents, are the alkaloid halichondrin B (**5**) a complex polyether obtained in very low yield from different sponge samples, and bryostatin 1 (**6**), a macrolide originated from bryozoan *Bugula neritina* (Figure 1) [29-30].

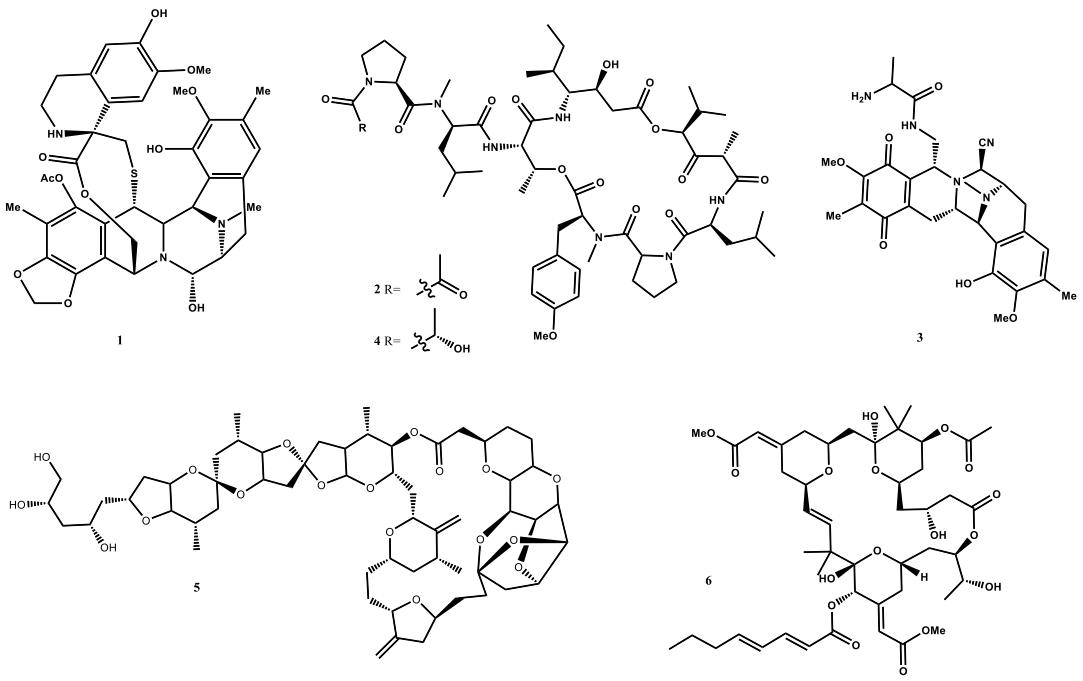

Figure 1. Structures of marine derivatives **1**-**6** involved in anticancer therapy.

Alongside the above-mentioned compounds **1**-**6**, the intense efforts performed both by academy and pharmaceutical industry allowed many compounds from ocean to reach the market and/or phase III clinical trials (see Table 1) underlining, thus, the incredible pharmacological potential of secondary metabolites from living organisms [19]. Moreover, different marine habitats play a key role in the production of different chemical class of metabolites featuring by an incredible structural diversity as well as high selectivity and specificity on biological targets. An important and additional feature of marine invertebrates is the evidence that several microorganisms, like bacteria and/or fungi, build up a symbiotic association with extra- and intracellular spaces of macroorganism tissues. About 40% of the biomass is often constituted by microorganisms and symbiotic bacteria which are mainly responsible for the synthesis of many bioactive compounds as has been clearly demonstrated [31-32].

Table 1. Marketed drugs and drug candidates from the ocean.

Marketed compounds		
Compounds	**Name**	**Use**
cytarabine	Cytosar-U®	cancer
eribulin mesylate	Halaven®	cancer
brentuximab vedotin	Adcetris®	cancer
polatuzumab vedotin	Polivy®	cancer
omega-3-acid ethyl esters	Lovaza®	hypertriglyceridemia
ethyl eicosapentaenoic acid	Vascepa®	hypertriglyceridemia
omega-3-carboxylic acids	Epanova®	hypertriglyceridemia
vidarabine	Vira-A®	antivirus
iota-carrageenan	Carragelose®	antivirus
Phase III clinical trials		
Compounds	**Name**	**Use**
tetrodotoxin	Tectin®	cancer-related pain
plinabulin	NPI-2358	cancer

The hypothesis of this symbiotic relationship by macro- and microorganisms is largely supported by experimental evidences. There are two principal reasons supporting this association; in fact, i) a wealth of prokaryotic cells sometimes has been found in animal tissues and ii) a close similarity between bacteria metabolites and those isolated invertebrates [32,33]. For example, it is known that several polyketides and non-ribosomal peptides, identified in a large number of sponges and tunicates during

pharmaceutical screening, are synthesised by megaenzymes such as polyketide synthetases (PKSs) and non-ribosomal peptide synthetases (NRPSs) that are almost exclusively of microorganism origin [34-36]. Despite many attempts executed by Faulkner and co-workers to show where natural metabolites were localized in bacteria cells, a possible transport across cells via exocytosis or sequestration mechanism may not be ruled out [37]. Consequently, the cultivation in laboratory scale of the suspected microbial collected either from surrounding water or from tissues of invertebrates might provide a satisfactory strategy to prevent the isolation of natural products in low quantities also if bacteria cultures are still largely complicated and difficult to realize [32].

CHAPTER 2

Marine and marine-based compounds as antiparasitic agents

2.1 The role of marine products in the drug discovery for malaria and neglected tropical diseases

A general discussion on the promising potential of marine natural products as medical tools against an array of diseases has been extensively achieved in recent reviews [38-40]. Historically, as well as described in the 1.2 paragraph of this thesis, most of marine compounds have been explored for their anticancer properties, even though the medical cares for other illnesses may be improved by marine metabolites. Indeed, a number of infectious diseases such as malaria, schistosomiasis, leishmania, tuberculosis and also several fungal infections have found suitable active compounds and/or drug candidate from marine resources [40-44]. Among the vastly described marine compounds yet, only few of these (compounds **7**-**15**) are reported in Figure 2 as illustrative representation to underline the widespread range of marine chemical scaffolds able to modulate the pharmacokinetic and pharmacodynamic properties of enzyme pathways and/or receptors in different infective agents.

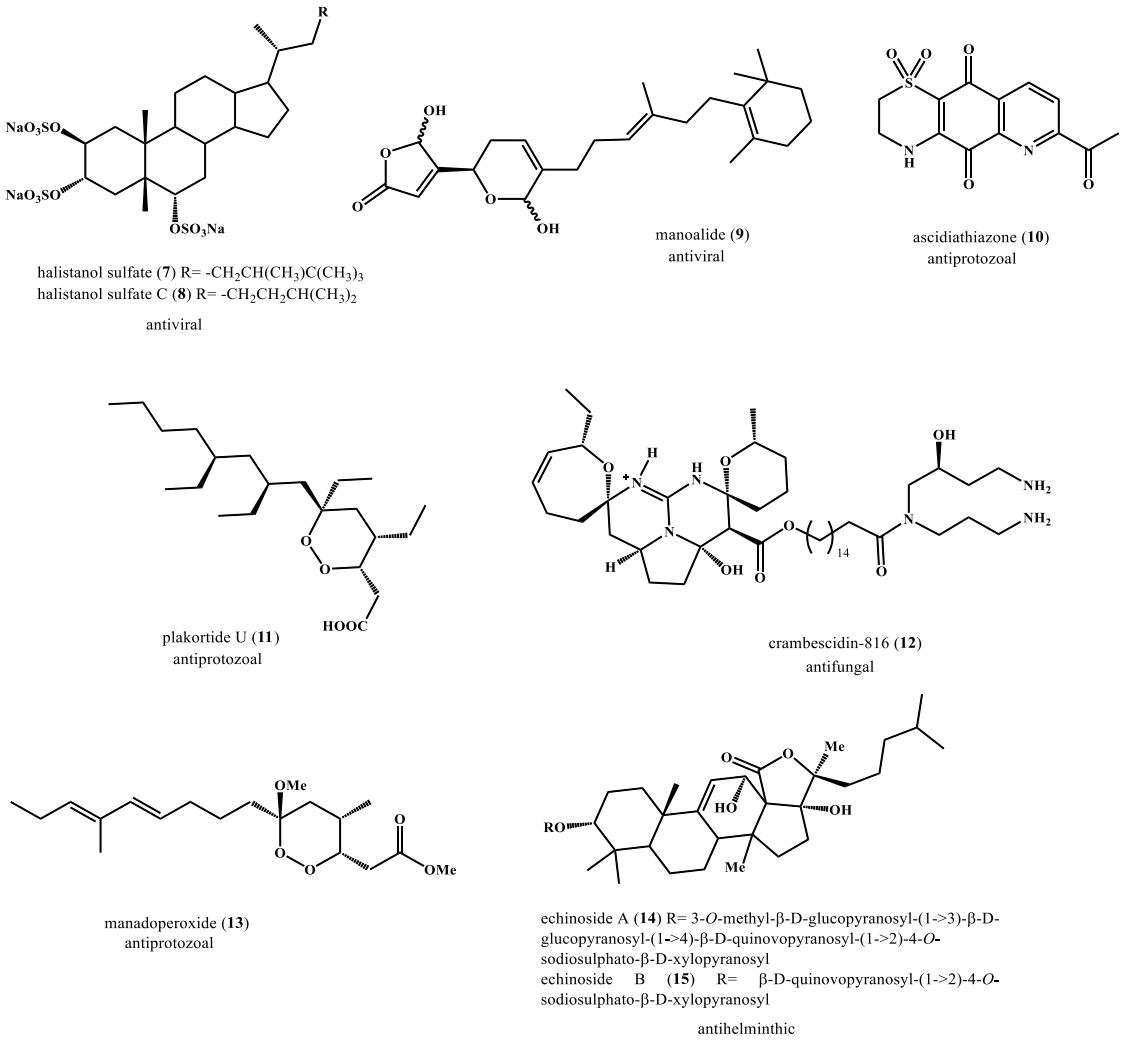

Figure 2. Examples of marine compounds (**7-15**) with antiviral, antiprotozoal, antifungal and anthelmintic activities.

Several pathologies, some above-mentioned, are provoked by unicellular and multicellular parasites and are classified as neglected tropical diseases since these are endemic in the poorest countries in tropical and sub-tropical region of the world, such as Africa, South America and most region of Asia [45]. The term neglected indicates the scarce interest of pharmaceutical industries to get involved in the development of

new therapeutic agents due to the low financial return as the affected populations are mainly low-income people. Furthermore, these diseases represent a severe issue for public health considering they are endemic in 149 tropical and subtropical countries, and affect more than 1 billion people, of which 875 million are children of school age [46]. The WHO lists almost 17 illnesses as neglected and, among them, which affect the population the most are schistosomiasis, leprosy, tuberculosis, leishmaniosis, dengue and Chagas disease [45]. Next to NTDs, malaria is still a serious problem in many countries of the world, especially sub-Saharan region where malaria infection is hurdle to social and economic growth beyond a health problem and it is estimated that one child dies every 30 seconds due to malaria. Surely, NTDs and malaria are the main diseases worldwide which present a still too high percentage of morbidity and/or mortality among the poorest people causing severe pains and disabilities [47-48].

However, in major cases for these diseases the current available therapeutics are quite limited, and the few effective ones cause severe side-effects. Additionally, where malaria and NTDs are co-endemic, it is worth mentioning the problem of co-infection which require the administration of more than one drug provoking drug accumulation and exacerbating the related toxic effects. For examples, another dramatic class of NTDs is represented by soil-transmitted helminths (STHs) infections such as schistosomiasis, onchocerciasis, dracunculiasis, and lymphatic filariasis. For these diseases, the people might be affected by more STHs parasites since the infections are facilitated by ingestion or direct contact with soil contaminated by worm eggs or larvae. In the group of NTDs responsible for the burden on global public health, schistosomiasis has been estimated to be the cause of ~4.5 million disability-adjusted life years [49]. Schistosomiasis is a NTD that may be caused by five different species of trematodes of

the family of Schistosomatidae. This pathology is also known as bilharzia by the physician Theodore Bilharz who was the pioneer in the study of this parasitology. It requires an intermediate host, preferentially aquatic snails, to continue its life-cycle before infecting humans as definitive host. Immune reactions in humans together with eggs laid contribute to develop a chronic disease which could be diagnosed only after severe organ damages. The dangerousness of schistosomiasis is also related to the fact that it causes an increase in the percentage of HIV transmission, further affirming the necessity of efficient pharmaceutical therapies [50].

Nevertheless, no global funds are reserved for research of new antischistosomal agents as well as for other NTDs with respect to malaria, HIV/AIDS and tuberculosis that are classified as the "big three" diseases in developing countries. For the latter, an international organization, "Global Fund to Fight AIDS, tuberculosis and malaria", invests every year capital for this struggle. On the other hand, there are not yet available public and/or private partnership for the eradication of schistosomiasis [51]. Currently, the only effective available agent for treatment of all types of human *Schistosoma* infections is praziquantel (**16**), while oxamniquine and metrifonate (**17**-**18**, Figure 3) are not preferred for clinical use. Commercial praziquantel is a racemic mixture of *R* and *S* isomers but only is *R*-isomer is responsible for antischistosomal properties and, at same time, in some strains are going to develop resistance phenomena as well as drug non-compliance in mass drug administration procedure [52-53].

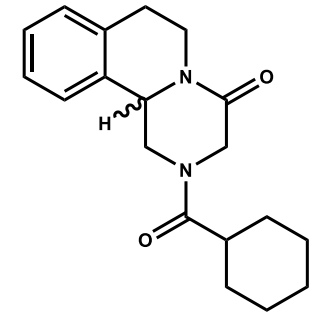

(±)-praziquantel (**16**)

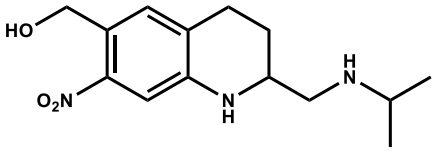

oxamniquine (**17**)

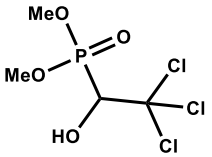

metrifonate (**18**)

Figure 3. Structures of the drug of choice for schistosomiasis, praziquantel (**16**), and of oxamniquine and metrifonate (**17**-**18**).

Thus, current therapies for NTDs are associated with other various limitations such as unfavourable toxicity profiles, complicated administration procedures and lengthy treatment duration. The continuous emerging of resistant strains, which inactivate drugs, increase the urgent need for new antiparasitic drugs. Thus, a constant need to bring to light and bare new antiparasitic drugs is required, even effective against more parasites in order to avoid the co-administration of drugs and able to bypass the problem of low funding.

To assess this opportunity, many pharmaceutical companies have decided to limit the costs of the development of brand-new therapeutic agents repurposing drugs, just approved for other diseases, for NTDs treatment. Accordingly, historically effective antimalarials have been tested against other underfunded parasite diseases resulting in activity. A great number of compounds such as artemisinin and its semisynthetic derivatives, mefloquine and chloroquine but also synthetic compounds such as several 1,4-naphthoquinones or quinoline-5,8-diones are some examples reported in literature

of how antimalarials have been shown schistosomicidal properties [51,54]. In this regard, it is well documented that both unicellular *Plasmodium* and multicellular *Schistosoma* feed on host haemoglobin causing an intense flux of ROS. To survive, both parasites have developed antioxidant systems based on the two electron donors, glutathione and thioredoxin, that are regenerated by NADPH-dependent reductases. In this way, the toxic free heme group can be converted in to insoluble hemozoin, achieving a potent detoxification of parasite intracellular compartment [54-57]. Thus, starting from these considerations, the physio-pathological similarities of *Plasmodium*, *Schistosoma*, and also other infectious parasites could inspire the possibility of a deep investigation of antiparasitic properties of novel identified compounds.

In this view, the exploration of metabolic content of marine environment may be further assessed in order to identify new suitable candidates for treatment of these pathologies considering also that surprising results in cancer treatment have been successfully shown by the employment of many marine natural products. Additionally, the isolation of new promising antiparasitic lead candidates is an important crossroads since it allows the identification of new active chemotypes which prompt the scientists to build up chemical libraries based on the model of natural compounds, too.

In this view, one of the main focus of my studies during the PhD course has been turned towards the search of novel secondary metabolites from marine invertebrates to be screened as antiparasitic agents (mainly as antimalarial, antischistosomal and antileishmanial), whose scaffold could be used as new chemical starting point to design and develop new drugs. Several efforts have been grounded in these three years, in fact, satisfactory results have been reached both by the broadening of novel marine

compounds framework and by the development of synthetical procedure which allowed to obtain libraries of compounds in a high outcome.

2.2 Two novel alkaloids from the Indonesian ascidian Polycarpa aurata and evaluation of the effects against Schistosoma mansoni

The deep analysis of the solitary ascidian *P. aurata*, collected along the Siladen coast (Indonesia) allowed for the isolation of four new secondary metabolites (compounds **19**-**22**) and even four known compounds (**23**-**26**, Figure 4) [58]. Among the novel compounds, two of them (**21**-**22**) belong to class of *para*-benzoyl derivates, whereas more fascinating were the two novel alkaloids named polyaurines A (**19**) and B (**20**) in which the presence of a 3-(*N*-methyl-methylcarbamate) linked to either methyl guanidine moiety or 1,2,4-thiadiazole ring, respectively, represented clearly examples of unusual functional groups in marine natural compounds. The structural elucidation required an extensive use of NMR spectroscopy with the acquisition of 1D and 2D experiments allowing the analysis of both homonuclear and heteronuclear correlations, as well as mass spectroscopy analysis to define molecular formula and mass fragmentation pattern. In addition, computational studies based on DFT calculation agreed univocally the proposed structure of polyaurine B (**20**) depicted in Figure 4 clarifying the ambiguity inherent to the rarely found 1,2,4-thiadiazole ring.

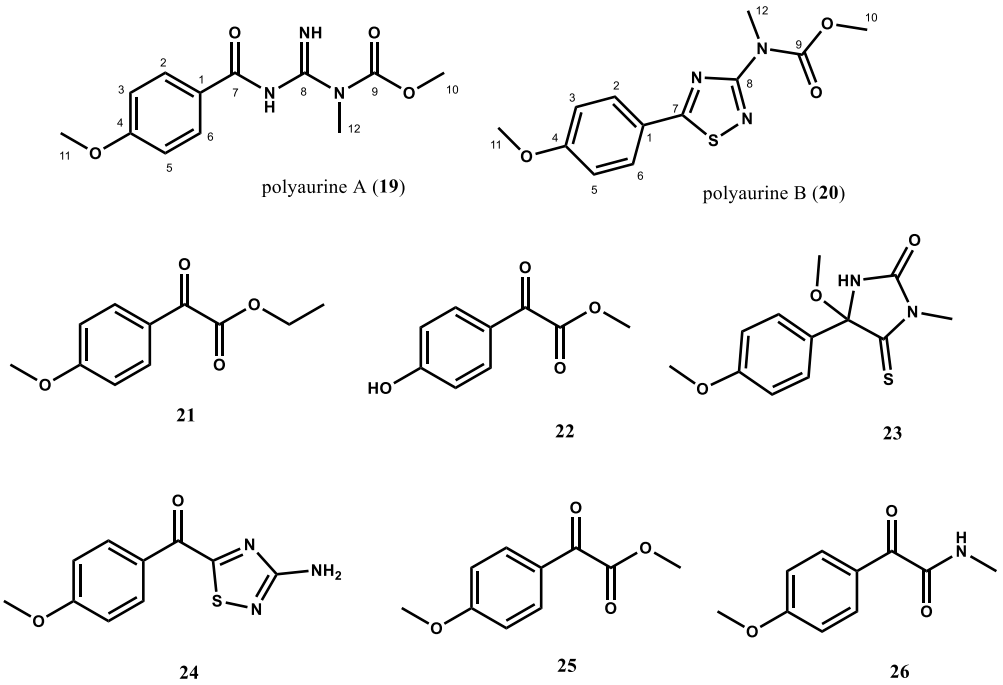

Figure 4. Structures of the novel (**19**-**22**) and known metabolites (**23**-**26**) from *P. aurata* samples.

Despite the low quantity isolated, the two new metabolites were subjected to a cytotoxicity and antiparasitic screening. The novelty brought by the latter two metabolites is thus underlined by the not-toxic effects on the growth of mammalian cells (NIH-3T3, mouse embryonic fibroblasts) and by the possibility of polyaurine A (**19**) to act on the shape and the development of the eggs produced by *S. mansoni* adult pairs. These results require that the ascidian *P. aurata* should be further investigated for its promising metabolic content.

2.2.1 An overview on the chemistry and pharmacology of the known Polycarpa sp. secondary metabolites

Ascidians of genus *Polycarpa*, common benthic invertebrates of the Indo-Pacific coral reefs, are renowned for the biosynthesis of various secondary metabolites and the majority of which contain one or more heteroatoms, often nitrogen and/or oxygen atoms while more rarely sulphur is observed. Many compounds isolated from different samples of *Polycarpa* species are alkaloids that sometimes present disulphide bonds in their structure. Previous chemical investigation by guided bioassays of *Polycarpa* species led to the isolation firstly of a dimeric disulphide, polycarpine (**27**, Figure 5), which tends to degrade slowly in the derivative **23** (Figure 4) mainly due to the silica gel used during the extraction procedures, and of an indole alkaloid, the *N,N*-didesmethylgrossularine-1 (**28**) [59]. Subsequently, the polycarpamines A-E (**29**-**33**), benzenoids derivatives with sulfur-containing functional groups, the polycarpaurines A-C (**34**-**36**) characterized by a 2-aminoimidazole ring along with polycarpathiamines A (**37**) and B (**24**, Figure 4) have been brought to light (Figure 5) [60-62].

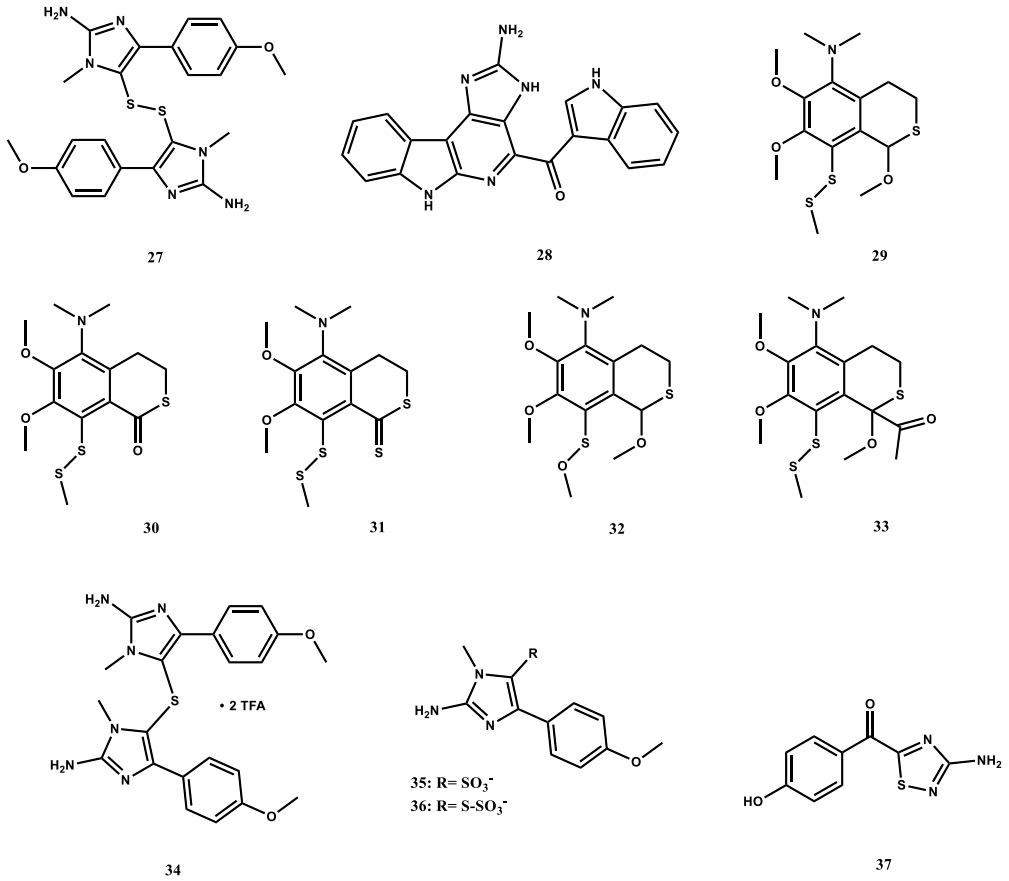

Figure 5. Known secondary metabolites (**27-37**) from *Polycarpa sp.*

Most of these metabolites have been also investigated for their effects on different target and their pharmacological potential needs to be mentioned. Particularly, the imidazole alkaloid polycarpine (**27**) has been shown to be a promising antitumor agent as well as able to induce apoptosis in different cell lines. Indeed, polycarpine (**27**) caused the inhibition of the enzyme inosine monophosphate dehydrogenase (IMPDH) which is used as a screening tool to detect antiproliferative drugs and in addition the anticancer effects have been also observed since compound **27** was responsible for apoptosis induction of JB6 cells through the p53- and caspase-3-dependent pathways [59,63-64]. Regarding the other known metabolites from *Polycarpa sp.*, interesting

biological properties have been demonstrated. Also other metabolites, like polycarpathiamine A (compound **37**) showed cytotoxic effects in submicromolar concentration inhibiting the growth of L5178Y mouse lymphoma cells *in vitro* as reported by Pham *et al.* [62]. Interestingly, compound **37** resulted 10-fold more active than the cytotoxic depsipeptide kahalalide F (**38**, Figure 6), isolated from the sea slug *Elysia rufescens* and used as positive control (IC_{50} of 4.3 μM). The term IC_{50} indicates the dose of compound necessary to inhibit cell growth by 50%. Apparently, the presence of a hydroxyl group on the aromatic ring of **37** should be crucial for the activity since polycarpathiamine B (**24**) was completely inactive [62].

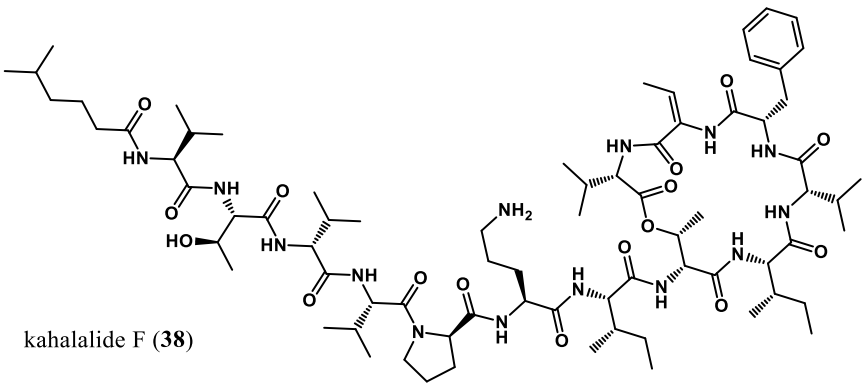

Figure 6. The marine-derived kahalalide F (**38**), a cytotoxic compound from the sea slug *Elysia rufescens*.

Instead, the *N,N*-didesmethylgrossularine-1 (**28**) raised interest for its interference on TNF-*α* production, resulting a promising lead candidate for drug discovery of chronic inflammatory diseases [65]. Lastly, the polycarpamines A-E (**29**-**33**), have been investigated for their antifungal properties enlarging in this way the overview of therapeutic application for *Polycarpa* secondary metabolites [60].

Next to these encouraging alkaloids, also different *para*-substituted benzoyl derivatives (**25**-**26** and **39**-**40**, Figures 4 and 7) have been yet reported in literature [66]. The peculiarity of these compounds lies in the structural analogy to hydroxyl-Dopa moiety contained in unstable peptides, known as tunichromes. Thus, the biosynthetic pathway of the latter might be, at least partially, derived from shikimic acid (**41**, Figure 7) [67].

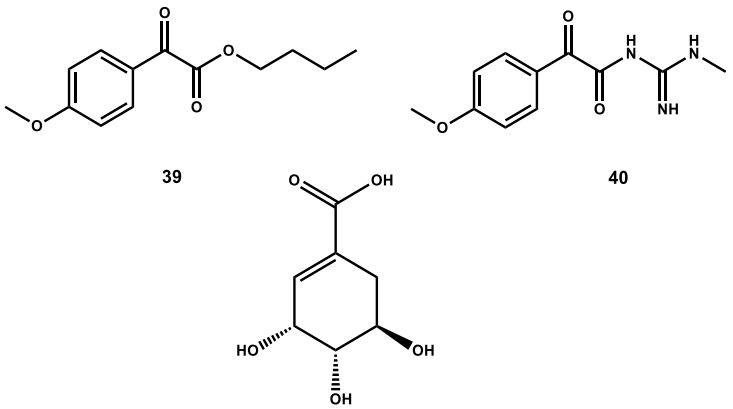

Figure 7. Structures of 4-methoxybenzoyl derivatives (**39** and **40**) and shikimic acid (**41**).

The high chemical diversity, and above all, the recovery of different kind of metabolites yielded by the chemical analysis of *Polycarpa sp.* samples, collected in different places and seasons, suggested that this invertebrate may not be the true bioproducer of these unique compounds. In fact, all the ascidians are filter feeders, seeping in planktonic organisms and microorganisms, and thus, the synthesis of secondary metabolites might involve planktonic biomass and/or symbiotic microorganisms [60]. Either way, the members of *Polycarpa* genus are doubtless an appealing source of potentially bioactive compounds.

2.2.2 Isolation and structural elucidation of novel secondary metabolites from the tunicate P. aurata

In the frame of an ongoing search of novel metabolites of marine origin, fresh specimen of *P. aurata* collected along Siladen coast (Indonesia, 1°37'41'' N 124°48'01'' E) have been frozen immediately after collection and kept frozen until the usage. To perform an exhaustive extraction of all metabolites, the tunicate samples were firstly thawed, subjected to homogenization and extracted several times with organic solvents. In particular, methanol and chloroform were used three time (each solvent 3 x 400 mL) to obtain a combined organic extract. The partitioning of the organic extract between ethyl acetate and water, and of the resulting water layer with *n*-butanol led to three different organic phases in which an initial separation of compounds was performed according to polarity of the latter, whereas the dry weight of extracted tunicates was 39.8 g.

My studies were carried on the lipid soluble portion. In fact, the ethyl acetate soluble material was chromatographed over silica gel by MPLC chromatographic techniques using mixtures hexane/EtOAc as mobile phase in different ratio by a gradient solvent system from 100% hexane to 100% chloroform and collecting eighteen fractions. A preliminary 1D NMR analysis on raw fractions revealed that the most valuable were the fractions from 6 to 9, i.e. those eluted with hexane/EtOAc 1:1 (v/v) which needed to be further investigated by other chromatographic techniques. Indeed, HPLC separations, in both different stationary and mobile phase, allowed to separate the highlighted fractions into individual compounds, yielding overall eight compounds in pure form as shown by NMR and HRESI-MS spectra (see Chapter 6), and of which, the structures have been reported in Figure 4 (**19**-**26**). The alkaloids polyaurine A (**19**) and B (**20**) and

two novel benzoyl derivatives, compounds **21** and **22**, have been afforded afterwards through HPLC separation on SiO_2 column of the above-mentioned fraction 6. Moreover, this chemical investigation has also permitted the isolation of four known compounds (**23**-**26**), already reported in literature as products of secondary metabolism of *P. aurata* and other *Polycarpa* species [59,62,66].

The ^1H chemical shifts of these compounds were compared to those of already described secondary metabolites. According to this, the presence in *P. aurata* organic extract of 4-methoxy-4-(4-methoxyphenyl)-1-methyl-5-thioxoimidazolidin-2-one (**23**) [59], of polycarpathiamine B (**24**) [62], of methyl 2-(4-methoxyphenyl)-2-oxoacetate (**25**) and of 2-(4-methoxyphenyl)-*N*-methyl-2-oxoacetate (**26**) was detected (Figure 4) [66]. The comparison of NMR resonances of the 2-oxo-2-phenylacetic acid strictly derived metabolites with those of compounds **21** and **22** allowed to easily identify the structures of novel benzoyl derivatives as ethyl 2-(4-methoxyphenyl)-2-oxoacetate (**21**) and 2-(4-hydroxyphenyl)-*N*-methyl-2-oxoacetamide (**22**). By the same HPLC gradient system (hexane/EtOAc 95:5 v/v), the investigated fraction yielded also the alkaloids **19** and **20**, which structures have been completely elucidated thanks to the progressive spectroscopic methods.

Structure elucidation of polyaurine A (**19**) was performed starting from the explanation of molecular formula. Indeed, a high-resolution ESI mass infusion revealed peaks at *m*/*z* 266.1129 $[M+H]^+$ and at *m*/*z* 288.0948 $[M+Na]^+$, suggesting a molecular formula of $C_{12}H_{16}N_3O_4$ and seven degrees of unsaturation. The MS/MS spectrum of compound **19** highlighted the presence of a fragment peak at *m/z* 135 which matched with a 4-methoxybenzoyl unit. This moiety was confirmed by the analysis of ^1H and ^{13}C resonances reported in Table 2, given that two deshielded aromatic protons at δ_H

8.17 (2H, *J*= 8.2 Hz, H-2/6) and δ_H 6.89 (2H, *J*= 8.2 Hz, H-3/5) assigned to two protonated carbons at δ_C 131.1 (C-2/6) and δ_C 113.0 (C-3/5) by 2D HSQC correlation along with two unprotonated carbons at δ_C 130.7 (C-1) and δ_C 162.4 (C-4), defined by HMBC spectrum analysis, agreed with a *para*-oxygenated benzoyl system. The methoxy group linked to the carbon C-4 was inferred by diagnostic ^{1}H (δ_H 3.84, 3H, C-11) and ^{13}C (δ_C 55.2, C-11) resonances, and by its HMBC key correlations with the quaternary carbon C-4 and with carbons C-3/5.

Table 2. ^{1}H (700 MHz) and ^{13}C NMR (125 MHz) spectroscopic data[a] of compounds **19** in $CDCl_3$.

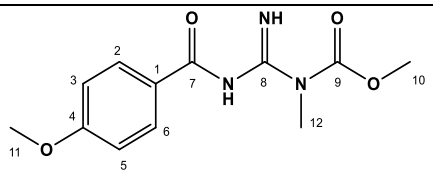

19[a]		
Pos.	δ_C	δ_H, **mult. (*J* in Hz)**
1	130.7	-
2	131.1	8.17, d (8.2)
3	113.0	6.89, d (8.2)
4	162.4	-
5	113.0	6.89, d (8.2)
6	131.1	8.17, d (8.2)
7	177.9	-
8	159.8	-
9	156.7	-
10	53.8	3.86, s
11	55.2	3.84, s
12	32.3	3.52, s
-NH	-	9.28, br.s; 10.58, br.s

[a] ^{1}H NMR and ^{13}C NMR shifts are referenced to $CDCl_3$ (δ_H = 7.26 ppm and δ_C = 77.0 ppm).

Additionally, diagnostic cross peak between H-2/6 and the carbonyl group at δ_C 177.9 (C-7) was recorded by HMBC spectrum assigning all resonances of the 4-methoxybenzoyl moiety and allocating five out of seven degrees of unsaturation. As

additional features, the ^{1}H spectrum of polyaurine A (**19**) in the low-field region showed two signals at δ_H 9.28 and at δ_H 10.58 ascribable to two -NH groups. Then, two methyl groups resonant as singlets at δ_H 3.86 (3H, s, Me-10) and δ_H 3.52 (3H, s, Me-12) were assigned to a methoxyl group (δ_C 53.8, C-10) and to a nitrogen linked methyl group (δ_C 32.3, C-12) respectively, according to their HSQC and HMBC correlations, and based on the expected chemical shift values. In the ^{13}C spectrum of compound **19** only two resonances (δ_C 159.8 and δ_C 156.7) belonging to two unprotonated sp^2 carbons remained to assign. The analysis of the whole HMBC correlations showed in Figure 8, and considering the defined molecular formula for **19**, allowed to identify a methyl-guanidine group and an unusual carbamate function.

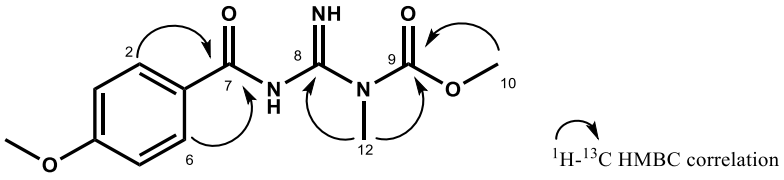

polyaurine A (**19**)

Figure 8. Key HMBC correlations for polyaurine A (**19**).

In fact, the structure depicted in Figure 4 for **19** has been univocally defined considering that *N*-methyl group (Me-12) presented key HMBC correlations with both the sp^2 carbons (δ_C 159.8 and δ_C 156.7) whereas the methoxyl group (Me-10) correlated only with the latter carbon (δ_C 156.7). In this way, all ^{1}H and ^{13}C resonances were assigned and reported in Table 2 completing the structural elucidation of the novel alkaloid polyaurine A (**19**).

As for polyaurine B (**20**), the molecular formula was determined as $C_{12}H_{13}N_3O_3S$ from HRESIMS in positive ion mode since the spectrum showed a pseudomolecular ion

peaks at *m*/*z* 280.0741 $[M+H]^+$ and at *m*/*z* 302.0558 $[M+Na]^+$. The evaluation of mass data indicated eight degrees of unsaturation while a deep NMR analysis allowed to suppose that the structure of **20** was composed of three subunits depicted in Figure 9, subsequently connected by diagnostic cross peaks recorded by HMBC experiment shedding light on the really atypical structure for a marine metabolite assigned to polyaurine B (**20**).

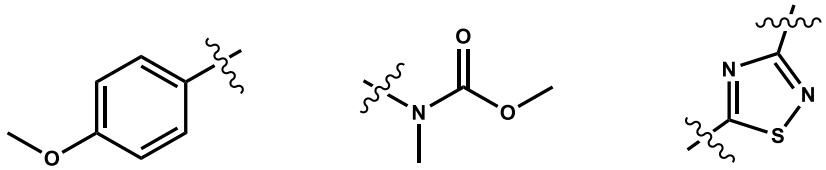

Figure 9. Subunits A-C of polyaurine B (**20**).

The subunit A is constituted of a *p*-methoxyphenyl group and was deduced by the typical resonances of aromatic protons in the low-field region of ^1H spectrum and also by the ^{13}C chemical shift analysis. The alkaloid **20** was characterized by aromatic methine protons at δ_H 7.88 (2H, d, *J*= 7.9 Hz, H-2/6) and δ_H 6.96 (2H, d, *J*= 7.9 Hz, H-3/5) linked to carbons C-2/6 and C-3/5 at δ_C 128.9 and δ_C 114.7, respectively. Bidimensional HSQC and HMBC experiments permitted to complete the assignment of all proton and carbon resonances into subunit A. Indeed, a direct coupling ^1J ^1H-^{13}C defined a methoxyl substituent (Me-11) by the correlation of proton resonance at δ_H 3.87 with the carbon at δ_C 55.5 (C-11), whereas into HMBC spectrum long range correlations among Me-11 and both C-4 (δ_C 162.7) and methine carbon at δ_C 114.7 (C-3/5) were recorded.

The ^{1}H NMR spectrum of polyaurine B (**20**) highlighted the presence of still two methyl singlets at δ_H 3.54 (3H, s, C-12) and at δ_H 3.85 (3H, s, C-10) linked to the relevant carbons at δ_C 36.1 (C-12) and δ_C 53.6 (C-10). These two resonances could be defined as a methyl group linked to a nitrogen atom and as a methoxyl substituent, respectively. In addition, HMBC correlations (Figure 10) of the latter protons with the same unprotonated sp^2 carbon at δ_C 154.9 led to the proposal of a *N*-methylcarbamate functionality (subunit B, Figure 9). According to molecular formula and remaining NMR resonances, the third moiety (subunit C, Figure 9) consisted of a 1,2,4-thiadiazole ring.

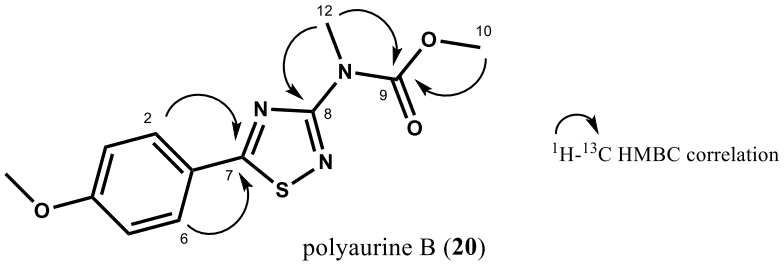

Figure 10. Key HMBC correlations for polyaurine B (**20**).

This motif occurs in nature only as this regioisomer and it was similarly found in previously discovered metabolites, polycarpathiamines A (**37**) and B (**24**), from *P. aurata* [62]. Generally, heterocycles are scaffolds commonly discovered in a wealth of natural products both from terrestrial plants and marine sources, particularly frequent in natural polyketides, alkaloids, vitamins, and phenylpropanoids harbouring one or two heteroatoms like nitrogen and/or oxygen and occasionally sulphur [68-70]. As for heterocyclic system with more than two heteroatoms, these portions are much less

abundant in nature although they constitute an enchanting group of molecules with a wide range of biological applications [71].

During this investigation, the attention has been focused on the "heteroatom rich" 1,2,4-thiadiazole ring which represents a case of choice for the uncommon heterocyclic moiety in natural products. The first example of 1,2,4-thiadiazole moiety identified in nature came from dendrodoine (**42**, Figure 11), a cytotoxic compound isolated from the tunicate *Dendrodoa grossularia* (Styelideae) collected off the coast of North Brittany (France) in 1980 [72]. Subsequently, only in 2013 the same ring was again discovered in polycarpathiamines (Figure 5), already mentioned *Polycarpa* metabolites [62]. From terrestrial sources, in 2012 a scalemic mixture (2:1) of indole alkaloids **43a** and **43b** (Figure 11) has been isolated from the root of herbaceous *Isatis indigotica* [73]. Another example, reported by Yang *et al.*, was penicilliumthiamine B (**44**, Figure 11) extracted from the fungus *Penicillium oxalicum* gathered from the gut of *Acrida cinerea*, a Chinese grasshopper [74].

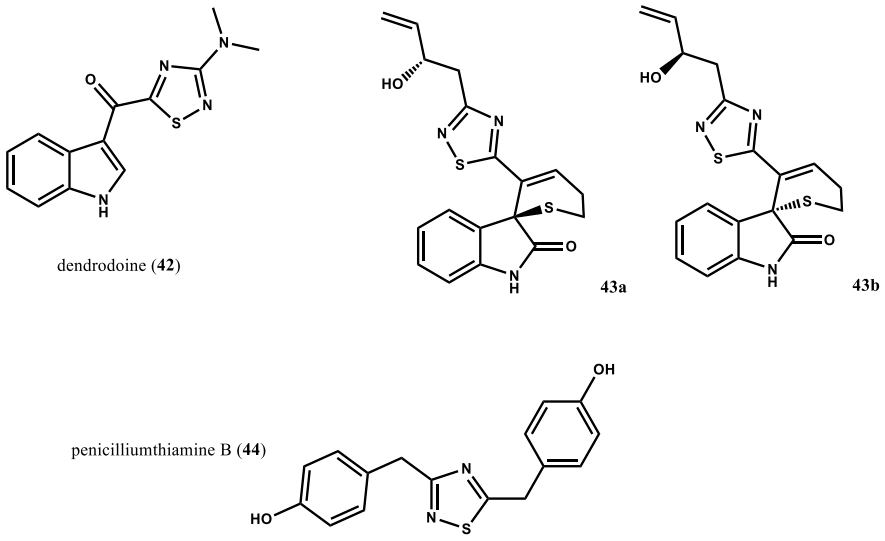

Figure 11. Examples of natural compounds with 1,2,4-thiadiazole ring (**42**-**44**).

In our case, the "heteroatom rich" 1,2,4-thiadiazole system was established having to satisfy other three degrees of unsaturation, and as a whole, allocate one sulphur, two nitrogen atoms and two sp^2 hybridized carbons at δ_C 187.1 and 165.8. The chemical shifts of the two carbons in-built into subunit C of compound **20** was revealed to be completely in agreement with those of known natural and also synthetic alkaloids exhibiting a 1,2,4-thiadiazole ring [62, 72-76]. Finally, HMBC correlations, showed in detail in Figure 10, connected the three subunits A-C.

Key ^{1}H-^{13}C long-range correlations were between aromatic protons H-2/6 (δ_H 7.88) and C-7 (δ_C 187.1) of the thiadiazole ring, and between the remaining carbon at δ_C 165.8 (C-8) and the protons of *N*-methyl group (δ_H 3.54) of subunit B. The whole pattern of δ_H and δ_C resonances were thus totally assigned, as reported in Table 3, suggesting the reported structure of polyaurine B (**20**, Figure 4).

Table 3. ^{1}H (700 MHz) and ^{13}C NMR (125 MHz) spectroscopic data[a] of compounds **20** in $CDCl_3$.

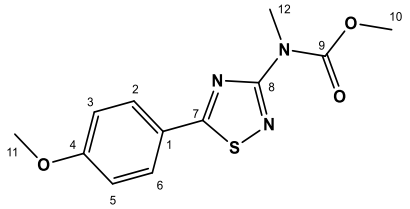

	20[a]	
Pos.	δ_C	δ_H, **mult. (*J* in Hz)**
1	123.2	-
2	128.9	7.88, d (7.9)
3	114.7	6.96, d (7.9)
4	162.7	-
5	114.7	6.96, d (7.9)
6	128.9	7.88, d (7.9)
7	187.1	-
8	165.8	-
9	154.9	-
10	53.6	3.85, s
11	55.5	3.87, s
12	36.1	3.54, s
-NH	-	-

[a] ^{1}H NMR and ^{13}C NMR shifts are referenced to $CDCl_3$ (δ_H = 7.26 ppm and δ_C = 77.0 ppm).

2.2.3 Theoretical QM calculations to substantiate polyaurine B structure

To further consolidate the evidence of a 1,2,4-thiadiazole ring in the structure of this marine metabolite **20**, quantum mechanical (QM) prediction of its ^{13}C NMR chemical shift values and DP4+ statistical analysis were performed.

In previous works [62,75,76], the regiochemistry of the heterocyclic ring has been confirmed only by synthesis, despite the spectroscopic means and biogenetic considerations. Nowadays, QM calculations of the NMR parameters profiles associated to the data processing of "computational toolboxes" may represent a valuable theoretical instrument as supplement to the spectroscopic analysis, both NMR and chiroptical, for structure elucidation of natural products. Indeed, beyond the regioisomer of 1,2,4-thiadiazole heterocyclic ring suggested according to NMR correlations and also comparing to literature data, it could be proposed on the whole six plausible regioisomers (**20a**-**20f**, Figure 12) compatible with the experimental NMR parameters. To unequivocally confirm the proposed regioisomer in compound **20**, the six alternatives were subjected to a *Density Functional Theory* (DFT) calculation of δ_C values using GIAO method. An optimization of geometry and energy of the compounds **20a**-**20f** were performed by DFT with mPw1PW91/6-311+G(2d,P) functional set combination.

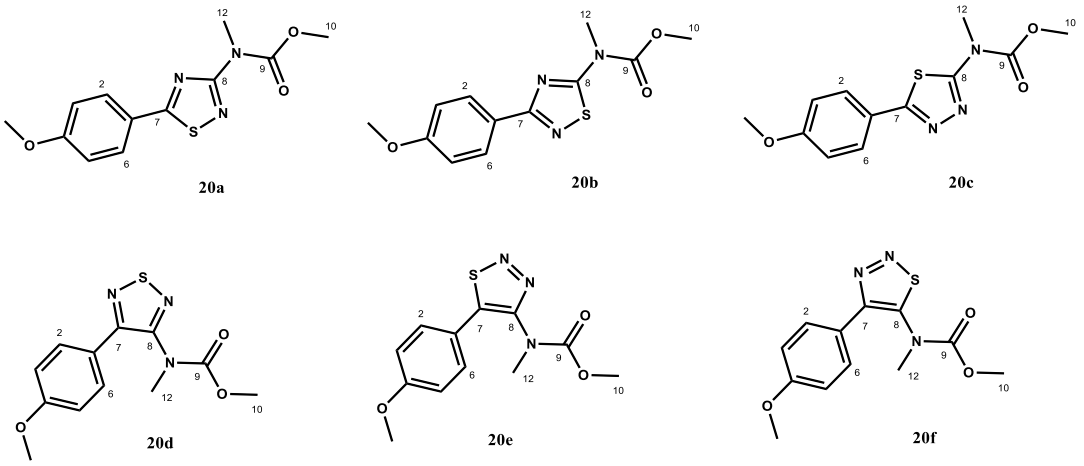

Figure 12. Putative regioisomers of the 1,2,4-thiadiazole ring in polyaurine B (**20**).

In Table 4 are reported the theoretical δ_C calculated for compounds **20a**-**20f** in comparison to those experimental recorded for the marine metabolite polyaurine B (**20**). The related calculated values of ^{13}C MAE and ^{13}C CMAE described in Table 5 resulted to be below 5 ppm for the isomer **20a** which is definitely established as the correct one. Indeed, an error value less than 5 ppm is considered acceptable for the theoretical chemical shifts predicted by DFT-NMR calculations.

Table 4. ^{13}C calculated and experimental NMR chemical shifts for isomers **20a**-**20f**. Chemical shifts were produced using tetramethylsilane (TMS) as reference compound.

Pos.	20a	20b	20c	20d	20e	20f	Experimental carbon
1	127.7	130.2	128.3	131.0	125.2	128.4	123.2
2	133.8	137.2	132.5	130.0	131.1	130.2	128.9
3	111.7	110.2	112.4	112.5	112.2	112.3	114.7
4	166.9	165.6	165.2	165.0	165.2	164.6	162.7
5	111.5	110.5	112.0	112.1	112.1	112.2	114.7
6	132.9	133.8	131.5	136.0	136.3	136.7	128.9
7	192.6	176.3	169.7	161.0	154.8	158.0	187.1
8	170.8	185.5	163.7	158.7	155.0	157.6	165.8
9	157.4	152.3	158.5	158.2	157.9	156.0	154.9
10	53.2	53.8	54.1	53.4	53.3	53.7	53.6
11	54.5	54.1	54.2	54.1	54.2	54.1	55.5
12	35.7	34.7	32.3	35.7	36.4	38.4	36.1

Additionally, ^{13}C NMR chemical shift pathways of the six regioisomers were subjected to a DP4+ statistical analysis (Table 5) which consist into the evaluation of the most consistent NMR data and allow to distinguish between several constitutional isomers. The computational analysis confirmed again **20a** as the correct regioisomer with the 100% of probability, confirming unequivocally the structure of the new isolated alkaloid polyaurine B (**20**, Figure 4).

Table 5. Calculation of the mean absolute errors (MAE) and correct MAE along and results of DP4+ statistical analysis for compounds **20a**-**20f**.

	MAE value (ppm)		^{13}C data DP4+ probability		
-	**^{13}C MAE**	**^{13}C CMAE**	**sDP4+**	**uDP4+**	**DP4+**
20a	3.2	1.7	100.00%	100.00%	100.00%
20b	5.6	5.3	0.00%	0.00%	0.00%
20c	3.9	4.2	0.00%	0.00%	0.00%
20d	5.1	6.4	0.00%	0.00%	0.00%
20e	5.6	7.3	0.00%	0.00%	0.00%
20f	5.2	6.6	0.00%	0.00%	0.00%

2.2.4 Evaluation of biological effects of polyaurine A and B on mammalian cells and against S. mansoni parasite

The alkaloids polyaurine A (**19**) and B (**20**) have been tested for their effects on the mammalian cells growth and also on the viability of blood-dwelling *S. mansoni* stages as well as egg production. Biological effects of the two novel compounds have been performed thanks to the active collaboration with the Institute of Cell Biology and Neurobiology of the National Research Council in Monterotondo (Rome), despite the small amount of tested compounds we managed to obtain by extraction procedure from the tunicate specimens. The effects on the viability of mammalian NIH-3T3 cell lines were evaluated and both compounds resulted not cytotoxic seeing as they showed an IC_{50} value higher than 100 μM in a dose-curve response. As for antiproliferative

properties, both polyaurine A (**19**) and B (**20**) resulted not active when tested against schistosomula, the larval form of *S. mansoni* parasite. Considering the low available quantity of **20** isolated, only polyaurine A was further investigated evaluating the effects on the viability of the adult worm pairs of the latter parasite as well as for the capability to impair the eggs production. The dose-curve response showed in Figure 13A polyaurine A (**19**) did not show any considerable effect on the viability of adult worms at both 20 and 50 μM during the seven days treatment, and at the same concentration also the total number of eggs laid by female worms of *S. mansoni* was similar to worms treated with DMSO as vehicle (Figure 13B). Interestingly, some eggs laid *in vitro* by **19**-treated parasite resulted to be deformed and egg fragments were present in plate dish together with vitelline cells, too (Figure 13C). It was possible to quantity the number of deformed and/or fragmented eggs at 72 h of treatment. By the observation of histograms shown in the Figure 13D it appeared that the percentage of damaged eggs is increased in the polyaurine A-treated samples with respect to the vehicle-treated ones ($p<0.05$) and this effect was also proved by carmine red-staining and confocal microscopy analyses which highlighted smaller size eggs in the ootype and uterus of *S. mansoni* parasites treated with compound **19** (Figure 13E).

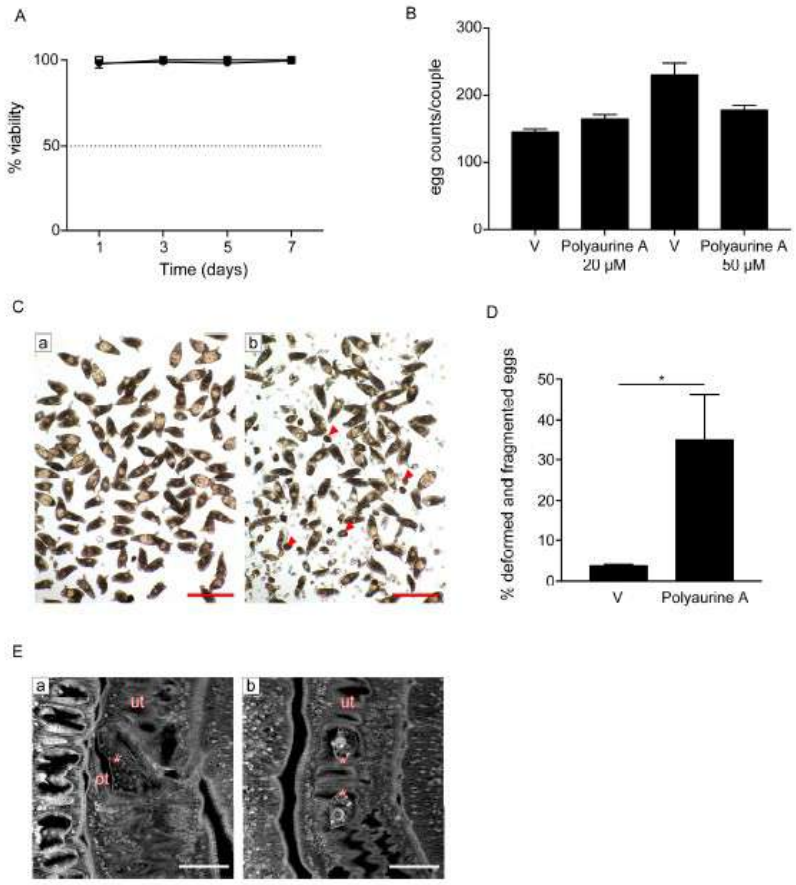

Figure 13. *Effects of polyaurine A on S. mansoni adult parasites and egg production:* A) Dose-curve response of worm viability. Adult worm pairs were treated with DMSO as vehicle (circle) 50 µM, and with **19** 20 µM (square) or 50 µM (triangle) and vehicle-treated samples is indicated as 100% viability. The data are the mean of three independent experiments ± SEM. B) Worm pairs were incubated with vehicle (V) or **19** at 20 and 50 µM; the eggs were counted at 72 hours. The data are the mean of three independent experiments ± SEM and eggs number normalized for worm couples. C) Microscopy images of *S. mansoni* eggs laid *in vitro* with (a) vehicle-treated samples or (b) 50 µM of polyaurine A (**19**). Deformed or fragmented eggs are indicated by red arrows. D) Histograms of the percentage of deformed and/or fragmented eggs counted after 72 h. Three independent experiments were performed counting 150-200 eggs/experiment. Asterisk indicates significant *t*-test *p*-value (*$p < 0.05$) relative to the comparison of 50 µM of **19**-treated samples with the V-treated ones. E) Representative confocal microscopy images of adult *S. mansoni* pairs treated with vehicle or 50µM of polyaurine A (72 h). Eggs in the ootype (a, vehicle) or uterus (b, polyaurine A) are indicated by asterisks. Abbreviations: ot: ootype;

ut: uterus. In all experiments, parasites or eggs received the same amount of DMSO (in volume) as the polyaurine A (**19**)-treated ones.

Conclusion: summing up, the eggs are a crucial element in the development of schistosomiasis infection since they permit the maintenance of parasite life-cycle and cause tissue damage into definitive host. Therefore, polyaurine A (**19**) represents an interesting example of not cytotoxic marine metabolite but able to impair the correct development of eggs in schistosomiasis. For this reason, this alkaloid is a promising bioactive natural compound that may be further investigated by electron microscopy and comparative proteomic studies in order to understand the egg phenotype and identify the putative target of polyaurine A. On the other hand, polyaurine B (**20**) may be considered as a fascinating example of how much varied the biogenetical pathways are since it belongs to the narrow cluster of molecules with the rarely found 1,2,4-thiadiazole ring. According to our knowledge, polyaurine B is also the first reported example of 3-(*N*-methyl-methylcarbamate) substituted 1,2,4-thiadiazole alkaloid originated from marine environment. Further contribution to its proposed structure is given by computational prediction of NMR parameters using DFT calculation that is becoming a fundamental tool to support the structure elucidation of natural products.

2.2.5 Materials and methods of P. aurata chemical investigation

*Collection, extraction and isolation of compounds **19-26***

Several samples of *P. aurata* were collected along the coast of Siladen in Indonesia and were identified by Dr. Masteria Yunovilsa Putra. Subsequently, the samples were

immediately frozen and kept so until the extraction. The extraction was performed with MeOH (3 x 400 mL) and then with $CHCl_3$ (3 x 400 mL) on thawed animals after homogenization. The extracts were combined and concentrated *in vacuo* obtaining an organic extract of *P. aurata*. The latter was solubilized in water and first partitioned with ethyl acetate (2 x 300 mL), and then with *n*-butanol (2 x 300 mL) giving three different organic extracts (EtOAc, *n*-BuOH and aqueous). The investigation of metabolic content was performed on the ethyl acetate-soluble material that was chromatographed by MPLC over a silica gel column with gradient elution 100% *n*-hexane→ EtOAc→ MeOH→ $CHCl_3$ yielding eighteen fractions. A preliminary 1D NMR analysis revealed that the most valuable were the fractions from 6 to 9, i.e. those eluted with hexane/EtOAc 1:1 (v/v) that were further purified by HPLC. The interesting fraction 6 was chromatographed by HPLC Luna 3 µm Silica column eluting with *n*-hexane/EtOAc (95:5) to afford in pure form polyaurine A (**19**, t_R= 9.2 min, 1.7 mg), polyaurine B (**20**, t_R= 12.7 min, 0.5 mg), compound **21** (t_R= 6.5 min, 0.2 mg), compound **22** (t_R= 19.1 min, 0.6 mg), and a mixture of compound **23** and **25** (t_R= 20.6 min). this mixture was further chromatographed by HPLC on reverse phase (Luna 3µm PFP column, MeOH/H_2O 75:25), affording as pure and individual compound **23** (t_R= 8.3 min, 0.5 mg), and compound **25** (t_R= 6.2 min, 0.7 mg). Regarding the pure compound **27** (t_R= 10.7 min, 0.5 mg), it was afforded by HPLC purification of fraction 7 using Luna 3 µm Silica column and *n*-hexane/EtOAc 85:15 as mobile phase. Definitely, fraction 8 was investigated by HPLC on SiO_2 (Luna 3 µm Silica column, *n*-hexane/EtOAc 9:1), yielding a fraction mainly composed of **24** (t_R= 22.4 min, 0.8 mg), then further purified on a RP-18 column (Luna 3µm PFP), with a mobile phase MeOH/H_2O 7:3 giving the pure compound **24** (t_R= 5.1 min, 0.4 mg).

*Polyaurine A (**19**):* yellow powder; ^{1}H and ^{13}C NMR data ($CDCl_3$) are reported in Table 2; HRESIMS: *m/z* 266.1129 $[M+H]^+$ (calcd. for $C_{12}H_{16}O_4N_3$ *m/z* 266.1135); *m/z* 288.0948 $[M+Na]^+$ (calcd. for $C_{12}H_{15}O_4N_3Na$ *m/z* 288.0955); 2D NMR spectra and mass spectrum are reported in Chapter 6.

*Polyaurine B (**20**):* yellow powder; ^{1}H and ^{13}C NMR data ($CDCl_3$) are reported in Table 3; HRESIMS: *m/z* 280.0741 $[M+H]^+$ (calcd. for $C_{12}H_{14}O_3N_3S$ *m/z* 280.0750); m/z 302.0558 $[M+Na]^+$ (calcd. for $C_{12}H_{13}O_3N_3SNa$ *m/z* 302.0570); 2D NMR spectra and mass spectrum are reported in Chapter 6.

*Compound **21**:* white powder; HRESIMS: *m/z* 209.0810 $[M+H]^+$ (calcd. for $C_{11}H_{13}O_4$: 209.0808); *m/z* 231.0630 $[M+Na]^+$ (calcd. $C_{11}H_{12}O_4Na$ *m/z* 231.0628); *m/z* 231.0370 $[M+K]^+$ (calcd. for $C_{11}H_{12}O_4K$ *m/z* 247.0367); ^{1}H NM and HRESIMS spectra are reported in Chapter 6.

*Compound **22**:* white powder; HRESIMS: *m/z* 181.0491 $[M+H]^+$ (calcd. for $C_9H_9O_4$: 181.0495); *m/z* 203.0309 $[M+Na]^+$ (calcd. for $C_9H_8O_4Na$ *m/z* 203.0315); ^{1}H NMR and HRESIMS spectra are reported in Chapter 6.

*Compound **23**:* yellow powder; $[\alpha]_D^{25}$= +33.5 (*c* 0.0002, CH_3OH); HRESIMS: *m/z* 289.0641 $[M+Na]^+$ (calcd. for $C_{12}H_{14}N_2O_3SNa$ *m/z* 289.0617); ^{1}H NMR ($CDCl_3$) and HRESIMS spectra are reported in Chapter 6.

*Compound **24**:* white powder; HRESIMS: *m/z* 236.0505 $[M+H]^+$ (calcd. for $C_{10}H_{10}N_3O_2S$: 236.0488); *m/z* 258.0327 $[M+Na]^+$ (calcd. for $C_{10}H_9N_3O_2SNa$ *m/z* 258.0308); ^{1}H NMR ($CDCl_3$) and HRESIMS spectra are reported in Chapter 6.

*Compound **25**:* colourless oil; HRESIMS: *m/z* 195.0647 $[M+H]^+$ (calcd. for $C_{10}H_{11}O_4$: 195.0652); *m/z* : 217.0465 $[M+Na]^+$ (calcd. for $C_{10}H_{10}O_4Na$ *m/z* 217.0471);

m/z 233.0205 $[M+K]^+$ (calcd. for $C_{10}H_{10}O_4K^+$ *m/z* 233.0211); ^1H NMR ($CDCl_3$) and HRESIMS spectra are reported in Chapter 6.

Compound ***26****:* colourless oil; HRMS (ESI): *m/z* 194.0806 $[M+H]^+$ (calcd. for $C_{10}H_{12}NO_3$: 194.0812); *m/z* 216.0625 $[M+Na]^+$ (calcd. for $C_{10}H_{11}NO_3Na$ *m/z* 216.0631); ^1H NMR ($CDCl_3$) and HRESIMS spectra are reported in Chapter 6.

Biological assays

Ethical statement: Animal work was approved by the National Research Council, Institute of Cell Biology and Neurobiology animal welfare committee (OPBA) and by the competent authorities of the Italian Ministry of Health, DGSAF, Rome (authorizations no. 25/2014-PRand no. 336/2018-PR). All experiments were conducted according to the 3R rules in the respect of all ethical and safety guidelines for the use of animals in biomedical research provided by Italian Legislative Decree 26/2014 and 2010/63/EU as well as by the International Guiding Principles for Biomedical Research involving animals (Council for the International Organizations of Medical Sciences, Geneva, Switzerland).

Maintenance of the S. mansoni life-cycle: A Puerto Rican strain of *S. mansoni* strains (Puerto Rico) were maintained in the intermediate host *Biomphalaria glabrata*, and in ICR (CD-1) outbred female mice as the definitive host [77]. Female 7-8-week-old mice (Envigo, Udine, Italy) were infected with by the tail immersion technique.

Preparation of parasites, viability assays and eggs production analysis: The larval form (schistosomula) was prepared by mechanical transformation of cercariae and following infection of female 7-8-week-old mice (Envigo, Udine, Italy) by tail immersion technique (150–200 double sex *S. mansoni* cercariae/mouse), while reversed perfusion of the hepatic portal system and mesenteric veins allowed to isolate adult

worm pairs 7-8 weeks post-infection. The schistosomula ATP-based assay was realized in 96-wells/cell culture black microplate (Greiner Bio-One S.r.l, Rome, Italy) with the CellTiterGlo (CTG) (Promega, Madison, USA) using 150-200 schistosmula/well and 50 μL of CTG [77]. The luminescence signal was measured with a Varioskan Lux and the Skanit software (ThermoFisher Scientific, Waltham, USA) calculating the percentage of dead schistosomula as ATP reduction against vehicle (negative control, 0% death) and against 50 μM of gambogic acid (positive control with 100% death).

For the adult worm viability assays, 5 adult male-female pairs were plated in tissue culture medium, and 24 h upon isolation of parasites from mice, were added DMSO as vehicle or polyaurine A at 20 and 50 μM, keeping under observation for seven days. A survival score was assigned daily based on phenotypes (plate-attached, movement, color, gut peristalsis, tegument damage, male-female pairing) with Leica MZ12 stereomicroscope. The score of viability was assigned in three independent experiments respect to DMSO. For *in vitro* eggs production assay, 5 adult worm pairs were treated with DMSO or polyaurine A (**19**), counting the number of eggs at 72 h of treatment the number was normalized to parasite pairs. Eggs images were recorded with a BX41 Olympus microscope and a brightfield objective 10 x served by a SPOT RT 220-3 Diagnostic Instrument Inc camera.

Confocal laser scanning microscopy analysis: Carmine-red staining was executed on parasites as described by Guidi *et al.* [78]. Images have been taken on an Olympus FV1200 confocal laser-scanning microscope using an UPlanFLN 40x immersion oil objective (NA = 1.30), a multiline argon laser at 488 nm as the excitation source and collecting images as a single stack.

Viability mammalian cell assay: NIH-3T3 cells were plated in 96-well plates (0.4 x 10^4 cells/well) and treated with compound **19** or **20** (increasing the concentration from 0.390 up to 100 μM) in complete tissue medium keeping for 72 hours at 37°C with 5% of CO_2. MTT assay was performed by using MTT at 1 mg/mL and solubilizing formazan crystals in DMSO. The plates were analyzed with the Varioskan Lux and the Skanit software (Thermo Fisher Scientific, Fisher Scientific; Waltham, USA) at 570 nm and 630 nm.

Statistical analysis: GraphPad Prism v.6.0c software is the software used to perform all statistical tests. All data are shown as the mean ± SEM while the differences in the number of abnormal/fragmented eggs were analyzed by Student's t-test ($p \leq 0.05$ was considered statistically significant).

2.3 Antiparasitic effects of marine sesquiterpene quinone avarone, of its semisynthetic dioxothiazine-derivative thiazoavarone, and of the hydroquinone avarol

Sponges of the genus *Dysidea* are for a long time reported as a hopeful source of various secondary metabolites which exert a wide range of biological activities. Most of the metabolites reported from sponges of the order Dictyoceratida are constituted of a decalin core structure to which quinone or hydroquinone moiety is linked as side chain. These compounds exhibit several interesting effects on many targets attracting in this way the attention of the scientists who might use these natural products both to elucidate intracellular process and to develop new leads in the drug discovery process [79-88].

Within a systematic analysis of macroflora and macrofauna of the Bay of Izmir on Aegean Sea (Turkey), a part of my PhD activity dealt with the study of the sesquiterpene-quinones fraction of *D. avara* aiming to enlarge the pharmacological characterization of these metabolites and, mainly, to explore their potential as antiparasitic agents. This chemical investigation afforded the isolation of the known sesquiterpene quinone avarone (**45**) along with the related reduced form avarol (**47**) from the sponge *D. avara* (Figure 14) [89-91]. In literature, various pharmacological properties of these two metabolites as well as of semisynthetic avarone-derivatives are known, thus highlighting a wide range of biological activities from anti-tumour, anti-inflammatory, antibacterial, antiviral to anti-psoriasis, anti-biofouling and antioxidant [79-88]. Recently, several articles have pointed out the worthy role of quinones as effective antimalarials mainly due to their redox active potential, in fact, the ability of

quinone ring to generate semiquinone radical species impairs *Plasmodium* defences causing parasite death [54,92-93]. Moreover, it is not unreasonable to affirm that a number of effective antimalarial compounds, either some already marketed like artemisinin, mefloquine and chloroquine, have been demonstrated as able to act in the eradication of schistosomiasis [51, 94-98]. Although a different biology distinguishes the unicellular from multicellular parasites, both *Plasmodium* and *Schistosoma* for example feed on haemoglobin indicating the presence of common metabolic pathways and/or targets which ensure drugs are efficacious in both pathologies [51,54, 99-100].

Additionally, it is also known that several marine metabolites characterized by a thiazinoquinone bicyclic moiety fused to the quinone ring have been demonstrated as active against *P. falciparum* strains [101-102]. Thus, the possibility to easily derivatize the quinone present in avarone (**45**) by coupling with hypotaurine in high yield and with completely regioselective outcome, led us to synthesise a novel thiazinoquinone derivative, named thiazoavarone (**46**, Figure 14).

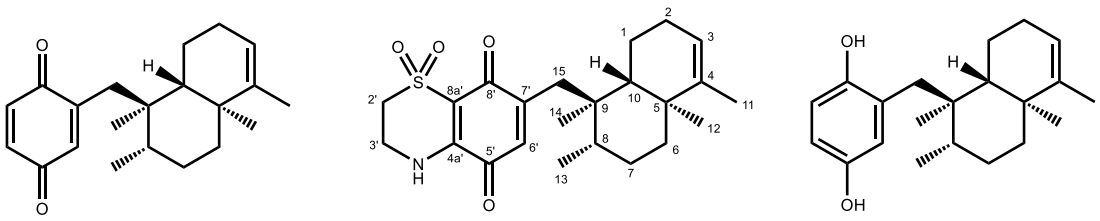

Figure 14. Structures of avarone (**45**), the dioxothiazine semisynthetic derivative thiazoavarone (**46**), and avarol (**47**).

This study has been performed as a part of an ongoing research for the group guided by Prof. Marialuisa Menna, in whose laboratory I spent the three years of doctorate. In

fact, the search of new antiparasitic drugs led to encouraging results when chemical libraries of thiazinoquinones have been prepared pointing out some crucial structural requirements for the activity and shedding light on the putative mechanism of action through computational studies. This analysis has identified the thiazinoquinone scaffold as an important active chemotype for malaria and schistosomiasis [103-105].

In accordance to the above described, the isolated sesquiterpenoid compound couple (**45** and **47**), and the semisynthetic derivative, thiazoavarone (**46**), have been included into pharmacological screening in order to shed light on the potential of these molecules in the fight against multiparasitism. In particular, the effects on D10 and W2 strains of *P. falciparum*, on V stage *Plasmodium* gametocytes, larval and adult form of *S. mansoni* worms and the effects on eggs production have been investigated. These three compounds have been also evaluated against *Leishmania infantum* and *tropica* as well as for the cytotoxic effects on human cell lines, microvascular endothelial (HMEC-1) and acute monocytic leukaemia (THP-1) cells [106].

The promising results carried out by compounds **45**-**47** on the tested parasites, and the computational studies including DFT calculations clearly support the hypothesis that in the antiparasitic activity a key role is played by the toxic semiquinone radical species. The latter species can be produced by both quinone- and hydroquinone-based compounds, while a different activity trend between the parasites may be addressed to morphological and/or metabolic differences in the targeted organisms.

2.3.1 The incredible perspective of terpenoid quinones/hydroquinones

A rich harvest of compounds with a terpenoid skeleton has been found in marine sponges. Among them, sponges of genus *Dysidea* are surely a reservoir of fascinating

quinones and hydroquinones which possess a drimane sesquiterpenoid residue. Since the first finding in 1974 by Minale *et al.* of the sesquiterpene quinone avarone (**45**) and its related hydroquinone avarol (**47**) from a *D. avara* collected in the Mediterranean Sea [89], an array of compounds belonging to this definite chemical class have been isolated from several *Dysidea* species, collected also in Indian and Pacific oceans [107-111].

The interest in this sesquiterpene units, tethered to a quinone or hydroquinone, arises from several reasons. Firstly, the 1,4-benzoquinone moiety and the relative reduced form are common structural features gathered in a great number of natural products from marine environment, in fact the couple oxidized/reduced form is often found. Then, the broad spectrum of biological activities showed by these compounds, generally ascribed to redox properties of quinone or hydroquinone system towards the generation of radical reactive species, and moreover the ability to interact with biomolecules also by nucleophilic addition, have always fuelled the attention to the analysis of the behaviour of these marine metabolites. Despite the high number of metabolites both chemically and biologically identified from *Dysidea sp.*, collected worldwide, the chemistry of these organisms is far from completely explored so much that several reviews are still published upgrading and reviewing the structures of *Dysidea* metabolites [112-113].

In addition, the attractive features of the unique structures have also made these metabolites intriguing targets and have spurred the development of regioselective strategies for their total synthesis [114-115]. The presence of several chiral centers in the rearranged sesquiterpenoid skeleton represents a hard challenge also for the synthesisers who have to synthesise the natural products in an enantioselective manner, and a common element in the whole enantioselective scheme has regarded the

assembling of the entire skeleton in which the decalin structure binds the quinone moiety. Regardless, the possibility to obtain natural products by synthesis is highly desirable and worthwhile for medical chemistry and pharmaceuticals as well as to understand the biogenetic origin and the enzymatic pathways involved in the production of natural products. Thus, the study of taxonomy has attracted the most attention of marine chemistry, too. The isolated compounds are generally classified according to the standard rules of organic chemistry but the correlation of the obtained data for a specific class or order holds a special importance in this field.

As above mentioned, terpenoid quinones and hydroquinones represent one of the most widespread groups of secondary metabolites isolated from sessile organisms and these have been classified as belonging to subgroup of quinoid compounds with a mixed shikimate-mevalonate biogenesis [116]. A representative group of correlated compounds is constituted of avarone and avarol (**45** and **47**, Figure 14) from *D. avara*, ilimaquinone (**48**) from *Petrosaspongia metachromia*, bolinaquinone (**49**) from *Dysidea sp.*, isospongiaquinone (**50**) from *Stelospongia conulata*, and several nakijiquinones (**51a-51d**) from *Spongia sp.* (Figure 15) [89,90,117-122].

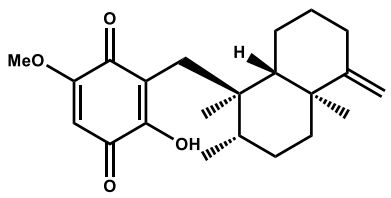

ilimaquinone (**48**)

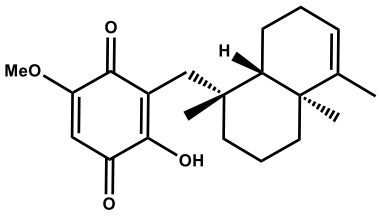

bolinaquinone (**49**)

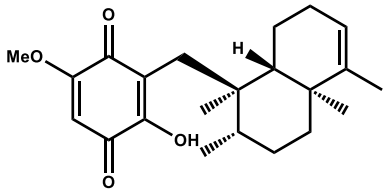

isospongiaquinone (**50**)

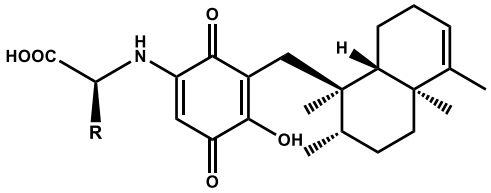

nakijiquinones

51a: R= -H
51b: R= -*i*Pr
51c: R= -CH_2OH
51d: R= -$CH(CH_3)OH$

Figure 15. Structures of 4,9-friedodrimane rearranged marine sesquiterpenoids (**48-51**) from order Dictyoceratida.

For the cited metabolites, biosynthetic pathways have been exhaustively studied and a 4,9-friedodrimane rearrangement for these marine sesquiterpenoids has been proposed [116]. It has been noted that although identified from different sponges and collected in different areas of the world, the membership to the same taxonomic order (Dictyoceratida) led to a structurally related compounds based on a common *trans*-decalin system, resulted in the rearrangement of drimane chain, attached to a (hydro)quinone moiety. If the double bond position and type of substituents on the quinone ring represent the main structural variations, the identical absolute configuration to all chiral centers with the only exception of C-8 in bolinaquinone (**49**)

confirms that the pathway of the formation of the sesquiterpenoid skeleton is the same for all related compounds. The strong interest into the study of behaviour of the main *D. avara* metabolites, avarone (**45**) and avarol (**47**), is again demonstrated by the fact that the quinoids biogenesis was firstly proposed for the hydroquinone avarol (Scheme 1) [116].

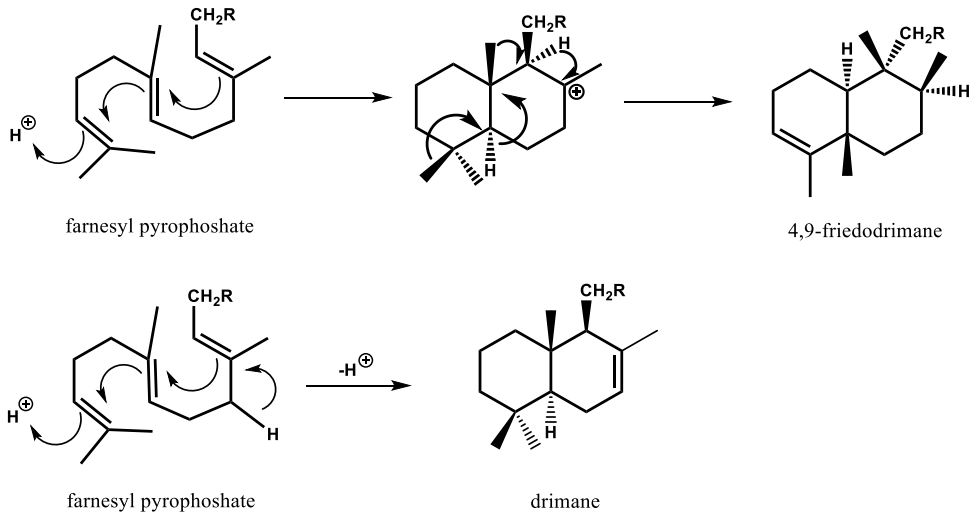

Scheme 1. Biogenesis of sesquiterpenoid skeleton.

As reported in Scheme 1, the farnesyl pyrophosphate (FPP) undergoes to a cyclization by an initial electrophilic attack at its *head*. In this way, a concerted process takes place giving rise to a bicyclic carbocation intermediate. This latter, after deprotonation, leads to 4,9-friedodrimane structure as final product. From this point, the process goes on with the active participation of several and different quinones in order to complete the synthesis of these various marine metabolites that, even though structurally correlated, exhibit different bioactivity from each other. Thus, the chemical

investigation of these marine organisms needs to be further scrutinized to shed light on novel intriguing sesquiterpene (hydro)quinones.

2.3.2 Chemical modification of avarone to synthesise thiazoavarone, a novel thiazinoquinone compound

The isolation of the two main secondary metabolites, avarone (**45**) and avarol (**47**), was achieved by sample of *D. avara* collected along the coast of Izmir Bay in Turkey (38° 24' 45 N 27° 8' 18 E) during the summer season and were immediately frozen (-25°C) on board to preserve the material quality as well as the metabolic content. The analysis of *Dysidea* and of other sponge, tunicate and octocoral samples, still in progress, is part of an investigational campaign of macroflora and fauna of the Aegean Sea in order to chemically explore this portion of marine environment.

According to this, thanks to the collaboration with the Department of Vocational School of Medicinal Health Services at Mugla University (Turkey) fresh specimens to investigate have been provided. As for *D. avara*, the extraction procedure was quite like to that reported in literature for *Dysidea sp.* and primarily to that described by Minale and co-workers, who first found the oxidized/reduced couple of compounds [89]. In detail, the thawed frozen sponge *D. avara* was subjected to several extraction with methanol, and then with dichloromethane affording a combined organic extract which was concentrated under pressure. The partitioning of the dry extract between water and *n*-butanol allowed to obtain an initial separation of the compounds according to their polarity. The *n*-butanol soluble material showed particularly interesting; indeed, it was

first chromatographed on RP-18 silica gel flash column, and subsequently, the most interesting fraction (eluted with a mixture MeOH/H_2O 8:2 v/v) was further purified by HPLC yielding the two metabolites, **45** and **47**. The structures of avarone (**45**) and avarol (**47**) were fully deduced comparing their spectral properties with those yet reported in literature [89-91]. In fact, the spectroscopic properties (^1H and ^{13}C chemical shifts), HRESIMS values and the value of specific optical rotation $[\alpha]_D^{25}$ enable to define for sure that the two metabolites were those already described.

The interesting pharmacological potential of these two compounds [82-88], and the reactivity of **45** in quinone addition-elimination processes [116,123], have inspired a depth investigation of both further pharmacological properties and the possibility to use the quinone moiety as starting point for chemical modifications.

From many years, the research group in which I performed my PhD was involved in the preparation of chemical libraries of thiazinoquinone compounds starting from low-cost reagents and by a versatile synthetic protocol [103-105]. The achieved results were encouraging: i) the thiazinoquinone moiety ascertained to be fundamental for the activity against unicellular and also multicellular parasites; ii) some crucial structural requirements were demonstrated in particular the regiochemistry of the heterocyclic ring with respect to the alkyl side chain; iii) the nature and the shape of alkyl chain affected compounds potency and, iv) SAR studies revealed that the corresponding quinone compound of the lead candidate, lacking of the 1,1-dioxo-1,4-thiazine ring was completely inefficacious. For a complete and in-depth description of the whole results achieved on this topic see Chapter 3 of this thesis and references 103-105.

To make a further exploration of this scaffold as multiparasitic agent, my research work has set up to make a coupling of **45** with hypotaurine (Scheme 2) in order to

synthesise a thiazinoquinone bicyclic moiety, taking advantages from its good availability. Beyond the novel semisynthetic compound, also the redox-active couple of natural derivatives (**45** and **47**) has been included into pharmacological screening in order to investigate the effects of a different quinone/hydroquinone scaffold against different human parasites. Here, the overall results are reported.

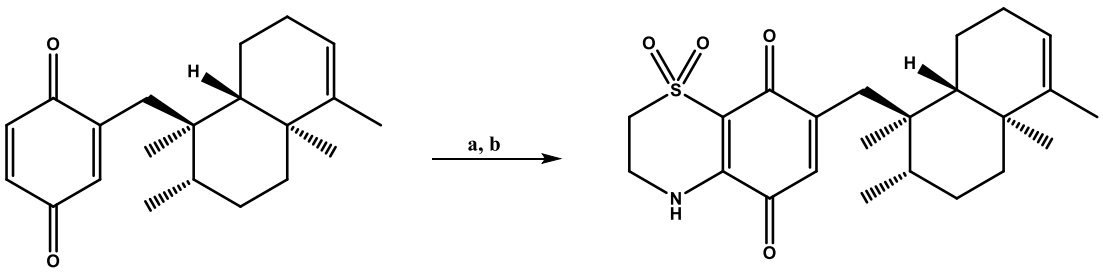

avarone (**45**) thiazoavarone (**46**)

Scheme 2. Coupling of the 1,4-benzoquinone moiety of avarone (**45**) with hypotaurine to synthesise thiazoavarone (**46**). Reagents and conditions: (**a**) hypotaurine, CH_3CN/EtOH 1:1, salcomine, 48h, rt; (**b**) HPLC on Luna 3 µm C-18 150 x 3.00 mm column, flow rate 0.5 mL/min, mobile phase MeOH/H_2O 75:25 v/v.

In Scheme 2 the synthesis of thiazoavarone (**46**) is described. The procedure is based on the use of a good portion (20.3 mg) of avarone to prepare the relevant thiazinoquinone derivative. The reaction grounded in the condensation of the 1,4-benzoquinone moiety of (**45**) with hypotaurine as nucleophilic reagent. In particular, the quinone was dissolved in a mixture of acetonitrile/ethanol (1:1) whereas a water solution of hypotaurine was added dropwise along with salcomine in portion as catalyst. The resultant mixture was stirred for 48 h at room temperature and since a chromophore

change occurred, it was possible to observe the variation of mixture colour from slight yellow to orange/red acting as a good indicator of the reaction outcome. After this time, the resulted mixture was concentrated *in vacuo* to remove most of ethanol, then was diluted with water and extracted with diethyl ether for three times. The orange organic layer was first washed with brine, made anhydrous over sodium sulphate and concentrated by rotary evaporator in order to give an orange crude residue. The crude material was purified by HPLC on a reverse phase silica gel column eluting with MeOH/H_2O 75:25 affording the pure thiazoavarone (**46**) which resulted in a satisfactory yield (46 %). The 1D NMR spectrum recorded firstly for the crude material, and then the mono- and bidimensional NMR experiments, mainly HSQC and HMBC, executed on the pure thiazoavarone (**46**) highlighted that the nucleophilic addition of hypotaurine was occurred and resulted to be completely regioselective. In fact, although avarone presents an unsymmetrical quinone moiety and thus the attack might take place on two different position, only one regioisomer was observed with respect to the results obtained by other synthetic derivatives [103-105].

The comparison of spectroscopic means between avarone (**45**) and the semisynthetic derivative (**46**) allowed immediately to observe in **46** the same decalin system of **45** and that the only differences were the lack in **46** of two protonic signals at δ_H 6.51 and 6.71 which clearly indicated the coupling of quinonic portion of avarone with hypotaurine to form the 1,1-dioxo-1,4-thiazine ring. Likewise, the additional heterocyclic nucleus was noticed by the analysis of ^1H and ^{13}C spectra which presented two deshielded methylene signals resonating as multiplets at δ_H 3.30 and 4.05 concerning to carbon resonances at δ_C 39.8 (C-3') and at δ_C 48.8 (C-2') owed to a nitrogen and sulfone-bearing carbons, respectively. The presence of heteroatoms was

further confirmed by mass spectroscopic infusion in positive mode of compound **46** which led to a molecular formula of $C_{23}H_{31}NO_4S$ (*m/z* $[M+Na]^+$ 440.1865, calcd. 440.1866). All ^1H and ^{13}C chemical shifts have been completely assigned (Table 6) as well as the coupling patterns noted by COSY, HSQC and HMBC experiments.

Table 6. ^{1}H (700 MHz) and ^{13}C (125 MHz) NMR data[a] of thiazoavarone (**46**) in $CDCl_3$.

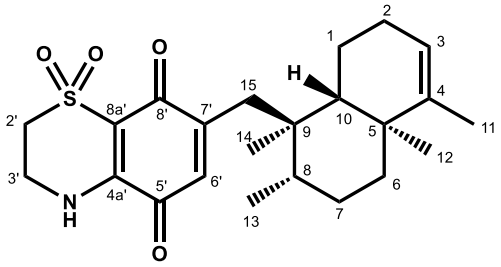

Pos.	δ_C	δ_H, mult. (*J* in Hz)	Pos.	δ_C	δ_H, mult. (*J* in Hz)
1'	-	-	**4**	143.7	-
2'	48.8	3.30, m	**5**	38.3	-
3'	39.8	4.05, m	**6**	35.8	1.03 [b], 1.64 [b]
4'	-	6.41, br s	**7**	27.3	1.38 [b]
4a'	143.2	-	**8**	37.1	1.25 [b]
5'	179.3	-	**9**	43.7	-
6'	131.8	6.50, s	**10**	47.5	1.03 [b]
7'	152.8	-	**11**	17.9	1.53, s
8'	177.1	-	**12**	20.0	0.99, s
8a'	111.6	-	**13**	16.7	0.96, d, (6.2)
1	19.3	1.50[b], 1.85, dd, (6.7, 13.2)	**14**	17.7	0.85, s
2	26.3	1.93 [b], 2.04 [b]	**15a**	35.6	2.50, d, (13.1)
3	120.9	5.2, br s	**15b**		2.70, d, (13.1)

[a] ^{1}H NMR and ^{13}C NMR shifts are referenced to $CDCl_3$ (δ_H = 7.26 ppm and δ_C = 77.0 ppm);
[b] Partially overlapped to other resonances

The univocally assignment of thiazinoquinone bicyclic system regiochemistry was indicated by key HMBC cross-peaks (Figure 16). Long-range correlations were observed for H-3' with C-2' and C-4a', for H-2' with C-3' and C-8a', for H-6' with C-4a', whereas the protons H-15a and H-15b correlated with the carbonyl group C-8'. The whole pattern of ^{1}H-^{13}C HMBC correlation had a key mean to indicate the relative position of side chain linked to the quinone ring with respect to the nitrogen atom of the thiazine portion, depicting a specific regiochemistry for **46**, as reported in Figure 16.

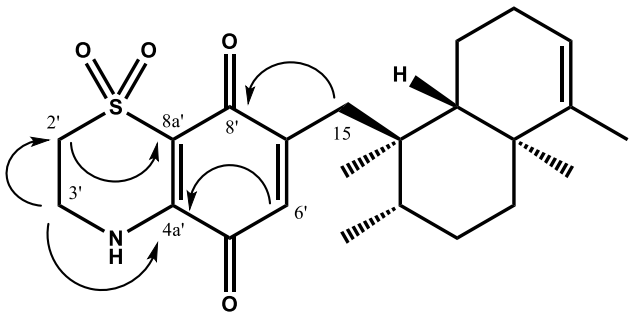

46

Figure 16. ^{1}H-^{13}C long range correlations (J^{2},J^{3}) recorded by HMBC spectrum in $CDCl_3$ of thiazoavarone (**46**).

2.3.3 Investigating the antiparasitic effects of avarone, avarol, and thiazoavarone

The compound **45-47** were tested against different strains of *P. falciparum* in order to determine their *in vitro* antiplasmodial activity at Department of Biomedical, Surgical and Dental Science of University of Milan. Particularly, the IC_{50} values were evaluated on chloroquine-sensitive (CQ-S) D10 and chloroquine-resistant (CQ-R) W2 strains of

malaria asexual parasite. Moreover, the effects on gametocytes stage V of the sexual parasite form were evaluated, too.

As showed in Table 7, the most potent compound of the series resulted to be thiazoavarone (**46**) with IC_{50} values in the range of nanomolar on both parasite strains. Interestingly, this semisynthetic derivative was more potent than the other synthetic compounds, including also the previously identified lead compound, on which my research work during the PhD has been focused [104].

Table 7. *In vitro* antimalarial activity against D10 (CQ-sensitive) and W2 (CQ-resistant) strains[a], and against gametocytes stage V of *P. falciparum (Pf)* from a 3D7 transgenic line.

Compounds	**D10** IC_{50} **(μM)**[b]	**W2** IC_{50} **(μM)**[b]	***Pf* Gametocytes Stage V** IC_{50} **(μM)**[b]
avarone (**45**)	2.74±0.51	2.09±0.52	15.53 ± 5.26
thiazoavarone (**46**)	0.38±0.15	0.21±0.03	15.01 ± 3.19
avarol (**47**)	0.96±0.24	1.10±0.15	9.30 ± 1.90
methylene blue	-	-	0.155 ± 0.05

[a]CQ has been used as positive control (D10 IC_{50} = 0.04 ± 0.01; W2 IC_{50} = 0.54 ± 0.28; not cytotoxic). [b]The results are the mean ± SD of IC_{50} of three independent experiments performed in duplicate.

The higher potency of thiazoavarone than the corresponding quinone avarone, lacking the thiazine moiety, confirmed once again the importance of this chemical scaffold in the development of new antimalarial leads. Unlike the results shown in chapter 3 and reference 104 where the 1,4-benzoquinone compounds were totally inactive when compared to the corresponding thiazinoquinone analogues, in this study

avarone is still active against both CQ-S and CQ-R strains of *P. falciparum*. Likewise, the hydroquinone compound avarol (**47**) exhibited a remarkable effect both on D10 and W2 strains and it was significant more potent as antimalarial than the oxidized form (**45**) showing also no-cross resistance with chloroquine.

Furthermore, the compounds **45**-**47** were tested on the *P. falciparum* sexual stage known as gametocytes stage V circulating in the bloodstream in order to assess in this way the potential effects on the malaria transmission blocking. The results reported in Table 7 evidenced that in this stage the tested compounds resulted much less potent than the asexual stage. Nonetheless, avarol (**47**) with an IC_{50} value of 9.30 μM was the most potent among the analysed compounds and proved as an interesting hit compound because its activity was comparable to that of OZ27, a drug into clinical development phase, which exhibited an IC_{50} of 6.4 μM [124].

The collaboration with University of Milan allowed to investigate also the antileishmanial activity realizing pharmacological assays against promastigote stage of *L. tropica* and *L. infatum* as well as against the clinically relevant form of this disease, *L. infantum* amastigotes. The obtained results (Table 8) provided points for some crucial remarks regarding the efficacy of compounds **45**-**47** in the eradication of cutaneous (*L. tropica*) and visceral (*L. infantum*) leishmaniasis. In detail, analogously to that verified for antimalarial effects, avarol (**47**) was the more active compound in the redox active couple avarone/avarol. In that case, the reduced form (**47**) resulted ~4-fold more potent than the oxidized form (IC_{50} 7.42 μM *vs* 28.21 μM). This result is not so surprising since a quite similar trend was already observed for a series of synthetic naphthohydroquinones which demonstrated themselves as better antileishmanial agents respect to the corresponding naphthoquinones [125].

Also the comparison avarone (**45**)/thiazoavarone (**46**) against *Leishmania* parasites showed a significant reduction of IC_{50} in thiazoavarone as result of the introduction of the heterocyclic ring, giving once again a meaningful emphasis to the role played by the thiazinoquinone scaffold. Summarizing, against the promastigote stage of both *Leishmania* parasites, avarol and thiazoavarone resulted to be effective in the range of micromolar and more potent than the natural sesquiterpene quinone avarone.

Table 8. Pharmacological results of the activity of compounds **45**-**47** against promastigote stage of *L. tropica* and *L. infantum*, and against amastigote stage of *L. infantum.*

Compounds	***L. tropica*** **promastigotes IC_{50} (μM)[a]**	***L. infantum***	
		promastigotes IC_{50} (μM)[a]	**amastigotes IC_{50} (μM)[b]**
avarone (**45**)	20.28 ± 3.56	28.21 ± 0.32	7.64
thiazoavarone (**46**)	9.52 ± 0.32	8.78 ± 0.26	4.99
avarol (**47**)	7.08 ± 1.91	7.42 ± 0.27	3.19
amphotericin B[c]	0.17 ± 0.04	0.20 ± 0.03	0.189

[a] Data are expressed as mean ± SD of three different experiments performed in duplicate; [b] Data are the mean of two different experiments in triplicate; [c] Amphotericin B was used as positive control;

The overview on the antileishmanial properties was completed by the evaluation of the effects on the amastigote stage of *L. infatum* (Table 8). Today, great efforts are made to fight this developmental stage of *Leishmania* stage since it is the main responsible of the most dangerous form of this infectious disease. In fact, amastigotes hit visceral organs and provoke death in most of the case if not promptly treated. Interestingly, all

tested compounds were from 2- to 4-fold more active on amastigotes than promastigotes.

To go further into the potential usefulness of these sesquiterpene compounds as antiplasmodial and/or antileishmanial agents, the viability effects on mammalian cells like HMEC-1 and THP-1 cell lines were evaluated; moreover, for each compound the selectivity index (SI) was also calculated, it achieved as ratio between IC_{50} on HMEC-1 cells and IC_{50} on parasite strains (Table 9).

Table 9. Effects of the compounds **45**-**47** on the viability of mammalian cells (HMEC-1 and THP-1), and related SI.

Compounds	**HMEC-1 IC_{50} (µM)[a]**	**THP-1 IC_{50} (µM)[b]**	**Selectivity index (SI)[c]**				
			SI_{D10}[c]	SI_{W2}[c]	SI_T[d]	SI_I[e]	SI_A[f]
avarone (**45**)	62.19 ± 1.98	>100	22.7	29.8	3.1	2.2	8.1
thiazoavarone (**46**)	3.31 ± 1.53	7.41	8.7	15.8	0.35	0.38	0.67
avarol (**47**)	36.85 ± 5.79	31.75	38.4	33.5	5.2	5.0	11.6

[a] Data are expressed as mean ± SD of three different experiments performed in duplicate.; [b] Data are the mean of two different experiments in duplicate; [c] SI= IC_{50} HMEC-1/ IC_{50} *P. falciparum* strains; [d] SI_T = IC_{50} HMEC-1 / IC_{50} *L. tropica* promastigotes; [e] SI_I= IC_{50} HMEC-1 / IC_{50} *L. infantum* promastigotes; [f] SI_A= IC_{50} HMEC-1 / IC_{50} *L. infantum* amastigotes;

Thiazoavarone (**46**) revealed the most cytotoxic compound in the series with IC_{50} values in the micromolar range (3.31 µM on HMEC-1 *vs* 7.41 µM on THP-1) and, consequently, displayed a very low SI as antiplasmodial and also as antileishmanial agent. The two marine sesquiterpenes, instead, showed greater values of IC_{50} than the semisynthetic thiazinoquinone on both tested cell lines. In particular, avarol (**47**)

exhibited moderate cytotoxic effects, whereas the corresponding oxidized form (**45**) had a low toxicity on the two treated cellular lines. In spite of the moderate toxicity, the hydroquinone compound (**47**) showed a better selectivity index than the other two compounds on all tested parasite stage with respect to HMEC-1 line cell (Table 9). Thus, considering the good IC_{50} values offered by this natural sesquiterpenoid hydroquinone against all tested strains of *P. falciparum*, *L. tropica* and *L. infantum*, the displayed SI greater than 10 allowed to consider avarol (**47**) as a really interesting compound to be further explored in efficacy and selectivity [126].

The couple of natural marine metabolites (**45** and **47**) and the semisynthetic derivative (**46**) have been investigated also for their effects on multicellular parasite. The series of compounds was indeed tested against larval and adult stage of the aetiological agent of schistosomiasis, the fluke *S. mansoni*, as well as for the ability to impair the eggs production. An organism-based approach relying on ATP quantitation in schistosomula was used to perform the *in vitro* assay. When tested against schistosomula, the thiazinoquinone derivative (**46**) demonstrated the most effective with LC_{50} (the concentration of the compound that kills 50% of the test animals during the observation) in the micromolar concentration range (5.90 μM) with respect to avarone and avarol, despite avarol was slightly more active than avarone (Table 10). In this developmental stage of *S. mansoni*, the heterocyclic ring is crucial for the activity and this remark agrees with the obtained results for synthetic thiazinoquinones tested for their schistosomicidal potential as well as for the antiplasmodial effects above-mentioned [104,105] (see Chapter 3). As for the synthesised chemical library of thiazinoquinones with various alkyl side chain, the absence of 1,1-dioxo-1,4-thiazine ring produced compound completely ineffective, hence the thiazinoquinone scaffold

confirmed itself as an active chemotype for development of new agents against *P. falciparum* and larval stage of *S. mansoni* [104, 105].

Table 10. Effects of the compounds **45**-**47** against schistosomula, the larval stage of *S. mansoni*

Compounds	***S. mansoni*** **schistosomula** LC_{50} **(μM)**[a]
avarone (**45**)	42.77 ± 1.90
thiazoavarone (**46**)	5.90 ± 2.59
avarol (**47**)	33.97± 5.52

[a]Data are expressed as mean ± SD of three different experiments.

Subsequently, all compounds of this study were tested against adult worm pairs and the effects on the worm viability were observed at different concentration. The results have been expressed as percentage of adult worm death after 7 days treatment (Figure 17). At 50μM, all three compounds were very active since they led to parasite death. Instead, at lower concentration (20 μM), only avarol was able to induce at least 80% of parasite death after 7 days which is considered an enough good ability to impair worm viability. Once again avarone was the least active of the series, while thiazoavarone was poorly effective at 20 μM even though strong lethal on schistosomula. The different activity of thiazoavarone passing from larval to adult stage of *S. mansoni* might be ascribed to the presence in adult worm of a double lipid bilayer, known as tegument [127], which interfere with the compound uptake, and in this case might reduce the effective active concentration of thiazoavarone.

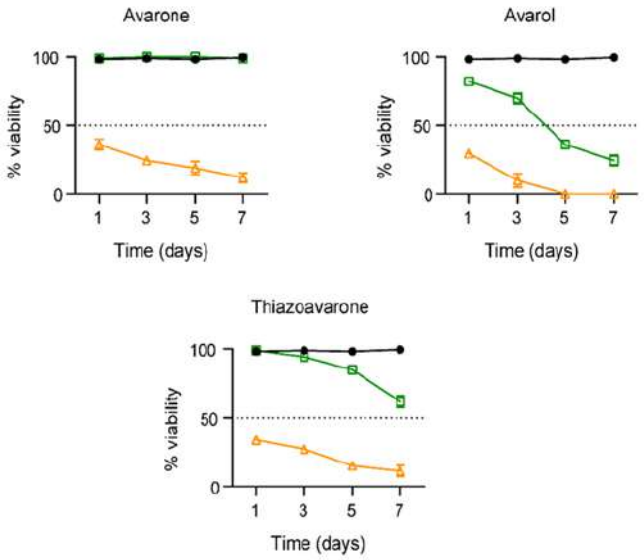

Figure 17. Evaluation of the effects on the *S. mansoni* adult worm viability of compounds **45**-**47**. Worm pairs were incubated with DMSO as vehicle (black circle) or with the indicated compounds at 50 µM (yellow triangle), 20 µM (green, square). After 7 days, the phenotype analysis was executed, and the results are the mean ± SEM of three independent experiments.

Finally, considering the role played by eggs in the maintenance of parasite life-cycle and into tissue damage in definitive host, the drug discovery of novel schistosomicidal agent require to take into account the production and the shape of eggs. For this reason, compounds **45**-**47** were assayed directly to the eggs laid *in vitro* by female worms and microscopic images of the effects on eggs maturation and/or damage are showed in Figure 18. The score related to egg maturation and morphology was assigned according to modern staging system reported in literature [128].

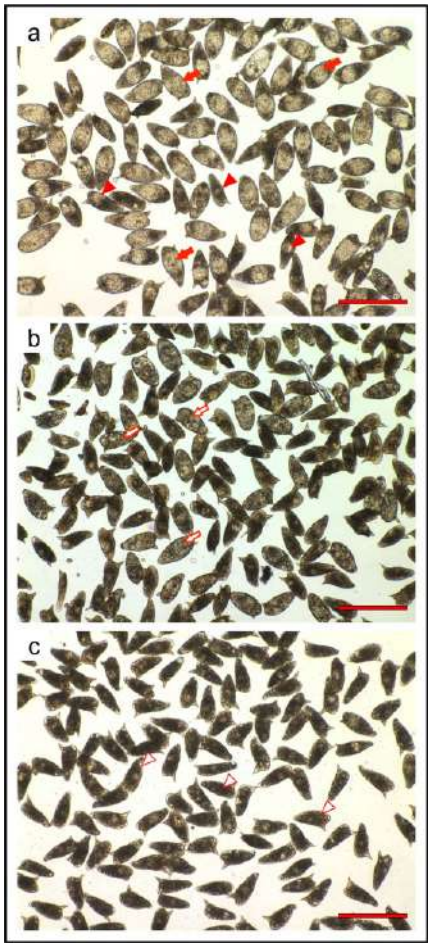

Figure 18. Representative images of thiazoavarone (**46**) effects on *in vitro*-laid eggs. (**a**) DMSO-treated eggs samples; (**b**) thiazoavarone-treated samples at 5 µM and (**c**) at 20 µM for 72 h. Filled red arrows indicate viable eggs at stages III-V; filled red triangle indicate viable eggs at stages I-II; red-edged arrows indicate damaged eggs at stages III-V; red-edged triangle indicates damaged eggs at stages I-II. Bar, 200 µm.

Regarding the influence on eggs production, thiazoavarone (**46**) was still one more time the most efficacious compounds. In Figure 18, the maturation stage of eggs is showed, and it can be noted that the thiazoavarone affected and impaired this stage at 5 µM, while at 20 µM provoked severe damages and the underdevelopment of eggs.

Similar effects were caused also by the natural metabolites, avarone (**45**) and avarol (**47**), but at a higher concentration (50 μM).

2.3.4 Conformational analysis and DFT calculations of avarone, thiazoavarone and avarol to rationalise SAR studies

To explore the putative mechanism of action of this interesting series of compounds against the different infectious parasites, as well as to rationalise the observed SARs, a conformational analysis and DFT calculations for compounds **45**-**47** have been performed by the research group of Prof. Caterina Fattorusso at Department of Pharmacy of University of Naples. First of all, for all compounds **45**-**47** have been generated the global minimum energy conformers (GM) through a systematic conformational analysis of all rotatable bonds. The obtained conformers have been subjected to an optimization of molecular mechanic (MM) geometry by the use of CFF force field and a distance dependent dielectric constant equal to 80 (Discovery Studio 2017, BIOVIA, San Diego, USA) [129]. Moreover, all the conformers showed an energy difference from the GM ≤ 3 kcal/mol.

The electron density analysis on the resulted conformers was performed by DFT calculation and the conductor-like polarizable continuum model (C-PCM) as solvation model was applied to mimic the aqueous environment [130]. Finally, the optimized conformers have been included into several families according to their torsion angles as reported in Tables 11-13.

Table 11. ΔE_{GM} values (kcal/mol) and torsion angle values (degrees) of the DFT conformers of avarone (**45**).

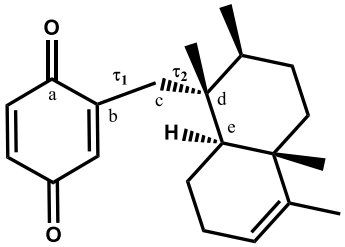

Conf.	ΔE_{GM} (kcal/mol)	Torsional Angles (°)	
		$\tau 1^a$	$\tau 2^b$
I	0.00	-91.95	64.65
II	0.01	101.16	60.62
III	1.20	-92.79	169.87
IV	1.25	96.73	-58.29
V	2.33	84.62	173.14
VI	2.64	-81.09	-54.96

[a]τ1 torsion angle is defined by a, b, c, and d atoms. [b]τ2 torsion angle is calculated considering b, c, d, and e atoms.

Table 12. ΔE_{GM} values (kcal/mol) and torsion angle values (degrees) of the DFT conformers of thiazoavarone (**46**).

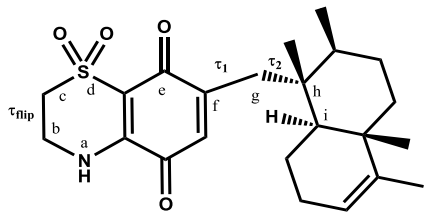

Conf.[a]	ΔE_{GM} (kcal/mol)	Torsional angles (°)	
		$\tau 1^b$	$\tau 2^c$
II	0.00	100.38	60.20
I	0.50	-110.21	55.83
IV	1.04	110.37	-72.73
III	1.25	-102.31	179.90
V	2.03	87.13	158.72
VI	3.02	-84.08	-54.03

[a]The value $\tau_{flip} \sim 60°$ led to the only reported conformational enantiomers. [b]τ1 torsion angle is defined by e, f, g, and h atoms. [c]τ2 torsion angle is calculated considering f, g, h, and i atoms.

Table 13. ΔE_{GM} values (kcal/mol) and torsion angle values (degrees) of the DFT conformers of avarol (**47**).

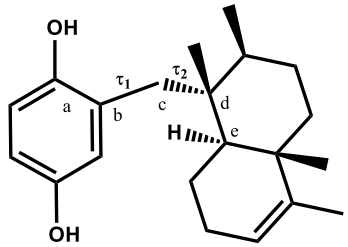

Conf.	ΔE_{GM} (kcal/mol)	Torsional Angles (°)	
		$\tau 1^a$	$\tau 2^b$
II	0.00	96.77	56.16
I	0.23	-104.40	59.80
III	1.45	-102.26	-179.87
IV	1.71	108.27	-69.84
V	2.12	89.20	179.85
VI	2.68	-86.45	-76.24

[a]τ1 torsion angle is defined by a, b, c, and d atoms. [b]τ2 torsion angle is calculated considering b, c, d, and e atoms.

The results carried out by the conformational analysis highlighted that the compounds **45**-**47** presented common features. In particular, the sesquiterpenoid moiety in all compounds has limited conformational freedom due to the electronic attraction between the hydrogen atoms of the methylene group of the side chain and the nearby quinone oxygen. Additionally, two specular sets of conformers with the same conformational energy, defined conformational enantiomers, have been obtained for thiazoavarone (**46**), due to two opposite flips of the thiazinoquinone ring with a specific torsional angle (τ_{flip}) ~ ± 60°. From Table 11-13, it is worth to observe as the torsional angle τ_1 may assume two possible values (~ ± 100°), and for each value, according to τ_2 values, only three possible orientation of the rigid sesquiterpene ring with respect to quinone/thiazinoquinone/quinol system (~+60°, ~-60°, ~180°) are accessible,

respectively. The overall results led to six possible conformers (named I-VI, Figure 19) for each compound (**45**-**47**).

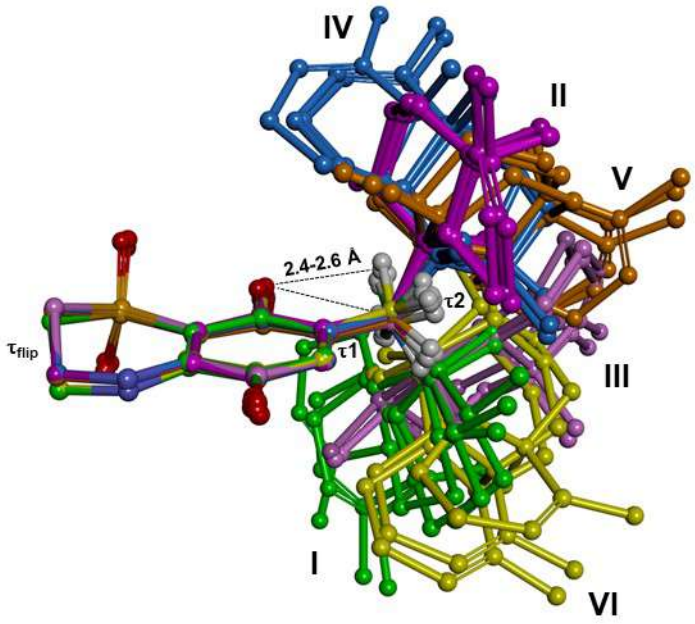

Figure 19. DFT conformers of compounds **45-47** superimposed by the carbon atoms of the quinone/hydroquinone ring. Carbon atoms are coloured according to conformer classification (I=green, II=magenta, III=pink, IV= light blue, V= orange, and VI=yellow); heteroatoms are coloured by atom type (H = white, O= red, N= blue, S= yellow). Hydrogens are omitted for sake of clarity, except for those of the first methylene group of the sesquiterpene moiety whose intramolecular distances from the close oxygen atom on the quinone ring are reported.

By the conformational analysis of the DFT optimized conformers, a certain rigidity of the sesquiterpene ring is suggested, and this evidence placed in a fixed position the methylene group of the sesquiterpenoid alkyl chain. In this way, since the putative mechanism of action concerns the formation of a toxic semiquinone radical species upon a one electron reduction/oxidation on the quinoid scaffold, the hydrogen atoms of this methylene group were at a suitable distance (≤ 3Å) from this oxygen-centered

radical, enabling the intramolecular radical shift from the oxygen to the side chain. Definitely, a putative carbon radical is so formed, and it is considered the toxic species for the parasites as it would be able to impair the parasite antioxidant defences [104,105].

To explore the redox properties of the tested compounds **45**-**47**, the two electrons/two protons quinone reduction pathway has been considered (Scheme 3) and, starting from the energetically favoured DFT minima I and II, all the species ($Q^{\bullet-}$, $QH^{\bullet}$, QH^-, QH_2) involved in this redox process have been generated.

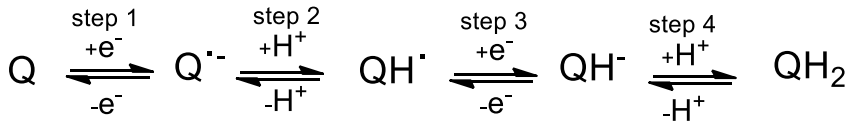

Scheme 3. Reduction pathway of quinone to hydroquinone in aqueous medium.

This computational investigation allowed to observe that although at first there are two quinone oxygen atoms that may be reduced/oxidized, and thus, two different semiquinones may be produced, only one reduction-site is more likely, and it depends from the localization of the highest occupied (HOMO) and the lowest unoccupied (LUMO) molecular orbital.

Indeed, in avarone (**45**) and thiazoavarone (**46**), the corresponding HOMO is located so as to make the quinone oxygen atom opposite to alkyl chain the most probable site for the reduction, whereas in avarol (**47**), the oxygen atom near to alkyl chain is indicated as the most feasible site to be oxidized according to the position of its LUMO

orbital (Figure 20). For the latter, it is remarkable to note that the oxidation of hydroquinone to quinone consists in an initial deprotonation step in a protic solvent (Scheme 3) and, by the pKa calculation, it was observed that the hydroxyl group nearby the sesquiterpene side chain is the first site to be deprotonated, further supporting the hypothesis of hydroquinone radical formation as described in Figure 20.

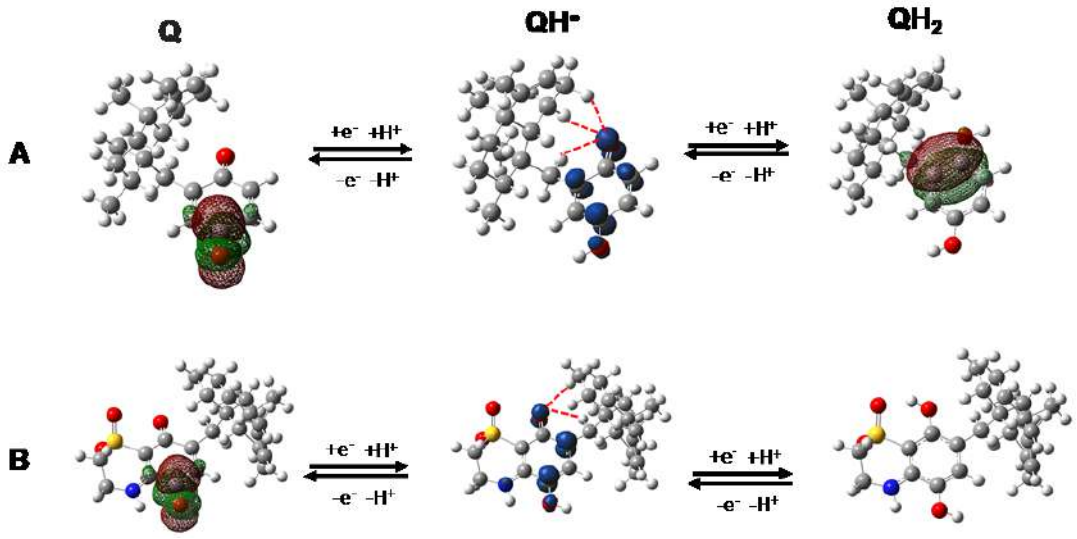

Figure 20. (**A**): DFT GM structures of avarone (Q), avarol (QH_2) and their semiquinone radical ($QH^{\bullet}$). (B) DFT GM structures of thiazoavarone (Q) together with its one- and two-electron reduced species $QH^{\bullet}$ and QH_2. Atoms possibly involved in an intramolecular radical shift are evidenced with red dashed lines. The LUMO of **45** and **46**, and the HOMO of **47** are visualized using GaussView with an isosurface value of 0.02 $e^-/a.u.^3$ The NBO spin density isosurface of the $QH^{\bullet}$ species is displayed using GaussView with an isosurface value of 0.01 $e^-/a.u.^3$. The blue surface (positive spin density) corresponds to an excess of α-electron density.

To further explore the propensity of avarone (**45**) and thiazoavarone (**46**) to be reduced by one-electron reduction and of deprotonated species (QH^-) of avarol (**47**) to

undergo a one-electron oxidation, the energy of lowest unoccupied molecular orbital (E_{LUMO}) and ionization potential (IP) were calculated, respectively. These parameters have been accompanied by the calculation of standard redox potential (E°), standard Gibbs free energy ($\Delta G°_{red,aq}$) of each electron-transfer reaction and standard Gibbs free energy for the protonation of reduced species ($\Delta G°_{H+}$) together with the energy of single occupied molecular orbital (E_{SOMO}) which indicates the tendency to delocalize unpaired electron, reporting the whole of data in Table 14 and 15.

Table 14. DFT calculated parameters and standard redox potentials (E°; Q/ $Q^{\bullet-}$) of compounds **45-47**.

Cmp.	Conf.	E_{LUMO}[a] (Q)	E_{SOMO}[a] ($Q^{\bullet-}$)	E_{SOMO}[a] ($QH^{\bullet}$)	$\Delta G°_{red,aq}$[a] (Q/ $Q^{\bullet-}$)	$E°$[b] (Q/ $Q^{\bullet-}$)	ΔG_{H+}[a] ($Q^{\bullet-}$/ $QH^{\bullet}$)
45/47	I	-10.62	-143.34	-106.45	-94.58	-328.57	-279.60
45/47	II	-10.68	-143.42	-106.60	-95.13	-304.65	-279.87
46	I	-17.76	-148.69	-158.60	-95.29	-297.63	-272.91
46	II	-17.83	-148.72	-159.93	-95.66	-281.68	-273.03

[a]kcal/mol. [b]mV.

Table 15. DFT calculated parameters and standard redox potentials (E°; $QH^{\bullet}/QH^{-}$) of compounds **45-47**.

Cmp.	Conf	$\Delta G°_{red,aq}$[a] ($QH^{\bullet}/QH^{-}$)	$E°$[b] ($QH^{\bullet}/QH^{-}$)	ΔG_{H+}[a] (QH^{-}/QH_2)	IP[a] (QH^{-})	E_{HOMO}[a] (QH_2)
45/47	I	-91.67	-454.64	-295.41	61.09	-158.06
45/47	II	-89.95	-529.31	-296.77	60.83	-156.34
46	I	-95.22	-300.60	-290.49	130.87	-158.18
46	II	-95.24	-299.70	-289.55	130.94	-159.27

[a]kcal/mol. [b]mV.

Accordingly, some crucial remarks can be done in agreement with the pharmacological results previously showed. Firstly, the comparison between the redox properties of the quinone avarone (**45**) and its semisynthetic derivative (**46**) showed as **46** has a major propensity to acquire one electron with respect to reactivity presented by avarone (**45**). The E_{LUMO} and $\Delta G°_{red,aq}$ values resulted lower in thiazoavarone than avarone, while E° was higher. At same way, thiazoavarone led to a more stable semiquinone radical species ($QH^{\bullet}$) than that obtained by reduction of avarone as proved by a lower E_{SOMO} value. This result agrees with the overall more potency of thiazoavarone than avarone confirming the key role exerted by the 1,1-dioxo-1,4-thiazine moiety on the electron affinity as one of main factors involved in the formation of the toxic semiquinone radical.

Nevertheless these considerations, the quinone derivative avarone (**45**) is still active against some developmental stages of tested parasites (i.e. D10 and W2 strains of *P. falciparum*, against gametocytes stage V, schistosomula and adult form of *S. mansoni* as well as on eggs production) contrarily to that happened for other synthetic quinones [104,105]. One possible reason for this ability might to be searched in the calculated semiquinone radical species (Figure 20) because, beyond the first methylene group, at least another hydrogen of the rigid sesquiterpene ring is placed at a distance ≤ 3Å such as to be subjected to intramolecular hydrogen radical shift. In line with this hypothesis, it can be explained also why thiazoavarone (**46**) results to be the most potent thiazinoquinone derivative yet prepared [104,105].

Some considerations can be proposed also to explain the better IC_{50} values showed by avarol (**47**) respect to that of the oxidized form (**45**). Avarol had a high propensity to be oxidized as demonstrated by the low values of E° and IP of the QH^- anion. On the

other hand, avarone didn't show appreciate values regarding the opposite reaction pathway. Thus, both compounds, avarone and avarol, were active against the different parasites but the hydroquinone metabolite resulted more potent than avarone and, at same time, avarol had the highest selectivity index respect the mammalian cells. The main reason might stay in the fact that both can generate the same semiquinone radical species, toxic for parasites, through the one-electron transfer reduction, and so both avarone and avarol resulted effective as antiparasitic agents. Additionally, the higher potency and selectivity of avarol into the redox active couple suggest that, in parasite cells, a bioactivation reaction partner binds preferentially the hydroquinone form rather than the oxidized form, while in human cells this bioactivation system seems to be not present.

The different activity could be influenced also by pharmacokinetic properties of compounds **45**-**47**, hence the distribution coefficient values (cLogD) of avarone, thiazoavarone and avarol have been calculated (Table 16, ACD/Percepta 2017).

Table 16. cLogD of compounds **45-47**.

Compound	**cLogD**[a]
avarone (**45**)	6.13
thiazoavarone (**46**)	3.83
avarol (**47**)	5.22

[a]cLogD calculated considering pH values: 7.4, 7.2 and 5.5.

According to Lipinski's rule for cell membrane drug diffusion, thiazoavarone (**46**) with a cLogD value of 3.83 confirmed its great active potential since this kind of cLogD

value is considered appropriate for passive diffusion. However, the lower effects of **46** against several developmental stages, for examples against gametocytes stage V, strains of *Leishmania* and adult worm pairs of *S. mansoni*, with respect to avarol (**47**) might depend on the better interaction of avarol with the large number of membrane transport proteins, since a cLogD>5 does not guarantee a good uptake by passive diffusion. It is worth to be mentioned that significant morphological changes occur in the parasite developmental stages and these may affect the absorption by passive diffusion impairing the efficacy of the tested compounds in comparison with what described also for schistosomicidal synthetic thiazinoquinones [105].

Conclusion: taking into account the whole results achieved by the chemical and pharmacological investigation of *D. avara*, the isolation of two known marine sesquiterpenoid compounds (**45** and **47**) was an interesting inspiration source to further investigate the biological potential of these metabolites. Additionally, the quinone moiety of avarone was used to prepare a novel thiazinoquinone derivative (**46**) through a feasible and cheap synthetic scheme. In spite of other synthetic thiazinoquinones, this procedure was completely regioselective leading to only one possible regioisomer even though avarone is an unsymmetrical quinone. Pharmacological analysis against *P. falciparum*, *S. mansoni*, *L. infantum*, *L. tropica* and on HMEC-1 and THP-1 as mammalian cells as well as computational studies of the compounds redox properties offered new points of discussion. Firstly, the heterocyclic system of **46** enhanced the effects on all parasite stages with respect to **45** lacking the 1,1-dioxo-1,4-thiazine moiety, confirming this scaffold as an active antiparasitic chemotype. Noteworthy, thiazoavarone (**46**) provided the most potent thiazinoquinone until now developed by us. As for the couple of marine metabolites, avarol resulted to be more potent than

avarone against overall infectious parasites while presented also the highest SI against mammalian cells.

To shed light on the putative mechanism of action of this series, several computational studies have been carried out. The results of computational investigation strongly support the hypothesis that the antiparasitic effects are related to the ability of compounds **45**-**47** to form a toxic semiquinone radical species by one-electron reaction and this radical could be formed starting both from quinone- and hydroquinone-based compounds. The effectiveness of **45-47** depends on also the plausible "through-space" intramolecular hydrogen radical shift thanks to suitable distances between the atoms of quinone oxygen and alkyl chain. In some developmental stages, the differences in the activity trend of compounds are mainly due to the morphological and/or metabolic changes in parasites affecting the cellular uptake of compounds. Thus, the selective toxicity against different parasite may be related to molecular pharmacokinetic properties as well as taking advantage of better affinity with bioactivation reaction partners.

2.3.5 Materials and methods of D. avara chemical investigation

*Isolation of **45** and **47**; synthesis of **46***

The fresh sample of *D. avara* was collected in the Bay of Izmir in Turkey (Narlidere, 38° 24' 45 N 27° 8' 18 E) and was immediately frozen at -25°C until the extraction. A voucher specimen is deposited at Mugla University, Turkey. The extraction of metabolic content was executed on the thawed and homogenized sponge using organic solvent, in particular MeOH (3 x 1 L) and, then, dichloromethane (3 x 1

L) affording a combined extract which was concentrated under pressure, while the sponge dry weight after extraction was 21.9 g. The procedure yielded an aqueous suspension that was partitioned against *n*-BuOH in a separating funnel. The collected butanol layer was subjected to solvent evaporation *in vacuo* and afford a brown oil (5.4 g). This material was firstly chromatographed on reversed phase (RP-18) silica gel flash chromatography with a gradient system water → methanol → chloroform, and then, the most interesting fraction further analysed. Indeed, the fractions eluted with MeOH/H_2O 8:2 (v/v) showed newsworthy properties when investigated by 1D NMR technique. According to this data, these fractions were investigated by HPLC on C-18 stationary phase (Luna 3 μm C-18, 150 × 3.00 mm, flow rate 0.5 mL/min) eluting with MeOH/H_2O 95:5 (v/v). Good results were achieved by this separation since were obtained avarol (**47**, 4.5 mg, t_R=5.4 min) and avarone (**45**, 26.8 mg, t_R=9.4 min) in pure state. These two metabolites were just elucidated as main constituent of *D. avara*, and thus, their structures were easily assigned by the comparison of their spectroscopic means with those reported in literature [89-91].

*Avarone (**45**):* yellow powder; $[\alpha]_D^{25}$= +2.6 (*c*= 0.0014, CH_3OH); HRESIMS: *m/z* 313.2156 $[M+H]^+$ (calcd. for $C_{21}H_{29}O_2$ *m/z* 313.2162); ^1H NMR in $CDCl_3$ and HRESIMS spectra are reported in Chapter 6.

*Avarol (**47**):* yellow powder; $[\alpha]_D^{25}$= +12.4 (*c*= 0.0018, CH_3OH); HRESIMS: *m/z* 315.2337 $[M+H]^+$ (calcd. for $C_{21}H_{31}O_2$ *m/z* 315.2319); ^1H NMR in $CDCl_3$ and HRESIMS spectra are reported in Chapter 6.

Taking advantage from the good availability of the natural product avarone, 20.3 mg of **45** (0.065 mmol) were used to prepare the thiazinoquinone derivative **46**. This quantity of **45** was dissolved in 12 mL of a mixture CH_3CN/EtOH 1:1 (v/v) and a water

solution of hypotaurine (7 mg, 0.065 mmol) was added dropwise alongside salcomine in portion as catalyst. The resulted mixture was kept under magnetic stirring for 48 h at rt, observing a color change from yellow to orange/red which indicated that the coupling was occurred. After this time, most of ethanol was removed *in vacuo* and the residue was poured in water before extracting the interesting product with diethyl ether (3 x 60 mL). The organic layer was first washed with brine, then dried over sodium sulfate, filtered and concentrated *in vacuo* by solvent removal. The resultant crude material was chromatographed by RP-18 HPLC (Luna, 3 μm C-18, 150 × 3.00 mm, flow rate 0.5 mL/min) affording the pure thiazoavarone (**46**, 46%, t_R=31.6 min, 11 mg).

*Thiazoavarone (**46**):* orange powder; $[\alpha]_D^{25}$= +19.2 (*c*= 0.0035, $CDCl_3$); ^1H and ^{13}C NMR data are described in Table 6. HRESIMS: *m/z* 440.1865 $[M+Na]^+$ (calcd. for $C_{23}H_{31}NO_4SNa$ *m/z* 440.1866); 1D and 2D NMR spectra along with mass spectrum are reported in Chapter 6.

Biological assays

P. falciparum growth assay: The CQ-S (D10) and the CQ-R (W2) strains of *Plasmodium* were maintained *in vitro* at 5% haematocrit medium (human type A-positive red blood cells) in RPMI 1640 (EuroClone, Celbio) supplemented with 1% AlbuMax (Invitrogen, Milan, Italy), 0.01% hypoxanthine, 20mM HEPES, and 2mM glutamine in an atmosphere constituted of 1% O_2, 5% CO_2, and 94% N_2, and at 37°C. Compounds were dissolved in DMSO, diluted with medium until <1% of DMSO, which is a nontoxic concentration to the parasite, and were placed in 96 well flat-bottom microplates. Asynchronous cultures (parasitemia of 1-1.5%; 1% final haematocrit) were aliquoted into the plates and incubated for 72 h at 37 °C. Finally, the parasite growth

was measured spectrophotometrically (OD_{650}) by observing the pLDH according to Makler's method [131].

Gametocytes cultivation: the transgenic *P. falciparum* 3D7 strain with 3D7elo1-pfs16-CBG99 expressing the *Pyrophorus plagiophthalamus* CBG99 luciferase under a gametocyte specific promoter was used in all the experiments. Gametocytes stage V were exposed to **45-47** after 11 days from NAG addition. Gametocytes stages were counted in Giemsa stained smears and the percentage of gametocytes stage V was higher than 80%.

Gametocyte compounds susceptibility assay: Compounds were incubated for 72 h at 37°C (under 1 % O_2, 5 % CO_2, 94 % N_2 atmosphere) in 96-well plate in complete medium after serial dilution. Gametocytes viability was measured by luciferase activity. Drug-treated gametocytes at 2% haematocrit were transferred to 96-well black microplates adding D-luciferin (1 mM in citrate buffer 0.1 M, 1:1 volume ratio at pH 5.5). Luminescence measurements were performed after 10 min with 500 ms integration time using a Sinergy 4 (Biotek) microplate reader and IC_{50} was extrapolated from the non-linear regression analysis of the concentration–response curve.

In vitro promastigote susceptibility assays: promastigote stage of *L. infantum* strain (MHOM/TN/80/IPT1) and *L. tropica* (MHOM/IT/2012/ISS3130) were cultured in Schneider's Drosophila medium with 10% heat-inactivated fetal calf serum (HyClone) at 24 °C. The medium was RPMI (EuroClone) supplemented with 10% heat-inactivated fetal calf serum (EuroClone), 20 mM Hepes, and 2 mM *L*-glutamine. To the IC_{50}, the MTT (3-[4.5-dimethylthiazol-2-yl]-2.5-diphenyltetrazolium bromide) assay was performed. Compounds were dissolved in DMSO, then the medium was added performing serial dilution and were placed in 96 wells round-bottom microplates.

Amphotericin B was used as positive control since it is a reference antileishmanial drug. 100 µL of the suspension of 5 x 10^6 parasites/mL were diluted in complete medium seeded into the plates, incubated for 72 hours at 24 °C. Then, 20 µL of MTT solution (5 mg/mL) were added into each well for 3 hours. After this time, plates were centrifuged and the resultant pellets was dissolved in 100 µL of lysing buffer consisting of 20% (w/v) of a solution of SDS (Sigma), 40% of *N*,*N*-dimethylformamide (Merck) in H_2O. The absorbance was measured spectrophotometrically at 550 and 650 nm. IC_{50} values are the mean of ± standard deviation of independent experiments performed in duplicate.

In vitro intracellular amastigote susceptibility assays: THP-1 cells were maintained in RPMI medium supplemented with 10% FBS (EuroClone), 50 µM 2-mercaptoethanol, 20 mM Hepes, 2 mM glutamine, at 37°C in 5% CO_2 and plated as 5x10^5 cells/mL in 16-chamber Lab-Tek culture slides (Nunc) with 0.1 µM phorbol myristate acetate (PMA, Sigma) for 48 h to have differentiation into macrophages. Then, cells were washed and infected with metacyclic *L. infantum* promastigotes in ratio of 1:10 (macrophage/promastigote) for 24 h before incubating with the tested compounds for 72 h. The percentage of infected macrophages in treated and non-treated cells was determined by light microscopy.

Cytotoxicity assays: HMEC-1 cell line was maintained in MCDB 131 medium (Invitrogen, Milan, Italy) supplemented with 10% fetal calf serum (HyClone, Celbio, Milan, Italy), 10 ng/ml of epidermal growth factor, 1 µg/mL of hydrocortisone, 2 mM glutamine and 20 mM Hepes buffer (EuroClone). HMEC-1 were plated at 10^5 cells/mL, while THP-1 at 5x10^5 cells/mL, in 96 wells flat bottom microplates. Monocytic cells were additionally treated with 0.1 µM PMA for 48h to achieve differentiation in

macrophages. Serial dilutions of **45-47** were realized and added to cell plates using MTT assay for cell proliferation evaluation conveying the results as IC_{50}.

In vitro effects on S. mansoni: see related section of 2.2.5 paragraph for experimental details regarding the viability effects on schistosomula and adult worm pairs as well as the impairing of eggs production.

Molecular modelling

Molecular modelling calculations were performed on E4 Server Twin 2 x Dual Xeon-5520, equipped with two nodes of Intel® Xeon® QuadCore E5520-2.26Ghz, 36 GB RAM. The graphics were carried out on Intel(R) Core (TM) i7-4790 processor and SGI Octane 2 workstations.

Conformational property analysis. ACD/Percepta software was used to calculate apparent pKa and clogD values of compounds **45-47** (Advanced Chemistry Development, Toronto, ON, Canada, 2017).

According to Henderson-Hasselbalch equation, compounds **45-47** were considered neutral in all calculations performed at pH 7.4 (blood pH value) and pH 7.2 (cytoplasm pH value). The compounds were built using the Small Molecule tool of Discovery Studio 2017 (Dassault Systèmes BIOVIA, San Diego) and subjected to molecular mechanic (MM) energy minimization ($\varepsilon = 80*r$) until the maximum RMS derivative was less than 0.001 kcal/Å, using Conjugate Gradient as minimization algorithm [132]. Conformational analysis was carried out on Search Small Molecule Conformations of Discovery Studio (2017) which was executed through a systematically varying of the rotatable bonds sp^3-sp^3 and sp^3-sp^2.The RMSD cut-off for structure selection was set to 0.01 Å and an energy threshold value of 10^6 kcal/mol was used as selection criteria. The generated structures were then subjected to MM energy minimization (CFF forcefield;

ε = 80*r) and the conformers within 5 kcal/mol from GM has been then subjected to DFT calculations using the Gaussian 09 package [133]. Partial charges, molecular orbitals and spin density have been calculated using the natural bond orbital (NBO) method grouping the resulting conformers into conformational families on the basis of dihedral angle values (i.e., τ1 and τ2) [134].

Calculation of redox properties. An appropriate way for calculating the redox potential of $Q^{\bullet -}$, $QH^{\bullet}$, QH^{-} and QH_2 states for each compound **45-47** is by using a thermodynamic cycle. Accordingly, the whole pattern of redox potentials was calculated by using the Born-Haber cycle (Scheme 4) and the equation system reported in literature [135-136].

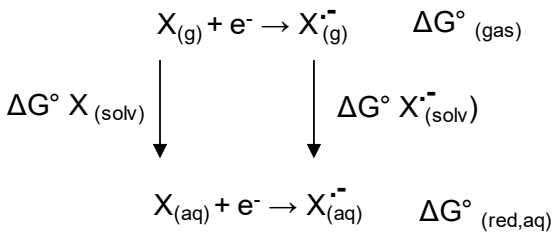

Scheme 4. Born-Haber cycle for a generic one-electron transfer reaction *in vacuo* and in aqueous solution.

CHAPTER 3

Synthesis of bioactive molecules inspired by marine substances

3.1 Marine chemical scaffold as lead for the drug design

The main disadvantage of the nature products chemistry is the isolation of few milligrams, often in the range of micrograms, of the pure compound that nowadays are enough for the planar structure elucidation but inadequate for a wide pharmacological screening. Accordingly, in the last century the natural products have been used not only as drugs but have also inspired the design and the synthesis of chemical libraries around natural product pharmacophores with the aim to identify new lead candidates more potent and selective than the natural derivatives.

Recently, the research group in which I attended my PhD have been involved in the isolation of a slightly cytotoxic and pro-apoptotic secondary metabolite, aplidinone A (**52**, Figure 21), from the Mediterranean ascidian *Aplidium conicum* [20, 137]. Its structure was characterized by an unusual 1,1-dioxo-1,4-thiazine ring for marine metabolites and the univocal structure elucidation was not completely allowed by the extensive NMR analysis. In fact, to define the structure of the heterocyclic ring, mainly regarding the relative position of nitrogen and sulphur in the ring, the NMR data was still uncertain. Computational studies of DFT were performed previously by others in the group on two theoretical models, A1 and A2 (**53** and **54**, Figure 21), to establish the regiochemistry of thiazinoquinone system in **52**, and the comparison of the experimental ^{13}C chemical shifts with those predicted allowed to assign the structure of aplidinone A as reported in Figure 21 [20]. Subsequently to further validate the structure of **52** made

by GIAO shielding calculations, a synthetic procedure was fine-tuned for A1 and A2, and thus the synthesis of these model compounds was performed [137].

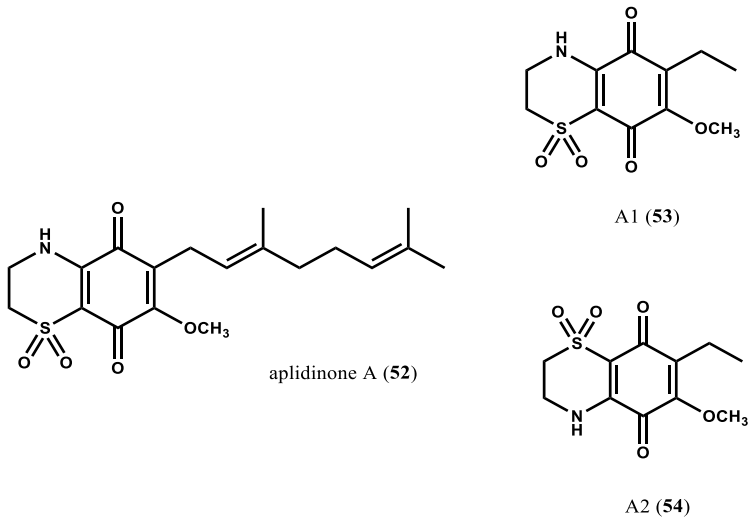

Figure 21. Structure of aplidinone A (**52**) and of two theoretical models A1 (**53**) and A2 (**54**).

On the other hand, a group of natural metabolites with a quinone structure was isolated from different marine invertebrates and, among them, some presented a thiazinoquinone bicyclic moiety. This group included xestoquinone (**55**), orlaquinone (**56**), ketoadociaquinones A and B (**57** and **58**) from *Xestospongia species* and thiaplakortones A-D (**59**-**62**) from *Plakortis lita* (Figure 22) [101, 138-139]. These metabolites resulted to be effective when tested against strains of *P. falciparum* and these studies demonstrated that the antiplasmodial activity was related to the possibility to undergo redox cycling, analogously to the naphthohydroquinone atovaquone, currently administrated in fixed-dose with proguanil (Malarone) [140]. In addition, the effects against *P. falciparum* were increased when a dioxothiazine ring was fused to the quinone moiety.

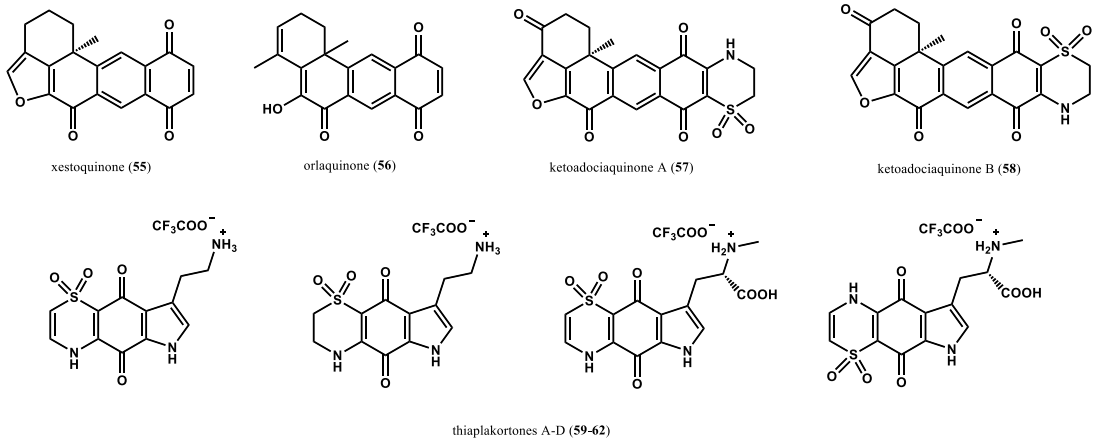

Figure 22. Natural antimalarial quinones (**55-62**) from marine invertebrates.

In the light of these considerations, the design and synthesis of a small chemical library of simplified analogues of compound **52** using the same synthetic procedure adopted for the achievement of the model compounds, A1 and A2, was performed. Definitely, the series of structurally related compounds was made available for an *in vitro* screening both of cytotoxicity and antiplasmodial effects [103,137].

Summarizing the obtained results, some of these synthetic compounds resulted to be active against D10 and W2 strains of *P. falciparum* exerted an IC_{50} values in the range of low micromolar concentration, while others were strongly cytotoxic and some derivatives showed a good selectivity index with respect to mammalian cells [103]. These preliminary studies highlighted some crucial structural requirements able to discern the antiplasmodial activity from the cytotoxicity: in particular, the regiochemistry of thiazinoquinone moiety influenced the antiplasmodial potency, while the length of alkyl chain linked at quinone ring moved the toxic effects from *Plasmodium* to human cells [103]. As for the effects on mammalian cells, the synthetic

derivatives inspired by aplidinone A (**52**) showed improved results with respect to the natural metabolite.

Thus, this kind of research clearly explains the potential of natural products as lead structure in medicinal chemistry campaigns, allowing to afford simplified analogues of natural compound with very often improved effects. For many aspects such as surely a better outcome, the synthetic analogues require less efforts to be obtained by chemical synthesis with respect to the natural metabolite.

Therefore, my attempts were focused on development of two different type of thiazinoquinone chemical libraries, built from same commercially available reagents and in few but efficient steps. The first synthesised series was aimed to investigate the role played by the nature and shape of side chain linked at quinone ring on the viability of *P. falciparum* and *S. mansoni* trying to shed light on the putative mechanism of action on parasites by computational means [104,105]. Instead, the second one was developed to broaden the knowledge regarding the antiproliferative effects of quinones and thiazinoquinones endowed with prenyl chains [141].

3.2 The role of thiazinoquinones in the fight of multiparasitism

The previous series of synthetic simplified thiazinoquinones inspired by aplidinone A (**52**) carried out a new antimalarial hit candidate (compound **54**, Figure 21) which showed an interesting antiplasmodial activity against both chloroquine sensitive and resistant strains of *P. falciparum* in the low micromolar concentration range (IC_{50} (D10)=2.45 μM; IC_{50} (W2)=2.37 μM) [103]. By combining computational and electrochemical studies, the efficacy of this compound was determined to be due to the

formation of a toxic semiquinone radical species which led to a stable adduct with Fe(III) of heme group impairing the *Plasmodium* antioxidant defences [137].

Taking into account the previous achievement, my objective has been to optimize the methoxy-thiazinoquinone scaffold in order to clarify the role of regiochemistry and nature of the alkyl side chain on the activity, and also to significantly improve the synthetic procedure with respect to that reported yet [137]. Moreover, the viability of different human line cells has been evaluated, too. Additionally, the demonstrated efficacy of several antimalarials as schistosomicidal agents encouraged the introduction of the methoxy-thiazinoquinones chemical library (Figure 23) also into a screening on viability of larval, juvenile and adult form of *S. mansoni* as well as on eggs production.

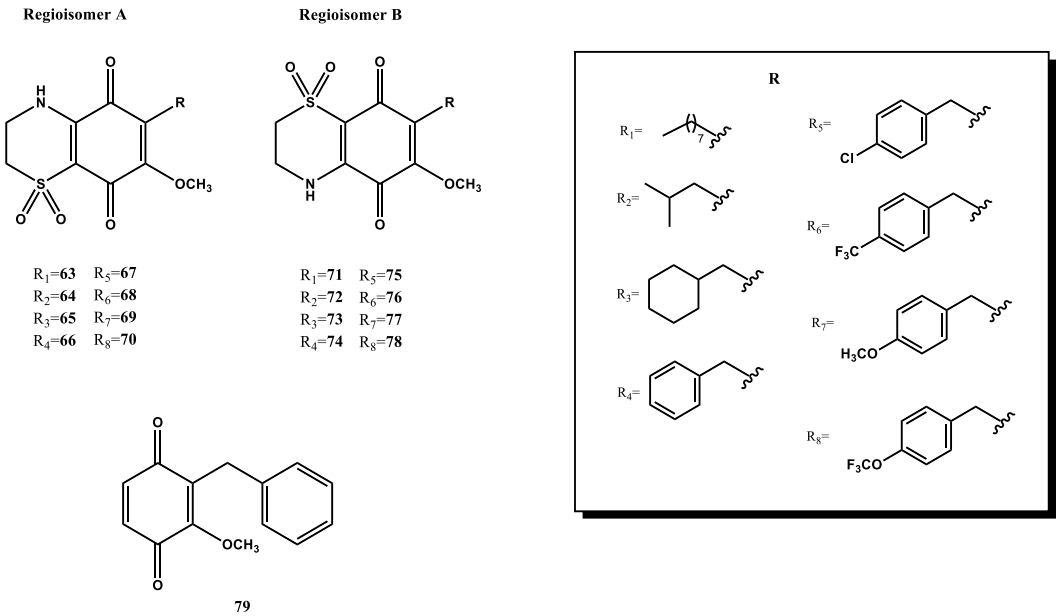

Figure 23. Synthetic chemical library of methoxy-thiazinoquinones (**63**-**79**) available for pharmacological screening.

This demanding and interdisciplinary work allowed to identify a new antimalarial lead candidate (compound **74**) with higher antiplasmodial potency and better SI than the starting hit (**54**); at once, electronic features of the heterocyclic ring together with steric properties of alkyl side-chain influenced the efficacy of several thiazinoquinones to act as multistage compounds affecting *S. mansoni* viability and eggs production.

The adopted synthetic procedure is based on commercially available reagents as starting material with the aim to reduce the costs of the whole synthesis since it is addressed to produce new effective and innovative leads for malaria and neglected diseases. Moreover, even though the procedure previously used for compounds **53**, **54**, **63** and **71** provided good yields for each step [137], the new methoxy-thiazinoquinones have been obtained with an improved procedure and optimized both for methoxy-thiazinoquinones with different alkyl side-chain and for those with a *p*-benzyl substituent on the quinone ring. Therefore, many efforts led to validate this efficient synthetic scheme which can be widened to a great variety of reactivity, enlarging the chemodiversity within the thiazinoquinone library.

3.2.1 Synthesis of compounds 64-70 and 72-79

The synthesis of compounds **64-65** and **72-73** starts from the 1,2,4-trimethoxybenzene (**80**) that it is subjected to alkylation reaction by treatment first with *n*-BuLi in THF as solvent and, then, with two different alkyl bromide (i.e. 1-bromo-2-methylpropane and bromomethylcyclohexane) to afford the 1,2,4-trimethoxy-3-alkylbenzenes **81-R_2** and **81-R_3**, respectively. Subsequently, each alkylbenzene was oxidized to the corresponding quinone by treatment with a dropwise addition of an aqueous solution of CAN with a large excess (molar ratio 4:1) of the latter, keeping the

resultant mixture at 0°C for 45 minutes. The oxidization afforded the quinones **82-R2** (65%) and **82-R3** (74%) with the process outcome clearly enhanced with respect to that already described [137]. At this point, a portion of each quinone was subjected to a coupling with hypotaurine. This reaction is based on a biomimetic addition of hypotaurine which allows the cyclization of the quinone ring to thiazinoquinone and requires the use of salcomine as catalyst. The nucleophilic addition of hypotaurine to unsymmetrical benzoquinone afforded two different regioisomers, named RA and RB, and thus from the quinone **82-R2** a mixture of **64** and **72** as well as from **82-R3** a mixture of **65** and **73** were obtained, respectively (Scheme 5).

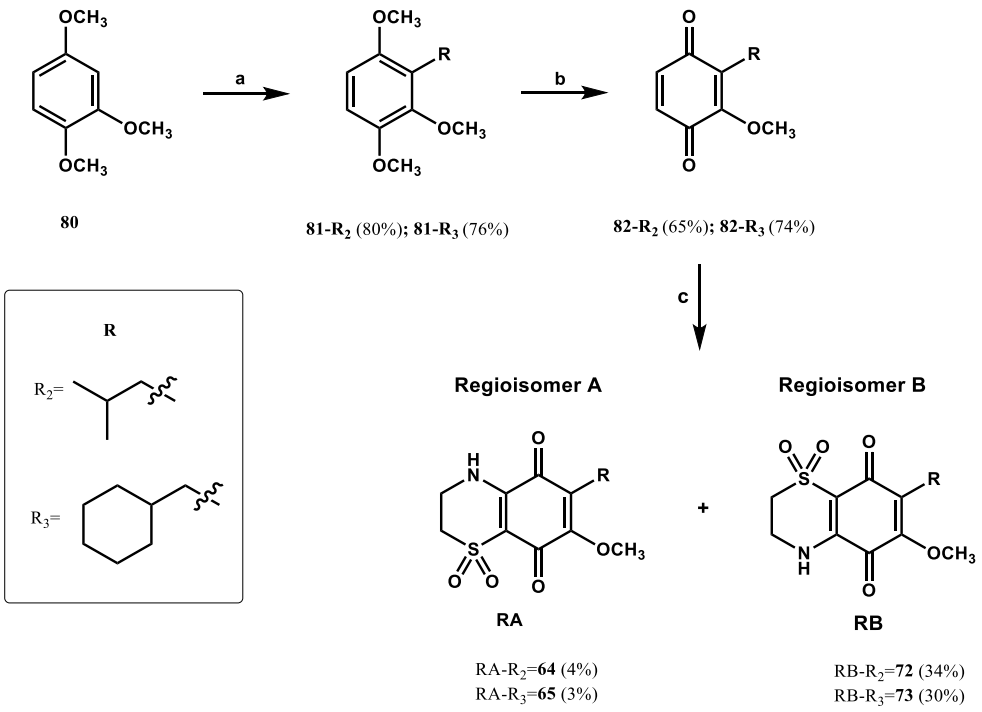

Scheme 5. Reagents and conditions: (**a**) (1) *n*-BuLi, THF, 0°C, 1h; (2) **81-R2**: 1-bromo-2-methylpropane, 0°C→rt, overnight; **81-R3**: bromomethylcyclohexane, 0°C→rt, overnight. (**b**) CAN, CH_3CN, 0 °C, 45 min. (**c**) hypotaurine, CH_3CN /EtOH, salcomine, rt, 48 h.

As for the benzyl derivatives **66-70** and **74-78**, the above protocol was slightly modified as reported in Scheme 6. Indeed, the lithiated of 1,2,4-trimethoxybenzene was treated with a suitable benzyl aldehyde, synthesising different biaryl alcohols (**83-R$_4$-R$_8$**), and not with an appropriate benzyl bromide since in this case the yield would result lower. Subsequently, the procedure is grounded on a reduction step, firstly adding trifluoroacetic acid and then triethylsilane in dichloromethane keeping the mixture under magnetic stirring overnight at room temperature. This reaction consists in the formation of an intermediate carbocation and for this kind of compounds, the yield has been demonstrated to be very high [142-143]. At this point, the synthesis returned to the same procedures as described below; therefore, in turn the oxidation of the intermediates **84-R$_4$-R$_8$** was occurred and then the condensation with hypotaurine was performed. Also for these derivative, the coupling with hypotaurine furnished a mixture of two regioisomers RA and RB (**66**/**74** for **79-R$_4$**; **67**/**75** for **85-R$_5$**; **68**/**76** for **85-R$_6$**; **69**/**77** for **85-R$_7$**; **70**/**78** for **85-R$_8$**).

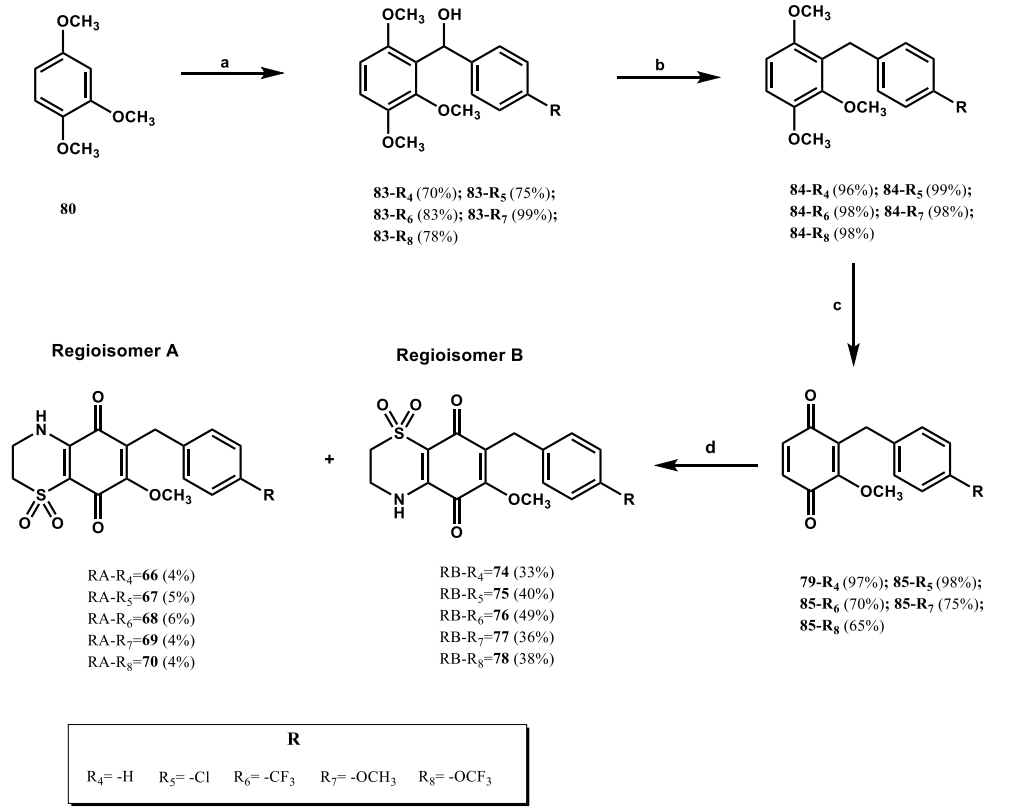

Scheme 6. Reagents and conditions: (**a**) (1) *n*-BuLi, THF, 0°C, 1h; (2) **83-R$_4$**: benzaldehyde, 0°C→rt, overnight; **83-R$_5$**: 4-chlorobenzaldehyde, 0°C→rt, overnight; **83-R$_6$**: 4-(trifluoromethyl)benzaldehyde, 0°C→rt, overnight; **83-R$_7$**: 4-methoxybenzaldehyde, 0°C→rt, overnight; **83-R$_8$**: 4 4-(trifluoromethoxy)benzaldehyde, 0°C→rt, overnight. (**b**) (1) TFA, CH_2Cl_2, rt, 10min; (2) TES, rt, 12h. (**c**) CAN, CH_3CN, 0°C, 45 min. (**d**) hypotaurine, CH_3CN /EtOH, salcomine, rt, 48h.

Despite this disadvantage, each mixture was easily separated into individual methoxy-thiazinoquinone by HPLC on silica gel, using hexane/EtOAc 6:4 (v/v) as mobile phase, and always a ratio of 9:1 in favour of RB was observed. Finally, all NMR resonances (δ_H and δ_C) were assigned by the analysis of mono- and bidimensional NMR experiments and reported in Tables 17-19; above all, the evaluation of key HMBC correlations and the comparison of NMR data with those of theoretical models A1/A2 allowed to univocally determine and distinguish the two regioisomers for each couple [20,137].

Table 17. ^{1}H (700 MHz) and ^{13}C (125 MHz) NMR data of compounds **64**-**65** and **72**-**73** in $CDCl_3$.

	64		**72**			**65**		**73**	
Pos	δ_C	δ_H, **mult. (*J* in Hz)**	δ_C	δ_H, **mult. (*J* in Hz)**	**Pos**	δ_C	δ_H, **mult. (*J* in Hz)**	δ_C	δ_H, **mult. (*J* in Hz)**
1	-	-	-	-	**1**	-	-	-	-
2	48.6	3.29, m	48.7	3.28, m	**2**	48.7	3.28, m	48.9	3.30, m
3	39.8	4.06, m	39.5	4.06, m	**3**	39.7	4.05, m	39.8	4.04, m
4	-	-	-	-	**4**	-	-	-	-
4a'	144.2	-	142.8	-	**4a**	144.6	-	142.5	-
5	179.5	-	176.5	-	**5**	180.4	-	176.5	-
6	127.7	-	152.9	-	**6**	126.7	-	153.5	-
7	157.6	-	138.8	-	**7**	158.6	-	137.8	-
8	174.1	-	178.1	-	**8**	173.2	-	179.0	-
8a'	109.1	-	110.2	-	**8a**	109.5	-	110.5	-
9	62.2	4.23, s	60.6	3.91, s	**9**	62.3	4.22, s	60.8	3.91, s
1'	34.9	2.28, d (7.3)	34.8	2.38, d (7.3)	**1'**	30.4	2.29, d (7.2)	31.4	2.40, d (7.1)
2'	28.1	1.75, m	28.3	1.87, m	**2'**	37.7	1.39, m	38.1	1.55, m
3'	22.6	0.86, d (6.7)	22.5	0.89, d (7.5)	**3'-7'**	33.2	1.56-0.92, m	33.4	1.53-0.95, m
4'	22.6	0.86, d (6.7)	22.5	0.89, d (7.5)	**4'-6'**	26.0	1.66-1.14, m	26.2	1.66-1.16, m
NH	-	6.71, brs	-	6.74, brs	**5'**	26.1	1.60, m	26.7	1.60, m
					NH	-	6.74, brs	-	6.43, brs

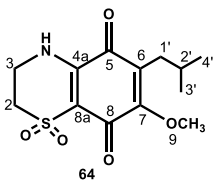

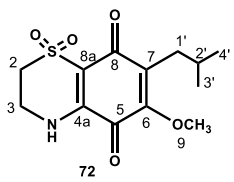

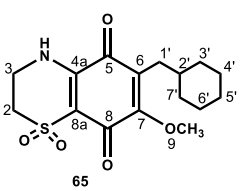

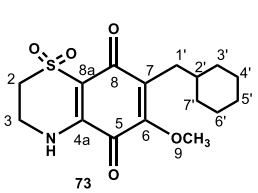

Table 18. ^{1}H (700 MHz) and ^{13}C (125 MHz) NMR data of compounds **66-70** in $CDCl_3$.

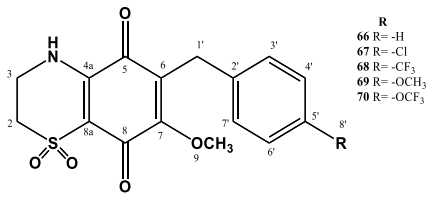

	66		**67**		**68**		**69**		**70**	
Pos	δ_C	δ_H, **mult. (*J* in Hz)**	δ_C	δ_H, **mult. (*J* in Hz)**	δ_C	δ_H, **mult. (*J* in Hz)**	δ_C	δ_H, **mult. (*J* in Hz)**	δ_C	δ_H, **mult. (*J* in Hz)**
1	-	-	-	-	-	-	-	-	-	-
2	48.3	3.24, m	48.2	3.24, m	49.0	3.23, m	48.2	3.24, m	48.3	3.24, m
3	40.0	4.02, m	40.1	4.02, m	40.4	4.03, m	40.1	4.02, m	40.0	4.02, m
4	-	-	-	-	-	-	-	-	-	-
4a'	144.3	-	144.2	-	142.5	-	142.8	-	144.3	-
5	179.2	-	179.1	-	176.2	-	179.3	-	178.2	-
6	127.0	-	127.2	-	152.8	-	127.0	-	135.8	-
7	157.5	-	157.3	-	136.1	-	157.5	-	152.5	-
8	17..1	-	173.0	-	178.0	-	173.1	-	175.1	-
8a'	109.5	-	109.1	-	110.4	-	109.2	-	109.2	-
9	63.3	4.29, s	63.2	4.29, s	62.1	3.92, s	63.3	4.29, s	61.1	4.29, s
1'	28.5	3.71, s	28.6	3.71, s	29.8	3.85, s	28.7	3.71, s	28.6	3.77, s
2'	138.9	-	137.8	-	137.8	-	129.6	-	135.0	-
3'-7'	128.8	7.19, d (7.3)	126.8	7.19, d (8.3)	126.4	7.49, d (8.3)	130.2	7.19, d (8.3)	127.8	7.30, d (8.3)
4'-6'	128.8	7.24, t (7.3)	127.6	7.24, d (8.3)	127.3	7.42, d (8.3)	113.8	6.75, d (8.3)	120.7	7.02, d (8.3)
5'	126.8	7.17, t (7.3)	133.2	-	133.1	-	158.2	-	147.9	-
8'	-	-	-	-	124.2	-	55.3	3.73, s	142.2	-
NH	-	6.74, brs	-	6.74, brs	-	6.48, brs	-	6.74, brs	-	6.80, brs

Table 19. ^{1}H (700 MHz) and ^{13}C (125 MHz) NMR data of compounds **74-78** in $CDCl_3$.

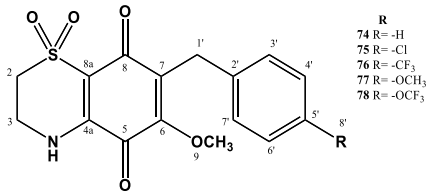

	74		**75**		**76**		**77**		**78**	
Pos	δ_C	δ_H, **mult. (*J* in Hz)**	δ_C	δ_H, **mult. (*J* in Hz)**	δ_C	δ_H, **mult. (*J* in Hz)**	δ_C	δ_H, **mult. (*J* in Hz)**	δ_C	δ_H, **mult. (*J* in Hz)**
1	-	-	-	-	-	-	-	-	-	-
2	49.3	3.24, m	48.2	3.24, m	48.8	3.23, m	48.3	3.24, m	48.8	3.27, m
3	40.6	3.99, m	40.1	4.02, m	40.1	4.03, m	40.0	4.02, m	39.9	4.03, m
4	-	-	-	-	-	-	-	-	-	-
4a'	142.6	-	142.8	-	143.0	-	144.3	-	142.6	-
5	176.1	-	179.3	-	177.0	-	178.2	-	176.9	-
6	152.9	-	127.0	-	152.7	-	135.8	-	152.9	-
7	136.0	-	157.5	-	136.2	-	152.5	-	136.5	-
8	178.1	-	173.1	-	178.1	-	175.1	-	177.9	-
8a'	110.5	-	109.2	-	110.1	-	109.2	-	110.1	-
9	62.0	3.87, s	63.3	3.90, s	60.9	3.92, s	61.1	3.89, s	60.8	3.94, s
1'	29.8	3.80, s	28.7	3.78, s	29.2	3.85, s	28.6	3.89, s	28.5	3.94, s
2'	138.1	-	129.6	-	129.6	-	135.0	-	134.9	-
3'-7'	130.0	7.28, d (7.3)	130.2	7.19, d (7.3)	130.5	7.49, d (7.3)	127.8	7.25, d (7.3)	130.7	7.32, d (7.3)
4'-6'	129.0	7.22, t (7.3)	113.8	7.16, d (7.3)	113.9	7.42, d (7.3)	120.7	6.76, d (7.3)	121.1	7.04, d (7.3)
5'	127.2	7.15, t (7.3)	158.2	-	158.2	-	147.9	-	147.8	-
8'	-	-	-	-	124.1	-	55.4	3.75, s	142.6	-
NH	-	6.45, brs	-	6.74, brs	-	6.48, brs	-	6.46, brs	-	6.47, brs

3.2.2 In vitro antiplasmodial activity and toxicity against human cells

The whole series of thiazinoquinones has been tested against chloroquine sensitive (D10) and resistant (W2) strains of *P. falciparum* in order to further investigate the propensity of this scaffold to impair *Plasmodium* viability and improve the results previously achieved, trying to lower the IC_{50} value < 1μM with respect to the hit candidate **54**. Additionally, the viability on two different mammalian cell lines, HMEC-1 and NIH-3T3, have been evaluated, too.

Interestingly, pharmacological assays performed at University of Milan corroborated the completely inactivity of the scaffold with regiochemistry A against *P. falciparum,* in fact, all synthesised RA (**64**-**70**) showed IC_{50} >10 μM that it is considered the cut-off for antiplasmodial activity. As for RB, compounds in which the nitrogen is at same side of methoxyl group, all thiazinoquinones were active in the range of micromolar concentration, but compound **74** resulted to be the most active thiazinoquinone synthesised up to now. As showed in Table 20, the presence of a benzyl group linked at quinone as side chain remarkably increased the antiplasmodial effects, and thus it was possible to identify a new lead candidate, compound **74**, which showed IC_{50} on both D10 and W2 strains in the range of sub-micromolar concentration. At same time, compound **74** did not exhibit a strong cytotoxicity on the tested mammalian cells and so was characterized by a good selectivity index that in each case was >25.

Regarding the series of *para*-benzyl substituted methoxy-thiazinoquinones (**75**-**78**), despite the electronic differences between *p*-OCH_3 and *p*-OCF_3 groups, it is worthy to be noted that the increase of thiazinoquinone potency, showed by **77** and **78** against *Plasmodium*, is verified when an oxygen atom is directly bonded to the aromatic ring with respect to compounds **75** and **76** (*p*-Cl *vs p*-CF_3). In addition, compound **78** with a

p-OCF_3 substituent, even though less active on chloroquine sensitive D10 (IC_{50}= 1.12 μM) compared to the lead candidate **74**, had effects on W2 strains in the same sub-micromolar range of compound **74** (Table 20). Instead, compound **77** in which a methoxy group is placed at *para* position on benzyl ring endowed with the same effects on D10 and W2 strains, while exhibited a better SI on HMEC-1 respect to compound **78**, and even it was not active on the second cell line tested (NIH-3T3, Table 20) since its IC_{50} resulted more than 100 μM. These effects on mammalian cells might be explained according to Lipinski's rule with which a distribution coefficient value (cLogD) >1 is required for drug passive diffusion [144], clarifying the influence of the size of alkyl substituent on human cell cytotoxicity (i.e. **54** *vs* **71** and **73**, see Table 23), too.

Table 20. *In vitro* antiplasmodial activity of the hit **54** and of compounds **71**-**78** together with the effects on mammalian cells and related SI.

Cmp.	D10 IC_{50} (μM)	W2 IC_{50} (μM)	HMEC-1 IC_{50} (μM)	NIH-3T3	SI[c]		SI[d]	
					D10	W2	D10	W2
54	2.45 ± 0.42	2.37 ± 0.42	NA	ND	-	-	-	-
71	0.82 ± 0.23	0.80 ± 0.36	5.52 ± 1.2	41.1 ± 8.9	6.7	6.9	50.1	51.4
72	1.26 ± 0.21	2.82 ± 0.81	28.6 ± 6.4	93.0 ± 6.9	21.2	9.4	73.8	32.9
73	2.37 ± 1.14	3.03 ± 1.14	3.9 ± 0.1	28.5 ± 3.4	1.6	1.3	12.0	9.4
74	0.60 ± 0.21	0.70 ± 0.22	17.6 ± 1.4	88.6 ± 7.7	29.3	25.2	147.7	126.5
75	1.63 ± 0.35	1.90 ± 1.05	8.51 ± 0.8	79.1 ± 9.3	5.2	4.5	48.5	41.6
76	5.06 ± 1.68	5.02 ± 1.81	20.4 ± 1.6	55.5 ± 2.7	4.0	4.1	11.0	11.1
77	1.21 ± 0.20	1.22 ± 0.24	17.9 ± 1.1	NA	14.8	14.7	-	-
78	1.12 ± 0.40	0.81 ± 0.19	3.59 ± 0.7	36.5 ± 5.4	3.2	4.4	32.6	45.0

[a]CQ as positive control: IC_{50} (D10)= 0.04 ± 0.01; IC_{50} (W2)= 0.54 ± 0.28; not cytotoxic. [b]Data are the mean ± SD of three different experiments in duplicate. [c]SI=IC_{50} on HMEC-1/IC_{50} *P. falciparum* strain. [d]SI=IC_{50} on NIH-3T3/IC_{50} *P. falciparum* strain.

Analogously, the presence of a chlorine or a trifluomethoxy- group (**75** and **78**) on the aromatic ring produced lipophilic derivatives (cLogD= 1.01 and 1.37, respectively) and reflected strong cytotoxic effects, whereas compound **77** with a cLogD of 0.33 (ACD/Percepta 2017) was the most polar thiazinoquinone in the series of benzyl derivatives exhibiting the worst ability to cross the lipidic membrane of HMEC-1 and especially of NIH-3T3. This assumption was not verified for the antiplasmodial effects because any correlation was observed between IC_{50} values on parasites and those on mammalian cells for these tested thiazinoquinones. Thus, the whole data corroborated the hypothesis that the entrance in parasite cells is due to membrane transport proteins expressed by *Plasmodium* though active transport processes in agreement with what approved for most of antimalarial agents [145-146].

The possibility of the semiquinone radical species produced following a one-electron reduction to form a stable adduct with Fe(III)-heme was previously suggested by electrochemical and computational studies, being the main responsible of antimalarial effects [103]. To support this hypothesis, RBCs infected with *P. falciparum* were firstly pre-treated with an increasing dose of NAC, and then, with the identified lead candidate **74**. NAC is known to be a note free radical scavenger, exerting an antioxidant function by the synthesis of GSH. Therefore, RBCs pre-treated with NAC are characterized by a greater quantity of GSH which avoids the free radicals accumulation and consequent cell damage. Accordingly, the potency of compound **74** was dose-dependent decreased by increasing doses of the antioxidant NAC (0.1 μM, IC_{50} (W2)= 0.7 ± 0.2; 1 μM, IC_{50} (W2)= 1.0 ± 0.2; 10 μM, IC_{50} (W2)= 1.3 ± 0.3). To investigate the effects on the sexual stage of *P. falciparum*, the lead candidate **74** was tested against gametocytes stage V, showing an IC_{50} of 13.8 ± 5.6 μM. Although

compound **74** did not exhibit a good transmission blocking potential, however it is an encouraging result comparing to other antimalarial drugs [124].

Finally, for this kind of methoxy-thiazinoquinones, the presence of the heterocyclic moiety is demonstrated to be crucial for the antiplasmodial activity since the quinone compound **79**, lacking the 1,1-dioxo-1,4-thiazine ring respect to the identified lead **74**, when included into pharmacological screening provided any effects against *Plasmodium* with respect to avarone (**45**) that resulted still active on the parasite.

3.2.3 Evaluation of schistosomicidal effects

The continuous search of antiparasitic agents able to act on more than one parasite in order to fight the dramatic effects related to co-infectious in the endemic countries, and the need of develop new antischistosomal therapeutic alternatives, given the evidences of praziquantel-resistant strains [52,53], led us to explore the pharmacological potential of the synthesised chemical library of methoxy-thiazinoquinones against *S. mansoni*. The main aim was to discover novel multistage compounds, i.e. compounds endowed with significant toxic effects on different developmental stage of the multicellular parasite. Accordingly, the whole library (**63-79**) was first tested on the larval stage of *S. mansoni*, named schistosomula, and then a selected set of active compounds was evaluated for their effects on the viability of juvenile and adult worms form as well as for the ability to impair eggs production and/or to provoke eggs damage. The *in vitro* assay on schistosomula was based on ATP quantitation in culture cells since ATP is a good indicator of metabolic activity of the larval stage. As for the antiplasmodial activity, all regioisomers A (**63-70**, incubated at

50 μM) did not show effects in term of reduction of schistosomula viability as well as the quinone derivative **79**. In fact, only a weak reduction of viability was observed but, in each case, the schistosomula survival was greater than the screening threshold (50%). Regarding the tested RB (**54** and **71-78**), all of them, except for **54**, were highly effective when tested at 50 μM, and a dose-response curve ranging from 0.78 μM up to 100 μM was determined in order to visualize each LC_{50} (Table 21).

Table 21. *In vitro* activity against larval stage of *S. mansoni* expressed as LC_{50} and related 95% confidence interval (CI) of compounds **71-78**.

Compounds	R	LC_{50} (μM)	95% CI
71	$-(CH_2)_7CH_3$	10.30	8.93-11.84
72	$-CH_2CH(CH_3)_2$	14.71	13.45-16.14
73	$-CH_2C_6H_{11}$	4.14	3.40-5.06
74	$-CH_2C_6H_5$	9.86	8.42-11.51
75	$-CH_2C_6H_4$-*p*-Cl	9.99	8.64-11.46
76	$-CH_2C_6H_4$-*p*-CF_3	5.00	4.18-5.96
77	$-CH_2C_6H_4$-*p*-OCH_3	13.92	12.52-16.03
78	$-CH_2C_6H_4$-*p*-OCF_3	5.57	4.81-6.39

Then, the selected set of thiazinoquinones (**71-78**) was investigated on the adult form (7-8 weeks old) of *S. mansoni*. In particular, adult worms couples were separately treated with two different concentration (50 and 100 μM) of each active thiazinoquinone and the effects on viability were monitored at 7 days upon treatment. Daily monitoring of worm's phenotype such as plate-attachment, movement, colour, gut peristalsis and tegument damage was executed in order to assign a score from 3 (normal effects) up to

0 (severe effects) to survivor worms. The most effective thiazinoquinones were those able to exhibit a percentage of adult worms survival less than 20% at 5 or 7 days (Figure 24) and, thus compounds **72**, **73**, **77** and **78** were tested at 20 µM and only **73** at 10 µM, too.

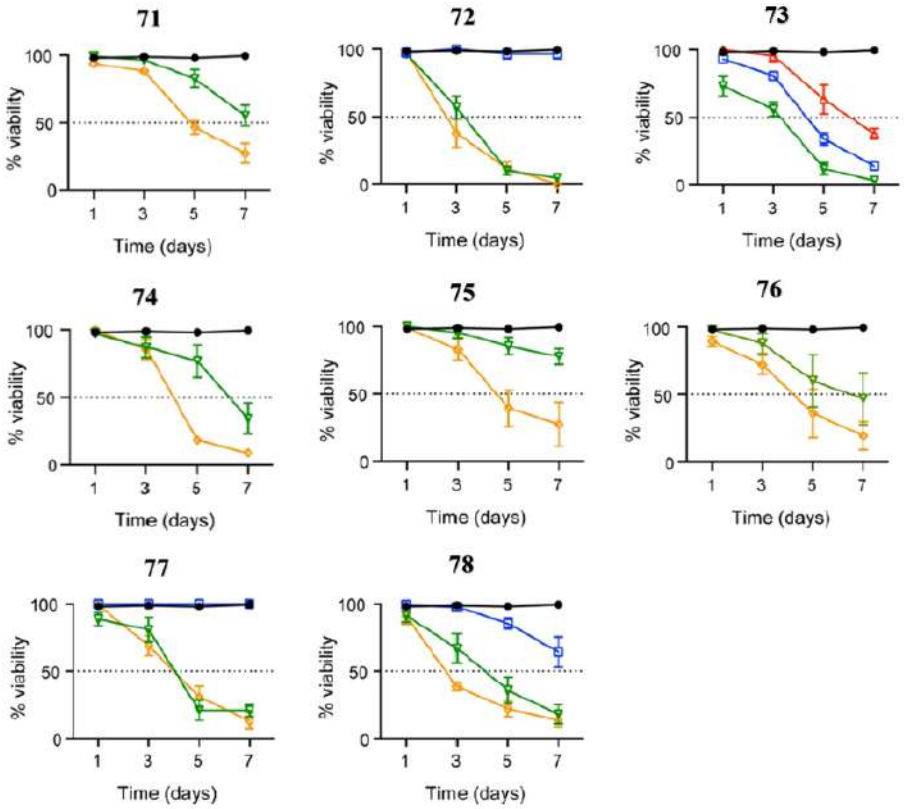

Figure 24. Effects of selected thiazinoquinones (**71**-**78**) on adult *S. mansoni* worm viability. Adult worm pairs were incubated with DMSO as vehicle (black, circle) or with compounds at 10 µM (red, triangle), 20 µM (blue, square), 50 µM (green, inverted triangle), and 100 µM (orange, diamond) monitoring the phenotypic alterations for 7 days. The % viability indicated on the y-axis is the mean ± SEM of three independent experiments.

The graphics reported instead in Figure 25 highlighted that the viability of adult worm pairs is time-dependent starting to be affected at least after 48h from treatment. Interesting effects were observed for **72**, **73** and **78** which caused complete death of the parasites at 100 and 50 μM. In addition, further investigations evidenced that compound **73** provoked parasite death when tested at 20 μM while compound **78** was the second one active at the same concentration even though it showed only a weak effect. Definitely, compound **73** resulted to be the only able to affect the adult worm viability also at 10 μM. Surprisingly, the satisfactory effects of **74** as antimalarial agent were not reflected on the adult worm pairs of *S. mansoni*.

In order to assess the multistage potential of above-mentioned compounds, the selected thiazinoquinones were additionally tested on the juvenile form (3-4 weeks old) of the neglected parasite and, as showed in figure 25, the results reflected what just described for the adult form. Indeed, compounds **72**, **73** and **78** continued to be the most effective and **73** was identified as the most potent methoxy-thiazinoquinone in the series since it induced complete worm death at 10 μM and was significantly active also at 5 μM.

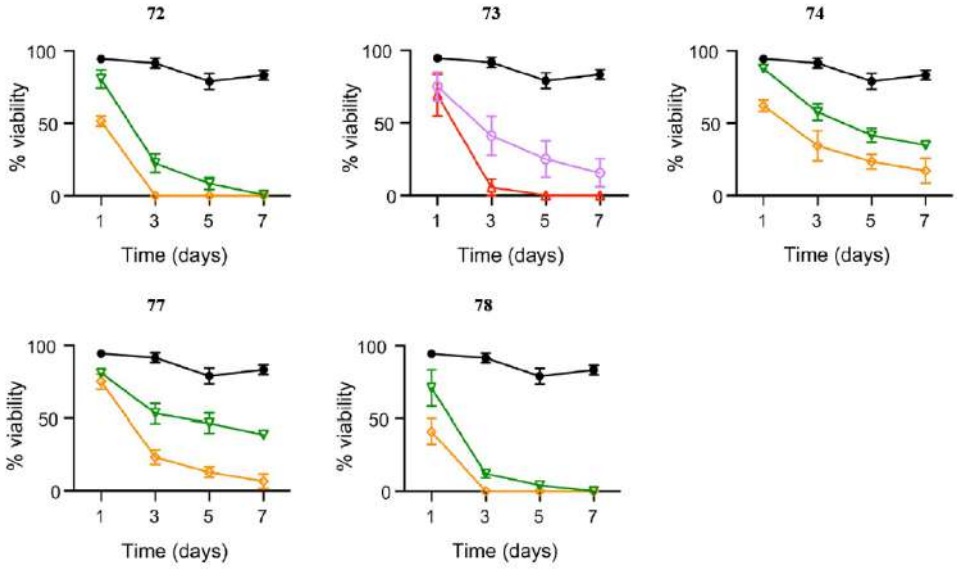

Figure 25. Effects of selected thiazinoquinones (**72**-**74** and **77**-**78**) on juvenile form of *S. mansoni*. Male worms were incubated with DMSO as vehicle (black, circle) or with compounds at 5 µM (violet, circle) 10 µM (red, triangle), 50 µM (green, inverted triangle), or 100 µM (orange, diamond) monitoring the phenotypic alterations for 7 days. The % viability indicated on the y-axis is the mean ± SEM of three independent experiments.

The high impact of eggs in the schistosomiasis transmission as well as in the tissue damages required to investigate the effects of the selected thiazinoquinones **72**-**74** and **77**-**78** on eggs-laying *in vitro*. The first assay was performed incubating eggs laid with a sub-lethal dose of the thiazinoquinones for 72 h in order to observe the interference on the global eggs count. No variations in the eggs count were highlighted but the eggs laid resulted dark and widespread damaged as showed by transmission electron microscopy images of compound **74**-treated samples (Figure 26). In these eggs, an increasing number of vacuoles and myelin bodies was observed alongside to an intense loss of internal structures in vitelline cells. Moreover, carmine red staining and confocal

microscopy analysis were performed to shed light on the male and female damaged systems into eggs according to Guidi *et al.* staging system approved [78]. A percentage ranging from 80-90% of eggs was arrested in stage I/II of maturation and all tested compounds (**72-74**, **77-78**) caused serious eggs damages at 5-10 μM.

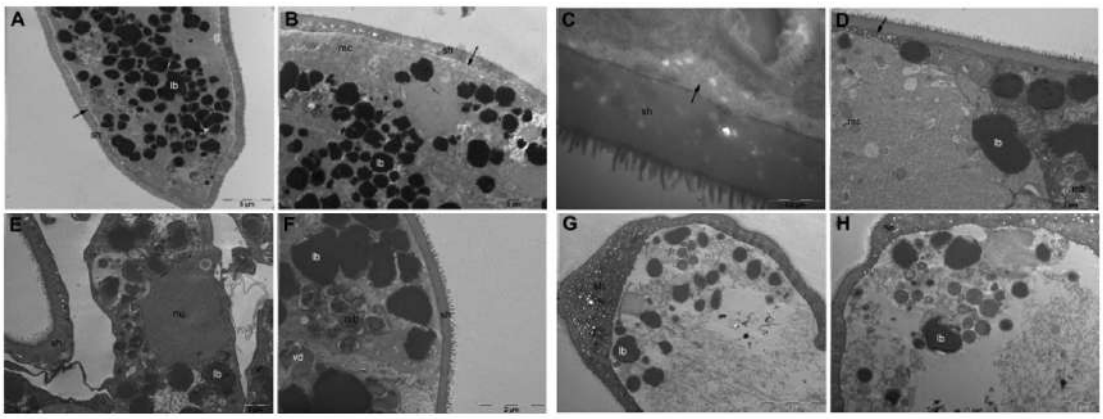

Figure 26. Transmission electron microscopy images of vehicle (DMSO)- and compound-**74**-treated eggs. (A-C) images of intact shell and distinct intracellular compartments for eggs laid *in vitro* treated with the vehicle. (D-F) Gradual loss of the intracellular compartments with appearance of myelin bodies in the vitelline cells. (G-H) lysis of the egg internal structures. Abbreviation: (sh) shell, (lb) lipid bodies, (vd) vitelline droplets, (nu) nucleus, (mc) mitochondria, (mb) myelin like structures, (arrow) cytoplasmic plates.

3.2.4 Computational studies on the synthesised thiazinoquinones

In order to gain light in the redox-based mechanism of action and rationalise the described SARs, a conformational analysis and DFT calculations have been performed by Prof. Caterina Fattorusso research group on these methoxy-thiazinoquinones taking

into account both features of inactive RA and active RB. First of all, the same computational approach applied for compounds **45**-**47** (see dedicated 2.2.4 paragraph) has been used to generate all possible conformers of the selected RA and RB thiazinoquinones together with **76** and **77** as representatives of *p*-benzyl substituted derivatives. As for thiazoavarone (**46**), two specular sets of conformers with same conformational energy have been generated for the analysed thiazinoquinones due to the two opposite ring flips (torsion angle τ_{flip} mean value ± 63°). At same time, in all conformers a limited conformational space has been demonstrated, considering that they showed the same orientation of methoxyl group ($\tau_{OMe} = \pm 63°$) while the R group on the quinone moiety is spatially fixed due to the electronic interaction between its first methylene group and the oxygen atoms of quinone ring and methoxyl group (~2.6 Å). Therefore, it is worth mentioning that these features are common for active and inactive regioisomers, independently from the nature and size of side chain. Thus, the highlighted antiparasitic effects on *Plasmodium* and *Schistosoma* are for sure not related to conformational properties of the thiazinoquinone scaffold.

Subsequently, the electronic properties of a set of selected thiazinoquinones (couples of regioisomers **65**/**73**, **66**/**74**, the quinone **79** as well as compound **76** and **77** for the benzyl derivatives, Figure 23) have been evaluated by DFT calculations miming the aqueous environment by C-PCM model [130]. Seeing as the antiparasitic mechanism of action of a wealth number of quinones is related to their redox properties and considering that the thiazinoquinone scaffold has been previously demonstrated to affect *Plasmodium* viability by the production of a semiquinone radical [103], the one electron reduction pathway has been considered (Scheme 3) and, starting from the quinone form (Q), the DFT minima have been calculated. According to the theory of

frontier orbitals which accounts the major propensity of LUMO orbital to accept the one electron during the reduction process, the localization and the energies of LUMO orbital of all DFT minima conformers have been calculated and reported in Table 22 [104,105].

Table 22. Calculated energy values (kcal/mol) of the LUMO orbitals of selected thiazinoquinones.

Compounds	Structure[a]	R	E_{LUMO}
65	RA	$-CH_2C_6H_{11}$	-14.27
66	RA	$-CH_2C_6H_5$	-15.53
73	RB	$-CH_2C_6H_{11}$	-19.74
74	RB	$-CH_2C_6H_5$	-20.49
76	RB	$-CH_2C_6H_4$-*p*-CF_3	-20.76
77	RB	$-CH_2C_6H_4$-*p*-OCH_3	-19.87
79	Q	$-CH_2C_6H_5$	-13.60

[a]Abbreviation: **RA**= regioisomer A; **RB**= regioisomer B; **Q**= 1,4-benzoquinone

In the all RA investigated, the lowest unoccupied molecular orbital resulted to be located on the quinone oxygen near to the methoxy group, instead for RB, LUMO was allocated on the quinone oxygen near to the R group bonded to quinone ring (Figure 27). The values of E_{LUMO} expressed as kcal/mol were lower for regioisomer B than regioisomer A and, interestingly, the quinone **79** lacking the heterocyclic ring showed the highest energy of LUMO value, hence lower propensity to undergo one electron reduction despite presented the same R group of the active RB **74** (Table 22). Furthermore, the reported values of E_{LUMO} are demonstrated as not related to the nature of R substituent since the energy of, e.g., **73** and **74** is in the same range. Thus, despite

two carbonyl oxygen might be involved in the one electron reduction, only the carbonyl group close to nitrogen is more subjected to the radical reduction. Additionally, the differences in term of antiparasitic activity between RA and RB on both *Plasmodium* and *Schistosoma* are not affected by lipophilic features since RA and RB have the same cLogD but strictly related to the regiochemistry of the thiazinoquinone bicyclic moiety [104,105].

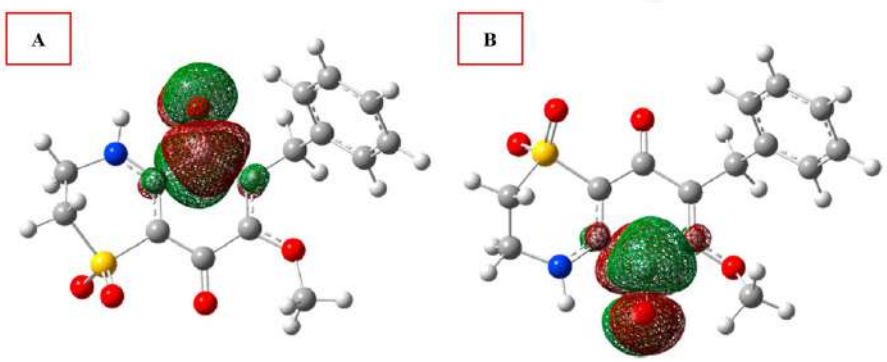

Figure 27. Localization of the LUMO orbital of compounds **66** and **74**. The ligands are displayed in *ball&stick* and colored by atom type (C=grey, O=red, N=blue, S=yellow and H=white). The orbitals were visualized using GaussView with an isosurface value of 0.02 e^{-}/a.u.^{3}

At this point, further computational dissertation allowed to shed new light on the putative antiplasmodial mechanism of action and on the pharmacokinetic properties which could explain the multistage against *S. mansoni*.

In particular, as above described and already reported in literature [103], the effect on *Plasmodium* viability depends on the formation of toxic semiquinone radical species. In this regard, considering a couple of regioisomers in which R is an aliphatic substituent (**65**/**73**) and the couple based on the new antimalarial lead candidate **74** and its inactive regioisomer **66**, the DFT minima conformers were generated and the electron spin

density was calculated. The results evidenced that, after generating an oxygen-centered radical, exists the possibility to delocalize the radical on the two regioisomers (RA and RB), but only in the active regioisomers (**73** and **74**) the appropriate intramolecular distance (2.6 Å, Figure 28) between the methylene of R group and the quinone oxygen allows a "through-space" hydrogen radical shift from the carbon of methylene to the oxygen atom. In this way, a carbon radical, the putative toxic species, is so formed on the R group of quinone side-chain and it could also account the higher potency of compound **74** since a more stable benzyl radical (**86**) is generated in spite of RB-thiazinoquinones with aliphatic substituent.

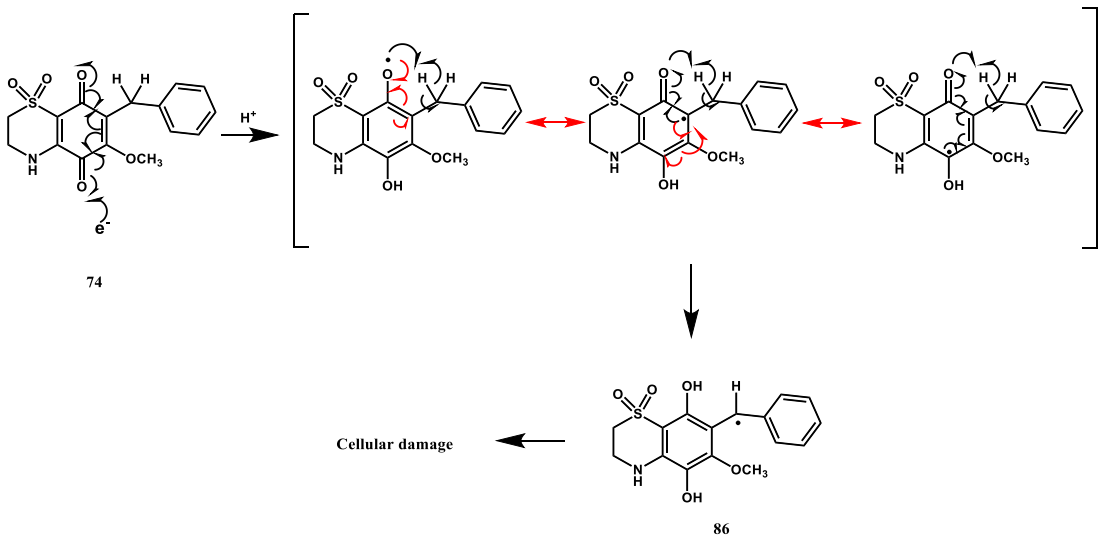

Figure 28. Proposed mechanism for the generation of the semiquinone radical by one-electron reduction of **74** followed by intramolecular hydrogen radical shift (red arrows indicate electron delocalization).

The observed discrepancies between the activity on different developmental stages of *S. mansoni* were not correlated to calculated cLogD values of the tested

thiazinoquinones (Table 23) since this parameter influence the compound intracellular uptake by passive diffusion according to Lipinski's rule [144].

Table 23. cLogD values at pH=7.4 and 7.2 calculated by ACD/Percepta 2017.

Compounds	Structure[a]	R	cLogD
65	RA	$-CH_2C_6H_{11}$	1.15
66	RA	$-CH_2C_6H_5$	0.41
71	RB	$-(CH_2)_7CH_3$	2.28
72	RB	$-CH_2CH(CH_3)_2$	-0.03
73	RB	$-CH_2C_6H_{11}$	1.15
74	RB	$-CH_2C_6H_5$	0.41
75	RB	$-CH_2C_6H_4$-*p*-Cl	1.01
76	RB	$-CH_2C_6H_4$-*p*-CF_3	0.99
77	RB	$-CH_2C_6H_4$-*p*-OCH_3	0.33
78	RB	$-CH_2C_6H_4$-*p*-CF_3	1.37

[a]Abbreviation: **RA**= regioisomer A; **RB**= regioisomer B;

Indeed, despite an optimal cLogD value, compounds as **71**, **75** and **76** are poor effective on the adult worm pairs probably due to scarce ability to cross the lipidic tegument. On the other hand, good antischistosomal properties of compounds **72**, **73**, **77** and **78** with much different lipophilic features might be attributed to facilitate diffusion or active transport processes by using membrane proteins. To substantiate this hypothesis, the structural similarity among **73** and antischistosomal choice drug praziquantel (PZQ, **16**) on which SAR studies demonstrated cyclohexyl substituent as a better substituent were taken in advantage, and structural comparison between these

highlighted multistage thiazinoquinones, PZQ, and adenosine, was explored. The use of adenosine in this step was corroborated by experimental evidences of its competitiveness with PZQ for nucleoside transporter [147].

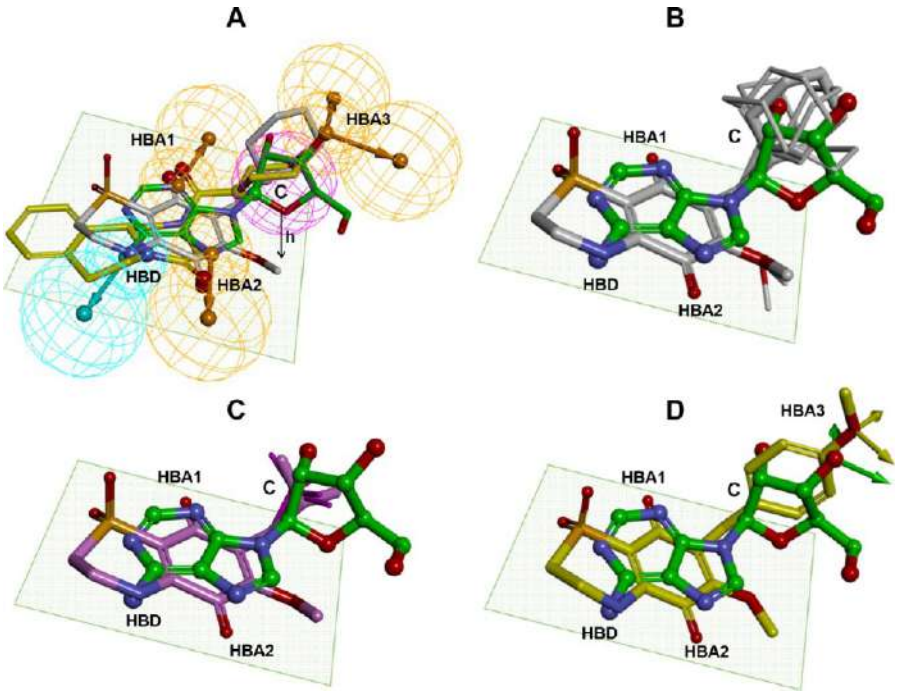

Figure 29. (**A**) Superimposition of adenosine (green), PZQ (yellow), and compound **73** (grey) by fitting the common structural features: (i) one H-bond donor (HBD; cyan); (ii) two H-bond acceptors (HBA; orange); (iii) a ring system containing a conjugated planar moiety (green plane), and (iv) a sizable carbon "side chain" with the first atom (C; magenta) placed at a height of ~1 Å from the ring plane. The comparison of the low energy conformers of **73** (grey; B), **72** (magenta; C), and **77** (yellow; D) with adenosine (green) is reported in (**B-D**). Heteroatoms are coloured by atom type (N = blue, O = red, S = orange), and lone pairs are evidenced with arrows.

In Figure 29, it is evidenced the good superimposition of the five-membered sugar moiety of adenosine and the cyclohexyl both of praziquantel and compound **73** as well as the isobutyl chain of **72**. Regarding the identified multistage *p*-benzyl derivatives, the

oxygen atom of *p*-OCH_3 and *p*-OCF_3 is overlapped to the 3'-OH of ribose of adenosine (HBA3, Figure 29D). Opposite situation occurred for the side-chain of thiazinoquinones **71**, (partially) **74**, **75** and **77** which are active against larval stage (schistosomula) and poor effective against adult form (Table 21 and Figure 24) seeing the shape and nature of R substituent did not fit with PZQ and/or adenosine structure. In any case, these SAR studies does not imply the same mechanism of action against *S. mansoni* for PZQ and the most active RB-methoxy-thiazinoquinone compound **73**.

Conclusion: overall these data clearly corroborated previous works on the role of the thiazinoquinone scaffold as an active chemotype for parasitic diseases. Among the rationalised chemical library of synthetic methoxy-thiazinoquinones (Figure 23), important structural requirements have been carried out, highlighting common featuring which ensure the presence of toxic effects on both *Plasmodium* and *Schistosoma* whereas other characteristics might affect the selectivity against mammalian cells or different parasite strains. Particularly, unlike that demonstrated for avarone (**45**, see paragraph 2.3.3), in these derivatives the 1,1-dioxo-1,4-thiazine ring is crucial for the activity because lack of the heterocyclic moiety produces totally inactive molecules. Moreover, the regiochemistry of the thiazinoquinone bicyclic system is extremely necessary to exert toxic effects on parasites since only when the methoxyl group is at same side of nitrogen atom, the thiazinoquinones result effective. Modulating the nature and the shape of R substituent placed on the quinone (Figure 23), the effectiveness on different organisms is influenced. Firstly, the cytotoxicity on mammalian cells is strongly dependent from the length of alkyl chain, instead for the antiplasmodial effects a benzyl substituent provided the better IC_{50} in the sub-micromolar concentration range

on D10 and W2 *P. falciparum* strains (0.60 and 0.70 μM, respectively) allowing to identify a new antimalarial lead candidate (**74**). On the other hand, to affect viability of different developmental stage of *S. mansoni* (eggs included) a cyclohexylmethyl is selected as the better substituent (**73**) even though comparable results have been achieved with variation in steric and electronic nature of R group i.e. **72**, **77** and in particular **78**.

Computational studies based on conformational analysis, DFT calculations and prediction of electronic features allowed to shed light on the putative mechanism of action of this promising bioactive chemical scaffold. The ability to impair parasitic intracellular structures is closely related to the formation of a toxic semiquinone radical species upon a one-electron reduction bioactivation step. This propensity is more accounted in regioisomer B due to the localization of LUMO orbital and the optimum distance (2.6 Å) between the first methylene of R group and the quinone or methoxyl oxygen atoms which permits a "through-space" hydrogen radical shift achieving the putative toxic species. To substantiate this hypothesis, the lead compound **74** might produce a benzyl radical more stable than that obtained by an aliphatic side-chain and, accordingly, with a *p*-OCF_3 substituent this trend is confirmed. The semiquinone radical is ascribed to be responsible also of the toxicity against the multicellular blood-dwelling *S. mansoni* even though compound **74** was less active as antischistosomal agent than antimalarial, while **73** showed a better overall activity profile against *S. mansoni* although less active as antimalarial. This discrepancy might be explained by the different ability to penetrate parasites that was demonstrated depending on membrane transport proteins expressed by parasites. Importantly, the different biology between the two discussed parasites and the morphological changes during the life cycle of *S.*

mansoni modify the compound pharmacokinetic toward a specific organism and clarify the different activity trend among *Plasmodium* and *Schistosoma* as well as among several parasite developmental stages.

3.2.5 Materials and methods for compounds 64-70 and 72-79

Synthesis of the methoxy-thiazinoquinone chemical library

The scheme of synthesis was successfully improved as regarding the yield of intermediates for each step as well as for final products modifying the starting material and the adopted organic chemistry reaction with respect to the already published work [137]. In this previous article, it is also reported the synthesis of compound **71** which was firstly included in the evaluation of its antischistosomal effects.

*Synthesis of 2-isobutyl-1,3,4-trimethoxybenzene (**81-R2**) and 2-(cyclohexylmethyl)-1,3,4-trimethoxybenzene (**81-R3**):* 10 mmol of 1,2,4-trimethoxybenzene (1.7 g) have been dissolved in 25 mL of anhydrous THF and 12.5 mL of *n*-BuLi 1.6 M (20 mmol) were added, keeping the mixture under argon at 0°C for 1h. Subsequently, for each mixture 20 mmol of 1-bromo-2-methylpropane (2.2 mL) or bromomethylcyclohexane (2.8 mL) were added leaving the mixture overnight under magnetic stirring at rt, monitoring the end of reaction by TLC (chloroform/hexane 7:3 as eluent). Then, the mixture was diluted with water (150 mL) and extracted with diethyl ether (3 x 80 mL). The organic layer was washed with brine, dried over Na_2SO_4, filtered and concentrated *in vacuo*. The crude material was so purified by flash chromatography on SiO_2 with

mobile phase hexane/EtOAc 9:1 affording the colourless oil **81-R$_2$** (1.8 g, 80%), and **81-R$_3$** (2.0 g, 76%), respectively.

*Compound **81-R$_2$**:* ^{1}H-NMR ($CDCl_3$): 6.68 (1H, d, *J*=8.8 Hz, H-6); 6.51 (1H, d, *J*=8.8 Hz, H-5); 3.79 (3H, s, -OCH_3); 3.78 (3H, s, -OCH_3); 3.73 (3H, s, -OCH_3); 2.49 (2H, d, *J*=7.3 Hz, CH_2); 1.89 (1H, m, *J*=7.3 Hz-6.7 Hz, CH); 0.86 (6H, d, *J*=6.7Hz, CH_3); HRESIMS: *m/z* 247.1314 $[M+Na]^+$ (calcd. for $C_{13}H_{20}O_3Na^+$ *m/z* 247.1305); ^{1}H NMR and HRESIMS spectra are reported in Chapter 6.

*Compound **81-R$_3$**:* ^{1}H-NMR ($CDCl_3$): 6.69 (^{1}H, d, *J*=8.8 Hz, H-6); 6.52 (1H, d, *J*=8.8 Hz, H-5); 3.80 (3H, s, -OCH_3); 3.78 (3H, s, -OCH_3); 3.74 (3H, s, -OCH_3); 2.50 (2H, d, *J*=7.4 Hz, CH_2-cyclohexyl); 1.55 (1H, m, CH); 1.53-0.95 (4H, m); 1.15-1.66 (4H, m), 1.60 (2H, m); HRESIMS: *m/z* 287.1626 $[M+Na]^+$ (calcd. for $C_{16}H_{24}O_3Na^+$ *m/z* 287.1618); ^{1}H NMR and HRESIMS spectra are reported in Chapter 6.

*Synthesis of 2-isobutyl-3-methoxycyclohexa-2,5-diene-1,4-dione (**82-R$_2$**) and 2-(cyclohexylmethyl)-3-methoxycyclohexa-2,5-diene-1,4-dione (**82-R$_3$**):* the oxidation reaction was executed on 780 mg of **82-R$_2$** and 925 mg of **82-R$_3$** (3.5 mmol). Each compound was separately dissolved in 90 mL of CH_3CN at 0°C and an aqueous solution of CAN (9.6 g, 17.5 mmol/100 mL) was added dropwise. The resultant orange mixture was kept under stirring in a cold-water bath for 45 minutes before to proceed with adding water (100 mL) and extract with diethyl ether (3 x 80 mL). The combined organic phase was first washed with brine, then dried over anhydrous sodium sulphate, filtered and concentrated by rotary evaporation. Compounds **82-R$_2$** (65%) and **82-R$_3$** (74%) were obtained after HPLC separation on silica gel column eluting with hexane/EtOAc 9:1.

Compound ***82-R2****:* ^{1}H-NMR ($CDCl_3$): 6.66 (^{1}H, d, *J*=10.0 Hz, H-6); 6.51 (1H, d, *J*=10.0 Hz, H-5); 3.99 (3H, s, -OCH_3); 2.34 (2H, d, *J*=7.3 Hz, CH_2); 1.81 (1H, m, *J*=7.3 Hz-6.7 Hz, CH); 0.89 (6H, d, *J*=6.7Hz, CH_3); HRESIMS: *m/z* 217.0841 $[M+Na]^+$ (calcd. for $C_{11}H_{14}O_3Na^+$ *m/z* 217.0835); ^{1}H NMR and HRESIMS spectra are reported in Chapter 6.

Compound ***82-R3****:* ^{1}H-NMR ($CDCl_3$): 6.69 (^{1}H, d, *J* = 8.8 Hz, H-6); 6.52 (1H, d, *J* = 8.8 Hz, H-5); 4.01 (3H, s, -OCH_3); 2.35 (2H, d, *J* = 7.4 Hz, CH_2-cyclohexyl); 1.55 (1H, m, CH); 1.53-0.95 (4H, m); 1.15-1.66 (4H, m), 1.60 (2H, m); HRESIMS *m/z* 257.1139 $[M+Na]^+$ (calcd. for $C_{14}H_{18}O_3Na^+$ *m/z* 257.1148); ^{1}H NMR and HRESIMS spectra are reported in Chapter 6.

Synthesis of compounds ***64****/****72*** *and* ***65****/****73****:* a portion of the two quinone compounds, 290 mg of **82-R2** and 350 mg of **82-R3** (1.5 mmol), was converted in the relevant quinone by a condensation reaction performed solubilizing each quinone in 20 mL of a mixture EtOH/CH_3CN 1:1, adding a water solution of hypotaurine (163.7 mg in 8 mL) in molar ratio of 1:1 together with salcomine in portion as catalyst. The mixture was left at rt for 48 h observing a colour changing from yellow to orange/red accounting the occurrence of the coupling. After that time, most of ethanol was removed by rotary evaporator before to dilute with water and extract with diethyl ether (3 x 60 mL). The organic layer was washed with saturated solution of NaCl, dried over Na_2SO_4, filtered and concentrated *in vacuo*. The solvent removal gave a mixture of the two regioisomers **64**/**72** (170 mg, 38 %) from the quinone **82-R2** and **65**/**73** (167 mg, 33 %) from **82-R3**. The individual compounds were achieved by HPLC on silica gel (column Luna 5µm, 250 x 4.60 mm, flow rate 1 mL/min) eluting with hexane/EtOAc 6:4 (v/v) of the crude material providing the pure thiazinoquinones **64** (RA, t_R=13.5 min, 8 mg) and **72** (RB,

t_R=24 min, 70 mg) as well as **65** (RA, t_R=11.8 min, 5 mg) and **73** (RB, t_R=21.4 min, 49 mg), respectively.

*6-isobutyl-7-methoxy-3,4-dihydro-2H-benzo[b][1,4]thiazine-5,8-dione 1,1-dioxide (**64**)*: ^{1}H and ^{13}C NMR data are reported in Table 17. HRESIMS: *m/z* 322.0727 $[M+Na]^+$ (calcd. for $C_{13}H_{17}NO_5SNa^+$ *m/z* 322.0720); NMR and HRESIMS spectra are reported in Chapter 6.

*6-(cyclohexylmethyl)-7-methoxy-3,4-dihydro-2H-benzo[b][1,4]thiazine-5,8-dione 1,1-dioxide (**65**)*: ^{1}H and ^{13}C NMR data are reported in Table 17. HRESIMS: *m/z* 362.1042 $[M+Na]^+$ (calcd. for $C_{16}H_{21}NO_5SNa^+$ *m/z* 362.1033); NMR and HRESIMS spectra are reported in Chapter 6.

*7-isobutyl-6-methoxy-3,4-dihydro-2H-benzo[b][1,4]thiazine-5,8-dione 1,1-dioxide (**72**)*: ^{1}H and ^{13}C NMR data are reported in Table 17. HRESIMS: *m/z* 322.0729 $[M+Na]^+$ (calcd. for $C_{13}H_{17}NO_5SNa^+$ *m/z* 322.0720); NMR and HRESIMS spectra are reported in Chapter 6.

*7-(cyclohexylmethyl)-6-methoxy-3,4-dihydro-2H-benzo[b][1,4]thiazine-5,8-dione 1,1-dioxide (**73**)*: ^{1}H and ^{13}C NMR data are reported in Table 17. HRESIMS: *m/z* 362.1038 $[M +Na]^+$ (calcd. for $C_{16}H_{21}NO_5SNa^+$ *m/z* 362.1033); NMR and HRESIMS spectra are reported in Chapter 6.

*Synthesis of compounds **83-R$_4$**, **83-R$_5$**, **83-R$_6$**, **83-R$_7$**, and **83-R$_8$**:* the synthesis of the first intermediate for the *p*-benzyl substituted series was performed using 1.0 mL (6.7 mmol) of 1,2,4-trimethozybenzene in 30 mL of THF each time and adding slowly 6 mL (10 mmol) of a solution of *n*-BuLi 1.6 M under Ar at 0°C for 1h. Subsequently, each formed lithiated was treated with a suitable aldehyde and thus, 10 mmol of benzaldehyde (1.0 mL) for **83-R$_4$**, 4-chlorobenzaldehyde (1.4 g) for **83-R$_5$**, 4-

(trifluoromethyl)benzaldehyde (1.40 mL) for **83-R$_6$**, 4-methoxybenzaldehyde (1.2 mL) for **83-R$_7$**, 4-(trifluoromethoxy)benzaldehyde (1.4 mL) for **83-R$_8$** were added keeping the resultant mixtures under magnetic stirring at rt overnight. Then, the mixtures were quenched with a saturated solution of NH_4Cl (30 mL) and extracted with diethyl ether (3 x 80 mL) before washing with brine, drying, filtering and concentrating *in vacuo*. The raw material was purified by HPLC on SiO_2 (Luna column Luna 5µm, 250 x 4.60 mm, flow rate 1 mL/min, eluent: hexane/EtOAc 8:2) and the corresponding biaryl alcohols were afforded **83-R$_4$** (1.3 g, 70% yield), **83-R$_5$** (1.5 g, 75%), **83-R$_6$** (1.9 g, 83%), and **83-R$_8$** (1.8 g, 78%). Regarding **83-R$_7$** (2.0, 99% g), it resulted sufficiently pure for following step.

*phenyl(2,3,6-trimethoxyphenyl)methanol (**83-R$_4$**):* ^{1}H-NMR ($CDCl_3$): 6.82 (1H, d, *J*=8.8 Hz, H-6); 6.62 (1H, d, *J*=8.8 Hz, H-5); 3.82 (3H, s, -OCH_3); 3.74 (3H, s, -OCH_3); 3.61 (3H, s, -OCH_3); 6.25 (1H, d, *J*=11.7 Hz, CH-OH); 7.36 (2H, d, *J*=7.0 Hz); 7.28 (2H, t, *J*=7.6Hz); 7.19 (1H, t, *J*=7.6Hz); 4.29 (1H, d, *J*=11.7Hz, -OH). HRESIMS: *m/z* 297.1109 $[M+Na]^+$ (calcd. for $C_{16}H_{18}O_4Na^+$ *m/z* 297.1097); NMR and HRESIMS spectra are reported in Chapter 6.

*(4-chlorophenyl)(2,3,6-trimethoxyphenyl)methanol (**83-R$_5$**)*: ^{1}H-NMR ($CDCl_3$): 6.82 (1H, d, *J*=8.8 Hz, H-6); 6.62 (1H, d, *J*=8.8 Hz, H-5); 3.81 (3H, s, -OCH_3); 3.72 (3H, s, -OCH_3); 3.62 (3H, s, -OCH_3); 6.24 (1H, d, *J*=11.7 Hz, CH-OH); 7.23 (2H, d, *J*=8.3 Hz); 7.27 (2H, d, *J*=8.3Hz); 4.29 (1H, d, *J* = 11.7Hz, -OH). HRESIMS: *m/z* 331.0719 $[M+Na]^+$ (calcd. for $C_{16}H_{17}ClO_4Na^+$ *m/z* 331.0708); ^{1}H and ^{13}C spectra are reported in Chapter 6.

*(4-(trifluoromethyl)phenyl)(2,3,6-trimethoxyphenyl)methanol (**83-R$_6$**):* ^{1}H-NMR ($CDCl_3$): 6.82 (1H, d, *J*=8.8 Hz, H-6); 6.62 (1H, d, *J*=8.8 Hz, H-5); 3.78 (3H, s, -OCH_3);

3.68 (3H, s, -OCH_3); 3.63 (3H, s, -OCH_3); 6.30 (1H, brs, CH-OH); 7.53 (2H, d, *J*=8.3 Hz); 7.50 (2H, d, *J*=8.3Hz); 4.29 (1H, brs, -OH). HRESIMS: *m/z* 365.0954 $[M+Na]^+$ (calcd. for $C_{17}H_{17}F_3O_4Na^+$ *m/z* 365.0971); ^1H and ^{13}C spectra are reported in Chapter 6.

*(4-methoxyphenyl)(2,3,6-trimethoxyphenyl)methanol (**83-R$_7$**):* ^1H-NMR ($CDCl_3$): 6.62 (1H, d, *J*=8.8 Hz, H-6); 6.20 (1H, d, *J*=8.8 Hz, H-5); 3.82 (3H, s, -OCH_3); 3.76 (3H, s, -OCH_3); 3.83 (3H, s, -OCH_3); 3.63 (3H, s, -OCH_3); 6.80 (1H, brs, CH-OH); 7.27 (2H, d, *J*=8.3 Hz); 6.82 (2H, d, *J*=8.3Hz); 4.60 (1H, brs, -OH). HRESIMS: *m/z* 327.1218 $[M+Na]^+$ (calcd. for $C_{17}H_{20}O_5Na^+$ *m/z* 327.1203); ^1H and ^{13}C spectra are reported in Chapter 6.

*(4-(trifluoromethoxy)phenyl)(2,3,6-trimethoxyphenyl)methanol (**83-R$_8$**):* ^1H-NMR ($CDCl_3$): 6.84 (1H, d, *J*=8.8 Hz, H-6); 6.63 (1H, d, *J*=8.8 Hz, H-5); 3.82 (3H, s, -OCH_3); 3.74 (3H, s, -OCH_3); 3.65 (3H, s, -OCH_3); 6.24 (1H, brs, CH-OH); 7.39 (2H, d, *J*=8.3 Hz); 7.13 (2H, d, *J*=8.3Hz); 4.34 (1H, brs, -OH). HRESIMS: *m/z* 381.0944 $[M+Na]^+$ (calcd. for $C_{17}H_{17}F_3O_5Na^+$ *m/z* 381.0920); ^1H and ^{13}C spectra are reported in Chapter 6.

*Synthesis of compounds **84-R$_4$**, **84-R$_5$**, **84-R$_6$**, **84-R$_7$**, and **84-R$_8$**:* 30 mL of CH_2Cl_2 were used to dissolve 650 mg (2.4 mmol) of **83-R$_4$**, 700 mg (2.3 mmol) of **83-R$_5$**, 1 g (2.9 mmol) of **83-R$_6$**, 1 g (2.9 mmol) of **83-R$_7$**, and 1 g (2.8 mmol) of **83-R$_8$**, respectively. The reaction provided for a slow addition from 500 to 800 μL of trifluoroacetic acetic of and, after 10 minutes, of triethylsilane (~1.1-1.6 mL) stirring the mixture at rt overnight. Each organic phase was subjected to quenching with aqueous solution of sodium carbonate and the solvent removed *in vacuo* affording pure compounds that were appropriate for the following reaction: 600 mg of **84-R$_4$**, 670 mg of **84-R$_5$**, 930 mg of **84-R$_6$**, 822 mg of **84-R$_7$**, and 937 mg of **84-R$_8$**.

*2-benzyl-1,3,4-trimethoxybenzene (**84-R4**):* ^{1}H-NMR ($CDCl_3$): 6.73 (1H, d, *J*=8.8 Hz, H-6); 6.56 (1H, d, *J*=8.8 Hz, H-5); 3.80 (3H, s, -OCH_3); 3.72 (3H, s, -OCH_3); 3.68 (3H, s, -OCH_3); 4.01 (1H, s, CH_2-benzyl); 7.22 (2H, d, *J*=7.0 Hz); 7.18 (2H, t, *J*=7.6Hz); 7.09 (1H, t, *J*=7.6Hz). HRESIMS: *m/z* 281.1154 $[M+Na]^+$ (calcd. for $C_{16}H_{18}O_3Na^+$ *m/z* 281.1148); ^{1}H NMR and HRESIMS spectra are reported in Chapter 6.

*2-(4-chlorobenzyl)-1,3,4-trimethoxybenzene (**84-R5**):* ^{1}H-NMR ($CDCl_3$): 6.76 (1H, d, *J*=8.8 Hz, H-6); 6.57 (1H, d, *J*=8.8 Hz, H-5); 3.80 (3H, s, -OCH_3); 3.72 (3H, s, -OCH_3); 3.70 (3H, s, -OCH_3); 3.99 (1H, s, CH_2-benzyl); 7.19 (2H, s); 7.17 (2H, s). HRESIMS: *m/z* 315.0770 $[M+Na]^+$ (calcd. for $C_{16}H_{17}ClO_3Na^+$ *m/z* 315.0758); ^{1}H and ^{13}C spectra are reported in Chapter 6.

*1,2,4-trimethoxy-3-(4-(trifluoromethyl)benzyl)benzene (**84-R6**):* ^{1}H-NMR ($CDCl_3$): 6.85 (1H, d, *J*=8.8 Hz, H-6); 6.65 (1H, d, *J*=8.8 Hz, H-5); 3.88 (3H, s, -OCH_3); 3.85 (3H, s, -OCH_3); 3.80 (3H, s, -OCH_3); 4.20 (1H, s, CH_2-benzyl); 7.57 (2H, d, *J*=8.0 Hz); 7.48 (2H, d, *J*=8.0 Hz). HRESIMS: *m/z* 349.1036 [M+Na]+ (calcd. for $C_{17}H_{17}F_3O_3Na^+$ *m/z* 349.1022); ^{1}H and ^{13}C spectra are reported in Chapter 6.

*1,2,4-trimethoxy-3-(4-methoxybenzyl)benzene (**84-R7**):* ^{1}H-NMR ($CDCl_3$): 6.77 (1H, d, *J*=8.8 Hz, H-6); 6.62 (1H, d, *J*=8.8 Hz, H-5); 3.84 (3H, s, -OCH_3); 3.78 (3H, s, -OCH_3); 3.77 (3H, s, -OCH_3); 3.74 (3H, s, -OCH_3); 3.99 (1H, s, CH_2-benzyl); 7.19 (2H, s); 6.80 (2H, s). HRESIMS: *m/z* 311.1259 $[M+Na]^+$ (calcd. for $C_{17}H_{20}O_4Na^+$ *m/z* 311.1254); ^{1}H and ^{13}C spectra are reported in Chapter 6.

*1,2,4-trimethoxy-3-(4-(trifluoromethoxy)benzyl)benzene (**84-R8**):* ^{1}H-NMR ($CDCl_3$): 6.81 (1H, d, *J*=8.8 Hz, H-6); 6.63 (1H, d, *J*=8.8 Hz, H-5); 3.86 (3H, s, -OCH_3); 3.80 (3H, s, -OCH_3); 3.79 (3H, s, -OCH_3); 4.08 (1H, s, CH_2-benzyl); 7.34 (2H, d, *J*=8.0

Hz); 7.11 (2H, d, *J*=8.0 Hz). HRESIMS: *m/z* 365.0979 $[M+Na]^+$ (calcd. for $C_{17}H_{17}F_3O_4Na^+$ *m/z* 365.0971); ^1H and ^{13}C spectra are reported in Chapter 6.

*Synthesis of compound **79** and **85-R5**:* 2.2 mmol (502 mg) of **84-R4** and 1.7 mmol (500 mg) of the compound **84-R5** were separately dissolved in 90 mL of acetonitrile with subsequently dropwise addition of aqueous solution of CAN (6.0 g, 11.0 mmol for synthesis of **79** and 4.6 g, 8.5 mmol for synthesis of **85-R5** in 100 mL of water) keeping in a cold bath. After stirring for 45 minutes at 0 °C, the orange mixture was poured into 100 mL of cold water and extracted with diethyl ether (3 x 90 mL). The combined organic layer was washed with brine, dried over Na_2SO_4, and filtered while the solvent removed *in vacuo*. The crude material contained the quinone **79** (487 mg) and **85-R5** (436 mg) in pure state for the following step.

*2-benzyl-3-methoxycyclohexa-2,5-diene-1,4-dione (**79**):* ^1H-NMR ($CDCl_3$): 6.66 (1H, d, *J* = 10.0 Hz, H-6); 6.57 (1H, d, *J* = 10.0 Hz, H-5); 4.02 (3H, s, -OCH_3); 3.77 (1H, s, CH_2-benzyl); 7.25 (2H, d, *J* = 7.0 Hz); 7.23 (2H, t, *J* = 7.6Hz); 7.16 (1H, t, *J* = 7.6Hz). HRESIMS: *m/z* 251.0689 $[M+Na]^+$ (calcd. for $C_{14}H_{12}O_3Na^+$ *m/z* 251.0679); ^1H NMR and HRESIMS spectra are reported in Chapter 6.

*2-(4-chlorobenzyl)-3-methoxycyclohexa-2,5-diene-1,4-dione (**85-R5**):* ^1H-NMR ($CDCl_3$): 6.66 (1H, d, *J*= 0.0 Hz, H-6); 6.57 (1H, d, *J*=10.0 Hz, H-5); 4.04 (3H, s, -OCH_3); 3.71 (1H, s, CH_2-benzyl); 7.19 (2H, d, *J*=8.5 Hz); 7.17 (2H, d, *J*=8.5 Hz). HRESIMS: *m/z* 285.0297 $[M+Na]^+$ (calcd. for $C_{14}H_{11}ClO_3Na^+$: 285.0289); ^1H and ^{13}C spectra are reported in Chapter 6.

*Synthesis of compound **85-R6**, **85-R7**, and **85-R8**:* 500 mg (1.5, 1.8 and 1.4 mmol, respectively) of the compounds **84-R6**, **85-R7** and **84-R8**, dissolved in 80 mL of acetonitrile, were treated with 100 mL of CAN solution (4.1 g, 7.5 mmol for **85-R6**, 5

g, 9 mmol for **85-R7**, and 4 g, 7.3 mmol for **85-R8**) at 0°C for 45 min. Then, the applied procedure was identical to the previous one, but the raw material afforded compound **85-R6** (310 mg, 70%) and **85-R8** (296 mg, 65%) as a result of HPLC separation on silica gel and hexane/EtOAc 9:1 (v/v) as mobile phase, whereas **85-R7** (348 mg, 75%) was obtained hereafter eluting with hexane/EtOAc 95:5 (v/v).

*2-methoxy-3-(4-(trifluoromethyl)benzyl)cyclohexa-2,5-diene-1,4-dione (**85-R6**):* ^{1}H-NMR ($CDCl_3$): 6.67 (1H, d, *J*=10.0 Hz, H-6); 6.59 (1H, d, *J*=10.0 Hz, H-5); 4.06 (3H, s, -OCH_3); 3.80 (1H, s, CH_2-benzyl); 7.50 (2H, d, *J*=8.0 Hz); 7.36 (1H, d, *J*=8.0Hz). HRESIMS: *m/z* 319.0545 $[M+Na]^+$ (calcd. for $C_{15}H_{11}F_3O_3Na^+$ *m/z* 319.0552); ^{1}H and ^{13}C spectra are reported in Chapter 6.

*2-methoxy-3-(4-methoxybenzyl)cyclohexa-2,5-diene-1,4-dione (**85-R7**):* ^{1}H-NMR ($CDCl_3$): 6.65 (1H, d, *J*=10.0 Hz, H-6); 6.57 (1H, d, *J*=10.0 Hz, H-5); 4.04 (3H, s, -OCH_3); 3.76 (3H, s, -OCH_3); 3.72 (1H, s, CH_2-benzyl); 7.19 (2H, d, *J*=8.0 Hz); 6.79 (1H, d, *J*=8.0Hz). HRESIMS: *m/z* 281.0768 $[M+Na]^+$ (calcd. for $C_{15}H_{14}O_4Na^+$ *m/z* 281.0784); ^{1}H and ^{13}C spectra are reported in Chapter 6.

*2-methoxy-3-(4-(trifluoromethoxy)benzyl)cyclohexa-2,5-diene-1,4-dione (**85-R8**):* ^{1}H-NMR ($CDCl_3$): 6.69 (1H, d, *J*=10.0 Hz, H-6); 6.60 (1H, d, *J*=10.0 Hz, H-5); 4.07 (3H, s, -OCH_3); 3.77 (1H, s, CH_2-benzyl); 7.28 (2H, d, *J*=8.0 Hz); 7.09 (1H, d, *J*=8.0Hz). HRESIMS: *m/z* 335.0496 $[M+Na]^+$ (calcd. for $C_{15}H_{11}F_3O_4Na^+$ *m/z* 335.0502); ^{1}H and ^{13}C spectra are reported in Chapter 6.

*Synthesis of thiazinoquinones **66**/**74**, **67**/**75**, **68**/**76**, **69**/**77**, and **70**/**78**:* compounds **79** (324 mg, 1.42 mmol), **85-R5** (400mg, 1.5 mmol), **85-R6** (250 mg, 0.85 mmol), **85-R7** (300 mg, 1.05 mmol), **85-R8** (200 mg, 0.64 mmol) were converted into thiazinoquinone bicyclic compound via nucleophilic addition. Thus, the quinones were

dissolved in ~30 mL of EtOH/CH_3CN 1:1 (v/v) and to each one hypotaurine (155 mg, 1.42 mmol for synthesis of **66**/**74**, 164 mg, 1.5 mmol for **67**/**75**, 92 mg, 0.85 mmol for **68**/**76**, 125 mg, 1.05 mmol for **69**/**77**; 70 mg, 0.64 mmol for **70**/**78**) in 2 mL of water was added dropwise, together with an in portion catalytic amount of salcomine. The resulting mixture was stirred for 48h at room temperature monitoring the reaction by TLC (chloroform/EtOAc 7:3). As for thiazinoquinones with aliphatic side chain as substituent, a colour variation from yellow to orange/red was observed. After this time, most of ethanol was evaporated under reduce pressure and the residue poured in water and extracted with diethyl ether (3 x 50 mL). Each resultant organic phase was washed with saturated solution of sodium chloride, dried over sodium sulphate, filtered and concentrated *in vacuo*. The crude residues contained always a mixture of the two regioisomers: **66** and **74** (175 mg, 37%), **67** and **75** (247 mg, 45%), **68** and **76** (189 mg, 55%), **69** and **77** (165 mg, 40%), **70** and **78** (113 mg, 42%). HPLC on SiO2 (column: Luna 5µm, 250 x 4.60 mm, flow rate 1 mL/min) with a mobile phase hexane/EtOAc 4:6 (v/v) provided the following pure compounds: **66** (7 mg) and **74** (63 mg); **67** (25 mg) and **75** (223 mg); **68** (20 mg) and **76** (169 mg); **69** (20 mg) and **77** (148 mg); **70** (12 mg) and **78** (100 mg).

The structural characterization and the univocal determination of regiochemistry of the thiazinoquinone system was achieved by 1D and 2D NMR analysis which allowed to assign all NMR resonances. ^{1}H and ^{13}C of these thiazinoquinones (**66**-**70** and **74**-**78**) are reported in Tables 18 and 19, instead NMR spectra as well as HRESIMS spectra are reported in Chapter 6.

*6-benzyl-7-methoxy-3,4-dihydro-2H-benzo[b][1,4]thiazine-5,8-dione 1,1-dioxide (**66**) and 7-benzyl-6-methoxy-3,4-dihydro-2H-benzo[b][1,4]thiazine-5,8-dione 1,1-*

*dioxide (**74**):* HRESIMS: *m/z* 356.0565 $[M+Na]^+$ (calcd. for $C_{16}H_{15}NO_5SNa^+$ *m/z* 356.0563).

*6-(4-chlorobenzyl)-7-methoxy-3,4-dihydro-2H-benzo[b][1,4]thiazine-5,8-dione 1,1-dioxide (**67**) and 7-(4-chlorobenzyl)-6-methoxy-3,4-dihydro-2H-benzo[b][1,4]thiazine-5,8-dione 1,1-dioxide (**75**):* HRESIMS: *m/z* 390.0169 $[M+Na]^+$ (calcd. for $C_{16}H_{14}ClNO_5SNa^+$ *m/z* 390.0173).

*7-methoxy-6-(4-(trifluoromethyl)benzyl)-3,4-dihydro-2H-benzo[b][1,4]thiazine-5,8-dione 1,1-dioxide (**68**) and 6-methoxy-7-(4-(trifluoromethyl)benzyl)-3,4-dihydro-2H-benzo[b][1,4]thiazine-5,8-dione 1,1-dioxide (**76**):* HRESIMS: *m/z* 400.0492 $[M-H]^-$ (calcd. for $C_{17}H_{13}F_3NO_5S$: 400.0461).

*7-methoxy-6-(4-methoxybenzyl)-3,4-dihydro-2H-benzo[b][1,4]thiazine-5,8-dione 1,1-dioxide (**69**) and 6-methoxy-7-(4-methoxybenzyl)-3,4-dihydro-2H-benzo[b][1,4]thiazine-5,8-dione 1,1-dioxide (77):* HRESIMS: *m/z* 364.0843 $[M+H]^+$ (calcd. for $C_{17}H_{18}NO_6S^+$ *m/z* 364.0849).

*7-methoxy-6-(4-(trifluoromethoxy)benzyl)-3,4-dihydro-2H-benzo[b][1,4]thiazine-5,8-dione 1,1-dioxide (**70**) and 6-methoxy-7-(4-(trifluoromethoxy)benzyl)-3,4-dihydro-2H-benzo[b][1,4]thiazine-5,8-dione 1,1-dioxide* (**78**): HRESIMS: *m/z* 418.0558 $[M+H]^+$ (calcd. for $C_{17}H_{15}F_3NO_6S^+$: 418.0555); *m/z* 440.0375 $[M+Na]^+$ (calcd. for $C_{17}H_{14}F_3NO_6SNa^+$ *m/z* 440.0386).

P. falciparum growth and drug susceptibility assay, cytotoxicity on HMEC-1 and THP-1, and molecular modelling: see paragraph 2.3.5 for experimental details.

In vitro effects on S. mansoni: see paragraph 2.2.5 for experimental details regarding ethical animal statements, viability effects on the different stages of the worm as well as the impairing of eggs production.

3.3 Exploring the pharmacological usefulness of meroterpenes to synthesise prenylated thiazinoquinones

My research activity during the PhD course has been also involved in the efforts to adapt the just reported synthetic procedure to the synthesis of a series of prenylated quinones and thiazinoquinones. These successful attempts took inspiration from the marine natural thiazinoquinone compound, aplidinone A (**52**, Figure 21) which has been previously reported as slightly cytotoxic on Jurkat leukaemia cell line exhibiting an IC_{50} value ~45μM [137]. Among natural metabolites, aplidinone A is a rare example of compounds endowed with a prenylated quinone moiety fused to 1,1-dioxo-1,4-thiazine ring. In fact, especially in the marine environment, most popular are the polyprenylated 1,4-benzoquinones and their corresponding hydroquinones [148-149]. These compounds, known as meroterpenes, have a wide occurrence in nature thanks to their huge structural diversity. It is worthy to be underlined that by the combination of a different number of prenyl units, many quinone compounds can arise broadening the pool of molecules belonging to this class. Often, the polyprenyl chains undergo to intramolecular reactions and consequent ring closure but also rearrangements can occur on these functionality groups giving rise to further compounds with poly- or macrocyclic structures. Alongside to this great structural diversity, meroterpenes show

also interesting biological activities mainly due to their chemical features [150-151]. The quinone scaffold is known to undergo redox cycling and, in this way, an oxidative burst is unleashed generating a huge, rapid and transient amount of ROS which are responsible of cellular damage. For this reason, quinones and hydroquinone, both natural and synthetic, found extensive application in the field of chemotherapy which is the most applied strategy for cancer treatment [148,150,151]. Additionally, from several years these fascinating group of bioactive molecules have been also subjected to a deeper investigation for cancer-preventive activity [152].

In this view, the encouraging results achieved by avarone (**45**) and avarol (**47**), glaring examples of the promising pharmacological potential of terpene-quinones/hydroquinones (see paragraphs 2.3-2.3.4 for details), the influence of length and shape of alkyl side chain of thiazinoquinone scaffold (see paragraph 3.2.2-3.2.4) against mammalian cells, and the cytotoxicity of aplidinone A (**52**, see reference 137) laid the groundwork to further explore the anticancer potential of terpene-quinones. Indeed, this work has envisaged to enlarge the synthetic chemical library of thiazinoquinones in order to further investigate the role played by heterocyclic ring and alkyl side chains on cytotoxic effects. For this reason, a small series of prenylated compounds (**87**-**90**, Figure 30) has been prepared following the previous reported procedure which is based on few and efficient synthetic steps (alkylation, oxidization and condensation via coupling with hypotaurine) and the 1,2,4-trimethoxybenzene as low-cost starting material. Then, the compounds **87**-**90** were included into screening to assess their effects on viability and proliferation of human breast cancer (MCF-7), pancreatic cancer (BxPC-3) and osteosarcoma (MG-63) cell lines [141].

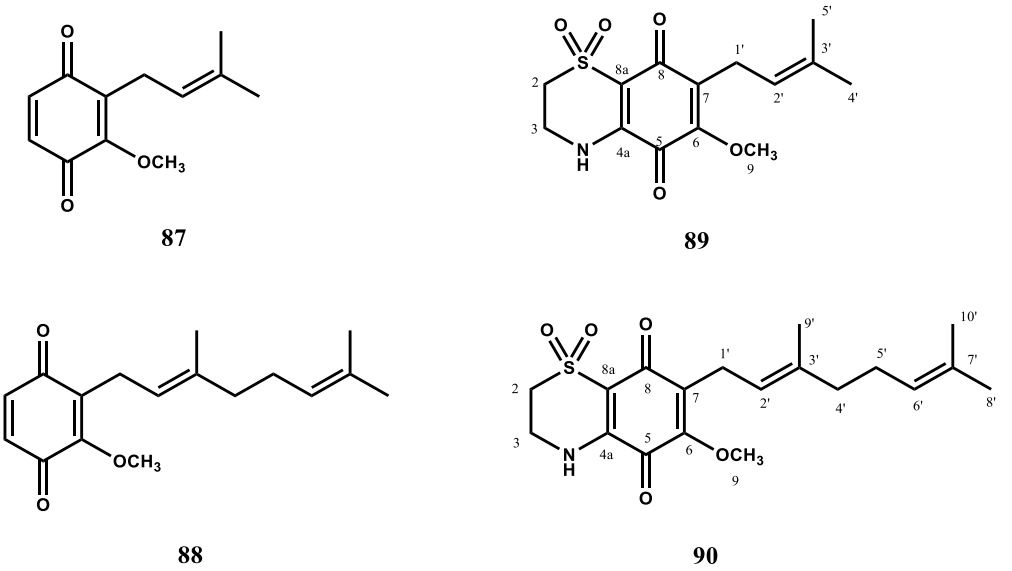

Figure 30. Structures of synthetic quinones (**87**-**88**) and thiazinoquinones (**89**-**90**) endowed with prenyl chains.

As above-mentioned, a THF solution of 1,2,4-trimethoxybenzene (**80**) was underwent to the treatment with *n*-BuLi added under argon atmosphere in an ice bath (Scheme 7). The first step allowed to generate the lithiated of 1,2,4-trimethoxybenzene that represent a good nucleophilic species able to react with a suitable allylic bromide, added subsequently. In particular, 1-bromo-3-methylbut-2-ene or (*E*)-1-bromo-3,7-dimethyl-2,6-octadiene were added to the mixture keeping at room temperature overnight the resultant mixtures. Under these conditions, the monoalkylation of aromatic ring of **80** resulted highly selective for the 3-position and the first two intermediates, **91-R$_1$** and **91-R$_2$**, were produced in high yield, too. Side products characterized by the alkylation of different positions on the aromatic ring, leading to mixtures of polyprenylated compounds, were avoid by this synthetic route with respect to the one just reported in literature [152]. In the first step, the use of *n*-butyllithium

(Scheme 7) ensured the selectivity on 3-position since the lithiated species is favoured by the presence of two methoxyl groups. Afterwards, each monoalkylated compound was oxidized with cerium ammonium nitrate which was employed always in large excess (molar ratio 4:1). The oxidation reaction with aqueous solution of CAN required to decrease the temperature since it dealt of an exothermic reaction, in fact the mixture was stirred in an ice bath to keep temperature at 0°C. In any case, the quinone compounds, **87** and **88**, were obtained in a satisfying yield (83 and 76%, respectively) with respect to another reported procedure for 3-prenylated compounds [152]. In fact, compound **88** has been already synthesise by a different chemical process and gave an overall outcome of about 45% [152], my attempts allowed to increase its total yield up to 74% and absence of polyprenylated compounds was also observed [141].

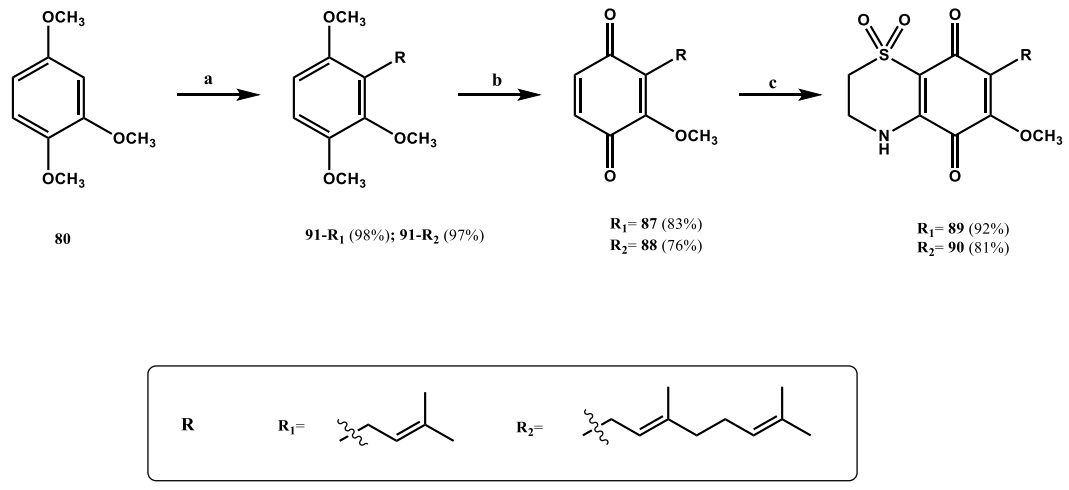

Scheme 7. Reagents and conditions: (**a**) (1) *n*-BuLi, THF, 0 °C, 1 h; **87-R1**: 1-bromo-3-methylbut-2-ene, 0 °C → rt, overnight. **87-R2:** (*E*)-1-bromo-3,7-dimethyl-2,6-octadiene, 0 °C → rt, overnight. (**b**) CAN, CH_3CN, 0 °C, 45 min. (**c**) hypotaurine, EtOH/CH_3CN, salcomine, rt, 48 h.

At this point, the conversion of the quinones **87** and **88** in the corresponding thiazinoquinone bicyclic compound, **89** and **90**, was performed by condensation with hypotaurine, and salcomine in catalyst amount (Scheme 7). At first instance, the occurrence of reaction was observed first by colour changing from yellow to orange/red, and then, by a preliminary NMR analysis on the raw material. In particular, the recorded ^{1}H NMR spectra highlighted the lack of two proton signals at δ_H 6.67 and 6.58 in **89** and of δ_H 6.67 and 6.59 for **90** which was ascribed to the fusion of quinone moiety to the dioxothiazine ring. Additionally, the condensation reaction of quinone compounds resulted to be completely regioselective even though the compounds **87** and **88** were unsymmetrical quinones. Only one of the two possible regioisomers was observed (Scheme 7), contrary to what befell for the other synthesised methoxy-thiazinoquinones (compounds **64**-**70** and **72**-**78**, Figure 23) but analogously to what occurred for the semisynthetic thiazoavarone (**46**, Figure 14) [104-106].

The main reason of this high regioselectivity might be explained by considering the greater steric hindrance exerted by prenylated chains in **87** and **88** (as well as by sesquiterpene moiety in avarone **45**) than the smaller substituent on the mentioned quinones (Schemes 5 and 6).

The thiazinoquinone compounds (**89** and **90**) have been obtained in pure state by HPLC chromatography on silica gel whereas mono- and bidimensional NMR analysis, especially HSQC and HMBC spectra, allowed to assign all proton and carbon resonances (Table 24).

Table 24. ^{1}H (700 MHz) and ^{13}C NMR (125 MHz) data[a] of compounds **89** and **90** in $CDCl_3$.

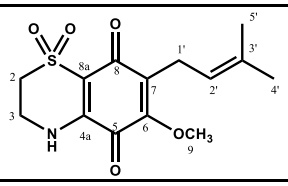

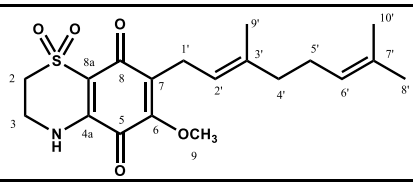

	89[a]		**90**[a]	
Pos.	δ_C	δ_H, **mult. (*J* in Hz)**	δ_C	δ_H, **mult. (*J* in Hz)**
1	-	-	-	-
2	49.0	3.29, m	49.0	3.28, m
3	39.9	4.04, m	39.7	4.04, m
4	-	-	-	-
4a	142.9	-	143.2	-
5	176.8	-	176.5	-
6	152.7	-	153.1	-
7	136.9	-	137.0	-
8	178.1	-	178.8	-
8a	110.2	-	109.8	-
9	60.8	3.91, s	61.0	3.89, s
1'	22.9	3.20, d (7.3)	22.9	3.20, d (5.5)
2'	119.1	5.04, t (7.6)	119.5	5.04, m[b]
3'	134.5	-	138.5	-
4'	17.8	1.72, s	39.9	1.93, m
5'	25.7	1.65, s	26.5	2.02, m
6'	-	-	124.5	5.04, m[b]
7'	-	-	131.8	-
8'	-	-	17.8	1.56, s
9'	-	-	16.9	1.71, s
10'	-	-	25.3	1.64, s
-NH		6.57, brs	-	6.84, brs

[a] ^{1}H NMR and ^{13}C NMR shifts are referenced to $CDCl_3$ (δ_H = 7.26 ppm and δ_C = 77.0 ppm). [b] Partially overlapped to other resonances.

Spectroscopic means and the HRESIMS data, which defined a molecular formula $C_{14}H_{17}O_5NS$ for **89** and $C_{19}H_{25}O_5NS$ for **90**, univocally determined the structure of the thiazinoquinone bicyclic moiety expect for the regiochemistry of this latter seeing as any HMBC correlation was observed between H-2 and C-8a and between H-3 and C-4a. To solve this issue, δ_H and δ_C recorded for the **89** and **90** and reported in Table 24 were compared to those predicted by theoretical means for the model compounds A1/A2 (**53**/**54**, Figure 21) [20]. The close agreement between the NMR resonances of the thiazinoquinone moiety both of **89** and **90** with the model compound A2 allowed to univocally define the regiochemistry of the bicyclic scaffold, placing the methoxyl group at same side of nitrogen atom as depicted in Figure 30.

3.3.1 Cytotoxicity assay

The synthetic series **87-90** was evaluated for the effects on viability and proliferation of MCF-7, BxPC-3 and MG-63, three different cell lines of human solid tumor. The cell viability was measured by xCELLigence system that it is a method based on a real-time analysis of cell growth by impedance measurements on the microelectronic sensors. According to this analyser, the electronic impedance resulted altered after the administration of drugs which provoke cell growth inhibition expressing the results as cell index (CI), a unit-less parameter explanatory of cell number and morphology. The biological assays envisaged to test compounds **87-90** at 10 μM for 72h with a real-time monitoring of cell proliferation alteration. The results of the effects on cell viability are reported in Figure 31 and showed that only geranylquinone **88** significantly affected the cell viability during the first 24 hours of treatment (selected time to point out subsequent investigations) and that BxPC-3 was

the most sensitive cell line. Instead, the compounds **87**, **89** and **90** that on MCF-7 and MG-63 cell lines resulted completely ineffective (Figure 32 A-C and G-I), on BxPC-3 caused only a slight reduction, approximatively 30%, of the slope of growth curve in comparison with DMSO used as control (Figure 32 D-F).

In the synthetic series, the highest antiproliferative activity was showed by the quinone **88** which revealed able to decrease the cell index within the range 50-60% at 10 μM with comparable effects on the three tested cell lines (Figure 32). Additionally, the effectiveness on mammalian cells was also demonstrated by a significant increase of cell doubling time.

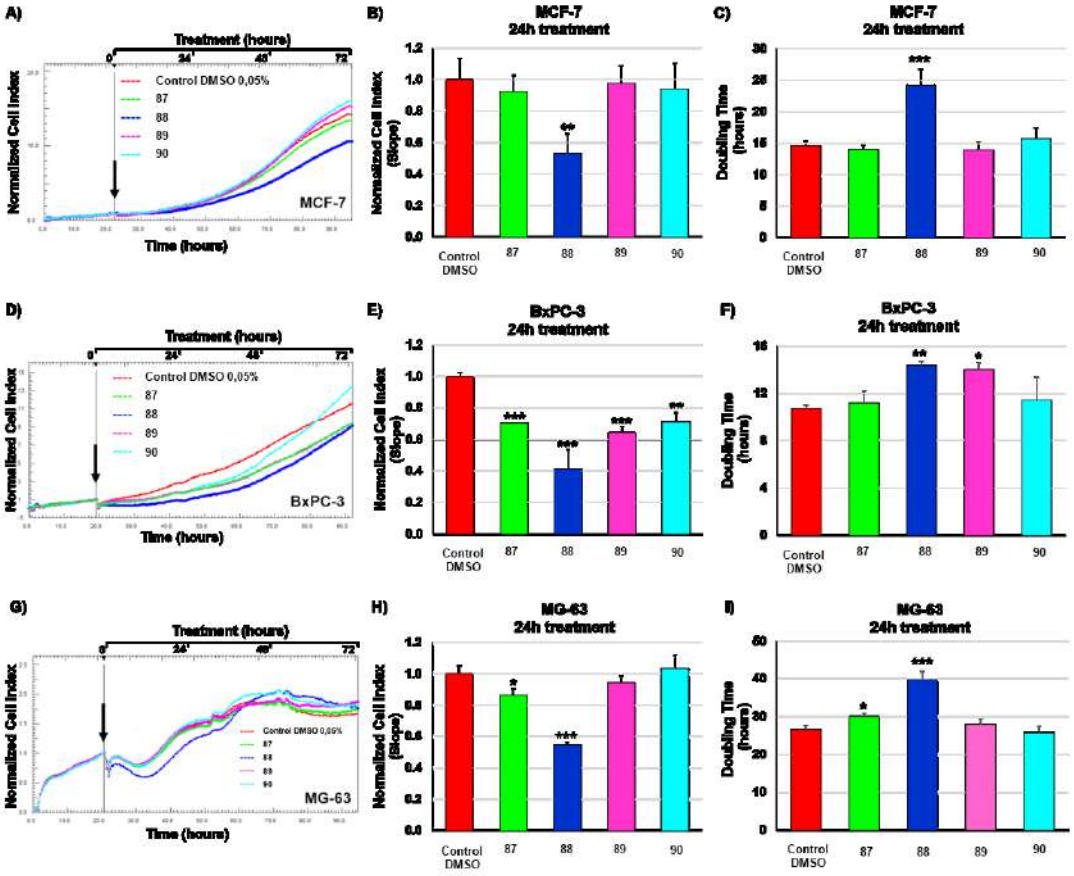

Figure 31. Real-time monitoring of cancer cell growth after treatment with compounds **87-90** at 10 µM and DMSO as vehicle (0.05%) using the xCELLigence System Real-Time Cell Analyzer. (**A**, **D**, **G**) Normalized cell index (NCI) graphics of MCF-7 (**A**), BxPC-3 (**D**), and MG-63 (**G**) cell lines treated with **87-90** and DMSO for 72 hours. The starting point of drug treatment was indicated by black arrow. (**B**, **E**, **H**) NCI changing of MCF-7 (**B**), BxPC-3 (**E**), and MG-63 (**H**) cells after 24h treatment with **87-90** and vehicle. Antiproliferative effects are reported as slope of NCI, referred to DMSO, and describe the changing rate of growth curves after drug exposure. (**C**, **F**, **I**) Doubling cell times of MCF-7 (**C**), BxPC-3 (**F**), and MG-63 (**I**) cells after 24h incubation with compounds **87-90** and 0.05% DMSO. Data are presented as mean ± SD of three independent experiments. * $p < 0.05$; ** $p < 0.01$; *** $p < 0.0001$.

Structure-relationship activity studies have been performed on the tested compounds with the aim to identify the key structural features responsible of cytotoxic effects. Notably, the length of prenyl chain strongly influenced the effects on cellular

growth because the presence of a second prenyl unit in the quinone **88** significantly increased the effects on the three cell lines with respect to compound **87**. At same time, the presence of a heterocyclic ring fused to the quinone moiety of **88**, generating the thiazinoquinone **90**, caused a dramatic reduction of its potency.

Many effective anticancer compounds are able to form covalent bonds with specific antitumor targets, e.g. the ubiquitin-proteasome pathway [153]. Thus, beyond the importance of prenyl chains (higher potency of **88** *vs* **87)**, the better antiproliferative activity exerted by geranylquinone **88** respect to the corresponding thiazinoquinone **90** might carried out by the interdiction of electrophilic sites in **90**. In fact, the conversion of the quinone moiety into related thiazinoquinone system embedded the electrophilic carbons 4a and 8a (Figure 30) into a bicyclic system forbidding the interaction with nucleophilic sites as can be the antitumor targets, decreasing so the potency.

To shed new light on the putative antiproliferative mechanism of action of the most interesting compound in the series, quinone **88**, its propensity to act either as apoptotic or cytostatic agent was investigated. To pursue this objective, the most sensitive BxPC-3 has been chosen as cell line on which perform the annexin V-FITC/PI assay and extrapolate the increase of cells death by apoptosis. The pancreatic cancer cells were incubated with different concentration of quinone **88** (5, 10 and 20 μM) for 24 h. After this time, flow cytometric detection allowed to observe that only ~11% of the treated pancreatic cells were early and late apoptotic cells and only at the highest concentration of **88** (20 μM, Figure 32). This low percentage of apoptotic cells, comparable to those obtained with DMSO as control, suggested that geranylquinone **88** has cytostatic effects and not cytotoxic.

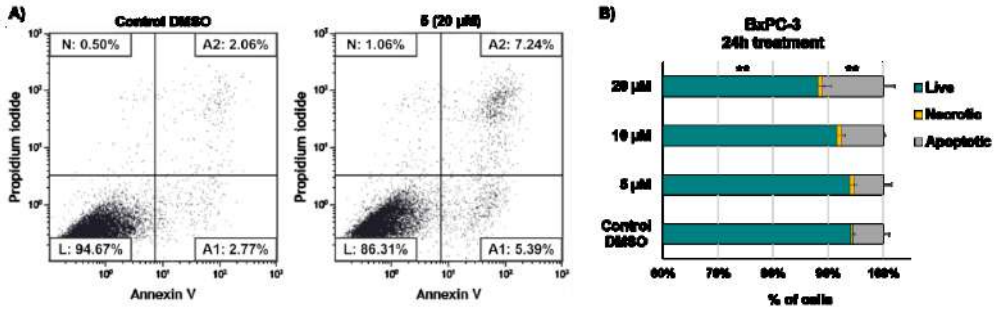

Figure 32. Flow cytometric detection of apoptosis and necrosis with Annexin-V-fluorescein isothiocyanate (FITC) and propidium iodide staining in BxPC-3 cells after 24h exposure to 5, 10 and 20 µM of **88** and DMSO vehicle. (**A**) Single representative experiment is showed as dot plots. Abbreviations: L, live cells; A1, early apoptotic cells; A2, late apoptotic cells; N, necrotic cells. (**B**) Percentage of live, necrotic, and apoptotic cells after 24h treatment with **88** at 5, 10, and 20 µM and DMSO vehicle. % apoptotic cells= sum of early and late apoptotic cells. Data are presented as mean ± standard deviation of three independent experiments. ** $p < 0.01$.

Thus, quinone compound **88** was investigated for the cell cycle arrest by flow cytometry and using the PI staining method. Cytostatic effect was demonstrated because, at concentration of 20 µM on BxPC-3 and after 24 hours incubated, the tested compound induced a significant increment of G0/G1 phase cells that resulted shifted from 45.7% to 62.8% (Figure 33).

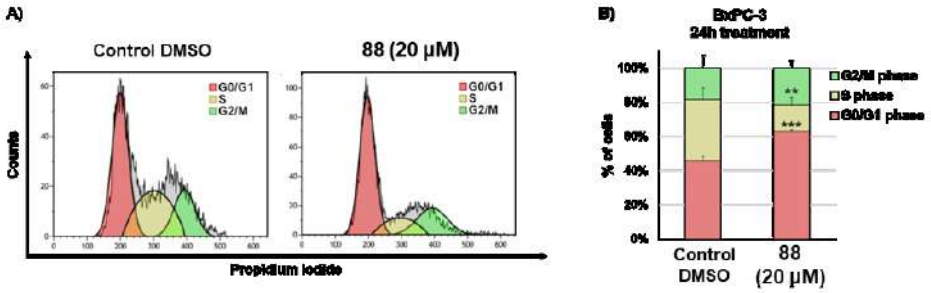

Figure 33. Cell cycle analysis through PI staining and flow cytometry of BxPC-3 cells after 24h treatment with compound **88** (20 µM)**.** DMSO is used as vehicle. (**A**) Single representative experiment described as cell cycle histogram. (**B**) Cell cycle distribution of BxPC-3 cells treated with quinone **88** (20 µM) for 24 hours. Data are presented as mean ± SD of four independent experiments. ** $p < 0.01$, *** $p < 0.0001$.

Conclusion: the synthesis and the pharmacological evaluation of compounds **87-90** have been performed. These compounds were inspired by the marine cytotoxic aplidinone A (**52**) and were prepared with the aim to further investigate the role played by prenyl units on quinone ring as well as the effects on mammalian cells of compounds in which the quinone moiety is fused with the 1,1-dioxo-1,4-thiazine ring. Following a procedure similar to that used for preparing the series of antiparasitic methoxy-thiazinoquinones, in few steps with high yield the intermediate prenylated quinones were converted into related thiazinoquinone compounds. Interestingly, contrary to the above-described compounds when prenyl substituents are placed as side chain at the quinone ring, the nucleophilic addition of hypotaurine occurred in a completely regioselective outcome leading only one regioisomer, probably due to the steric hindrance exerted by the prenyl substituent. Previously, cytotoxicity of thiazinoquinones was demonstrated to be related to the length of the side substituent

which influenced the compound uptake by passive diffusion. Here, quinones **87** and **88** as well as thiazinoquinones **89** and **90** were tested on three different mammalian cancer cells, MCF-7, BxPC-3 and MG-63, offering interesting results. In particular, only the geranylquinone **88** showed significant effects on BxPC-3 when tested at 10 μM resulting an interesting cytostatic agent able to cause cell cycle arrest in G0/G1 phase, while the sites targeted by cellular constituents were hidden by the presence of the heterocyclic system which drastically reduces the biological effects. Thus, the putative mechanism of action on specific solid tumours seems, almost in first instance, not strictly correlated to the electronic features of quinone compounds and hence remarks the importance of enhancing the efficacy of natural and synthetic prenylated compounds in the field of anticancer drug discovery.

3.3.2 Materials and methods for compounds 87-90

*Synthesis of 1,2,4-trimethoxy-3-(3-methylbut-2-en-1-yl)benzene (**91-R$_1$**) and (E)-2-(3,7-dimethylocta-2,6-dien-1-yl)-1,3,4-trimethoxybenzene (**91-R$_2$**):* as for the first intermediate of antiparasitic thiazinoquinones, the commercially available 1,2,4-trimethoxybenzene (**80**, 500 μL, 3.4 mmol) was dissolved in anhydrous THF (15 mL) and subjected to addition of *n*-BuLi solution 1.6 M (2.5 mL, 4 mmol) stirring the mixture under Ar atmosphere for 1h at 0°C. Then, using a molar ratio of 1.2:1 respect to **80**, 4 mmol of 1-bromo-3-methylbut-2-ene (470 μL) for compound **91-R$_1$** and (*E*)-1-bromo-3,7-dimethyl-2,6-octadiene (800 μL) for compound **91-R$_2$** were separately added to the obtained lithiated of **80**, stirring overnight the mixture under Argon atmosphere and increasing gradually the temperature (0°C → rt). After 12 hours passed,

a saturated solution of NaCl (30 mL) was used to quench the resultant mixtures which was subsequently extracted with diethyl ether (2 x 50 mL). The combined organic layers were dried over anhydrous sodium sulphate, filtered and concentrated under reduced pressure affording **91-R1** (787 mg, 98%) and **91-R2** (1.0 g, 97%) in a sufficiently pure state to be used in the following reaction.

*1,2,4-trimethoxy-3-(3-methylbut-2-en-1-yl)benzene (**91-R1**):* dark yellow oil; ^{1}H NMR ($CDCl_3$, 500 MHz): 6.72 (1H, d, *J*=8.9 Hz), 6.57 (1H, d, *J*=8.9 Hz), 5.23 (1H, t), 3.84 (3H, s), 3.83 (3H, s), 3.79 (3H, s), 3.39 (2H, d, *J*=7.0 Hz), 1.81 (3H, s), 1.69 (3H, s). ^{13}C NMR ($CDCl_3$, 125 MHz): 154.6, 150.5, 149.7, 133.8, 127.5, 125.3, 112.4, 108.1, 63.3, 58.8, 58.6, 28.4, 25.8, 20.4; HRESIMS: *m/z* 259.1307 $[M+Na]^+$ (calcd. for $C_{14}H_{20}O_3Na$ *m/z* 259.1305); NMR and HRESIMS spectra are reported in Chapter 6.

*(E)-2-(3,7-dimethylocta-2,6-dien-1-yl)-1,3,4-trimethoxybenzene (**91-R2**):* dark yellow oil; ^{1}H NMR ($CDCl_3$, 500 MHz): 6.73 (1H, d, *J* = 8.9 Hz), 6.58 (1H, d, *J* = 8.9 Hz), 5.24 (1H, t), 5.10 (1H, t), 3.84 (6H, s), 3.80 (3H, s), 3.41 (2H, d, *J* = 6.9 Hz), 2.08 (2H, dd, *J* = 7.5, 6.9 Hz), 2.00 (2H, m), 1.81 (3H, s), 1.67 (3H, s), 1.60 (3H, s); ^{13}C NMR ($CDCl_3$, 125 MHz): 154.9, 150.6, 149.9, 137.3, 133.6, 127.8, 127.3, 125.8, 112.3, 108.3, 63.4, 58.9, 58.5, 42.5, 29.4, 28.2, 25.6, 20.4, 18.8; HRESIMS: *m/z* 327.1942 $[M+Na]^+$ (calcd. for $C_{19}H_{28}O_3Na$ *m/z* 327.1931); NMR and HRESIMS spectra are reported in Chapter 6.

*Synthesis of 2-methoxy-3-(3-methylbut-2-en-1-yl)cyclohexa-2,5-diene-1,4-dione (**87**) and synthesis of (E)-2-(3,7-dimethylocta-2,6-dien-1-yl)-3-methoxycyclohexa-2,5-diene-1,4-dione (**88**):* a portion of the corresponding alkylated 1,2,4-trimethoxybenzene was oxidized with a large excess of CAN (molar ratio 1:4). In detail, 310 mg (1.3 mmol) of **91-R1** and 130 mg (0.43 mmol) of **91-R2** were respectively dissolved in 50 and 20

mL of acetonitrile in ice bath with the following dropwise addition of CAN solution (2.9 g, 5.2 mmol in 9 mL of water for **91-R1** and 938 mg, 1.7 mmol in 5 mL of water for **91-R2**). The resultant mixture was kept at 0°C for 45 minutes and the end of reaction was monitored by TLC on silica Gel 60 F254 plates (20 x 20.2 mm), eluting with chloroform/EtOAc 7:3 and revealing the spots by UV lamp then by spraying with 2 N sulphuric acid and heating at 120 °C. The obtained orange liquid was so diluted in 100 mL of water and extracted with diethyl ether (2 x 100 mL). The organic layer was washed with brine, dried, filtered and concentrated *in vacuo*. The solvent removal gave a crude residue that in each two case was further purified by HPLC on silica gel. In particular, the pure compound **87** (221 mg, 83%, t_R=4.9 min) was obtained by HPLC on Luna 3µm, 150 x 4.6mm column, flow rate 1 mL/min and a mixture hexane/EtOAc 9:1 (v/v) as mobile phase. The quinone **88** (80 mg, 76%, t_R=20.4) was instead achieved chromatographing the raw material on the same column but using a mobile a mixture hexane/EtOAc 98:2 (v/v).

*2-methoxy-3-(3-methylbut-2-en-1-yl)cyclohexa-2,5-diene-1,4-dione (**87**):* yellow powder; ^{1}H NMR ($CDCl_3$, 500 MHz): 6.67 (1H, d, *J* = 9.5 Hz), 6.58 (1H, d, *J* = 9.5 Hz), 5.04 (1H, t, *J* = 6.9 Hz), 4.01 (3H, s), 3.13 (2H, d, *J* = 7.3 Hz), 1.73 (3H, s), 1.66 (3H, s); ^{13}C NMR ($CDCl_3$, 125 MHz): 187.4, 183.4, 155.0, 136.8, 136.1, 134.4, 131.9, 119.4, 60.7, 25.2, 22.3, 17.5; HRESIMS: *m/z* 229.0839 $[M+Na]^+$ (calcd. for $C_{12}H_{14}O_3Na$ *m/z* 229.0835); NMR and HRESIMS spectra are reported in Chapter 6.

*(E)-2-(3,7-dimethylocta-2,6-dien-1-yl)-3-methoxycyclohexa-2,5-diene-1,4-dione (**88**):* yellow powder; ^{1}H NMR ($CDCl_3$, 500 MHz): 6.67 (1H, d, *J*=9.5 Hz), 6.59 (1H, d, *J*=9.5 Hz), 5.05 (2H, m, overlapped), 4.02 (3H, s), 3.16 (2H, d, *J*=7.3 Hz), 2.05 (2H, m), 1.96 (2H, m), 1.73 (3H, s), 1.65 (3H, s), 1.58 (3H, s); ^{13}C NMR ($CDCl_3$, 125 MHz):

δ 187.8, 183.7, 155.2, 137.1, 136.6, 134.4, 132.2, 131.3, 123.9, 119.6, 60.8, 39.5, 26.5, 25.4, 22.4, 17.7, 16.0. HRESIMS *m/z* 275.1645 $[M+H]^+$ (calcd. for $C_{17}H_{23}O_3$ *m/z* 275.1642); NMR and HRESIMS spectra are reported in Chapter 6.

*Synthesis of 6-methoxy-7-(3-methylbut-2-en-1-yl)-3,4-dihydro-2H-benzo[b][1,4]thiazine-5,8-dione-1,1-dioxide (**89**) and (E)-7-(3,7-dimethylocta-2,6-dien-1-yl)-6-methoxy-3,4-dihydro-2H-benzo[b][1,4]thiazine-5,8-dione-1,1-dioxide (**90**):* the quinone compound **87** (137 mg, 0.67 mmol) and **88** (14 mg, 0.049 mmol) were converted into relevant thiazinoquinone derivatives by biomimetic coupling with hypotaurine via nucleophilic addition. To realize this synthesis, the addressed amount of **87** was solubilized in 15 mL of a mixture EtOH/CH_3CN 1:1 (v/v) while quinone **88** in 5 mL of the same mixture. At this point, a solution of hypotaurine (66.4 mg, 0.67 mmol in 3 mL for **87** and 6.0 mg, 0.049 mmol in 500 µL for **88**) was added dropwise to dissolved quinone whereas salcomine in portion was used as catalyst of this reaction. The resultant mixtures were kept at rt for 48 h under magnetic stirring. The end of the reaction could be observed by colour changing from yellow to orange/red and by TLC. The solvent removal *in vacuo* afforded a crude material that was dissolved in water (60 mL) and extracted with diethyl ether (3 x 60 mL) was performed. Afterwards, the organic phase was washed with NaCl solution, dried over Na_2SO_4, filtered and concentrated by rotary evaporator. The pure thiazinoquinones **89** and **90** were purified by the respective raw material by HPLC on silica gel (Luna 3µm column, 150 x 4.6 mm, flow rate 1 mL/min) and mobile phase hexane/EtOAc 1:1 (v/v) affording **89** (190 mg, 92%) and **90** (15.1 mg, 81%).

*6-methoxy-7-(3-methylbut-2-en-1-yl)-3,4-dihydro-2H-benzo[b][1,4]thiazine-5,8-dione-1,1-dioxide (**89**):* slight orange powder; HRESIMS: *m/z* 312.0909 $[M+H]^+$ (calcd.

for $C_{14}H_{18}O_5NS$ *m/z* 312.0901); *m/z* 334.0728 $[M+Na]^+$ (calcd. for $C_{14}H_{17}O_5NSNa$ *m/z* 334.0720); ^1H and ^{13}C NMR data are reported in Table 24; NMR and HRESIMS spectra are reported in Chapter 6.

(*E)-7-(3,7-dimethylocta-2,6-dien-1-yl)-6-methoxy-3,4-dihydro-2H-benzo[b][1,4]thiazine-5,8-dione-1,1-dioxide (**90**):* slight orange powder; HRESIMS *m/z* $[M+H]^+$ calcd. for $C_{19}H_{26}O_5NS$: 380.1526, found 380.1519; HRESIMS: *m/z* 402.1337 $[M+Na]^+$ (calcd. for $C_{19}H_{25}O_5NSNa$ *m/z* 402.1346); ^1H and ^{13}C NMR data are reported in Table 24; NMR and HRESIMS spectra are reported in Chapter 6.

Cell cultivation and antiproliferative assays

American Type Culture Collection (ATCC, Manassas, VA, USA) was the supplier of MCF-7, BxPC-3 and MG-63 cells. The medium used to cultivate MCF-7 and MG-63 was DMEM, while BxPC-3 cells were cultivated in RPMI medium, at 37°C and a 5% CO_2. Both medium were supplemented with 10% fetal bovine serum, penicillin-streptomycin (100 U/mL), and 2 mM L-glutamine. Cell morphology was monitored by inverted optical microscope and 0.05% trypsin-EDTA allowed to detach cells to perform *in vitro* assays. Antiproliferative assays were performed by using the *xCELLigence* System Real-Time Cell Analyzer (ACEA Biosciences, San Diego, CA, USA) [154]. MCF-7 cells were seeded at a cell density of 3000 cells/well, BxPC-3 at 2500 cells/well, and MG-63 cells at 4000 cells/well. Approximately 24 h after seeding, 10 μM of compounds **87-90** and 0.05% DMSO as vehicle were added to cancer cells and treated for 72 hours. The results were expressed as normalized cell index (NCI) values obtained just before drug treatment and it was meant as $NCI = CI_{\text{end of treatment}}/CI_{\text{normalization time}}$. Real-time NCI proliferation curves were generated through the Real-Time Cell Analyzer (RTCA)-integrated software. The effects on cellular growth of

compounds **87-90** are expressed either as cell index slopes relative to controls with DMSO or as cell doubling times. These parameters were calculated using the RTCA-integrated software within a 24-hour time window.

Apoptosis assay and cell cycle analysis

BxPC-3 cells were treated with different concentration of compound **88** (5, 10, and 20 μM). After treatment BxPC-3 cell line was stained with annexin-V-fluorescein isothiocyanate (FITC) and propidium iodide, using the FITC Annexin V Apoptosis Detection kit I (Becton Dickinson, BD, Franklin, NJ, USA) for flow cytometric detection of apoptotic and necrotic cells. As for cell cycle analysis, BxPC-3 cells were treated with 20 μM of **88** for 24 h, then the cells were permeabilized with 70% cold EtOH (1 h) and stained for 30 minutes with a solution of 50 μg/mL propidium iodide (Sigma Aldrich, St. Louis, MO, USA) and 10 μg/mL RNase A (EuroClone S.p.A., Milan, Italy) in calcium and magnesium-free PBS. Four independent experiments were carried out analysing the samples by Kaluza software (Beckman Coulter) and acquiring 10,000 events for each sample.

Statistical analysis

Data represent the mean (±SD) of at least three independent experiments. The one-way analysis of variance (ANOVA) method was applied to compare means of more than two groups and Dunnett's method was used as post-hoc test to compare multiple groups versus a control group. Two-group comparisons were performed using Student's t-test. P-values <0.05 were considered to be statistically significant. Statistical analysis was performed using the GraphPad Prism Software Version 5.

CHAPTER 4

Challenges in the configuration assignment of natural products

4.1 Application of several tools for stereochemical assignment of natural products

Above the 80% of both terrestrial and marine natural products are chiral and most of them have multiple chiral centers [155]. The chirality is ubiquitous in the nature as demonstrated by the fact that peptides, carbohydrates and nucleic acids, three of main biological natural metabolites classes, have several unsymmetrical centers which are strictly involved into interaction with cellular receptors and enzymes. Indeed, even though in living matters mixtures of enantiomers are produced, generally one only stereoisomer is responsible of bioactivity by stereoselective interaction with the cellular biological pattern [156]. Accordingly, the isolation of new natural metabolite requires that the elucidation of planar structure is always accompanied by a complete stereochemical assignment which includes the determination of its relative and absolute configuration. Stereochemical assignment, especially for natural products, represents a demanding work for the chemists worldwide since it has to take into consideration the reduced availability of the substrate and that any information is known, except for possible common biogenetic characteristic with structurally related compounds [157-158]. Furthermore, few micrograms are sufficient to shed light on the planar structure of novel natural compounds while more efforts, in term of costs and man-hours, are required for the configurational analysis needing a carefully data acquisition on a case-by-case basis [159].

In this view, an important period of my PhD course has been involved in solving the issue of stereochemical assignment of a recently isolated marine natural acyclic and polysubstituted polyketide, named phosphoeleganin (**92**, Figure 34), isolated from the Mediterranean ascidian *Sydnium elegans*. The stereostructure elucidation of this compound has represented a hard challenge in the field of natural products chemistry since the so much flexible skeleton of phosphoeleganin and the presence of five chiral centers required many integrated approaches with a rigorous acquisition of data by the combination of different tools [160-161]. Chemical degradation and manipulation of the marine polyketide together with chiral derivatizations applied to an extensive use of the 1D and 2D NMR spectroscopy allowed to assign the absolute configuration at C-8, C-15 and C-16 as well as the relative configuration of the diol C-11/C-12 leading to two alternative stereostructures, defined as 8*S*, 11*S*, 12*R*, 15*S*, 16*R* and 8*S*, 11*R*, 12*S*, 15*S*, 16*R* which diverged for the absolute configuration at C-11 and C-12 [160]. Hence, my research activity was focused on the completing of absolute configuration assignment of **92** determining the univocal stereostructure depicted in Figure 34 [161]. Aiming by this purpose, further chemical chiral derivatizations on **92** were avoided due to the low availability of the natural metabolite. Thus, my work has rather returned to the synthesis of diastereoisomeric model compounds with known stereochemistry in order to apply the logic envisaged by the Universal NMR Database (UDB) concept [162-163]. This innovative method allowed to assign the absolute configuration to a great number of complex, acyclic and hydroxylated polyketides by the comparison of NMR parameters of models reported into database and experimental δ_H and δ_C data. In this case, the absence of suitable compounds which might mimic the C-8/C-12 stereocluster of phosphoelaganin (**92**) inspired the synthesis of the 8,9-*anti* stereoisomers of the

tetradecane-5,8.9-triol necessary to apply the UDB concept and complete the stereostructure of phosphoeleganin [161].

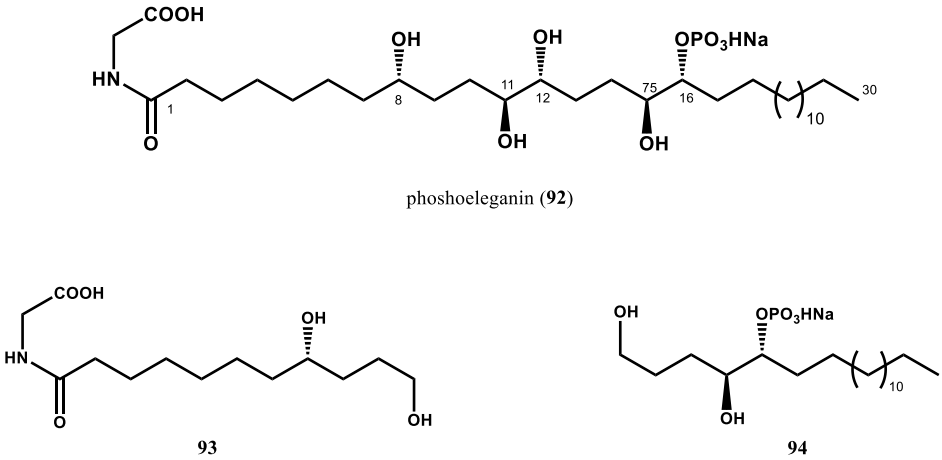

Figure 34. Structure of phosphoeleganin (**92**) and its fragments **93** and **94** obtained by oxidative cleavage with periodic acid HIO_4.

Additionally, an active collaboration with the Shanghai Institute of Materia Medica at Chinese Academy of Sciences enabled evaluation of the pharmacological properties of **92** alongside to its two fragment compounds (**93** and **94**, Figure 34). All three compounds showed no cytotoxicity on the tested mammalian cells but interesting inhibitory effects on the human protein tyrosine phosphatase 1B with the whole molecule **92** moderately more active than the two related fragments [160]. To further explore the role of simplified analogues of **92** on the tyrosine phosphatase 1B, I'm still involved in the building of a rationalized chemical library of polyoxy-, polyacetoxy- and even phosphorylated compounds to assess the potential of this chemical class as well as to discover putative pharmacophore sites against the PTP1B. Moreover, the importance of small fragments with known stereochemistry, as support to the

configurational assignment strongly encourages the broadening of this kind of NMR database with novel classes of compounds by using organic synthesis.

4.2 Toward the application of UDB concept

Stereochemical elucidation is a significant challenging topic that can be achieved by different techniques such as NMR, X-ray diffraction o crystallography, chiroptical methods as well as synthetic approach. Undoubtedly, NMR spectroscopy currently represents the main instrument which allows to assign relative and absolute configuration considering its various advantages such as the availability of instruments in most laboratories and the feasible recovering of the small amount utilised. Primarily, relative configuration of small molecules featuring rigid moieties into their structures is efficiently assigned by the analysis of homonuclear correlation constants ($^{3}J_{H,H}$) and NOE effects. Nevertheless, most of natural products are characterized by flexible and acyclic structures which give rise to a more complicated elucidation. In these cases, Murata method focused on the *J*-based configurational analysis, in particular, on the measurement of $^{2,3}J_{C,H}$ and $^{3}J_{H,H}$ by NMR experiments (HETLOC, HSQC-TOCSY, and phase sensitive HMBC as main) allows to solve the issue of relative configuration assignment just in stereocenters with 1,2 or 1,3 relative position on an acyclic moiety since this approach is based on short-range interactions [164]. However, its applicability to flexible structures is still limited. On the other hand, once the relative configuration is established, the use of chiral derivatizing agents (CDAs), likewise α-methoxyphenylacetic acid (MPA), 9-anthrylmethoxyacetic acid (9-AMA) Boc-phenylglycine (BPG), and α-methoxy-α-(trifluoromethyl)phenylacetic acid (MTPA), permits to assign the absolute configuration of unknown compounds by converting a

pure stereoisomer into two diastereoisomeric compounds thanks to chiral auxiliary reagents and calculating the chemical shifts differences ($\delta\Delta$) among the two diastereoisomers. At this point, the $\delta\Delta$ distribution around the chiral center is compared to an appropriate empiric model allowing to assign the absolute configuration [165].

To avoid limitations of Murata method and also the chemical manipulation of the natural metabolite, quantum mechanical calculations and the use of synthetic model compounds for comparative studies of NMR parameters are becoming powerful tools in the field of stereochemical assignment. In the first case, QM calculations take advantage of complex mathematical equations in order to predict the NMR parameters (δ_H and δ_C) and the *J*-coupling constants of suitable candidates. Subsequently, these calculated values are compared with those experimentals for the evaluation of their fitting to accept or reject the proposed stereostructures [166-167].

Instead, regarding the studies based on the comparison of NMR resonances between natural products and libraries of synthetic compounds with known stereochemistry, a great contribution in the development of this successful approach arises from a database of spectroscopic information proposed by Kishi and co-workers, known as UDB-NMR [162-163].

From several years, Kishi and colleagues got strongly involved into structural and stereostructural elucidation of natural and synthetic polyketides as well as marine toxins. In these works, they observed that structural properties of a compound depend on specific stereochemical rearrangements of the substituents on carbon backbone and these are not dependent from the rest of the molecule. Hence, acyclic, polysubstituted and conformationally flexible natural products featuring many chiral centers may be considered as composed of several stereogenic clusters which are independent from

each other when separated by two or more methylene groups. Accordingly, the relative and, then, absolute configuration of each stereogenic cluster can be assigned through the comparison of its protonic and carbon NMR resonances with those of model compounds with known stereochemistry displaying the same connectivity [162-163]. On this basis, Kishi's group compilated an NMR database through synthetic efforts to produce stereochemical motifs endowed with the most common functionality groups by contributing to solve the problem of stereostructures of newly discovered polyols and polyacetoxy-compounds without degradation and/or chiral derivatization of the substrate.

4.3 Completing the absolute configuration assignment of phosphoeleganin by combined approaches

The combination of different methods as NMR analysis, organic synthesis and the fruitfulness of chiral derivatizing agents with a rigorous data acquisition led to the unequivocal determination of the whole stereochemistry of the natural phosphorylated polyketide, phosphoeleganin (**92**), depicted as 8*S*, 11*S*, 12*R*, 15*S*, 16*R* (Figure 34). This approach was executed in order to assign the absolute configuration of the last two stereocenters, C-11 and C-12, in the natural metabolite through the application of the UDB concept proposed by Kishi [162-163]. Accordingly, the C-8/C-12 stereocluster of phosphoeleganin (**92**) was taken into account searching suitable diastereoisomeric model compounds into UDB-NMR database since previous work allowed to determine the absolute configuration at C-8 as *S* and a relative configuration as *anti* at 1,2-diol system (C-11/C-12) [160]. Unfortunately, any appropriate compound with known

stereochemistry and same connectivity of C-8/C-12 stereocluster of **92** has been found in the database to execute comparative studies of NMR resonances. Hence, the synthesis of the 8,9-*anti* stereoisomers of tetradecane-5,8,9-triol was necessary in developing a synthetic scheme starting from the (*Z*)-4-decenal (**95**) as starting material. The whole synthesis of model compounds is reported in Scheme 8 and envisaged to convert the compound **95** to (*Z*)-tetradec-8-en-5-ol (**96**) as racemic mixture via coupling with *n*-BuLi in a THF solution at 0°C. Subsequently, the dihydroxylation reaction of compound **96** using OsO_4 1% in a mixture of acetone/water 9:1 and 4-methylmorpholine *N*-oxide (NMO), followed by HPLC separation on reversed phase of the reaction raw material, afforded two diastereoisomeric mixtures (***rac*-97** and ***rac*-98**) as racemate of the four desired stereoisomers.

The stereochemical assignment of these compounds required first to separate into individual compounds both diastereoisomeric mixtures, and then to apply Riguera method based on the double derivatization by the use of CDAs [168-170]. Riguera's group proposed an appealing approach to the problem of determining absolute configuration of the acyclic *sec*/*sec*-1,*n*-diols by chiral derivatization and NMR spectroscopy [168-170]. The method envisaged to use the two enantiomers, *R* and *S*, of an appropriate chiral derivatizing agent and to calculate the chemical shift differences ($\delta\Delta^{RS}$ or $\delta\Delta^{SR}$) between the two diastereoisomeric compounds considering the shielding and deshielding effects that the CDAs exerted on the chemical shift values. According to an appropriate empiric model, the coherent distribution of $\delta\Delta$ signs (positive and negative) around the stereogenic carbon allowed to deduce the absolute configuration for the stereocenter. Additionally, Riguera *et al.* demonstrated that when MTPA esters are prepared, a loss of confidence in the assignment is observed whereas a more

homogenous sign distribution is observed with MPA derivatives. Therefore, α-methoxyphenylacetic acid is currently considered the CDA of choice [169].

In this regard, each mixture (***rac*-97** and ***rac*-98**) was treated with three equivalents of the *R*-α-methoxyphenylacetic acid to afford two mixtures of the *tris*-*R*-MPA esters (**97a**/**97b** and **98a**/**98b**) that were separately chromatographed by HPLC on SiO_2 column affording the four triester derivatives in pure form (Scheme 8).

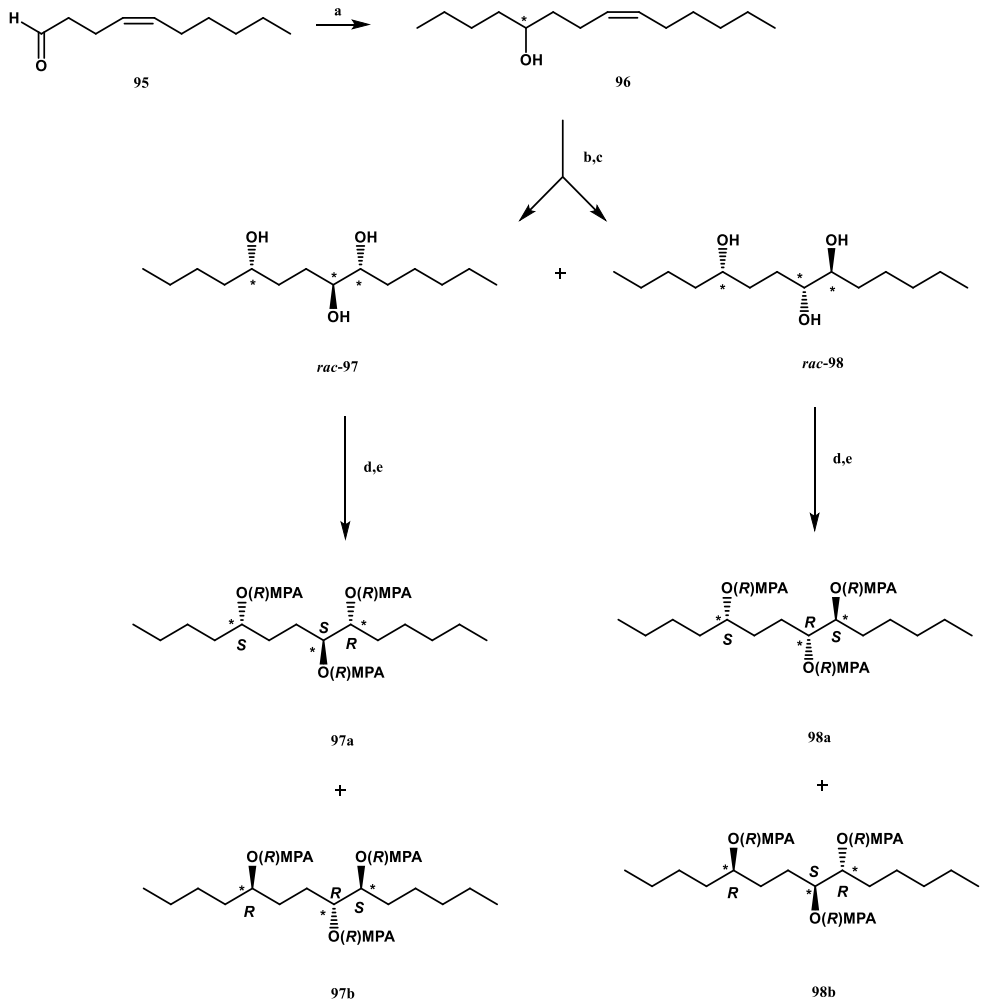

Scheme 8. Reagents and conditions: (**a**) *n*-BuLi, anhydrous THF, −78 °C (10 min), rt (8 h); (**b**) NMO, 1% OsO_4, acetone/H_2O 9:1, rt, overnight; (**c**) HPLC on reversed phase, Luna C-18 10 µm, MeOH/H_2O. (**d**) EDC, DMAP, (*R*)-MPA, CH_2Cl_2, rt, overnight. (**e**) HPLC on SiO_2, Luna 3 µm column, hexane/EtOAc 85:15 v/v.

Following this approach, the $\delta\Delta^{RS}$ for the couple **97a**/**97b** and **98a**/**98b** have been calculated in order to establish the relative configuration for C-8/C-11 portion and subsequently the absolute configuration of each stereoisomer. It is worthy to be mentioned that in the analysed case, it was not necessary perform the derivatization with both *R* and *S* enantiomers of MPA (double derivatization). Indeed, the *S*-MPA derivative of compound **97a** is the enantiomer of *R*-MPA derivative of **97b**, as well as occurs into couple **98a**/**98b**, and consequently, their NMR resonances are identical. The evaluation of signs distribution of $\delta\Delta$ in the couple **97a**/**97b** and **98a**/**98b**, in comparison with the trend of values reported by Riguera for the acyclic *sec*/*sec*-1,4-diols (Figure 35) [170], allowed to determine a 5,8-*anti* relative configuration in the compounds **97a** and **97b**, whereas a *syn* configuration for the same fragment in the compounds **98a** and **98b**.

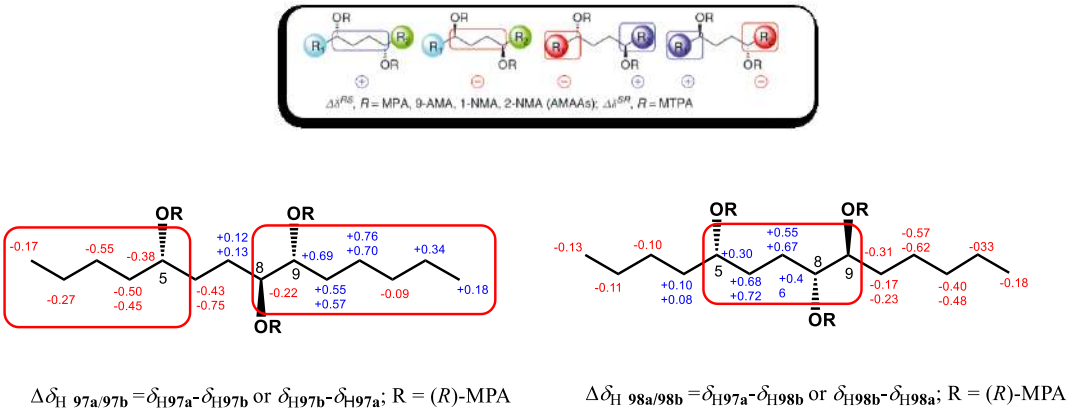

Figure 35. Pattern of $\delta\Delta_H$ sign distribution for the *tris*-*R*-MPA esters for the pairs **97a**/**97b** and **98a**/**98b** according to Riguera's model.

As shown in Figure 35, it has been observed that the signs distribution of $\delta\Delta$ values was not perfectly homogenous due to the anisotropic effects of MPA units too close to each other that influenced the δ_H values of diagnostic protons. Despite Riguera approach might be deemed acceptable small anomalies in the $\delta\Delta$ distribution, the relative configuration of C-5/C-8 portion of the synthesised triesters (and accordingly, the absolute configuration of each compound) was substantiated by a one-pot stereoselective synthesis of a tetrahydrofuran ring via *in situ* cyclic ortho esters [171].

This reaction required to obtain the enantiomerically pure (5*S*, 8*S*, 9*R*)- and (5*S*, 8*R*, 9*S*)-tetradecan-5,8,9-triol (**99** and **100**) by base-catalysed methanolysis of compounds **97a** and **98a**, respectively (Scheme 9). After the hydrolysis conducted with sodium hydroxide, the pure triol **99** was dissolved in dichloromethane and subjected to addition of trimethyl orthoacetate which led to the formation *in situ* of the cyclic ortho ester **101**. By this one-pot synthesis, BF_3 allowed to ionize the intermediate **101** generating an acetoxonium species in which the hydroxyl group placed at C-5 displayed an intramolecular nucleophilic displacement to C-8 obtaining the cyclic ether **102**. Analogously, the triol **100** proceeded the same chemical treatment generating the ether **103** (Scheme 9).

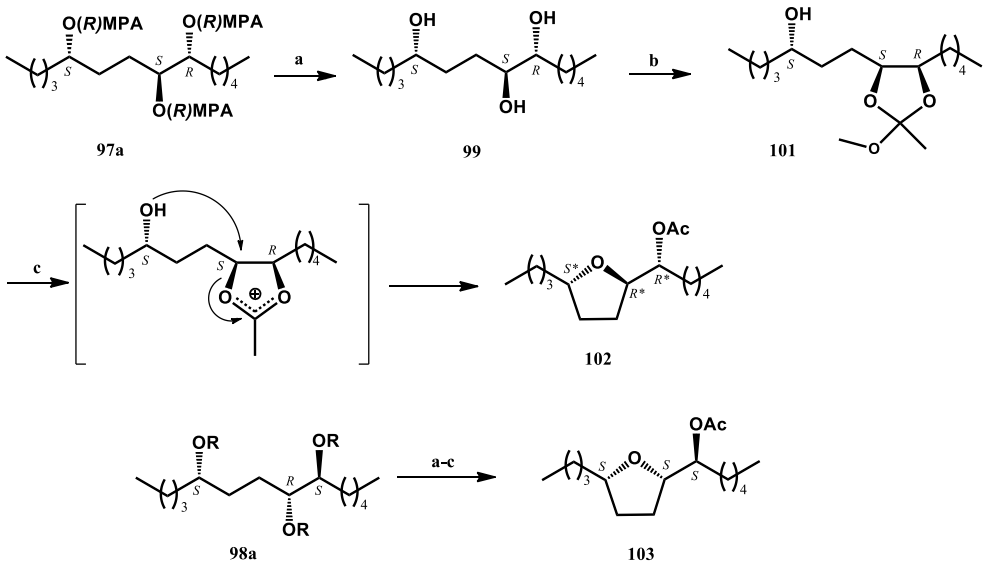

Scheme 9. Reagents and conditions: (**a**) NaOH, MeOH, r.t., overnight (**b**) $MeC(OMe)_3$ (1.2 equiv), PPTS (0.1 equiv), CH_2Cl_2, 15 min., r.t.; (**c**) BF_3•Et_2O (0.1 equiv), 0°C, H_2O/Acetone 9:1.

The analysis of constant dipolar couplings recorded by ROESY experiments executed on the ethers **102** and **103** shed light on the *trans* and *cis* relationship within the tetrahydrofuran ring. In fact, only in the case of ether **103**, deriving from the putative 5*S*, 8*R*, 9*S* model compound **100**, a strong ROE correlation was detected between H-5 and H-8, while no correlation was observed in the ROESY spectrum of compound **102** (Figure 36).

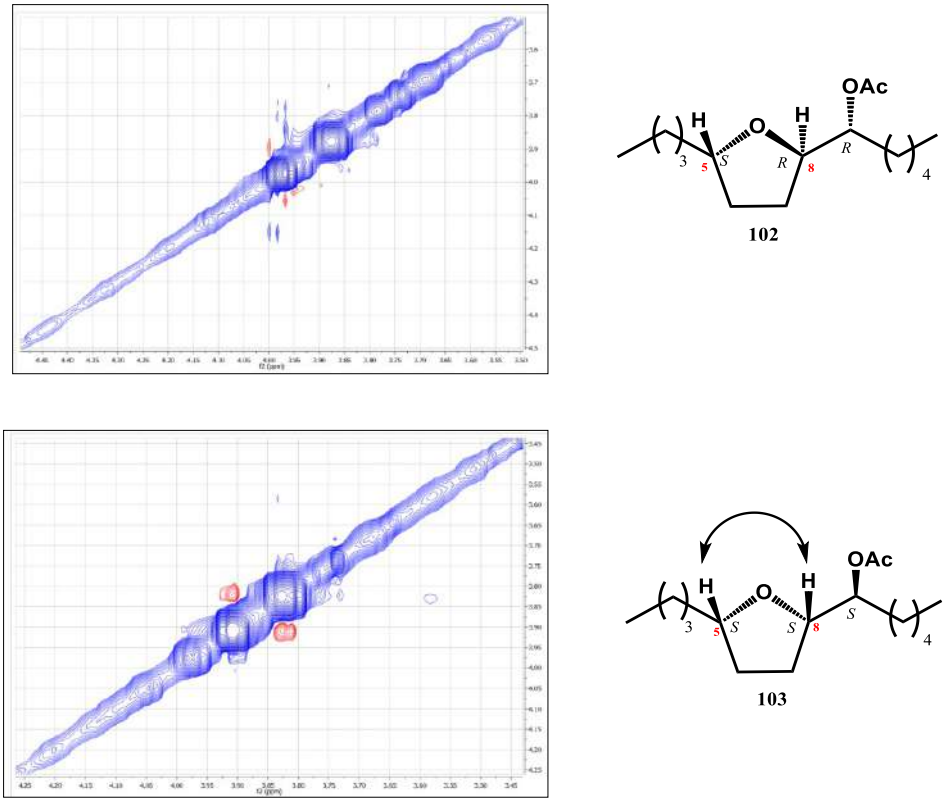

Figure 36. Enlargement of 2D ROESY spectra of compounds **102** and **103**.

Thus, a *cis* relationship was assigned across the compound **103** while the ether **102** showed a *trans* tetrahydrofuran ring. The 2D NMR key correlations alongside the stereochemical outcome of the one-pot cyclization reaction, in which the configuration at C-8 is inverted after the nucleophilic displacement, agreed with the patterns of sign distribution previously described through Riguera's approach confirming the stereochemical assignment showed in Figure 35 and Scheme 8. Therefore, an absolute configuration 5*S*, 8*S*, 9*R* and 5*S*, 8*R*, 9*S* were unequivocally and univocally assigned to compound **99** and **100**, respectively.

According to the UDB concept based on the comparison of δ_H and δ_C of diastereoisomeric model compounds with known stereochemistry and those of stereoclusters in natural polyketides with unknown stereochemistry, protonic and carbon chemical shifts of **99** and **100**, used as models, were compared with those of the C-8/C-12 fragment of **92** (Figure 37).

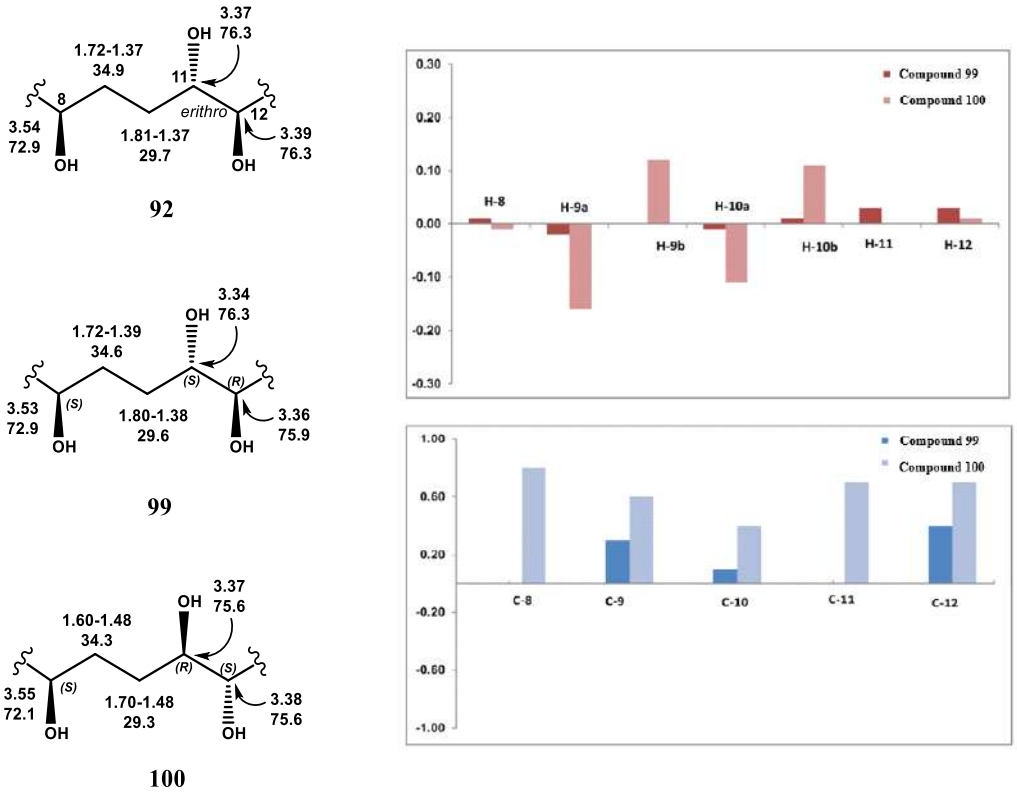

Figure 37. Comparison of δ_H and δ_C between **92**, **99** and **100** together with $\Delta\delta_H$ *(*$\delta_{H\ 92}$ - $\delta_{H\ 99\ or\ 100}$**)** and $\Delta\delta_C$ *(*$\delta_{C\ 92}$ - $\delta_{C\ 99\ or\ 100}$**)**.

From this evaluation (Figure 37), a close correlation between the chemical shifts of compound **99** and the stereocluster of **92** was depicted as confirmed by values of mean absolute error (MAE: ^{13}C = 0.16; ^{1}H = 0.02 for compound **99** *vs* ^{13}C = 0.64 and ^{1}H = 0.07 for compound **100**).

Finally, the *anti*-configuration at fragment C-8/C-11 of phosphoeleganin (**92**) was defined and, together with the known configuration at C-8 as *S*, allowed to definitely assign the absolute stereochemistry at C-11 and C-12 resulted to be *S* and *R*, respectively. Hence, the stereostructure of the phosphorylated marine polyketide **92** was unequivocally completed by the combination of organic synthesis for diastereoisomeric compounds and the application of the logic of UDB.

4.4 Design and synthesis of simplified analogues of phosphoeleganin

The reliability and usefulness of UDB-NMR database for stereochemical assignment of acyclic polyols is out of the question. In this view, Kishi and co-workers have been involved in the creation of different kind of NMR data collections based first on all the possible diastereoisomers of an unknown compound achieved by synthesis, and then, on the assembling of chemical shift and spin-coupling constant profiles [162,163,172]. In the aim to enlarge the chemical classes of compounds included into NMR database, acetylated and phosphorylated polyols (**104**-**106**, Figure 38) have been designed and prepared up to now starting from the (5*S*, 8*S*, 9*R*)-tetradecane-5,8,9-triol (**99**, Scheme 9), previously synthesised and characterized by NMR. In fact, these mentioned functionality groups widely occur in many natural polyketides, so synthetic model compounds with known stereochemistry might get easier the protocol of stereostructural determination.

Additionally, phosphoeleganin (**92**) and its degradation products (**93** and **94**, Figure 34) demonstrated to be active against human protein tyrosine phosphatase 1B and the natural polyketide **92** resulted more effective than the two fragments (IC_{50} (**92**)= 11 μM;

IC_{50} (**93**)= 24 μM; IC_{50} (**94**)= 28 μM). Considering that also the two fragments of **92** preserved good effects against PTP1B, these pharmacological results encouraged the possibility to investigate the biological properties of simplified analogues of the natural marine polyketide since they might contribute to discover structural requirements essential for the bioactivity.

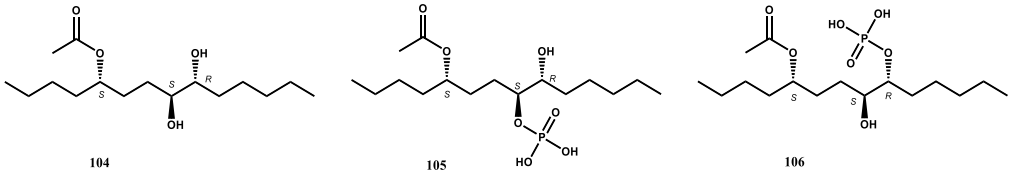

Figure 38. Structure of compounds **104-106** designed from (5*S*, 8*S*, 9*R*)-tetradecane-5,8,9-triol (**99**).

Phosphorylation and dephosphorylation events of regulatory and signalling proteins involved into cellular communication and homeostasis are monitored by the coordinated action of protein tyrosine kinases and phosphatases. The dysregulation of phosphorylation status of amino acids in proteins within the cells is closely related to onset of diabetes, cancer, neurological and metabolic disorders as well as autoimmune syndromes [172-177]. Even to the past two decades, PTKs inhibitors were the most involved compounds in the drug discovery programs but, nowadays, the understanding of phosphatases biological role has demonstrated that the aberrant activity of PTPs is linked to countless diseases [177]. Among these enzymes, PTP1B is the most studied isoform since it is involved in the insulin signal regulation. Alteration in the functionality of PTP1B implicates a persistent dephosphorylation of insulin receptor causing insulin-resistant and onset of type II diabetes. Thus, these discoveries have highlighted the PTP1B as interesting therapeutic target [173,176,178].

On this basis, the enantiomerically pure triol **99** has been used to prepare several simplified analogues of the marine metabolite that are going to be used as support in the configurational analysis of polyketides and evaluated for the effects against the PTP1B at the Institute of Materia Medica (Shanghai).

The synthetic route is reported in Scheme 10 and consisted in a series of highly efficient reactions. Firstly, the triol **99** is dissolved in 2,2-dimethoxypropane with a catalytic amount of *p*-toluenesulfonic acid keeping the mixture under magnetic stirring overnight. The resultant mixture was quenched with a saturated solution of $NaHCO_3$ and the solvent removal afforded the acetonide intermediate **107** sufficiently pure for the subsequent synthetic step. In fact, compound **107** was directly treated with acetic anhydride in pyridine as solvent and the mixture was stirred at rt overnight. After this time, the mixture was cooled and subjected to addition of MeOH before removing the solvent *in vacuo*. The procedure resulted efficient because afforded compound **108** in high outcome and so **108** underwent the hydrolysis of acetonide group in acid environment yielding compound **105** in pure form.

At this point, the acetylated polyol **105** was converted into phosphate monoesters by a phosphorylation reaction by one-pot method. From many years, this reaction is in-depth performed since the introduction of a phosphate group on a carbon skeleton can widely modify the pharmacokinetic and pharmacodynamic properties of a molecule. Moreover, several inconvenient as the formation of pyrophosphates as side products and/or the need to use a great excess either of the substrate or the phosphorylation reagent were intrinsic to the proposed protocols [179]. An improvement of the results was achieved by a one-pot method which increase the yield of phosphate monoesters and avoid the production of pyrophosphates [180].

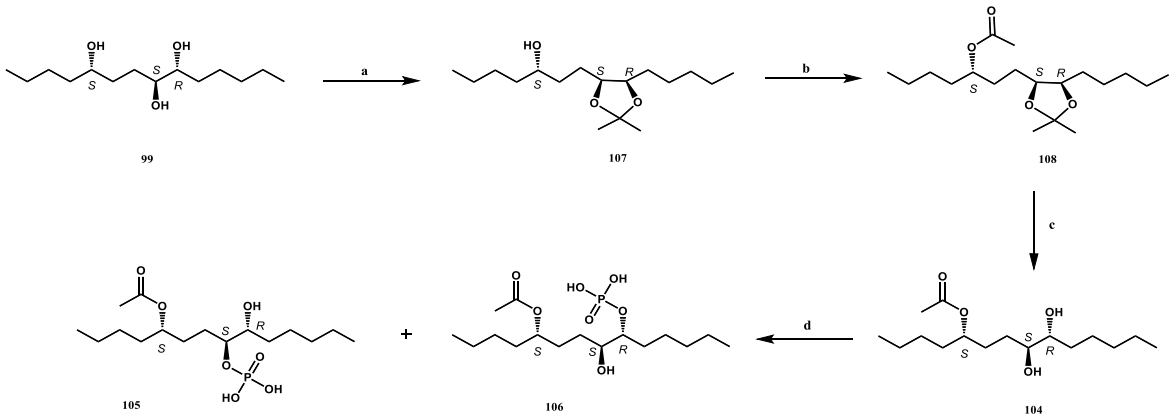

Scheme 10. Reagents and conditions: (**a**) 2,2-dimethoxypropane, *p*-toluenesulfonic acid, rt, overnight. (**b**) Ac_2O, pyridine, rt, overnight. (**c**) HCl 1%, MeOH/H_2O 9:1, rt, overnight. (**d**) (1) Cl_3CN; (2) $(n\text{-Bu})_4NH_2PO_4$, CH_3CN, rt, 2h.

The straightforward method starts from the commercially available tetrabutylammonium dihydrogen phosphate which reacts with trichloroacetonitrile giving rise to a mixed anhydride-like activated phosphate, i.e. the trichloroacetimidate. The latter is subjected to nucleophilic attack by the hydroxyl group of the alcohol yielding the corresponding phosphate monoester and trichloroacetamide (Scheme 11), according to the mechanism proposed by Lira *et al.* [180].

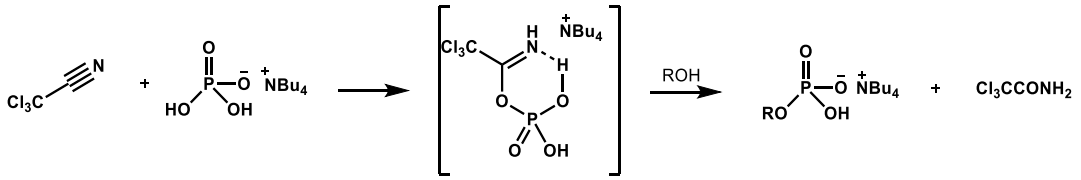

Scheme 11. Proposed mechanism for the formation of phosphate monoesters *via* reactive mixed anhydride.

As reported into Scheme 11, compound **104** is dissolved in acetonitrile and trichloroacetonitrile is added to mixture. Subsequently, tetrabutylammonium dihydrogen phosphate in acetonitrile is slowly added and the resultant mixture is stirred for 2 h at rt. After solvent removal under N_2, the raw material is chromatographed by HPLC on reversed phase eluting with MeOH/H_2O 75:25 with 0.1% TFA collecting a fraction constituted by the mixture of compounds **105** and **106**. Thus, the two phosphorylated compounds **105** and **106** were obtained in pure form by a further HPLC (MeOH/H_2O 6:4 + 0.1% TFA).

All compounds have been completely characterized by NMR spectroscopy and HRESI mass spectrometry in order to unequivocally define the whole structure and distinguish among the structural isomers. In particular, ^{1}H-^{1}H correlations recorded in COSY and TOCSY experiments permitted to assign the whole spin system, whereas diagnostic peaks in HSQC and HMBC defined the correlation between protons and heteronuclei, building up the skeleton of each molecule. The ^{1}H and ^{13}C NMR chemical shifts of compounds **104-106** are reported in Table 25.

Table 25. ^{1}H (700 MHz) and ^{13}C NMR (125 MHz) data[a] of compounds **104-106** in CD_3OD.

	104		**105**		**106**	
Pos.	δ_C	δ_H, **mult.**	δ_C	δ_H **mult.**	δ_C	δ_H **mult.**
1	14.1	0.91, t	14.1	0.91, t	14.1	0.91, t
2	23.5	1.33[b]	23.3	1.34[b]	23.4	1.31[b]
3	28.4	1.28[b]-1.32[b]	28.4	1.28[b]-1.32[b]	28.4	1.28[b]-1.37[b]
4	34.7	1.56[b]	34.6	1.57[b]	34.8	1.55[b]
5	76.0	4.82, ddd	76.0	4.87, ddd	76.0	4.87, ddd
6	31.5	1.52[b] -1.83[b]	30.7	1.61[b]-1.86[b]	31.6	1.60[b]-1.82[b]
7	29.4	1.31[b]-1.68[b]	27.3	1.65[b]-1.69[b]	29.3	1.38[b]-1.61[b]
8	79.5	3.29, ddd	82.4	4.11, ddd	74.0	3.66, dt
9	79.6	3.33, dt	73.8	3.66, dt	82.9	4.15, ddd
10	33.5	1.62[b] -1.35[b]	33.5	1.40[b]-1.56[b]	31.5	1.60[b] -1.68[b]
11	26.5	1.34[b] -1.54	26.4	1.33[b] -1.56[b]	25.6	1.41[b] -1.48[b]
12	32.7	1.33[b]	32.7	1.33[b]	32.8	1.33[b]
13	23.5	1.34[b]	23.3	1.34[b]	23.4	1.36[b]
14	14.1	0.91, t	14.1	0.91, t	14.1	0.91, t
-CH3	20.9	2.02, s	20.9	2.02, s	20.9	2.03, s
-CO	173.7	-	173.7	-	173.6	-

[a]^{1}H NMR and ^{13}C NMR shifts are referenced to CD_3OD (δ_H = 3.31 ppm and δ_C = 49.0 ppm). [b]Partially overlapped to other resonances.

***Conclusion*:** database of spectroscopic information is an innovative and efficient tool to solve the absolute stereochemical assignment of acyclic and polysubstituted polyketides. This approach does not require degradation or chemical derivatization of the natural metabolite, rather the comparison of ^{1}H and ^{13}C chemical shifts of unknown

compound with those of synthesised diastereoisomeric model compounds allows to unequivocally assign the absolute stereochemistry.

As for phosphoeleganin (**92**), completing the configurational analysis at C-11 and C-12 was performed preparing model compounds with known stereochemistry and same connectivity of stereocluster C-8/C-12 of the marine metabolite seeing as no suitable compounds for the comparison were found into Kishi's database. The diastereoisomers (**97a**/**97b** and **98a**/**98b**, Scheme 8) were synthesised by an efficient route while their stereostructural elucidation was executed through the application of different methods. Firstly, Riguera's method based on the use of CDAs was carried out by the analysis of anisotropic effects that chiral auxiliary agents exerted on chemical shift values, and then to substantiate the achieved results, stereoselective synthesis and a deep analysis of ROESY diagnostic peaks was brought out. Application of the UDB-NMR concept led to a closely correlation among the analysed stereocluster of **92** and of **99** endowed with a 5*S*, 8*S*, 9*R* absolute configuration allowing to complete the absolute configuration assignment of the marine phosphorylated polyketide which resulted to be 8*S*, 11*S*, 12*R*, 15*S*, 16*R* [161].

Taking into account the difficult of the natural products manipulation due to the limited availability, it is worth enlarging the pool of model compounds within the UDB-NMR database synthesising new chemical classes of diastereoisomers. Accordingly, polyoxi-, polyacetoxy- and phosphorylated compounds (**104**-**106**) have been prepared up to now with an efficient synthetic route which avoids the most common side products (e.g. pyrophosphates). This work is ongoing for a double reason: firstly, working as support for stereostructural elucidation of complex, acyclic or macrocyclic, and polyfunctionalised polyketides, and in this view synthetic phosphorylated compounds

represent a great novelty, while on the other hand, shedding light on the structural elements required for the inhibitory activity on PTP1B, currently the most validate target for treatment of type II diabetes.

Finally, this project will have to be directed also to the use of the other available stereoisomers (**97b**, **98a**, **98b**) applying the synthetic procedure described in Schemes 9 and 10 in order to provide the database of more stereoisomers as aid in the stereochemical assignment and investigate their pharmacological properties on the same target.

4.5 Materials and methods

*Synthesis of compounds **96-106***

*(Z)-tetradec-8-en-5-ol (**96**):* 424 mg (2.7 mmol) of *cis*-4-decenal were dissolved in 20 mL of THF and 2.0 mL of *n*-BuLi 1.6 M (3.3 mmol) were added dropwise at -78°C for 10 minutes. Subsequently, the mixture was stirred for additional 8 hours at rt before quenching with a saturated solution of NH_4Cl (40 mL) and extracting with EtOAc (2 x 60 mL). The combined organic layer was dried over sodium sulphate, filtered and the solvent removed *in vacuo* yielding the desired alcohol **96** in pure form (524 mg, 90%).

*Compound **96**:* colourless oil; ^{1}H-NMR ($CDCl_3$): 0.84 (6H, m, H-1 and H-14); 1.20-1.51 (14H, overlapped, H-2-H-4, H-9, H-11/H-13); 1.96 (2H, m, H-5); 5.32 (2H, m, H-6 and H-7); 2.10 (1H, m, H-8a); 2.06 (1H, m, H-8b); 3.54 (1H, m, H-10); ^{13}C-NMR ($CDCl_3$): 14.1 (CH_3, C-1); 22.5 (CH_2, C-2); 22.7 (CH_2, C-3); 22.4 (CH_2, C-4); 71.5 (CH, C-5); 27.1 (CH_2, C-6); 27.7 (CH_2, C-7); 129.1 (CH, C-8); 130.5 (CH, C-9); 29.3 (CH_2,

C-10); 31.4 (CH_2, C-11); 37.0 (CH_2, C-12); 37.1 (CH_2, C-13); 14.1 (CH_3, C-14) ESIMS: *m/z* 213.22 $[M+H]^+$; ^1H and ^{13}C NMR spectra are reported in Chapter 6.

(5S, 8S*, 9R*)- and (5S*, 8R*, 9S*)-tetradecan-5,8,9-triol (**rac-97** and **rac-98**):* the alcohol **96** (495 mg, 2.3 mmol) was treated with NMO (410 mg, 3.5 mmol) and OsO_4 (6 mg, 1 mol%) in 10 mL of acetone/H_2O 9:1 (v/v) stirring overnight at rt. After this time, the mixture was quenched with saturated solution of Na_2SO_3 and subjected to extraction with EtOAc (3 x 50 mL). The organic layer was dried over sodium sulphate, filtered and concentrated by rotary evaporation. A portion of the raw material was chromatographed by HPLC on reversed phase (Luna C-18 10 μm column, eluent MeOH/H_2O 7:3, flow rate 3 mL/min) to afford two mixture of diastereoisomeric compounds as racemate, ***rac*-97** (55.1 mg, t_R=12.6 min) and ***rac*-98** (61.4 mg, t_R=14.4 min).

*Compound **rac*-97**: white powder; ^1H-NMR ($CDCl_3$): 0.92 (3H, t, *J* = 7.6 Hz, H-1); 1.43 (1H, overlapped, 1H-2a); 1.32 (1H, overlapped, H-2b); 1.32 (2H, overlapped, H-3); 1.46 (1H, m, H-4a); 1.42 (1H, overlapped, H-4b); 3.53 (1H, m, H-5); 1.72 (1H, m, H-6a); 1.39 (1H, overlapped, H-6b); 1.80 (1H, m, H-7a); 1.39 (1H, overlapped, H-7b); 3.34 (1H, m, H-8); 3.36 (1H, m, H-9); 1.60 (1H, overlapped, H-10a); 1.36 (1H, overlapped, H-10b); 1.54 (1H, m, H-11a); 1.33 (1H, overlapped, H-11b); 1.32 (2H, overlapped, H-12); 1.34 (2H, overlapped, H-13); 0.92 (3H, t, *J* = 7.6 Hz, H-14); ^{13}C NMR ($CDCl_3$, signals assigned from HSQC data): 14.1 (CH_3, C-1); 28.7 (CH_2, C-2); 32.8 (CH_2, C-3); 37.9 (CH_2, C-4); 72.9 (CH, C-5); 34.6 (CH_2, C-6); 29.6 (CH_2, C-7); 76.3 (CH, C-8); 75.9 (CH, C-9); 33.4 (CH_2, C-10); 26.4 (CH_2, C-11); 32.8 (CH_2, C-12); 23.7 (CH_2, C-13); 14.1 (CH_3, C-14); ESIMS: *m/z* 247.22 $[M+H]^+$; ^1H and ^{13}C NMR spectra are reported in Chapter 6.

Compound ***rac*-98**: white powder; ^{1}H-NMR ($CDCl_3$): 0.92 (3H, t, J = 7.6 Hz, H-1); 1.44 (1H, overlapped, 1H-2a); 1.33 (1H, overlapped, H-2b); 1.32 (2H, overlapped, H-3); 1.46 (1H, m, H-4a); 1.42 (1H, overlapped, H-4b); 3.55 (1H, m, H-5); 1.60 (1H, overlapped, H-6a); 1.53 (1H, overlapped, H-6b); 1.70 (1H, overlapped, H-7a); 1.48 (1H, overlapped, H-7b); 3.37 (1H, m, H-8); 3.38 (1H, m, H-9); 1.60 (1H, overlapped, H-10a); 1.36 (1H, overlapped, H-10b); 1.54 (1H, overlapped, H-11a); 1.33 (1H, overlapped, H-11b); 1.32 (2H, overlapped, H-12); 1.34 (2H, overlapped, H-13); 0.92 (3H, t, J = 7.6 Hz, H-14); ^{13}C NMR ($CDCl_3$, signals assigned from HSQC data): 14.1 (CH_3, C-1); 28.7 (CH_2, C-2); 32.8 (CH_2, C-3); 37.9 (CH_2, C-4); 72.1 (CH, C-5); 34.3 (CH_2, C-6); 29.3 (CH_2, C-7); 75.6 (CH, C-8); 75.6 (CH, C-9); 33.4 (CH_2, C-10); 26.4 (CH_2, C-11); 32.8 (CH_2, C-12); 23.7 (CH_2, C-13); 14.1 (CH_3, C-14); ESIMS: *m/z* 247.25 $[M+H]^+$; ^{1}H and ^{13}C NMR spectra are reported in Chapter 6.

Synthesis of compounds ***97a*/*97b*** *and* ***98a*/*98b****:* a portion of each racemic (***rac*-97** and ***rac*-98**) mixture was subjected to esterification by coupling with *R*-MPA. In detail, 5.1 mg of ***rac*-97** (0.05 mmol) were dissolved in 3 mL of dry CH_2Cl_2 to which 37.4 mg (0.195 mmol) of *N*-(3-Dimethylaminopropyl)-*N*′-ethylcarbodiimide (EDC), 11.8 mg (0.096 mmol) of dimethylaminopyridine (DMAP), and 6.3 mg of (*R*)-MPA (0.195 mmol) were added in portion. As for compounds **98a**/**98b**, 18.1 mg of ***rac*-98** (0.074 mmol) were dissolved in 3 mL of dry CH_2Cl_2 to which 63.3 mg (0.334 mmol) of EDC, 18.1 mg (0.148 mmol) of DMAP and 54.8 mg of (*R*)-MPA (0.334 mmol) were added in portion. Each mixture was kept under magnetic stirring and N_2 atmosphere overnight at rt. Then, the solvent removal gave two mixtures of diastereoisomeric triesters (**97a**/**97b** and **98a**/**98b**) which were separately chromatographed by HPLC on silica gel (Luna SiO_2 3 μm, eluting with hexane/EtOAc 85:15, flow rate 1 mL/min) affording the

four pure trimester **97a** (2.1 mg, t_R=3.74 min), **97b** (2.3 mg, t_R=4.64 min), **98a** (7.8 mg, t_R=3.12 min), **98b** (8.0 mg, t_R=4.32 min) as individual compounds.

*Compound **97a***: colourless oil; ^{1}H-NMR ($CDCl_3$): 0.67 (3H, t, *J* = 7.6 Hz, H-1); 0.98 (2H, overlapped, H-2); 0.61 (2H, m, H-3); 0.98 (1H, overlapped, H-4a); 0.94 (1H, overlapped, H-4b); 4.42 (1H, m, H-5); 0.88 (1H, overlapped, H-6a); 0.56 (1H, m, H-6b); 1.14 (1H, m, H-7a); 0.93 (1H, overlapped, H-7b); 4.66 (1H, m, H-8); 5.09 (1H, m, H-9); 1.39 (1H, overlapped, H-10a); 1.36 (1H, overlapped, H-10b); 1.22 (2H, overlapped, H-11); 1.22 (2H, overlapped, H-12); 1.25 (2H, overlapped, H-13); 0.86 (3H, t, *J* = 7.6 Hz, H-14); ^{13}C NMR ($CDCl_3$, signals assigned from HSQC data): 13.5 (CH_3, C-1); 22.1 (CH_2, C-2); 26.2 (CH_2, C-3); 33.4 (CH_2, C-4); 74.9 (CH, C-5); 29.1 (CH_2, C-6), 24.0 (CH_2, C-7); 74.7 (CH, C-8); 74.1 (CH, C-9); 29.9 (CH_2, C-10); 24.9 (CH_2, C-11); 31.1 (CH_2, C-12); 22.3 (CH_2, C-13); 13.7 (CH_3, C-14); ESIMS: *m/z* 713.36 $[M+Na]^+$; ^{1}H spectrum is reported in Chapter 6.

*Compound **97b***: colourless oil; ^{1}H-NMR ($CDCl_3$): 0.84 (3H, t, *J* = 7.6 Hz, H-1); 1.25 (2H, overlapped, H-2); 1.16 (2H, overlapped, H-3); 1.48 (1H, m, H-4a); 1.39 (1H, m, H-4b); 4.80 (1H, m, H-5); 1.31 (2H, overlapped, H-6); 1.02 (1H, m, H-7a); 0.80 (1H, overlapped, H-7b); 4.88 (1H, m, H-8); 4.40 (1H, m, H-9); 0.84 (1H, overlapped, H-10a); 0.79 (1H, overlapped, H-10b); 0.52 (1H, m, H-11a); 0.46 (1H, m, H-11b); 1.31 (2H, overlapped, H-12); 0.91 (2H, m, H-13); 0.68 (3H, t, *J* = 7.6 Hz, H-14); ^{13}C NMR ($CDCl_3$, signals assigned from HSQC data): 13.8 (CH3, C-1); 22.3 (CH2, C-2); 27.1 (CH2, C-3); 33.9 (CH2, C-4); 74.7 (CH, C-5); 30.4 (CH2, C-6); 25.5 (CH2, C-7); 74.4 (CH, C-8); 74.7 (CH, C-9); 26.9 (CH2, C-10); 23.9 (CH2, C-11); 30.3 (CH2, C-12); 22.1 (CH2, C-13); 13.5 (CH3, C-14); ESIMS: *m/z* 713.36 $[M+Na]^+$; ^{1}H spectrum is reported in Chapter 6.

Compound ***98a***: colourless oil; ^{1}H-NMR ($CDCl_3$): 0.68 (3H, t, *J* = 7.6 Hz, H-1); 1.05 (2H, m, H-2); 0.83 (2H, overlapped, H-3); 1.31 (1H, overlapped, H-4a); 1.29 (1H, overlapped, H-4b); 4.83 (1H, m, H-5); 1.46 (1H, overlapped, H-6a); 1.42 (1H, overlapped, H-6b); 1.44 (1H, overlapped, H-7a); 1.37 (1H, overlapped, H-7b); 5.07 (1H, m, H-8); 4.69 (1H, m, H-9); 0.99 (2H, overlapped, H-10); 0.59 (1H, overlapped, H-11a); 0.54 (1H, overlapped, H-11b); 0.82 (1H, overlapped, H-12a); 0.74 (1H, m, H-12b); 0.91 (2H, m, H-13); 0.67 (3H, t, *J* = 7.6 Hz, H-14); ^{13}C NMR ($CDCl_3$, signals assigned from HSQC data): 13.7 (CH_3, C-1); 22.1 (CH_2, C-2); 26.7 (CH_2, C-3); 33.4 (CH_2, C-4); 74.2 (CH, C-5); 29.9 (CH_2, C-6); 25.9 (CH_2, C-7); 74.5 (CH, C-8); 74.8 (CH, C-9); 27.6 (CH_2, C-10); 23.9 (CH_2, C-11); 30.9 (CH_2, C-12); 22.1 (CH_2, C-13); 13.7 (CH_3, C-14); ESIMS: *m/z* 713.37 $[M+Na]^+$; ^{1}H spectrum is reported in Chapter 6.

Compound ***98b***: colourless oil; ^{1}H-NMR ($CDCl_3$): 0.81 (3H, t, *J* =7.6 Hz, H-1); 1.16 (2H, overlapped, H-2); 0.93 (2H, overlapped, H-3); 1.21 (1H, overlapped, H-4a); 0.99 (1H, overlapped, H-4b); 4.53 (1H, m, H-5); 0.74 (2H, overlapped, H-6); 0.89 (1H, overlapped, H-7a); 0.77 (1H, overlapped, H-7b); 4.61 (1H, m, H-8); 5.00 (1H, m, H-9); 1.22 (1H, overlapped, H-10a); 1.16 (1H, overlapped, H-10b); 1.16 (2H, overlapped, H-11); 1.22 (2H, overlapped, H-12); 1.24 (2H, overlapped, H-13); 0.85 (3H, t, *J* = 7.6 Hz, H-14); ^{13}C NMR ($CDCl_3$, signals assigned from HSQC data): 13.8 (CH_3, C-1); 22.4 (CH_2, C-2); 27.1 (CH_2, C-3); 33.4 (CH_2, C-4); 73.9 (CH, C-5); 28.8 (CH_2, C-6); 22.6 (CH_2, C-7); 74.2 (CH, C-8); 74.4 (CH, C-9); 29.6 (CH_2, C- 10); 29.4 (CH_2, C-11); 31.4 (CH_2, C-12); 22.4 (CH_2, C-13); 13.9 (CH_3, C-14); ESIMS: *m/z* 713.36 $[M+Na]^+$; ^{1}H spectrum is reported in Chapter 6.

*Synthesis of (5S, 8S, 9R)-tetradecan-5,8,9-triol (**99**) and (5S, 8R, 9S)-tetradecan-5,8,9-triol (**100**):* the base-catalysed hydrolyses of compound **97a** (2 mg, 0.003 mmol)

and **98a** (4.8 mg, 0.007 mmol) were executed in 3 mL of MeOH and few drops of water with 400 mg (10 mmol) of NaOH keeping overnight at rt, respectively. Then, each mixture was diluted with HCl solution (0.1 M) and extracted with *n*-BuOH (3 x 20 mL). The resultant organic layers were dried over Na_2SO_4 and concentrated *in vacuo* and each raw material was purified by HPLC on RP-18 (Luna 5 μm C-18 column, MeOH/H_2O 7:3 as eluent) affording the pure triol **99** (2 mg, t_R=12.6 min; $[\alpha]^{25}_D$ +3.7 with c 0.009 in MeOH) and the triol **100** (3.6 mg, t_R=14.4 min; $[\alpha]^{25}_D$ +1.5 with c 0.015 in MeOH).

*Compound **99***: white powder; ^{1}H-NMR ($CDCl_3$): 0.92 (3H, t, *J* = 7.6 Hz, H-1); 1.43 (1H, overlapped, H-2a); 1.32 (1H, overlapped, H-2b); 1.32 (2H, overlapped, H-3); 1.46 (1H, m, H-4a); 1.42 (1H, overlapped, H-4b); 3.53 (1H, m, H-5); 1.72 (1H, m, H-6a); 1.39 (1H, overlapped, H-6b); 1.80 (1H, m, H-7a); 1.39 (1H, overlapped, H-7b); 3.34 (1H, m, H-8); 3.36 (1H, m, H-9); 1.60 (1H, overlapped, H-10a); 1.36 (1H, overlapped, H-10b); 1.54 (1H, m, H-11a); 1.33 (1H, overlapped, H-11b); 1.32 (2H, overlapped, H-12); 1.34 (2H, overlapped, H-13); 0.92 (3H, t, *J* = 7.6 Hz, H-14); ^{13}C NMR ($CDCl_3$, signals assigned from HSQC data): 14.1 (CH_3, C-1); 28.7 (CH_2, C-2); 32.8 (CH_2, C-3); 37.9 (CH_2, C-4); 72.9 (CH, C-5); 34.6 (CH_2, C-6); 29.6 (CH_2, C-7); 76.3 (CH, C-8); 75.9 (CH, C-9); 33.4 (CH_2, C-10); 26.4 (CH_2, C-11); 32.8 (CH_2, C-12); 23.7 (CH_2, C-13); 14.1 (CH_3, C-14); HRESIMS: *m/z* 247.2266 $[M+H]^+$ (calcd. for $C_{14}H_{31}O_3$ *m/z* 247.2268).

*Compound **100***: white powder; ^{1}H-NMR ($CDCl_3$): 0.92 (3H, t, *J* = 7.6 Hz, H-1); 1.44 (1H, overlapped, H-2a), 1.33 (1H, overlapped, H-2b); 1.32 (2H, overlapped, H-3); 1.46 (1H, m, H-4a); 1.42, (1H, overlapped, H-4b); 3.55 (1H, m, H-5); 1.60 (1H, overlapped, H-6a), 1.53 (1H, overlapped, H- 6b); 1.70 (1H, overlapped, H-7a); 1.48

(1H, overlapped, H-7b); 3.37 (1H, m, H-8); 3.38 (1H, m, H-9); 1.60 (1H, overlapped, H-10a); 1.36 (1H, overlapped, H-10b); 1.54 (1H, overlapped, H-11a); 1.33 (1H, overlapped, H-11b); 1.32 (2H, overlapped, H-12); 1.34 (2H, overlapped, H-13); 0.92 (3H, t, J = 7.6 Hz, H-14); ^{13}C NMR ($CDCl_3$, signals assigned from HSQC data): 14.1 (CH_3, C-1); 28.7 (CH_2, C-2); 32.8 (CH_2, C-3); 37.9 (CH_2, C-4); 72.1 (CH, C-5); 34.3 (CH_2, C-6); 29.3 (CH_2, C-7); 75.6 (CH, C-8); 75.6 (CH, C-9); 33.4 (CH_2, C-10); 26.4 (CH_2, C-11); 32.8 (CH_2, C-12); 23.7 (CH_2, C-13); 14.1 (CH_3, C-14); HREIMS: *m/z* 247.2267 $[M+H]^+$ (calcd. for $C_{14}H_{31}O_3$ *m/z* 247.2268).

*Synthesis of compounds **102**:* 10.4 mg (0.042 mmol) of the triol **99** were dissolved in 5 mL of CH_2Cl_2, whereas 7 µL of trimethyl orthoacetate ($MeC(OMe)_3$, 1.2 equiv) and 0.100 mg of pyridinium *p*-toluensulfonate (PPTS, 0.1 equiv) were added to the resultant mixture under magnetic stirring at rt. After 15 minutes, the mixture was cooled up to 0°C and 0.53 µL of boron trifluoride diethyl etherate ($BF_3 \cdot Et_2O$, 0.1 equiv) were added. TLC allowed to observe the consuming of intermediate orthoester before quenching with a mixture H_2O/acetone 9:1 and removing the solvent *in vacuo*. The cyclization of compound **99** yielded the compound **102** quantitatively.

*Compound **102***: white powder; ^{1}H-NMR ($CDCl_3$): 0.87 (3H, t, J = 7.6 Hz, H-1); 1.30 (2H, overlapped, H-2); 1.31 (1H, overlapped, H-3a); 1.25 (1H, m, H- 3b); 1.56 (H, m, H-4a); 1.38 (1H, overlapped, H-4b); 3.88 (1H, m, H-5); 1.98 (1H, m, H-6a); 1.44 (1H, overlapped, H-6b); 1.96 (1H, m, H-7a); 1.58 (1H, overlapped, H-7b); 3.98 (1H, m, H-8); 4.86 (1H, m, H-9); 1.53 (2H, overlapped, H-10); 1.27 (2H, overlapped, H-11); 1.28 (2H, overlapped, H-12); 1.30 (2H, overlapped, H-13); 0.92 (3H, t, J = 7.6 Hz, H-14); 2.08 (3H, s, COOCH3); ^{13}C NMR ($CDCl_3$, signals assigned from HSQC data): 14.1 (CH_3, C-1); 22.8 (CH_2, C-2); 28.4 (CH_2, C-3); 35.5 (CH_2, C-4); 79.6 (CH, C-5); 32.4

(CH_2, C-6); 28.4 (CH_2, C-7); 79.3 (CH, C-8); 75.7 (CH, C-9); 31.1 (CH_2, C-10); 31.9 (CH_2, C-11); 25.6 (CH_2, C-12); 22.8 (CH_2, C-13); 14.1 (CH_3, C-14); 21.3 (CH_3); 171.4 (CO); HREIMS: *m/z* 271.2270 $[M+H]^+$ (calcd. for $C_{16}H_{31}O_3$ *m/z* 271.2273). NMR spectra are reported in Chapter 6.

*Synthesis of compounds **103**:* the same procedure for **102** was adopted also for the cyclization of the triol **100** 10.5 mg (0.042 mmol) synthesising the cyclic ether **103**, quantitatively.

*Compound **103***: white powder; ^{1}H-NMR ($CDCl_3$): 0.87 (3H, t, *J* = 7.6 Hz, H-1); 1.30 (2H, overlapped, H-2); 1.31 (1H, overlapped, H-3a); 1.25 (1H, m, H-3b); 1.56 (1H, overlapped, H-4a); 1.40, (1H, overlapped, H-4b); 3.81 (1H, m, H-5); 1.92 (1H, overlapped, H-6a); 1.44 (1H, overlapped, H-6b); 1.89 (1H, overlapped, H-7a); 1.62 (1H, overlapped, H-7b); 3.91 (1H, m, H-8); 4.87 (1H, m, H-9); 1.56 (2H, overlapped, H-10); 1.27 (2H, overlapped, H-11); 1.28 (2H, overlapped, H-12); 1.29 (2H, overlapped, H-13); 0.87 (3H, t, *J* = 7.6 Hz, H-14); 2.09 (3H, s, $COOCH_3$); ^{13}C NMR ($CDCl_3$, signals assigned from HSQC data): 14.1 (CH_3, C-1); 22.9 (CH_2, C-2); 28.5 (CH_2, C-3); 35.5 (CH_2, C-4); 80.1 (CH, C-5); 31.2 (CH_2, C-6); 27.8 (CH_2, C-7); 79.6 (CH, C-8); 75.9 (CH, C-9); 31.2 (CH_2, C-10); 31.9 (CH_2, C-11); 25.2 (CH_2, C-12); 22.6 (CH_2, C-13); 14.1 (CH_3, C-14); 21.3 (CH_3); 171.4 (CO); HREIMS: *m/z* 271.2269 $[M + H]^+$ (calcd. for $C_{16}H_{31}O_3$ *m/z* 271.2273); NMR spectra are reported in Chapter 6.

*Synthesis of compound **104-108**:* to obtain the novel derivatives from the pure compound (5*S*, 8*S*, 9*R*)-tetradecan-5,8,9-triol (**99**) was necessary repeating the procedure already described which afforded 24.0 mg of the pure triol [161].

*Synthesis of compound **107**:* the compound **99** (24.0 mg, 0.1 mmol) was subjected to reaction with 2,2-dimethoxypropane to afford the acetonide derivative **107**. In detail,

the triol was dissolved in 6 mL of 2,2-dimethoxypropane and a catalytic amount of *p*-toluenesulfonic acid was added in one portion, stirring the resultant mixture overnight at rt. Then, a saturated $NaHCO_3$ solution quenched the reaction and the desired product (25.6 mg, 92%) was extracted with EtOAc (2 x 30 mL).

*Compound **107***: colourless oil; ^{1}H NMR (CD_3OD): 0.93 (3H, H-1); 1.32 (2H, H-2); 1.32-1.43 (2H, H-3); 1.42-1.46 (2H, H-4); 3.53 (1H, H-5); 1.34-1.68 (2H, H-6); 1.34-1.61 (2H, H-7); 4.02 (1H, H-8); 4.05 (1H, H-9); 1.47-1.48 (2H, H-10); 1.34-1.54 (2H, H-11); 1.34 (2H, H-12); 1.34 (2H, H-13); 0.91 (3H, H-14); 1.30 (3H, CH_3, H-1'); 1.39 (3H, CH_3, H-3'); ^{13}C NMR (CD_3OD): 14.1 (CH_3, C-1); 23.5 (CH_2, C-2); 28.7 (CH_2, C-3); 37.9 (CH_2, C-4); 73.9 (CH, C-5); 34.9 (CH_2, C-6); 27.5 (CH_2, C-7); 79.0 (CH, C-8); 79.5 (CH, C-9); 30.4 (CH_2, C-10); 26.4 (CH_2, C-11); 32.8 (CH_2, C-12); 23.7 (CH_2, C-13); 14.1 (CH_2, C-14); 108.5 (C, C-2'); 28.5 (CH_3, C-1'); 25.7 (CH_3, C-3'); NMR spectra are reported in Chapter 6.

*Synthesis of compound **108***: acetylation reaction was carried out on 24 mg (0.083 mmol) of the acetonide **107** in pyridine (3 mL) as solvent with a great excess of acetic anhydride, leaving the resultant mixture for 18 h at rt. After this time, the excess of acetic anhydride was destroyed cooling the mixture at 0°C in an ice-bath and adding ~10 mL of MeOH. The solvent removal *in vacuo* afforded compound **108** in a quantitative amount (26.9 mg, 98%).

*Compound **108***: colourless oil; ^{1}H NMR (CD_3OD): ^{1}H NMR (CD_3OD): 0.91 (3H, H-1); 1.34 (2H, H-2); 1.28-1.32 (2H, H-3); 1.56 (2H, H-4); 4.87 (1H, H-5); 1.51-1.80 (2H, H-6); 1.44 (2H, H-7); 3.99 (1H, H-8); 4.05 (1H, H-9); 1.42-1.45 (2H, H-10); 1.44-1.50 (2H, H-11); 1.32 (2H, H-12); 1.34 (2H, H-13); 0.92 (3H, H-14); 1.30 (3H, CH_3, H-1'); 1.39 (3H, CH_3, H-3'); 2.02 (3H, $COCH_3$); ^{13}C NMR (CD_3OD): 14.1 (CH_3, C-1);

23.4 (CH_2, C-2); 28.4 (CH_2, C-3); 34.6 (CH_2, C-4); 75.6 (CH, C-5); 31.8 (CH_2, C-6); 26.6 (CH_2, C-7); 79.0 (CH, C-8); 79.0 (CH, C-9); 30.7 (CH_2, C-10); 26.6 (CH_2, C-11); 32.8 (CH_2, C-12); 23.4 (CH_2, C-13); 14.5 (CH_2, C-14); 108.5 (C, C-2'); 28.5 (CH_3, C-1'); 25.7 (CH_3, C-3'); 173.7 (CO); 20.9 ($COCH_3$); HRESIMS: *m/z* 351.2505 $[M+Na]^+$ (calcd. for $C_{19}H_{36}O_4Na$ *m/z* 351.2506); NMR and HRESIMS spectra are reported in Chapter 6.

*Synthesis of compound **104***: hydrolysis of the protective acetonide group on the 1,2-diol system was performed dissolving 25.0 mg of **108** (0.076 mmol) in 6 mL of a mixture MeOH/H_2O (9:1) adding dropwise 50 µL of HCl 37% (p/p). The mixture was kept at 4°C for 36 h before removing the solvent by rotary evaporator. The raw material was purified by HPLC on C18 reversed phase (Luna 5 µm C18 column, MeOH/H_2O 7:3 as mobile phase, flow rate 1 mL/min) to yield the acetylated compound **104** (21.4 mg, 97%).

*Compound **104***: white powder; ^1H and ^{13}C NMR data are reported in Table 25; NMR and HRESIMS spectra are reported in Chapter 6.

*Synthesis of compounds (5S,8S,9R)-9-hydroxy-8-(phosphonooxy)tetradecan-5-yl acetate (**105**) and (5S,8S,9R)-8-hydroxy-9-(phosphonooxy)tetradecan-5-yl acetate (**106**)*: 16 mg (0.055 mmol) of compound **104** in 3 mL of acetonitrile were treated with 40 µL (0.400 mmol) of trichloroacetonitrile, following by dropwise addition of 50 mg (0.147 mmol) of tetrabutylammonium dihydrogenphosphate, previously solubilised in 1 mL of acetonitrile. The reaction was kept under magnetic stirring at rt for 2 h and the solvent removal *in vacuo* afforded a raw material which was first purified by HPLC on RP-18 (5 µm C18 column, MeOH:H_2O 75:25 + 0.1% TFA) and a collected fraction was found to contain a mixture of two isomeric phosphorylated compounds, **105** and **106**

(6.2 mg, 31%). This fraction was further purified by HPLC on RP-18 using a Synergy 4 μm Polar column and MeOH/H_2O 6:4 + 0.1% TFA as mobile phase affording compound **105** (3.9 mg, t_R= 27.4 min) and **106** (2.3 mg, t_R= 28.8 min) in pure form.

*Compound **105***: colourless oil; HRESIMS: *m/z* 369.2036 $[M+H]^+$ (calcd. for $C_{16}H_{34}O_7P$ *m/z* 369.2037); ^1H and ^{13}C NMR data are reported in Table 25; NMR and HRESIMS spectra are reported in Chapter 6.

*Compound **106***: colourless oil; HRESIMS: *m/z* 369.2035 $[M+H]^+$ (calcd. for $C_{16}H_{34}O_7P$ *m/z* 369.2037); ^1H and ^{13}C NMR data are reported in Table 25; NMR and HRESIMS spectra are reported in Chapter 6.

CHAPTER 5

Current methodologies for structural elucidation

5.1 Introduction

The analytical characterization of organic molecules is a fundamental requirement in environmental, food and medicinal chemistry as well as in the field of natural products. As for the chemistry of marine products, several troubles affect the structural elucidation of new secondary metabolites. Mainly, due to the complicated procedures of collection and identification of the biological material accounting the fundamental need of marine environment safeguard, the scientists constantly face with samples in the range of micrograms, even nanograms, whence efficiently separate pure compounds. Accordingly, structural elucidation requires to use non-destructive techniques preserving the integrity of compounds in order to enable performing biological assays. As a consequence of these needs, methodologies in isolation and structural characterization of novel natural compounds are becoming endowed with more sensitivity.

Indeed, to deal with the issue of tiny quantities isolated from marine sources, refined analytical and chromatographic procedures have been efficiently developed. Additionally, these isolation techniques luckily have increased also the number of compounds that may be recovered and thus, the structural and stereostructural elucidation topic is primarily based on the modern mass spectrometry and NMR spectroscopy techniques, often assisted by computational tools allowing to support the qualitative analysis of compounds with a quantitative evaluation, too.

5.1.1 Chromatographic procedures

The first step to isolate marine metabolites is an efficient extraction of the biomass, generally lyophilized, thawed and ground, with different organic solvents or mixtures of them (methanol, ethanol, acetone, chloroform as most used). Afterwards, the combined organic extracts were subjected to partitions with solvents affording phases with different polarity grade. The interesting fractions are subjected to subsequent purification procedures mainly by solid-liquid chromatography in which a liquid mobile phase is forced on a solid phase, named stationary phase. In this way, liquid mixtures of dissolved compounds are separated into individual compounds according to their polarity and the different interaction with the column (stationary phase).

The most commonly used techniques are medium and high pressure liquid chromatography, MPLC and HPLC. The first one provides a better resolution than open-column, working at a pressure of ~5-40 bar allowing to load large amount of sample (100 mg-100 g) and gain time with respect to other purification methods. As for HPLC, it represents the most widely applied chromatographic technique and, in fact, it finds a variety of industrial and scientific applications in the field of pharmaceutical, forensic and environmental analysis. In the field of natural products chemistry, the HPLC can present the last step in the scale of purification since its versatility allows to choose optimized conditions both as stationary and mobile phase, providing compounds in pure form with high yield.

Accordingly, this technique has been extensively used during my PhD research activity with semipreparative aims to separate and purify natural compounds as well as intermediate and final compounds of synthetic procedures. In particular, Knauer K-501

and Shimadzu LC-10AT systems, both equipped with a Knauer K-2301 reflective index detector, have been used to execute the HPLC separations.

5.1.2 Mass spectrometry

Determining the molecular formula, based on the mass-to-charge ratio (*m/z*) of ions generated from the molecules, is the first step in the structure determination of natural compounds and an important element to confirm if a chemical reaction is occurred. It is an analytical destructive technique which consists in an initial ionization and transfer in gas phase of the molecules into a source. During this phase, the ions can fragment, or the fragments may be generated by the collision of ions with gas in the source. The resultant *m/z* fragment values provide important information for the structure determination. Subsequently, the produced ions are transmitted to the mass analyser where the ions are separated according to their *m/z* ratio and finally, the *m/z* values of a compound are measured by the detector.

Natural and synthetic compounds described in my thesis have been investigated by a Thermo LTQ Orbitrap XL mass spectrometer (Thermo-Fisher) recording spectra by infusion in an electrospray ionisation source (ESI) and using MeOH to solubilize the compounds. Orbitrap analyser consists in a central rod-like electrode bordered by a barrel-shaped external electrode and the ions are injected into barrel electrode rolling around central electrode. The harmonic oscillations of ions together with the application of Fourier transform allows to determine the *m/z* ratio. The LTQ-orbitrap, endowed with a compact design, combines into a single instrument the ion trap and Fourier transform technologies providing high mass resolution (> 150000) and high mass accuracy (1-2 ppm) [181].

5.1.3 Nuclear magnetic resonance

Nuclear magnetic resonance (NMR) is surely the most widely applied and preeminent spectroscopic technique for determining the structure of organic compounds. As opposed to mass spectrometry which is a very sensible analytical method but destructive, NMR is a non-destructive procedure that allows to record good data with the modern instrument providing structural determination starting from samples weighing satisfactory results in structural determination of compounds weighing less than a milligram. The sample is contained into a 5 mm glass tube and oriented among the poles of a strong magnetic field while an appropriate radiofrequency radiation with adequate energy is broadcast in the sample. By varying the magnetic field over a small range, the NMR spectrum is acquired observing the radiofrequency released from the sample. Beyond the standard ^{1}H and ^{13}C experiments, more information can be understood by 2D NMR experiments. In fact, the univocal and unequivocal structure of the isolated natural compounds as well as the synthetic substances was afforded by the analysis of 2D NMR diagnostic cross peaks of the most used bidimensional experiments.

In particular, COSY and TOCSY experiments represent homonuclear chemical shift correlation experiments that have been recorded in order to determine the connectivity between the protons into the molecule. The COSY experiment identifies proton scalarly coupled through directly *J*-coupled spins, whereas TOCSY is very useful for molecules composed by many separate spin systems. For each spin system, spin-spin couplings are transferred along the chain, and thus any proton of the spin system can give rise to a peak. Homonuclear correlation related to dipolar coupling

between the nuclei depending on the geometry and spatial distance between protons are highlighted instead by diagnostic peaks of NOESY and ROESY experiments.

Heteronuclear correlations are evidenced by 2D HSQC and HMBC spectra in which a one-bond ^{1}H-^{13}C or two- and three- ^{1}H-^{13}C bond couplings are observed, respectively. In other words, HSQC spectra show the correlation between a proton chemical shift with the carbon directly bonded ($^{1}J_{CH}$). Instead, HMBC is the experiment in which are observed the correlations proton-carbon two or three bond away ($^{2,3}J_{CH}$) while the direct correlations ($^{1}J_{CH}$) are suppressed, suggesting the connection among fragments and assembling the whole structure.

In the three years of PhD course, I had the opportunity to acquire 1D and 2D experiments on Varian Inova 700 and 500 (Agilent Technology) and Bruker Avance Neo 400 spectrometer (Bruker) equipped with a ^{13}C enhanced HCN Cold Probe and RT-DR-BF/1H-5mm-OZ Smart Probe, respectively. Chemical shifts were referenced to residual solvent signal as internal standard and expressed in ppm. The 1D spectra have been transformed at 64 K points (digital resolution of 0.09 Hz) for an accurate measurements of coupling constants. Two and three bond ^{1}H-^{13}C connectivities were determined by gradient 2D HMBC experiments optimized for a $^{2,3}J$ of 8 Hz.

CHAPTER 6

Spectroscopic data

^{1}H NMR of polyaurine A (**19**) in $CDCl_3$

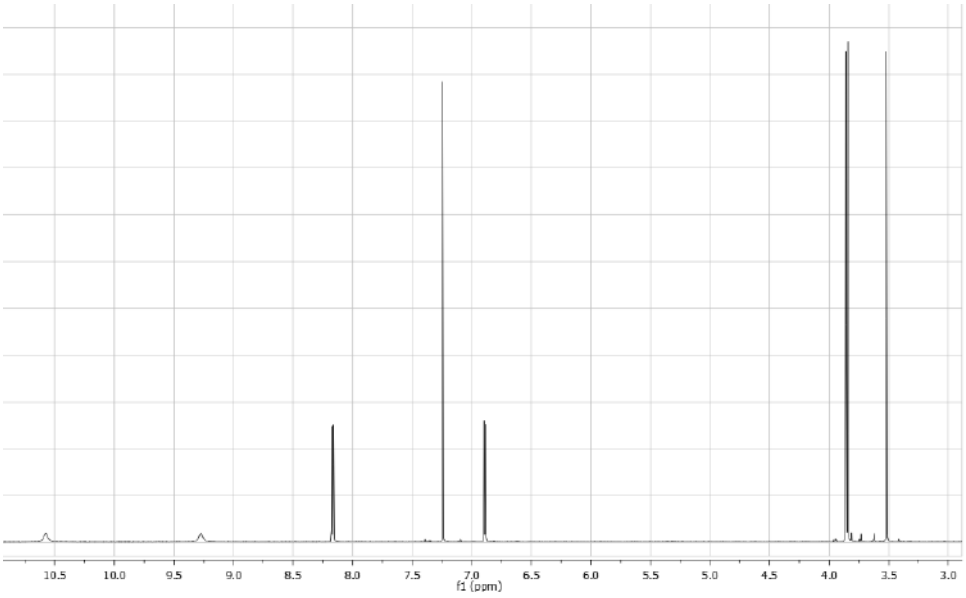

^{13}C NMR of polyaurine A (**19**) in $CDCl_3$

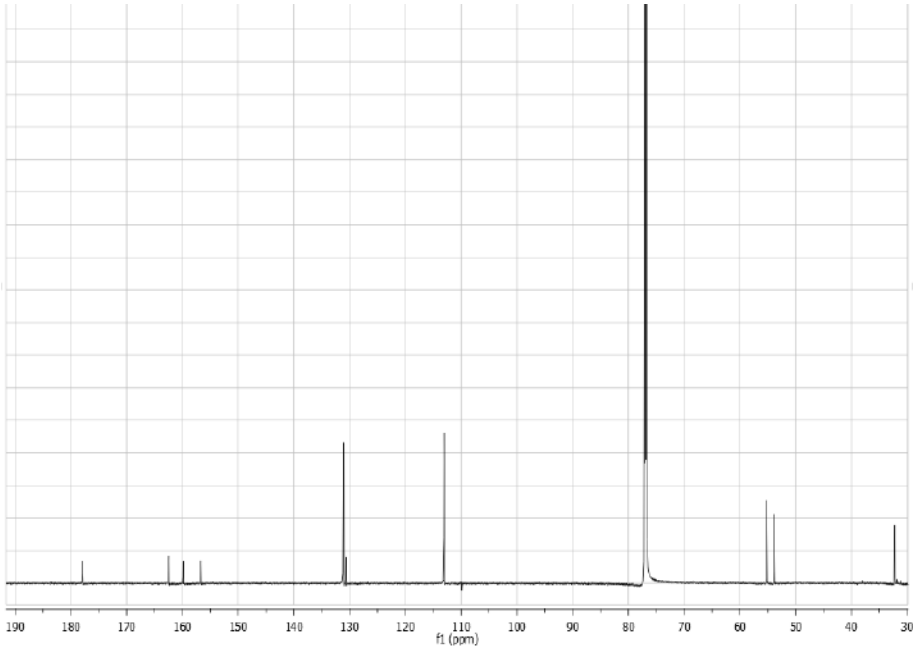

COSY spectrum of polyaurine A (**19**) in $CDCl_3$

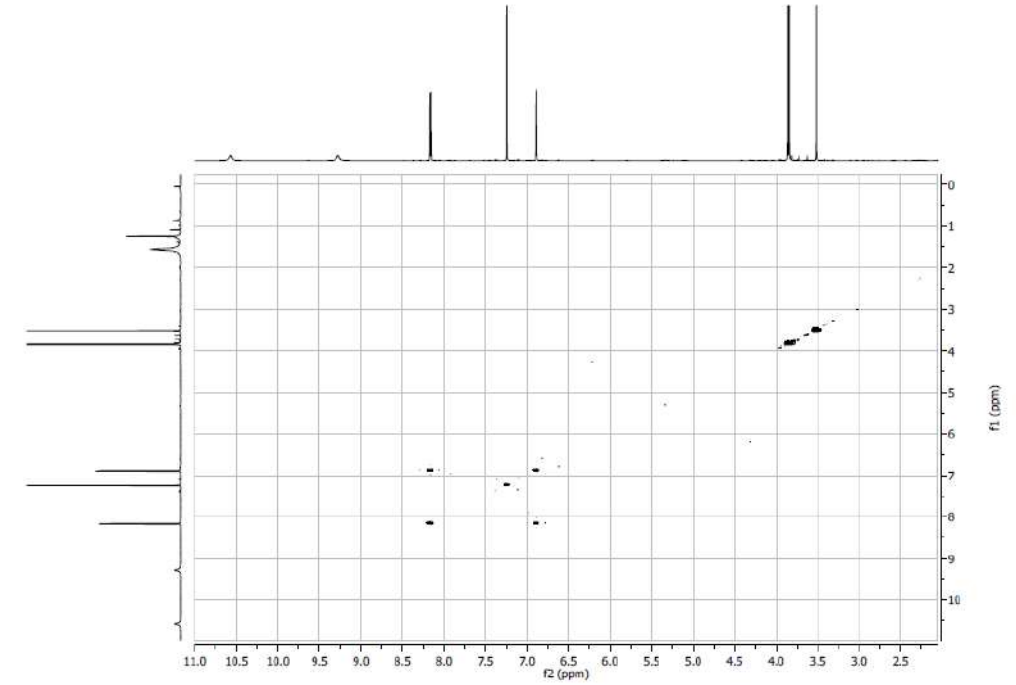

HSQC spectrum of polyaurine A (**19**) in $CDCl_3$

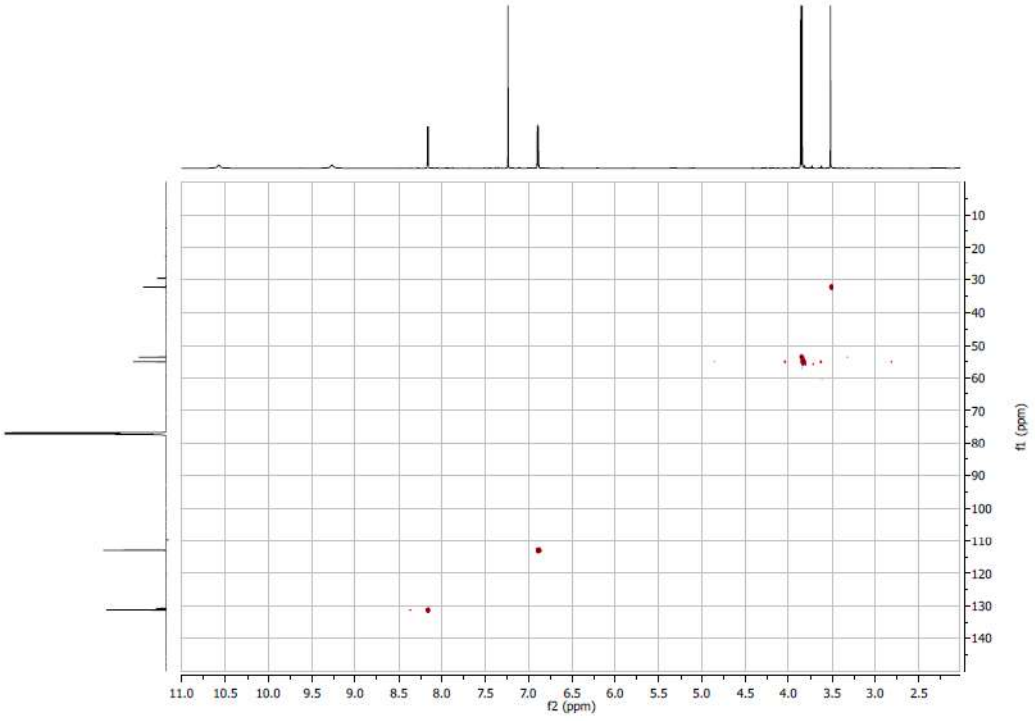

HMBC spectrum of polyaurine A (**19**) in $CDCl_3$

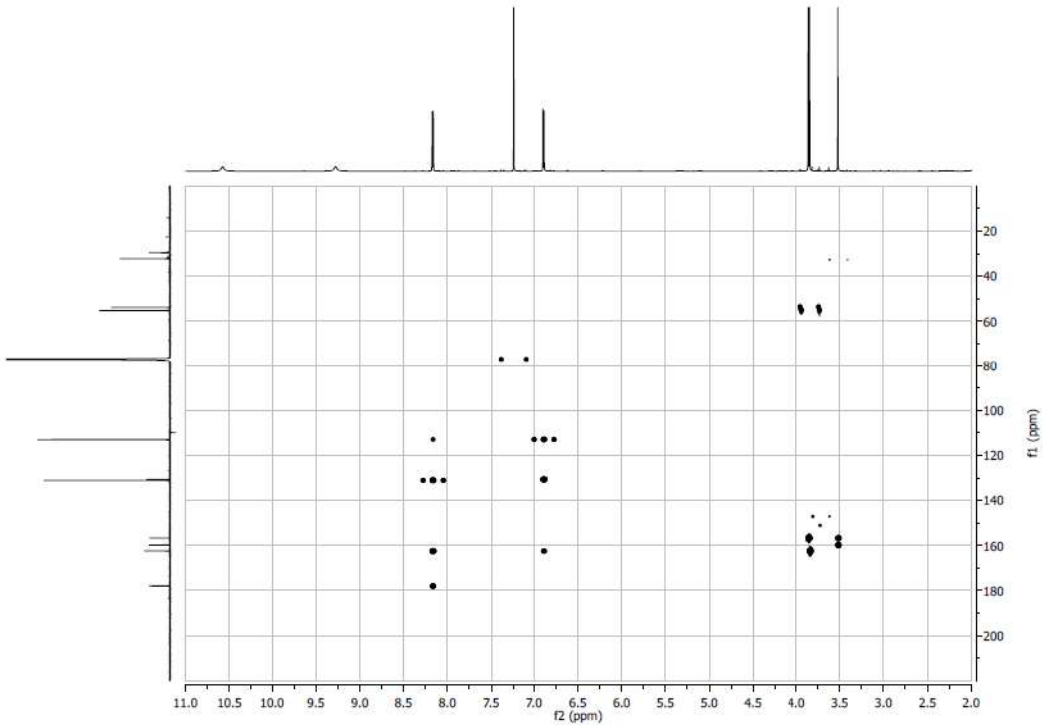

HRESIMS spectrum of polyaurine A (**19**)

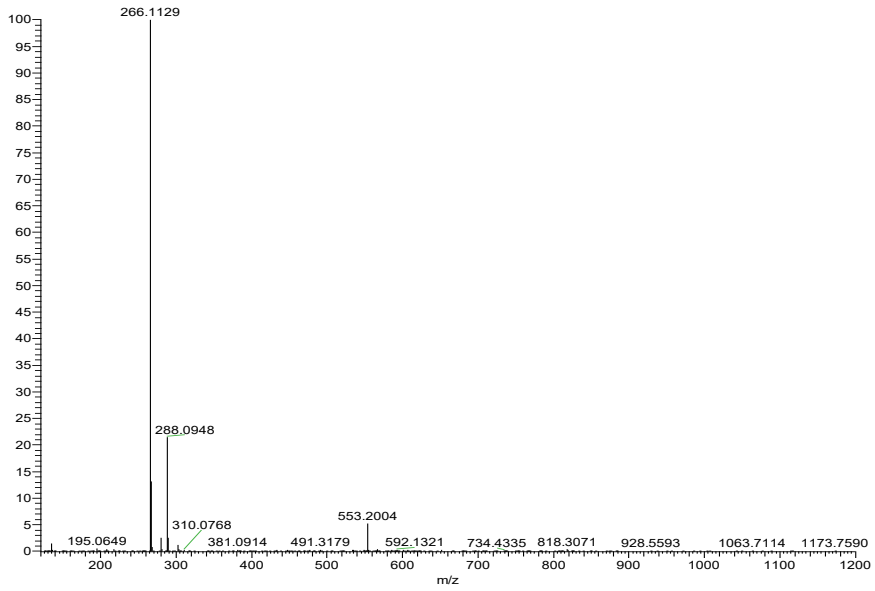

^{1}H NMR of polyaurine B (**20**) in $CDCl_3$

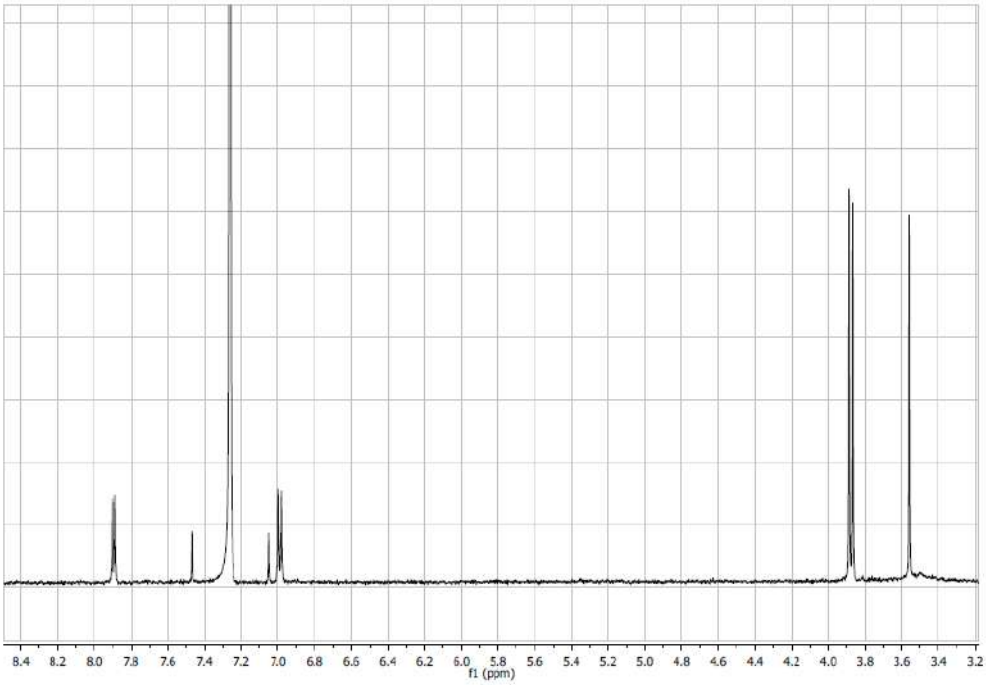

^{13}C NMR of polyaurine B (**20**) in $CDCl_3$

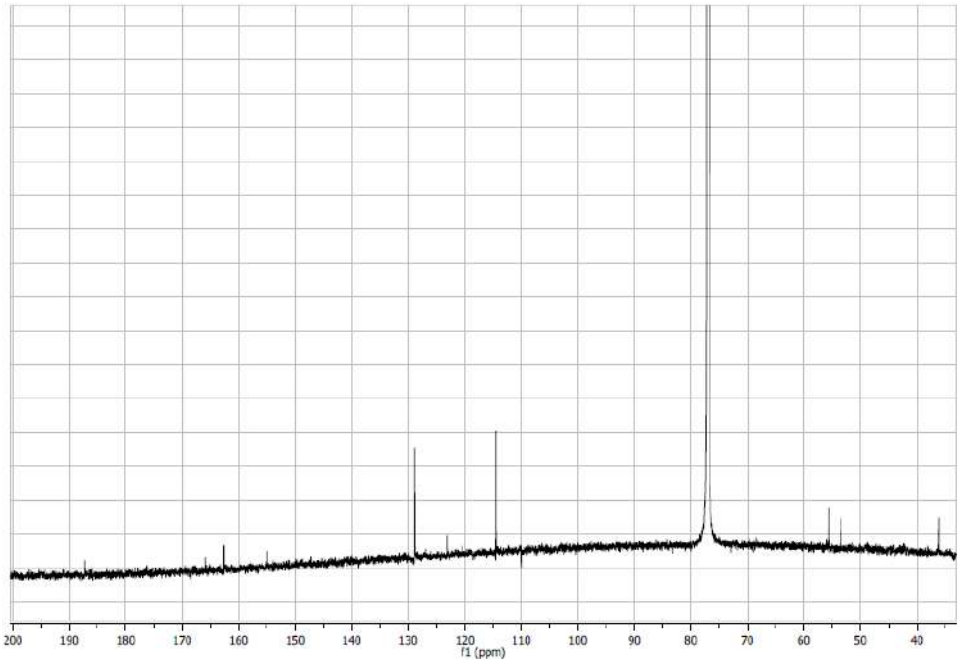

COSY spectrum of polyaurine B (**20**) in $CDCl_3$

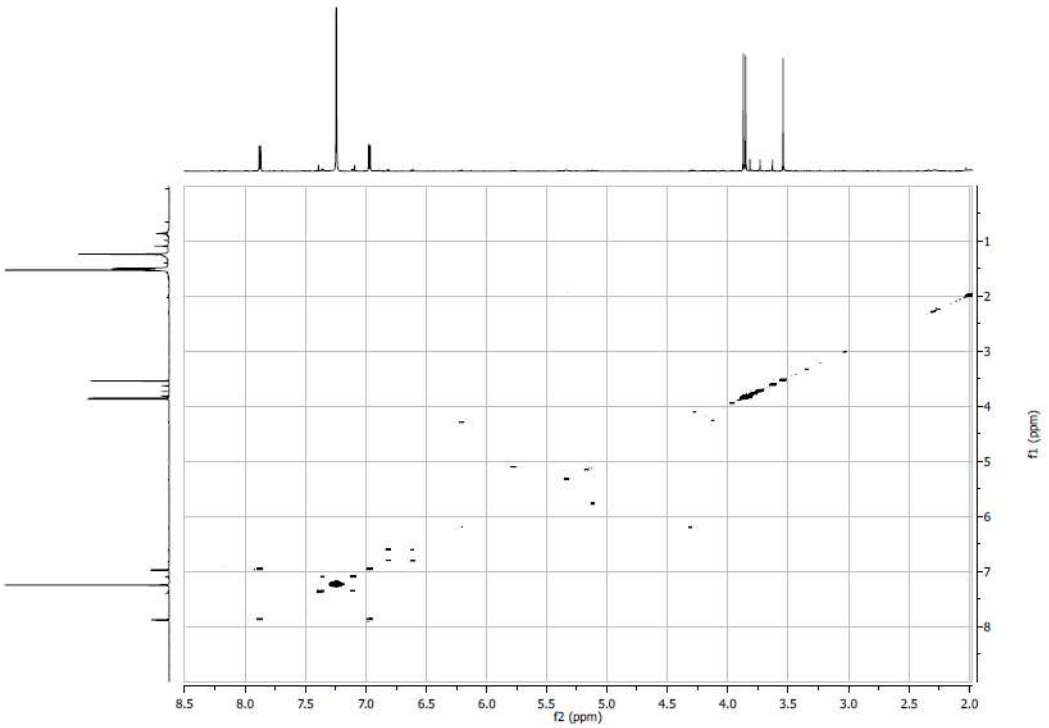

HSQC spectrum of polyaurine B (**20**) in $CDCl_3$

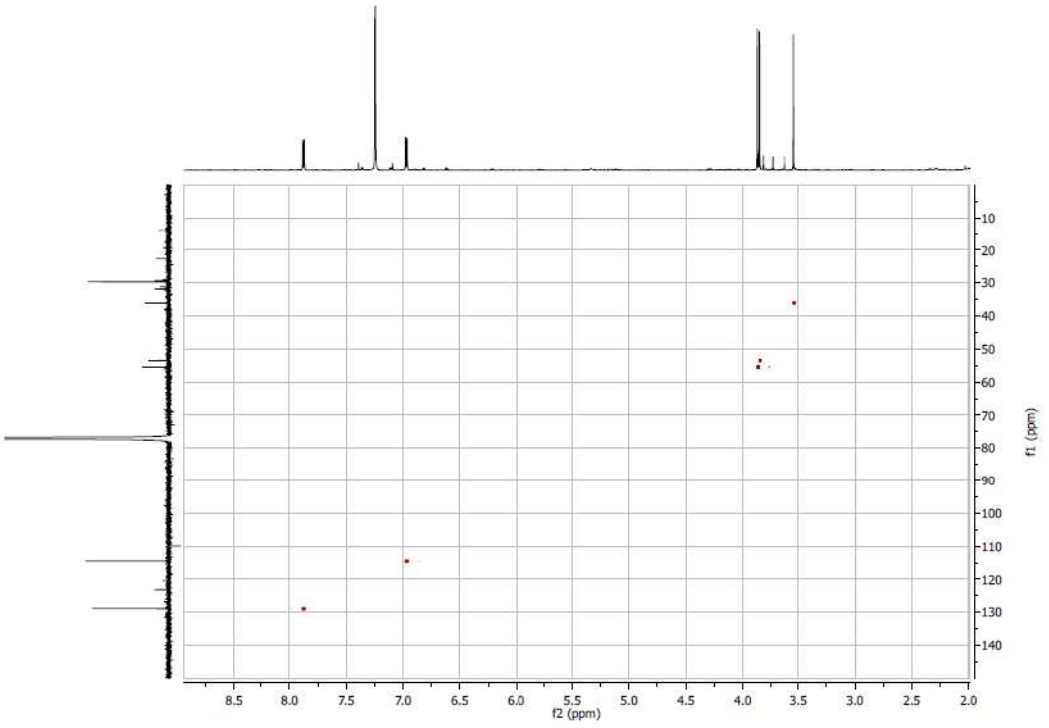

HMBC spectrum of polyaurine B (**20**) in $CDCl_3$

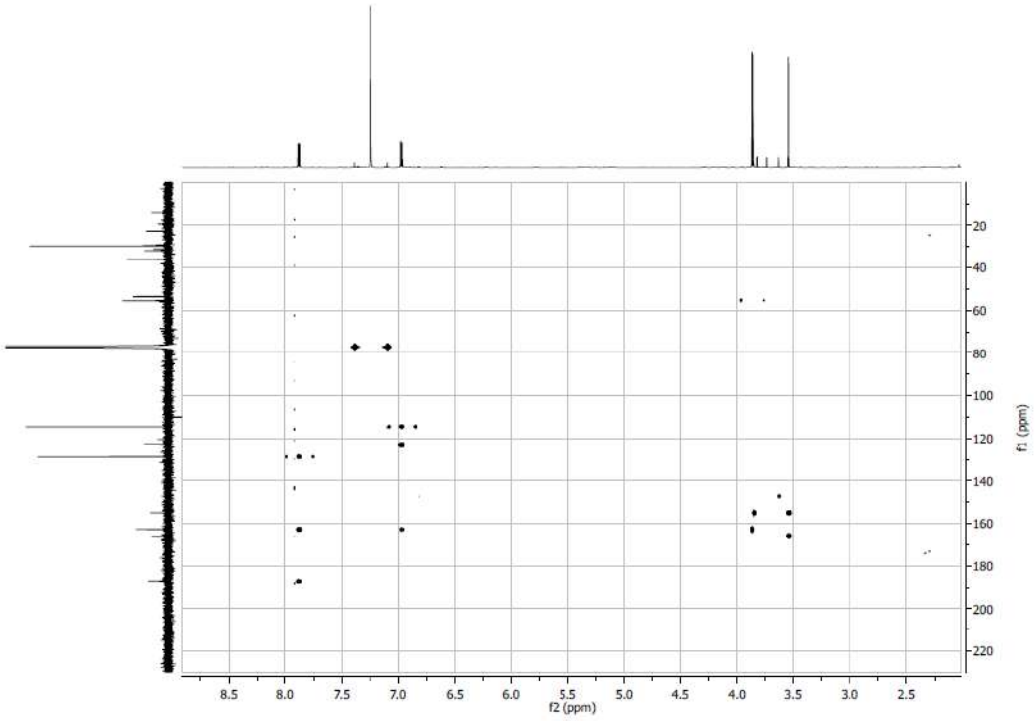

HRESIMS spectrum of polyaurine B (**20**)

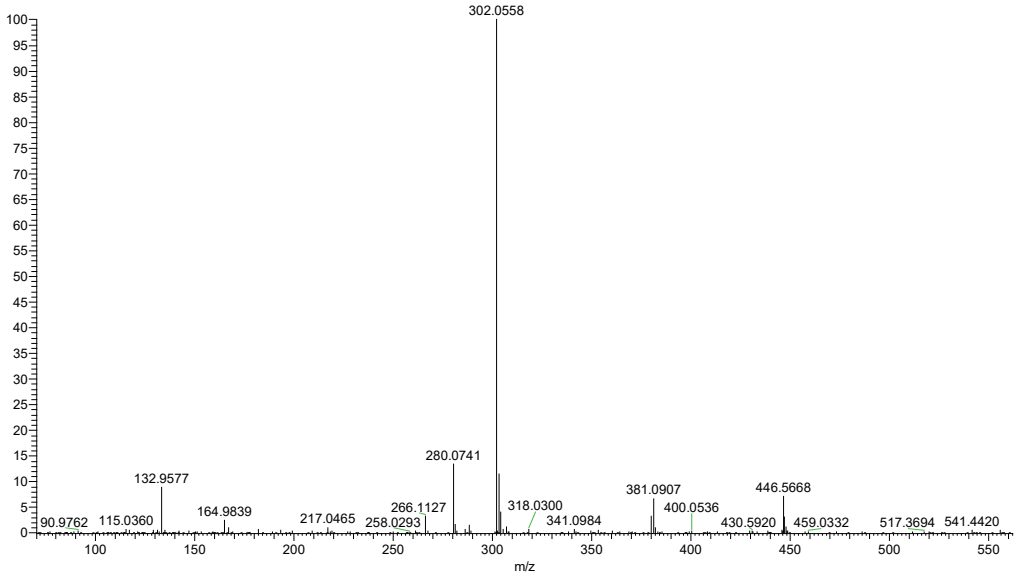

^{1}H NMR of compound **21** in $CDCl_3$

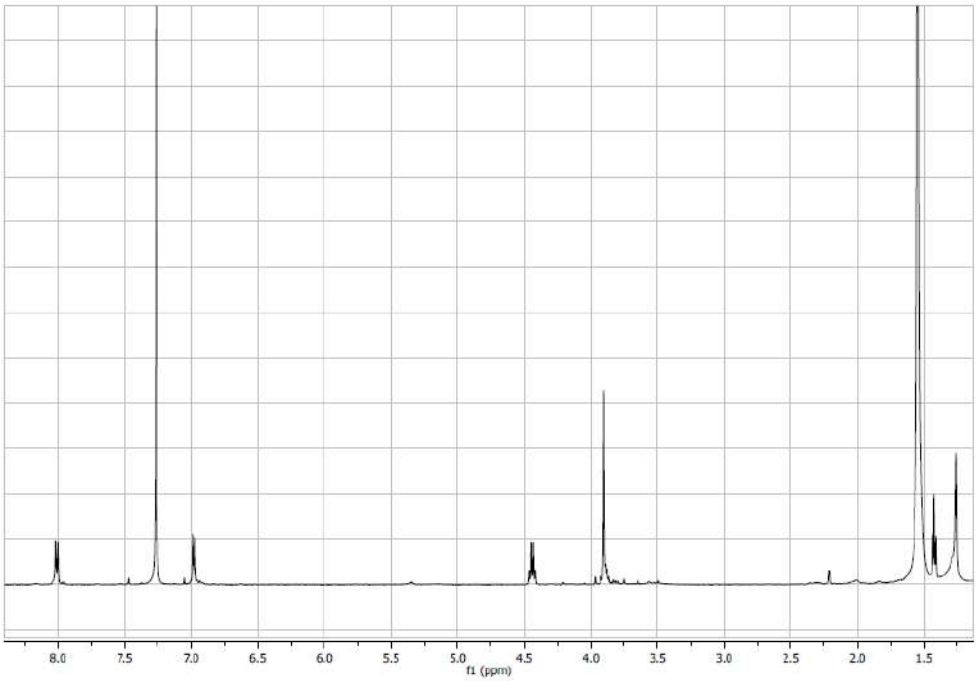

HRESIMS spectrum of compound **21**

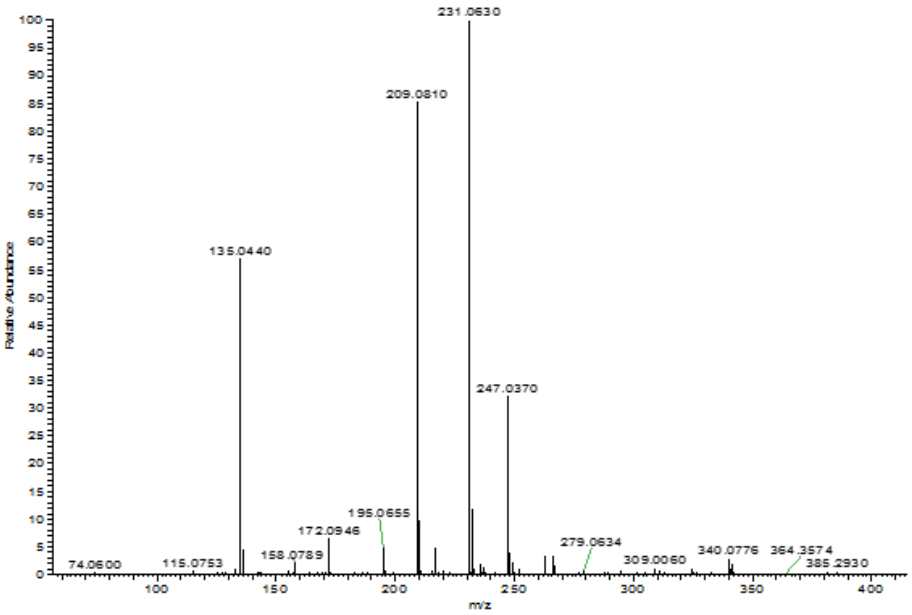

^{1}H NMR of compound **22** in $CDCl_3$

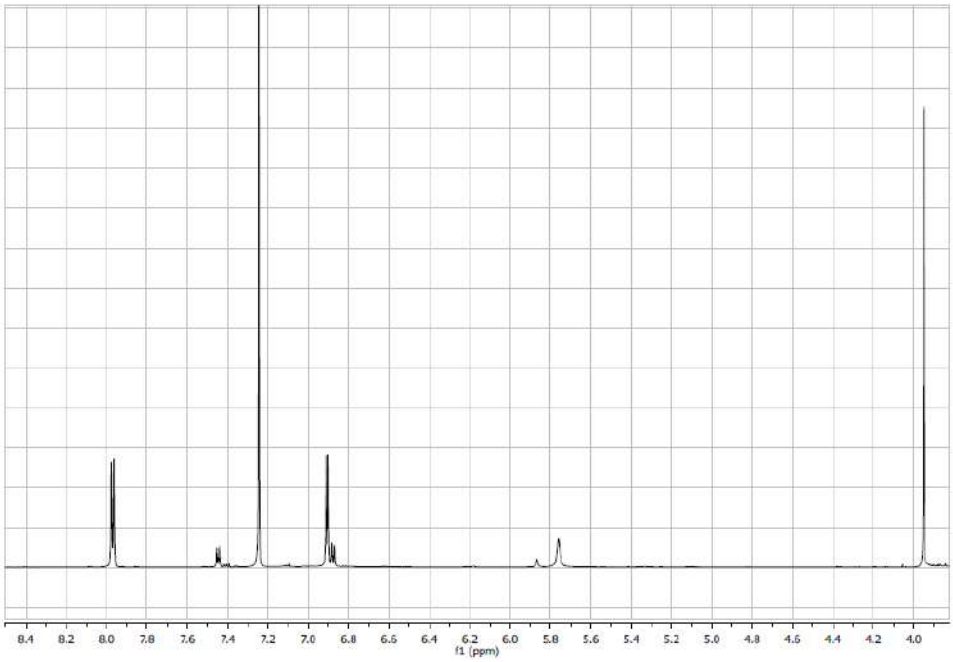

HRESIMS spectrum of compound **22**

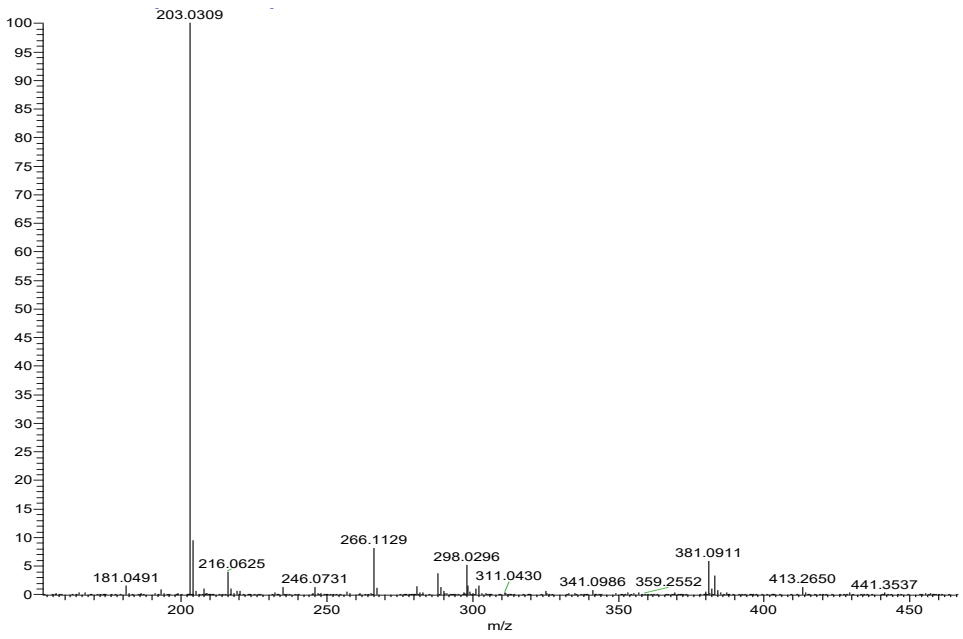

^{1}H NMR of compound **23** in $CDCl_3$

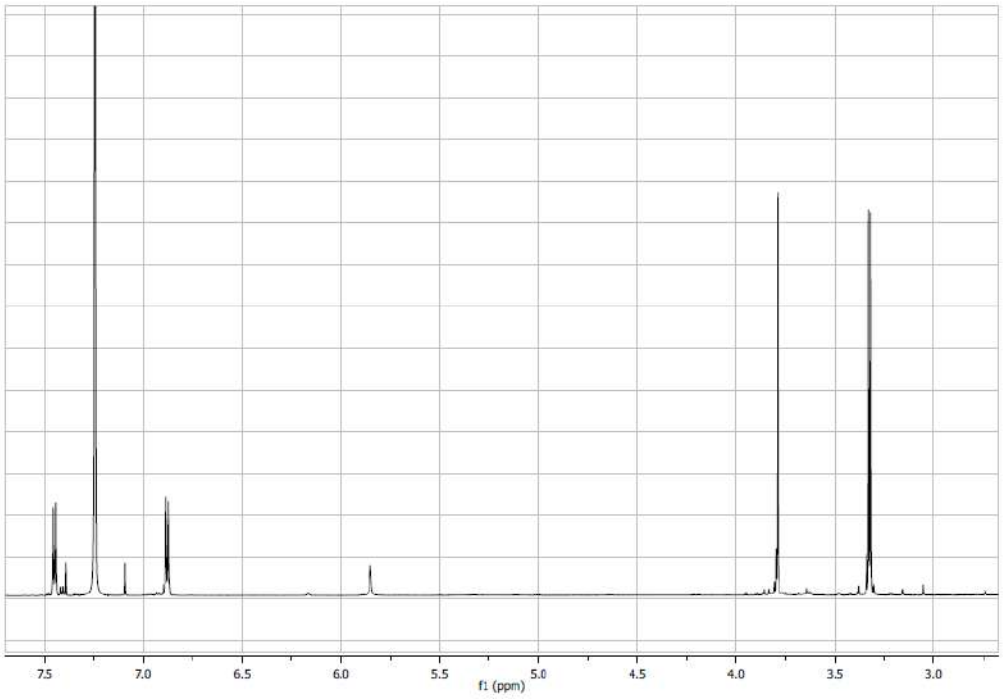

HRESIMS spectrum of compound **23**

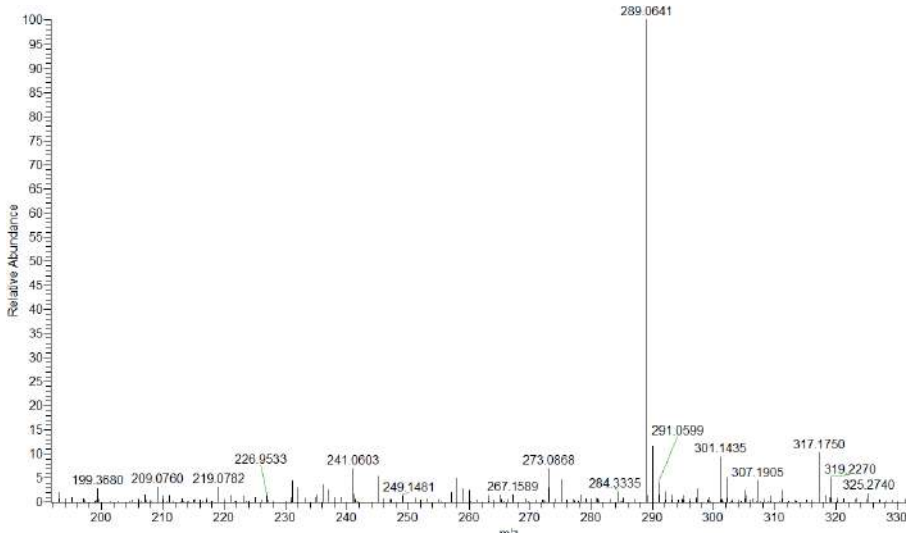

HRESIMS spectrum of compound **24**

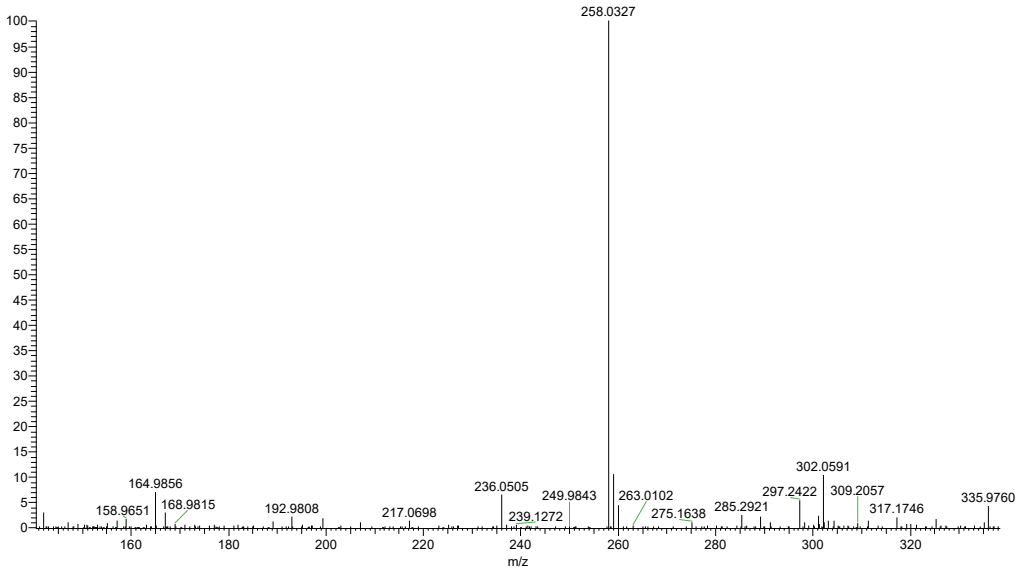

^{1}H NMR of compound **24** in $CDCl_3$

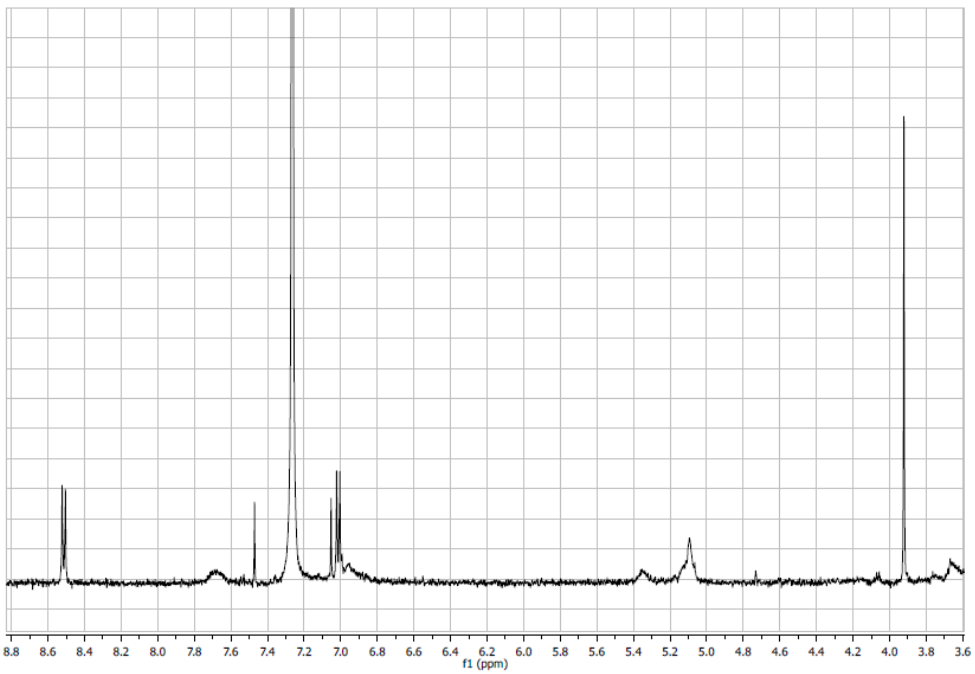

^{1}H NMR of compound **25** in $CDCl_3$

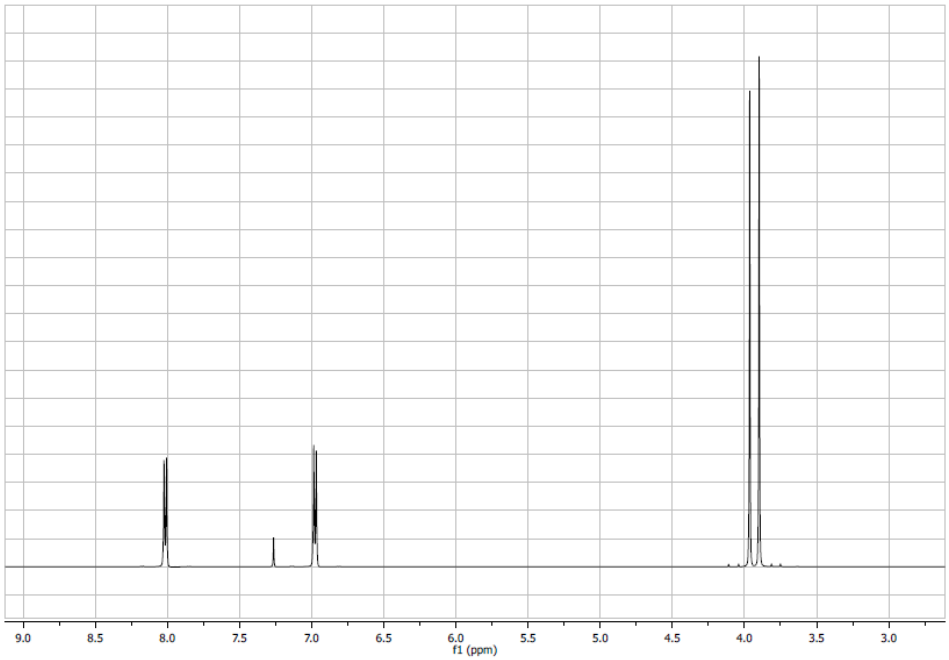

HRESIMS spectrum of compound **25**

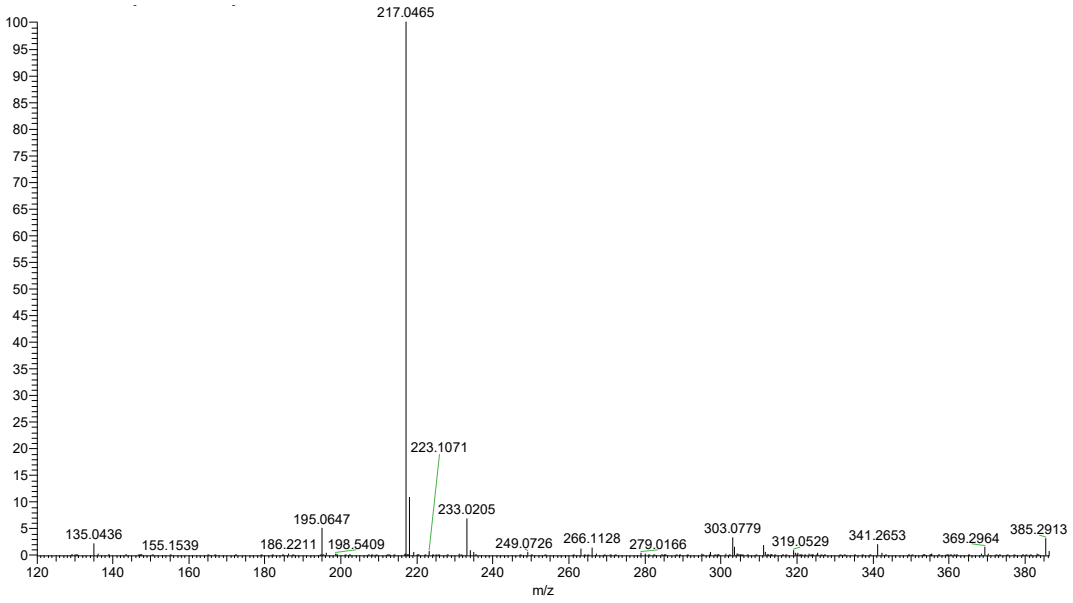

^{1}H NMR of compound **26** in $CDCl_3$

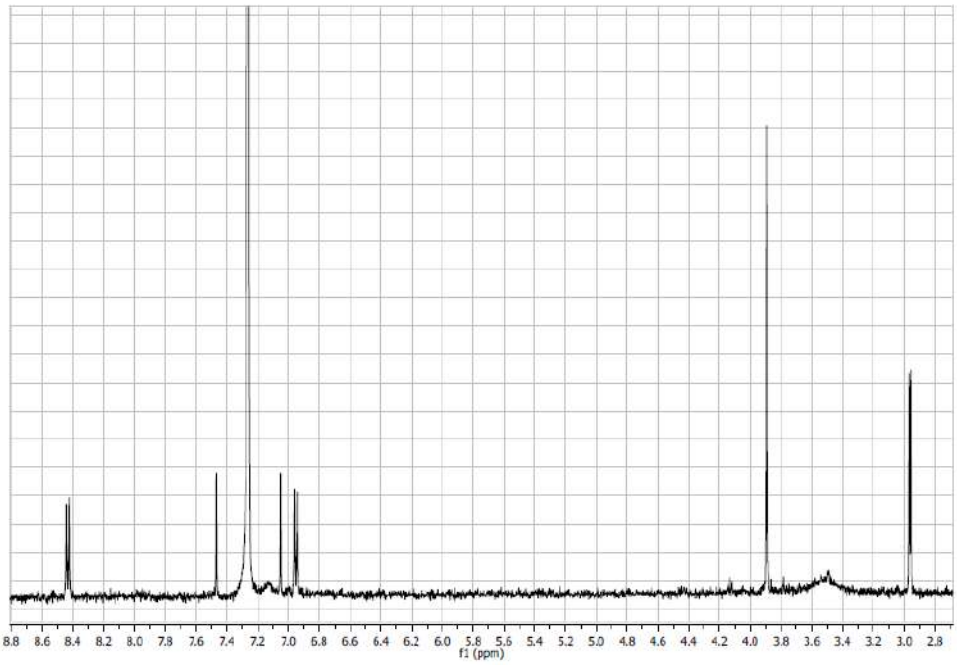

HRESIMS spectrum of compound **26**

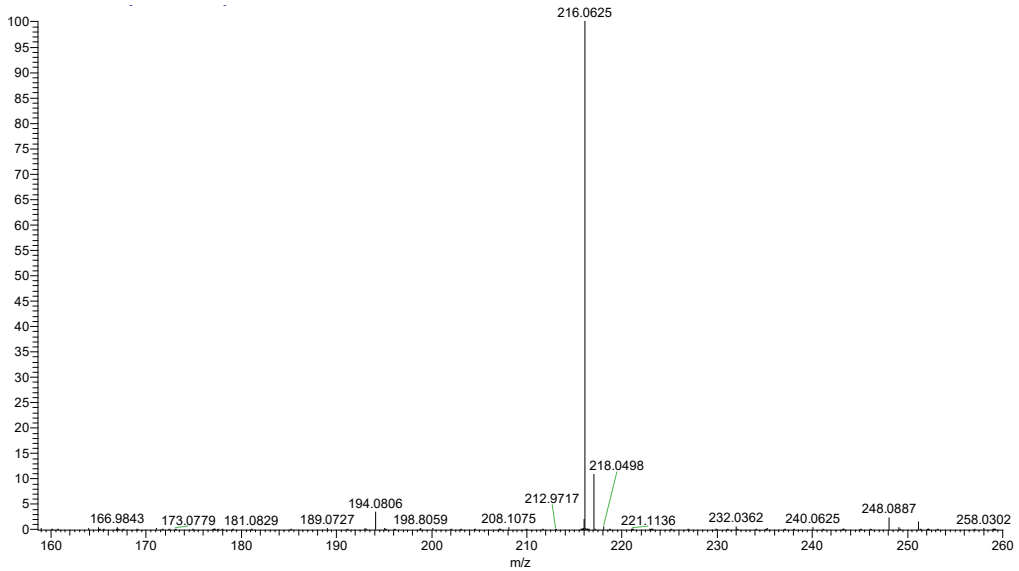

^{1}H-NMR of avarone (**45**) in $CDCl_3$

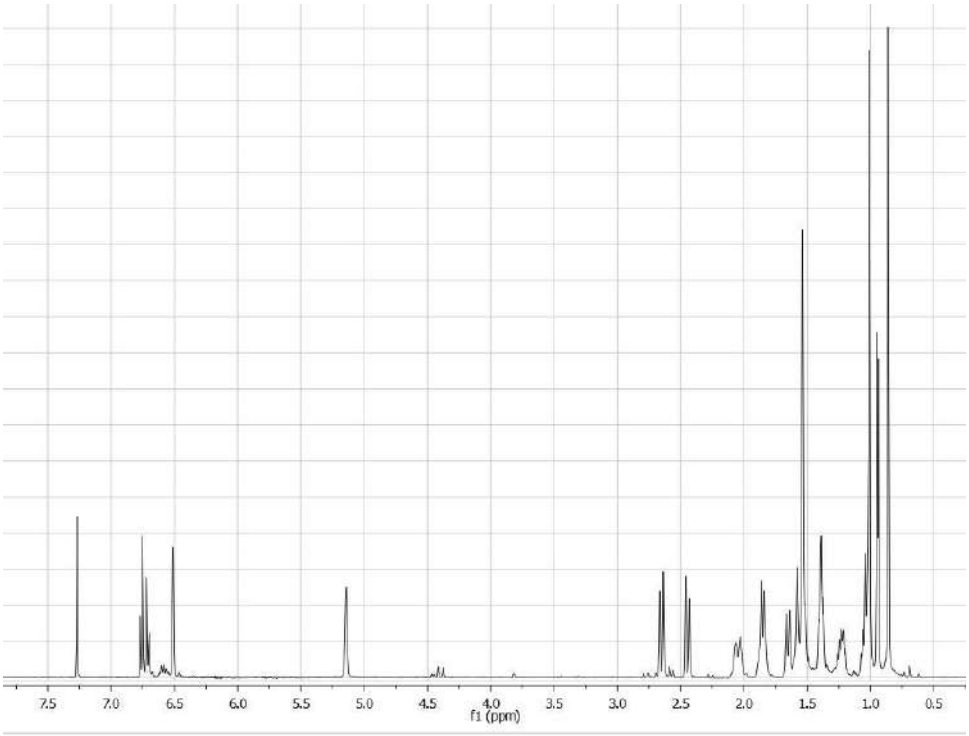

HRESIMS spectrum of avarone (**45**)

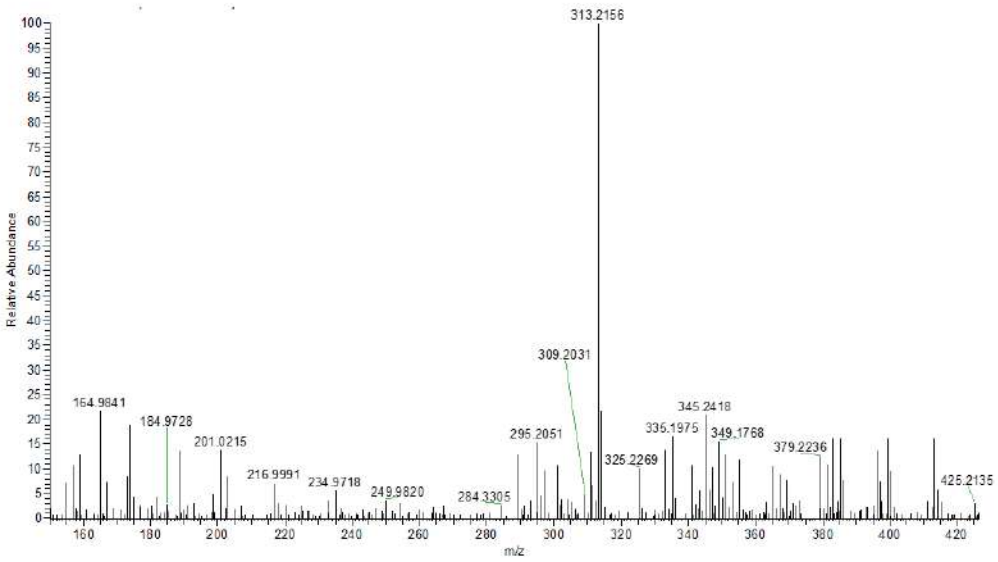

^{1}H NMR of thiazoavarone (**46**) in $CDCl_3$

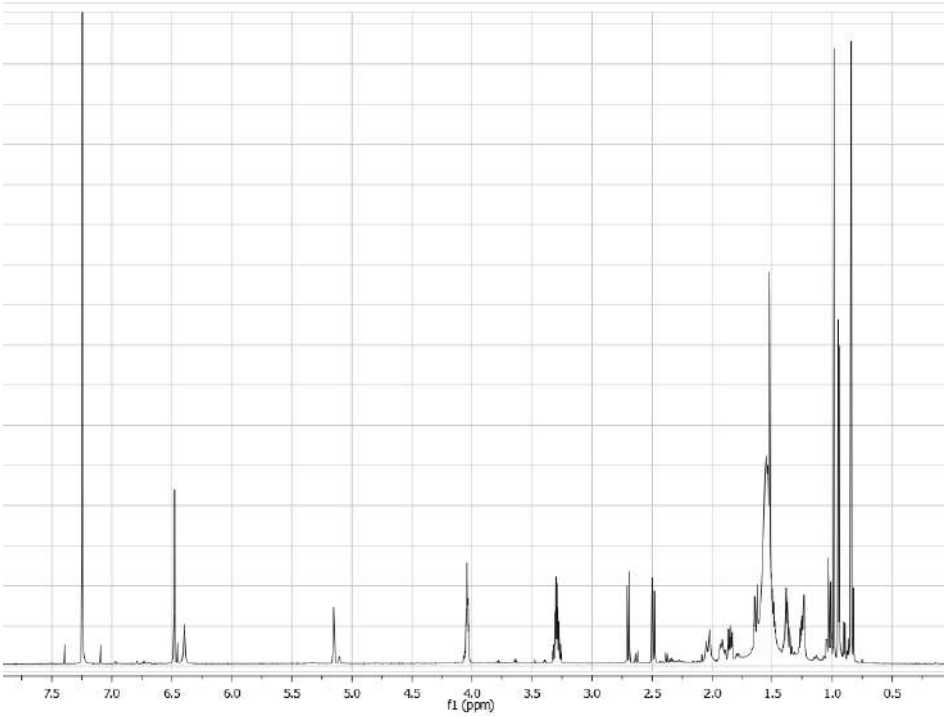

COSY spectrum of thiazoavarone (**46**) in $CDCl_3$

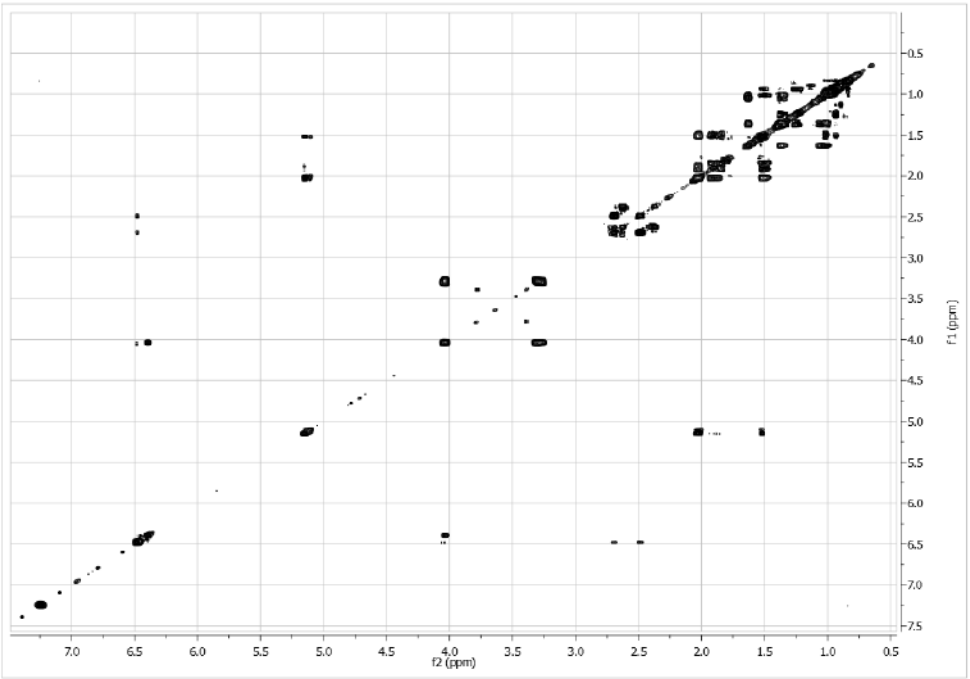

HSQC spectrum of thiazoavarone (**46**) in $CDCl_3$

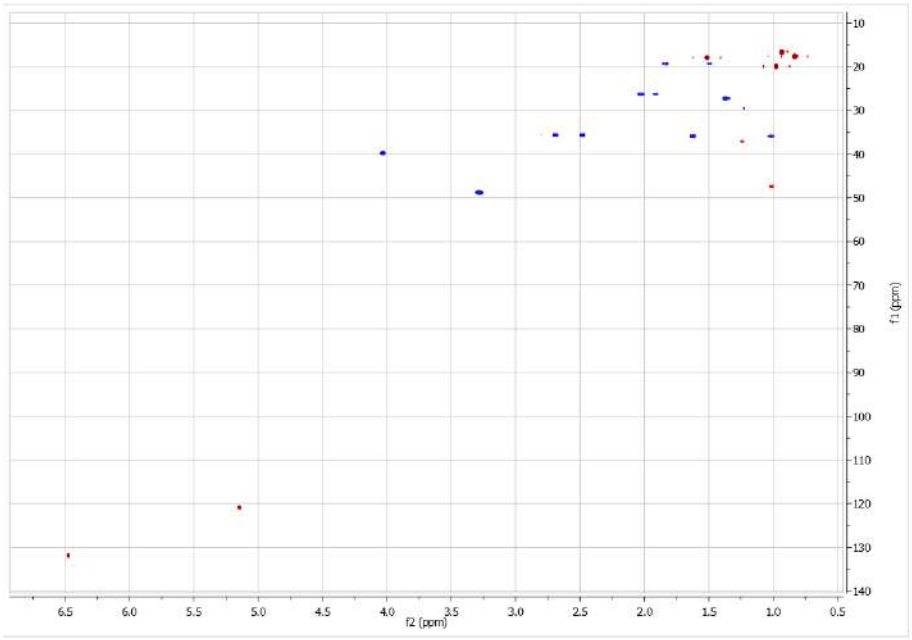

HMBC spectrum of thiazoavarone (**46**) in $CDCl_3$

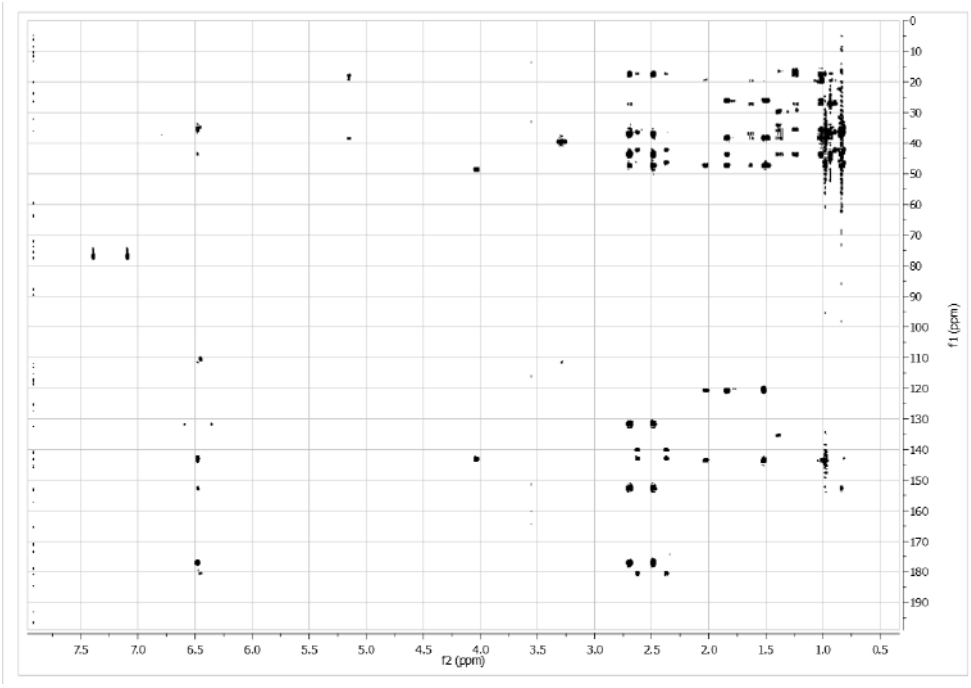

HRESIMS spectrum of thiazoavarone (**46**)

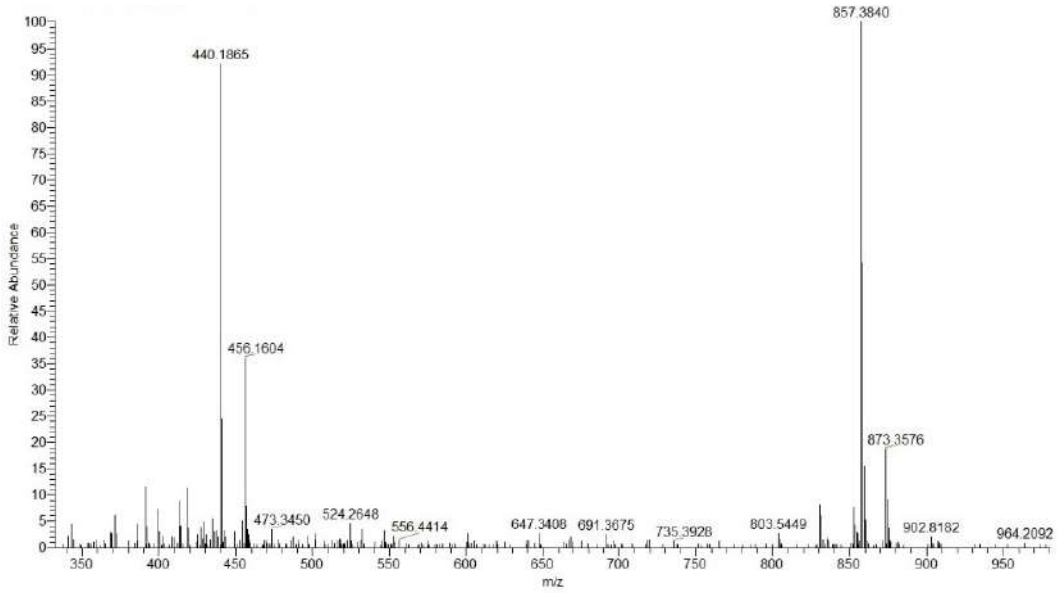

^{1}H-NMR spectrum of avarol (**47**) in $CDCl_3$

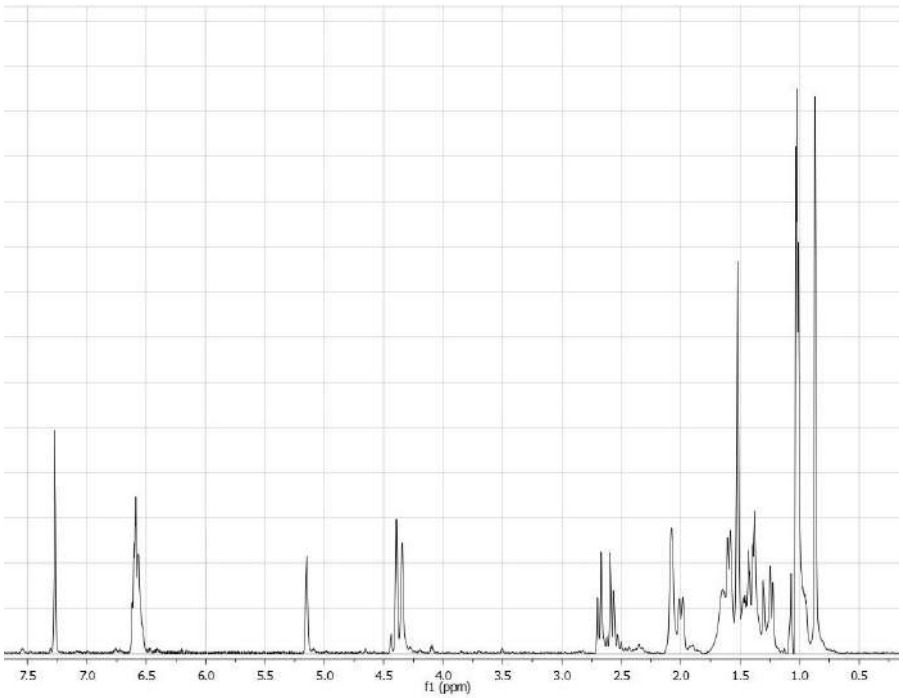

HRESIMS spectrum of avarol (**47**)

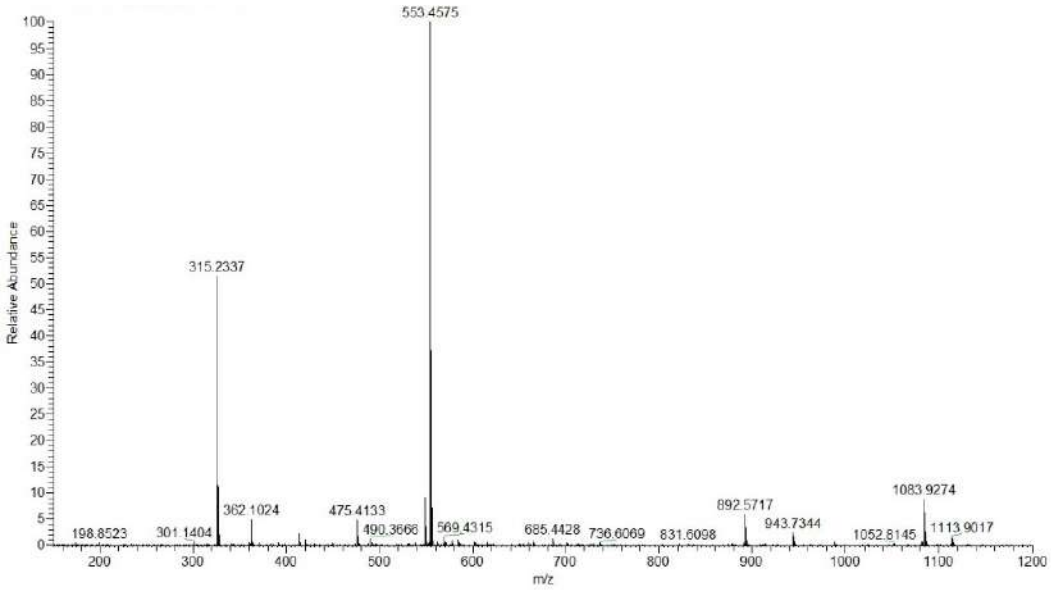

^{1}H NMR of compound **64** in $CDCl_3$

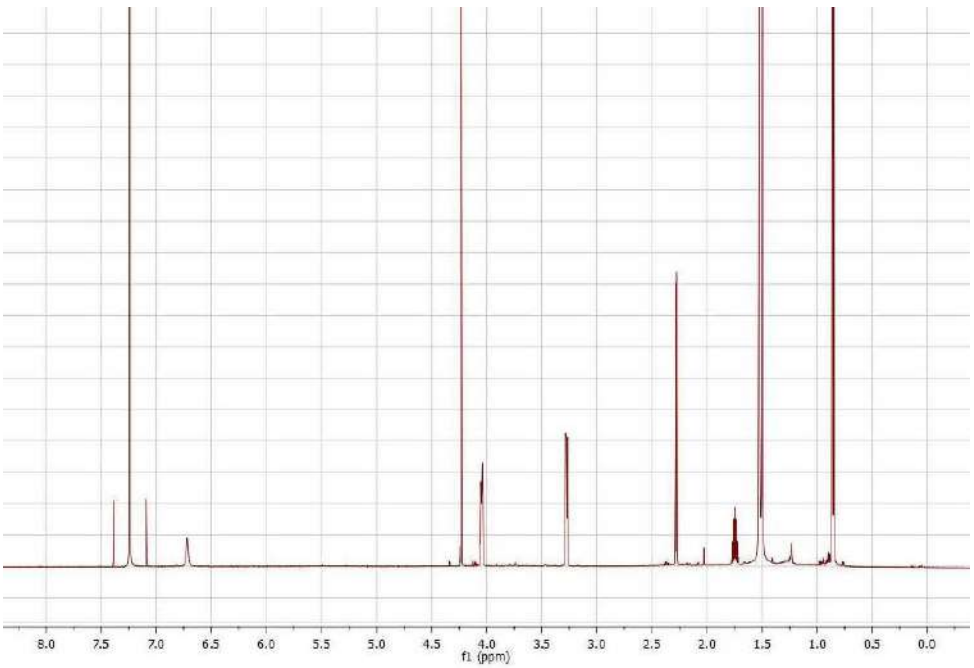

HRESIMS spectrum of compound **64**

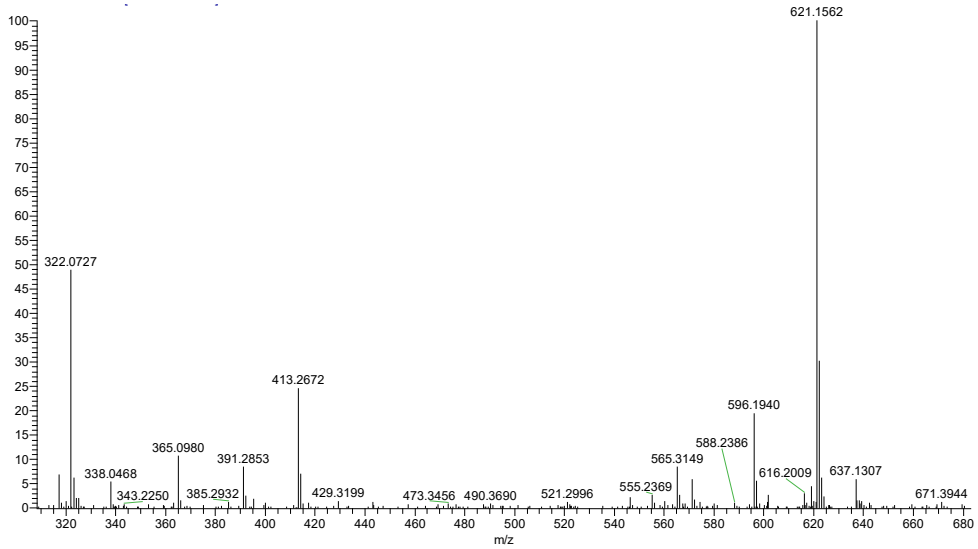

^{1}H NMR of compound **65** in $CDCl_3$

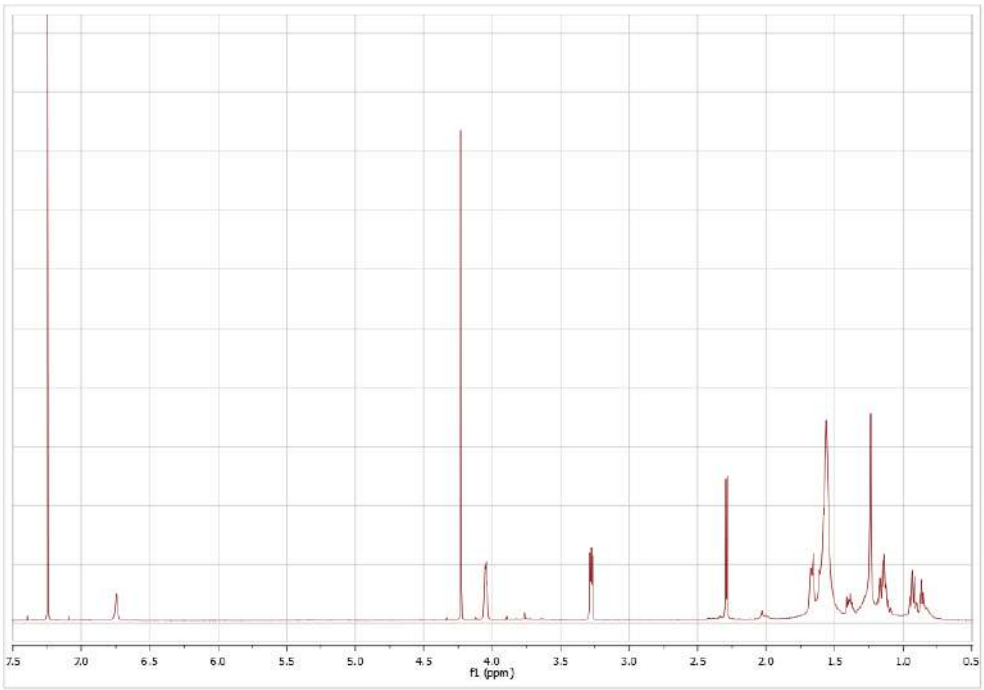

HSQC spectrum of compound **65** in $CDCl_3$

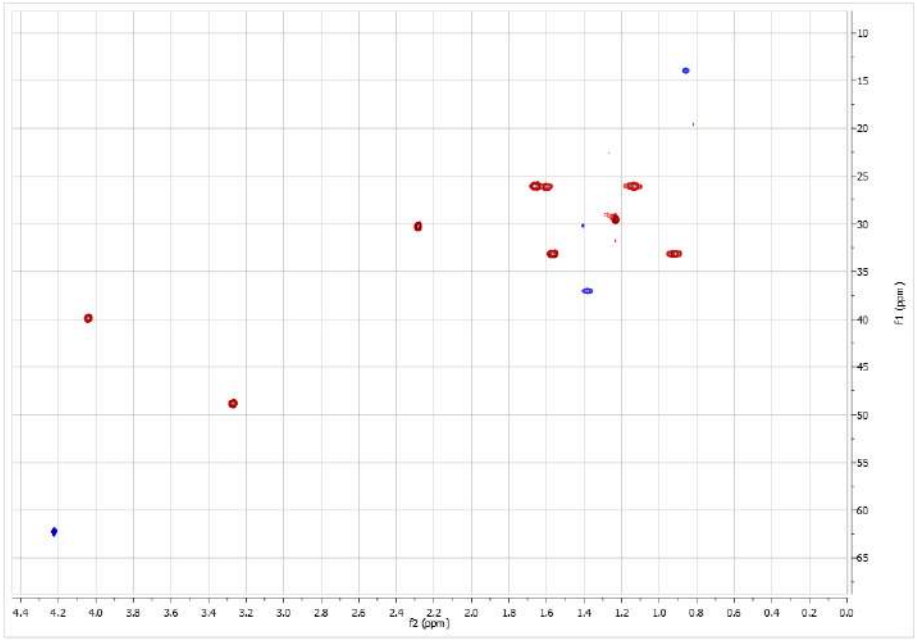

HMBC of compound **65** in $CDCl_3$

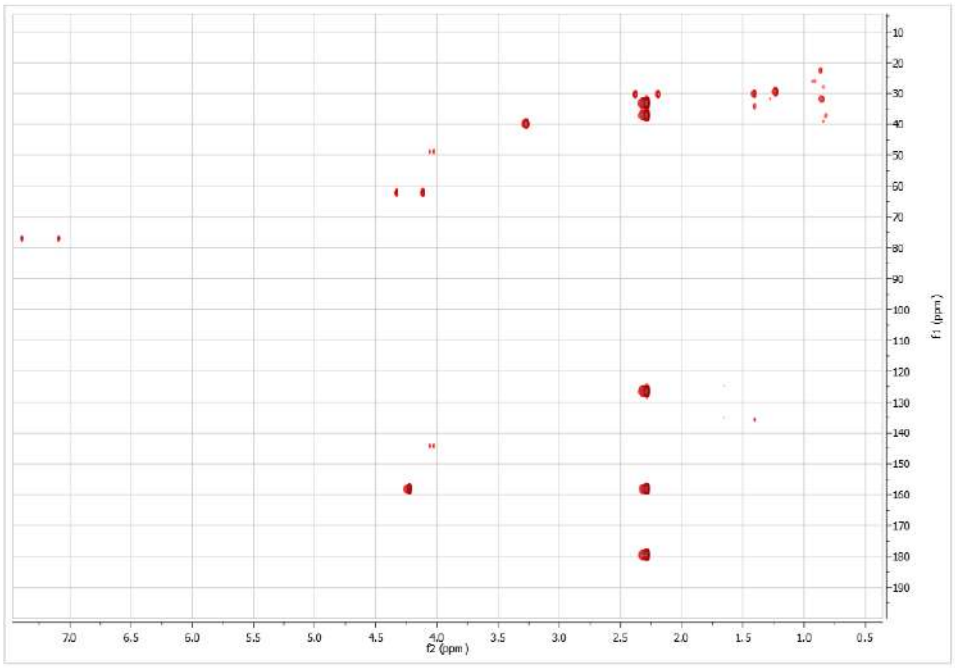

HRESIMS spectrum of compound **65**

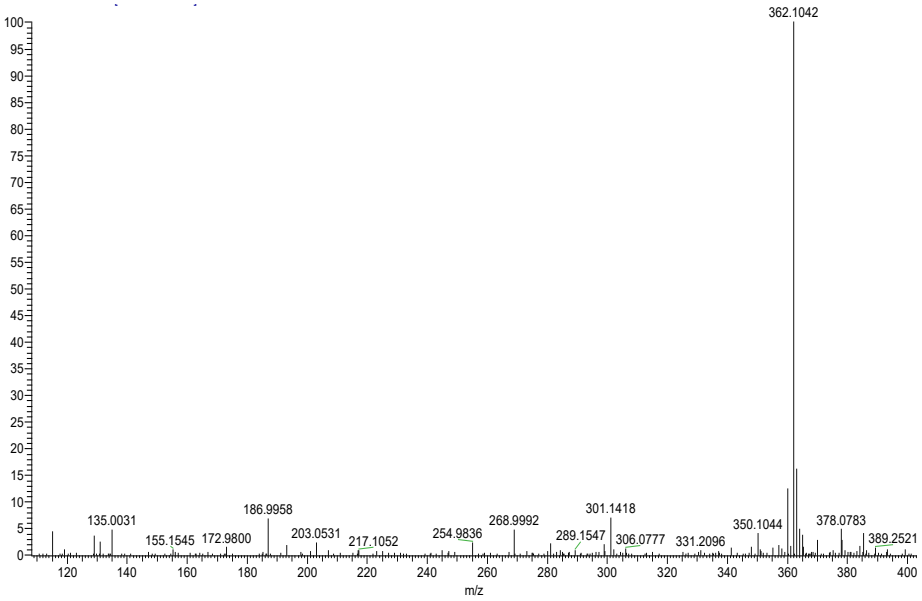

^{1}H NMR of compound **66** in $CDCl_3$

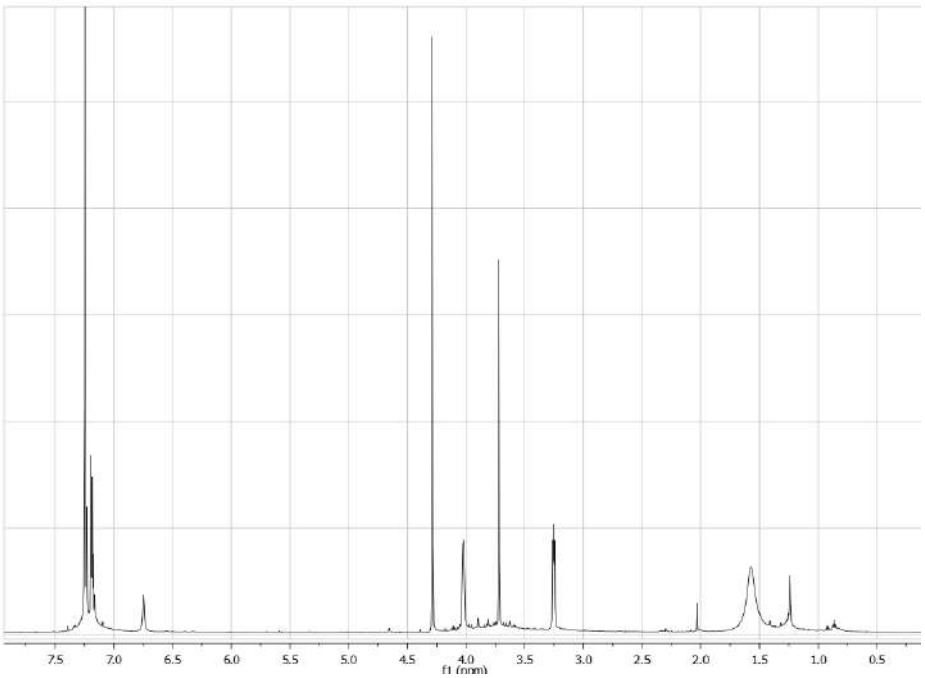

HSQC of compound **66** in $CDCl_3$

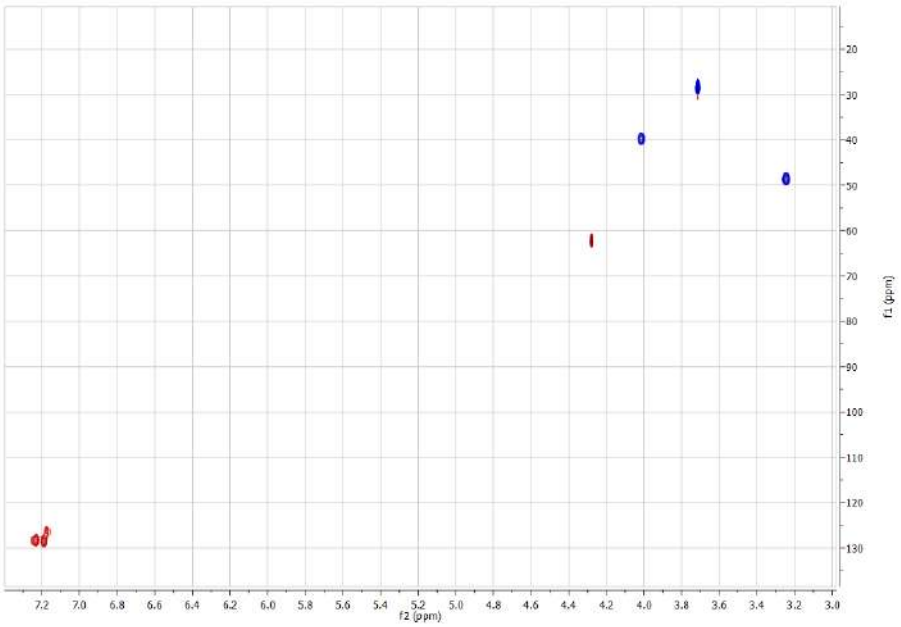

HMBC NMR of compound **66** in $CDCl_3$

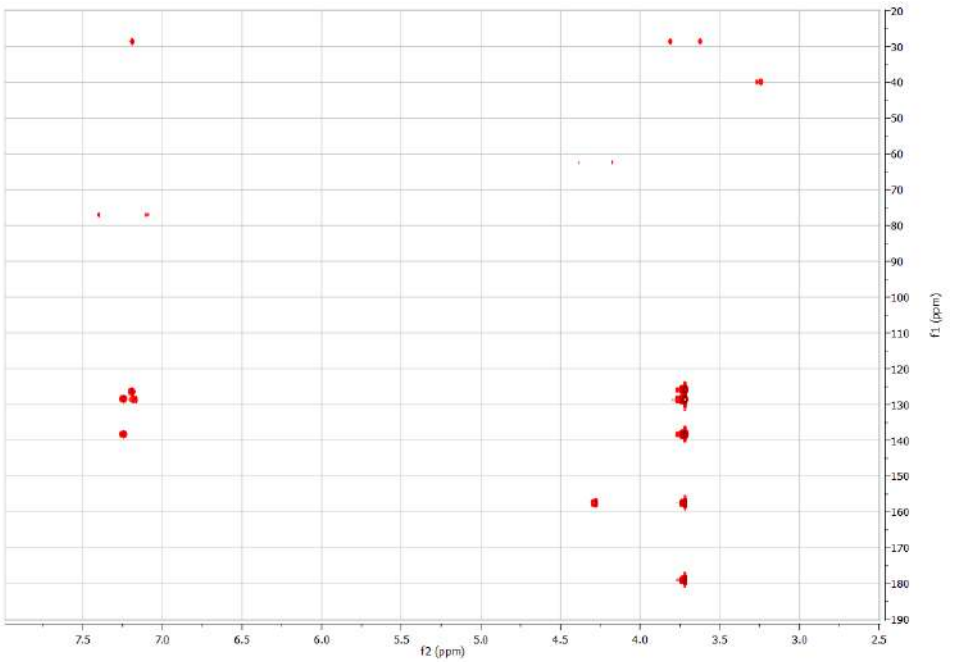

HRESIMS spectrum of compound **66**

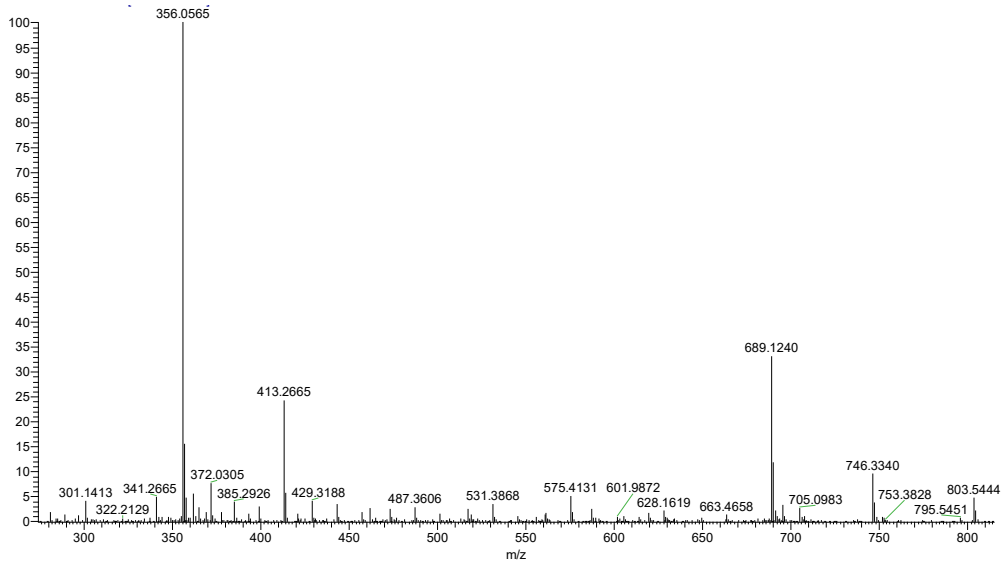

^{1}H NMR of compound **67** in $CDCl_3$

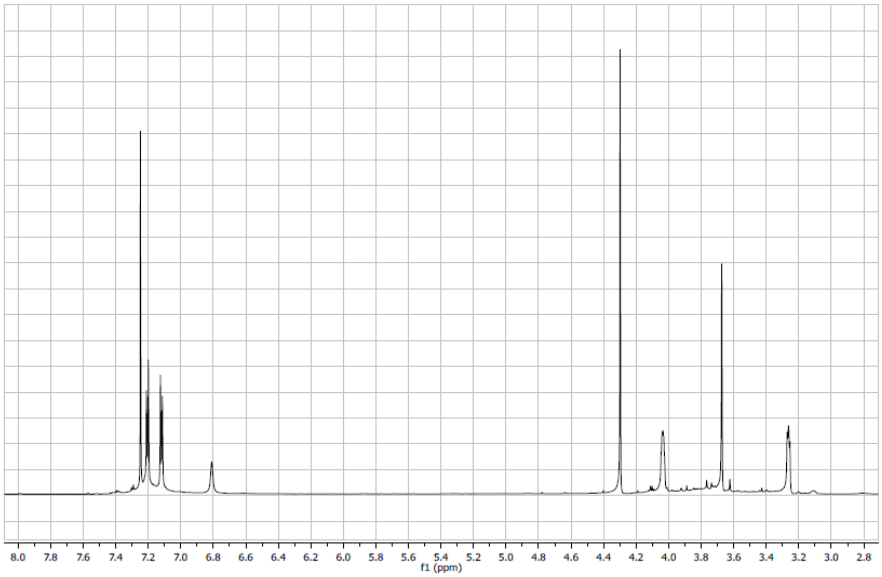

HMBC spectrum of compound **67** in $CDCl_3$

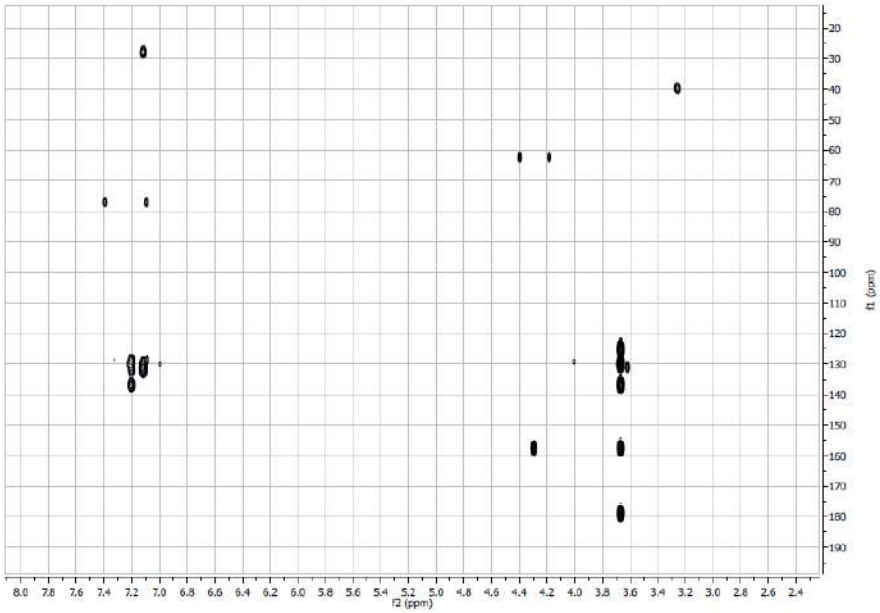

HRESIMS spectrum of compound **67**

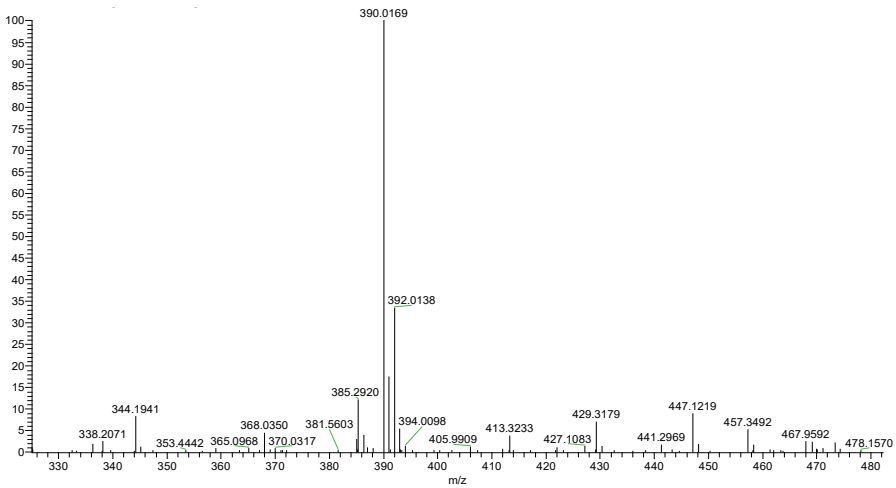

^{1}H NMR of compound **68** in $CDCl_3$

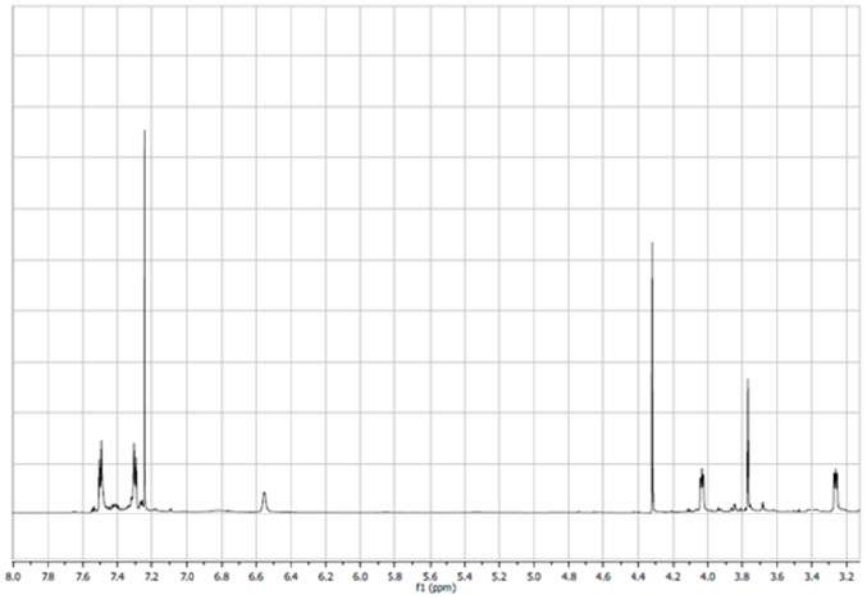

HMBC spectrum of compound **68** in $CDCl_3$

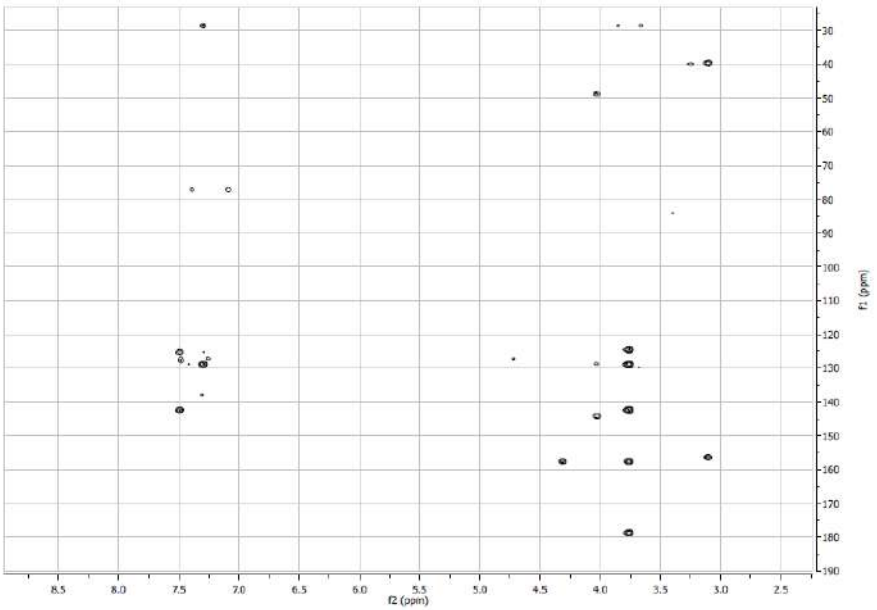

HRESI MS spectrum of compound **68**

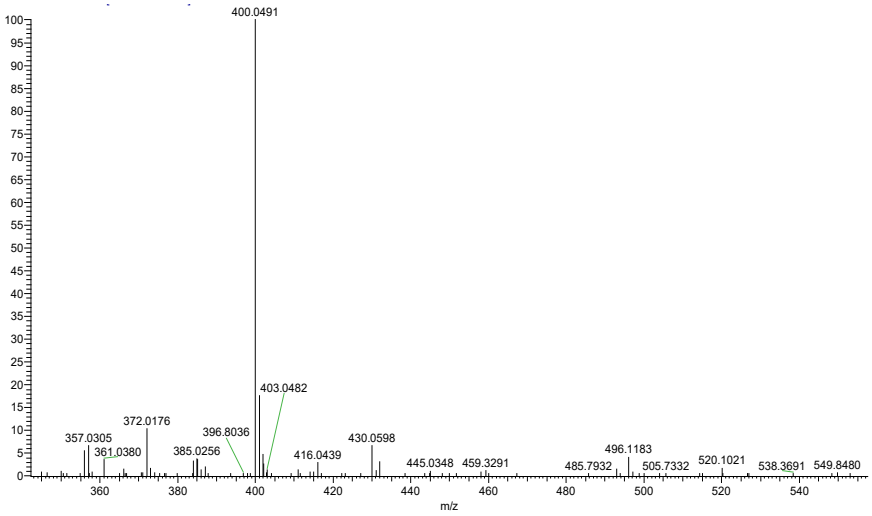

^{1}H NMR of compound **72** in $CDCl_3$

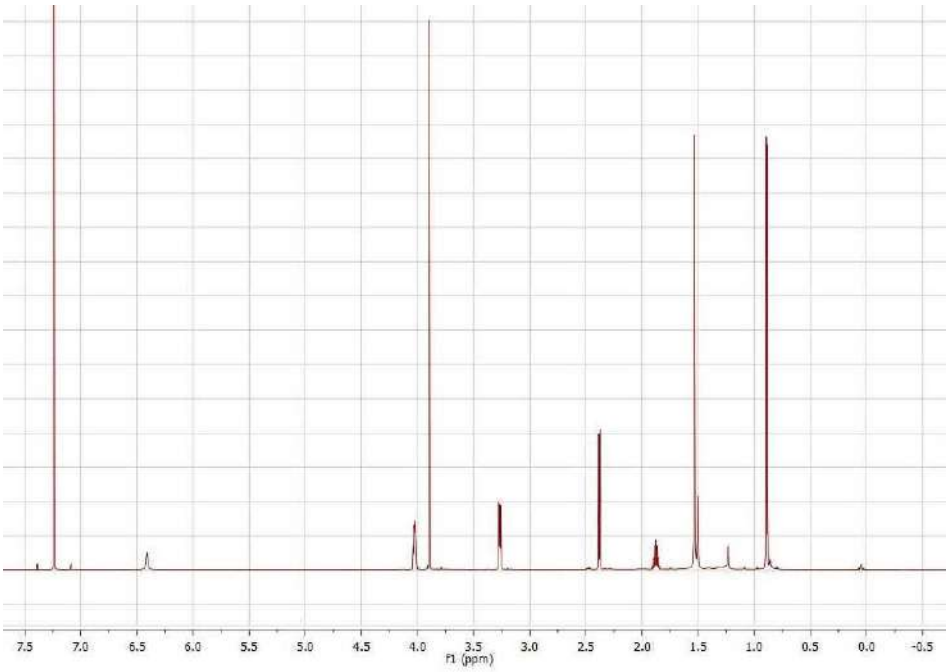

HRESIMS spectrum of compound **72**

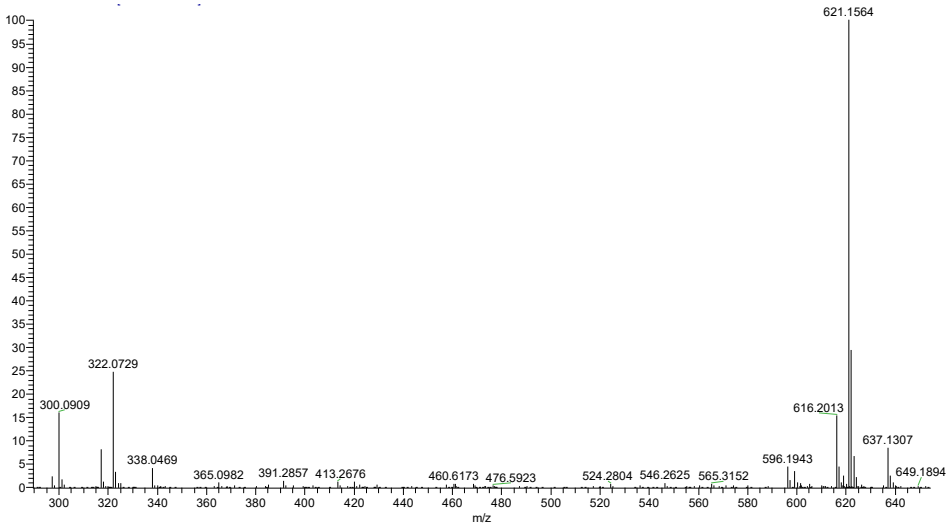

^{1}H NMR of compound **73** in $CDCl_3$

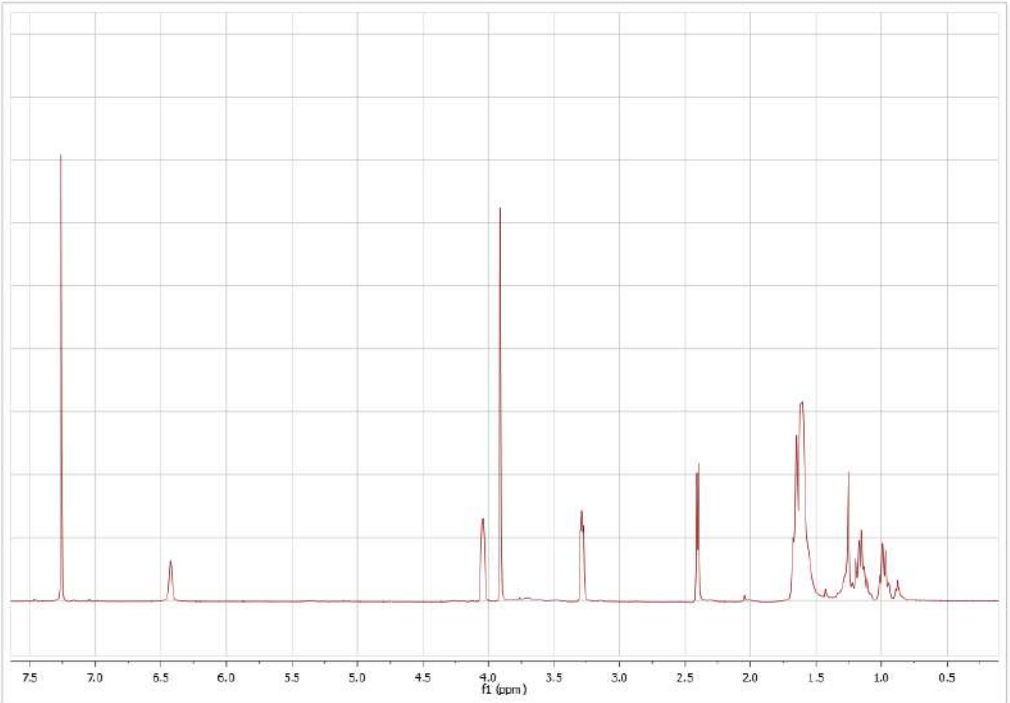

HSQC spectrum of compound **73** in $CDCl_3$

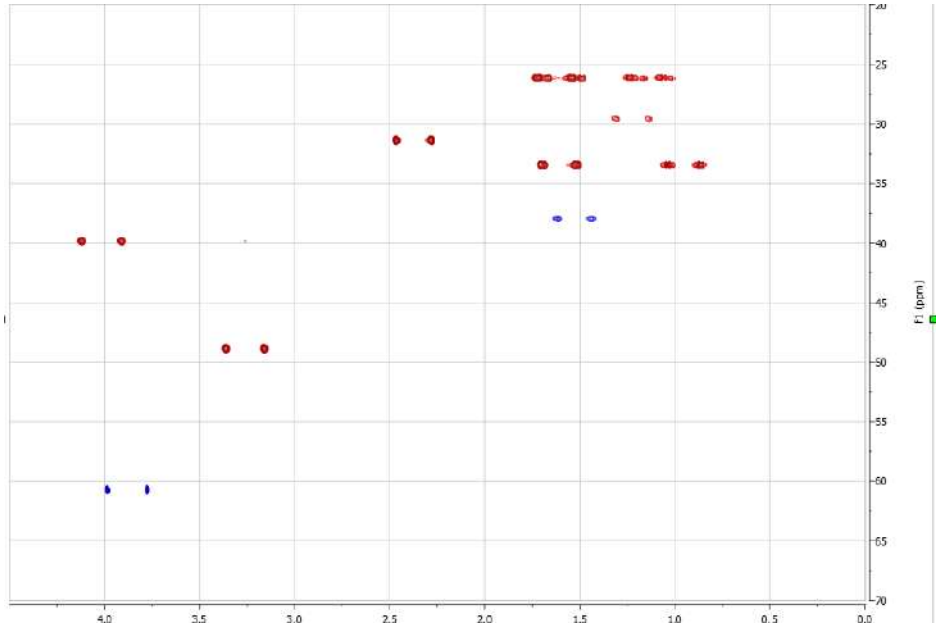

HMBC spectrum of compound **73** in $CDCl_3$

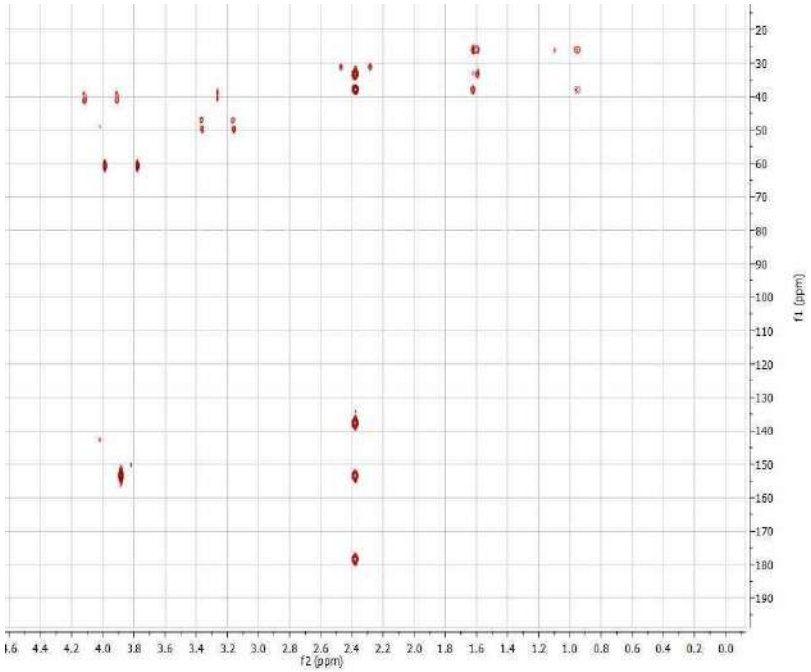

HRESIMS spectrum of compound **73**

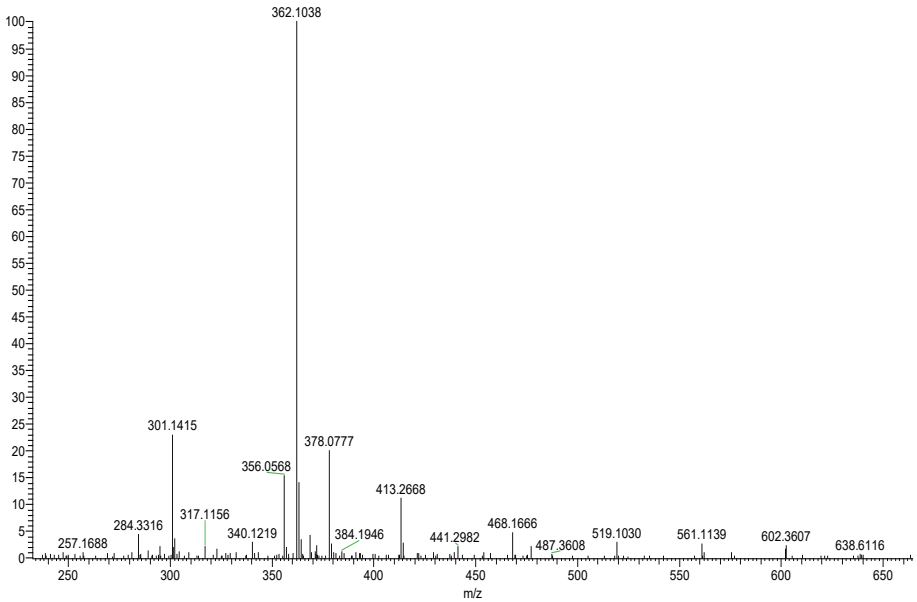

^{1}H NMR of compound **74** in $CDCl_3$

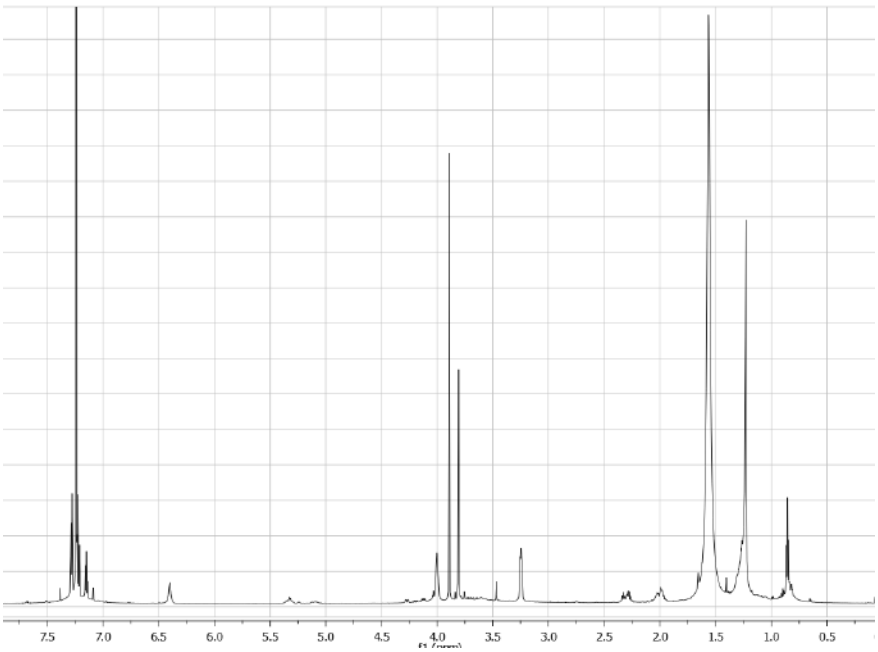

HSQC spectrum of compound **74** in $CDCl_3$

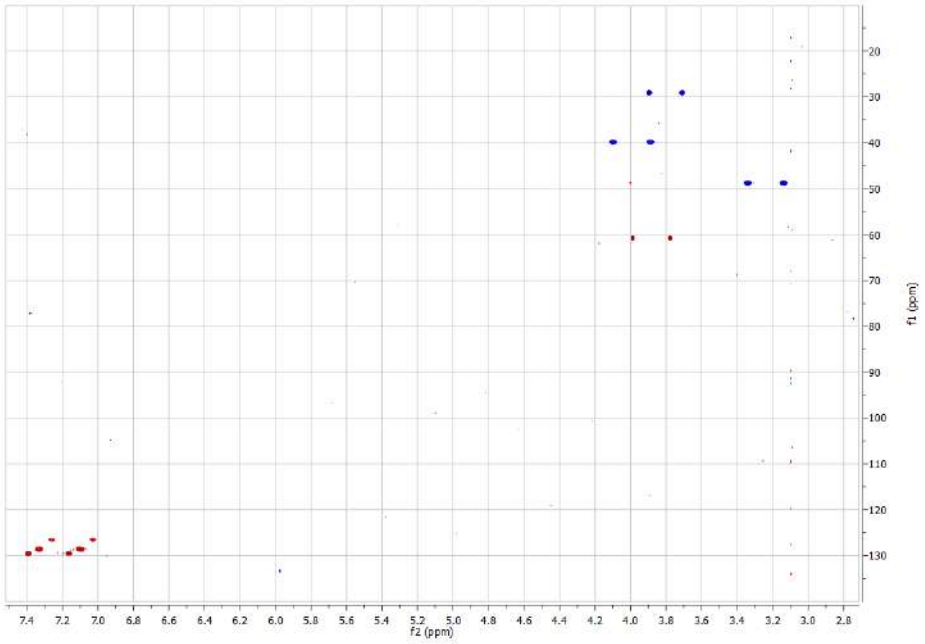

HMBC spectrum of compound **74** in $CDCl_3$

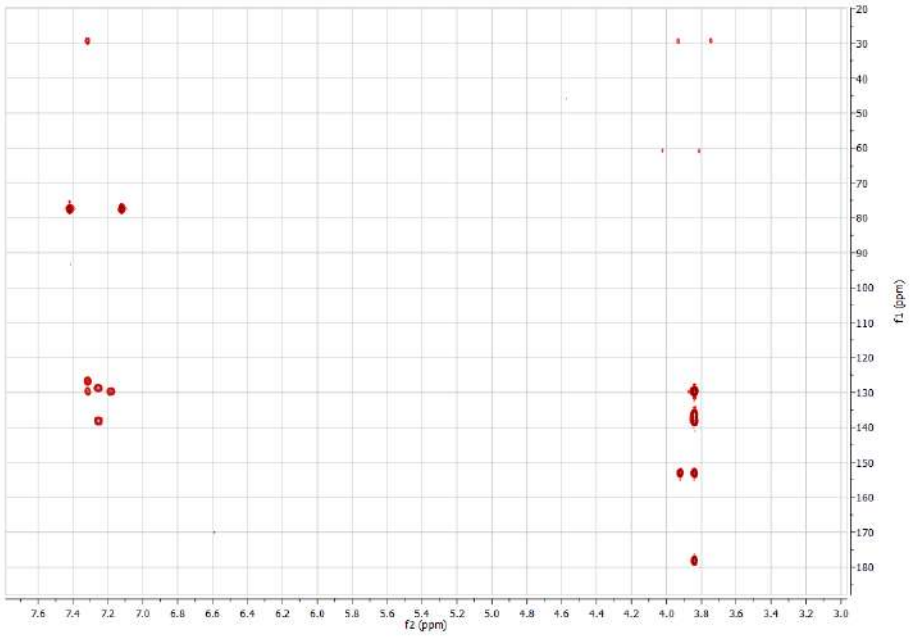

HRESIMS spectrum of compound **74**

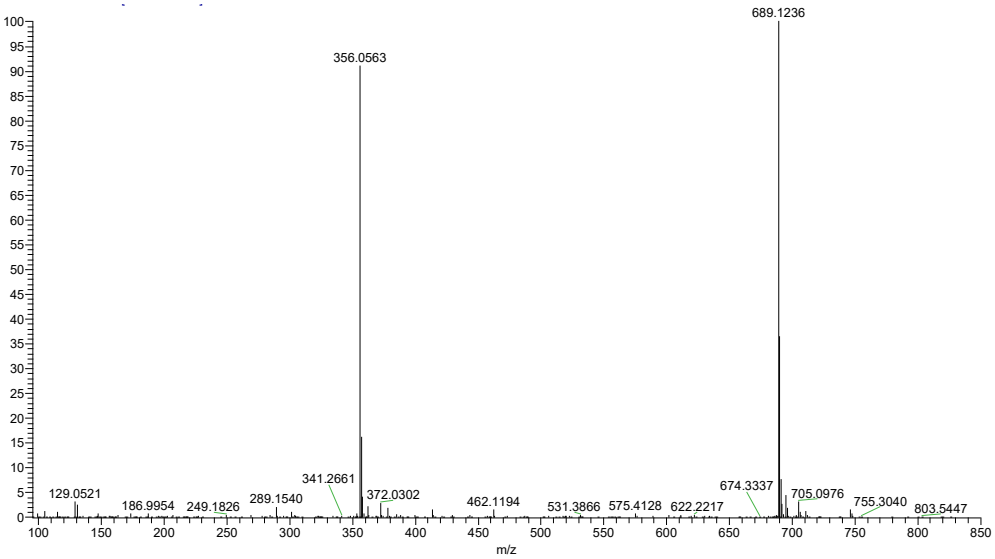

^{1}H NMR of compound **75** in $CDCl_3$

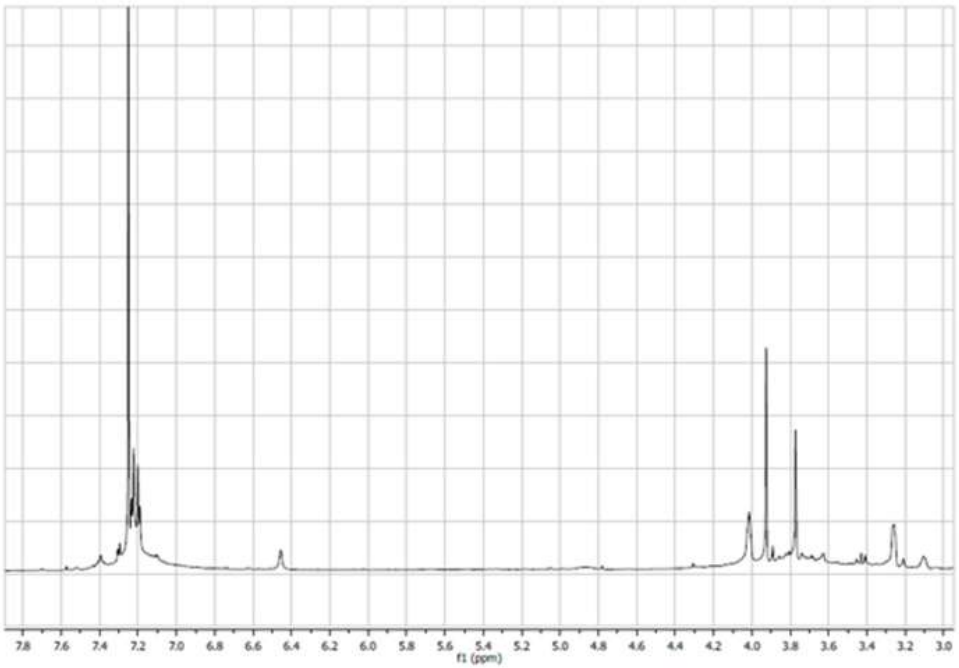

HMBC spectrum of compound **75** in $CDCl_3$

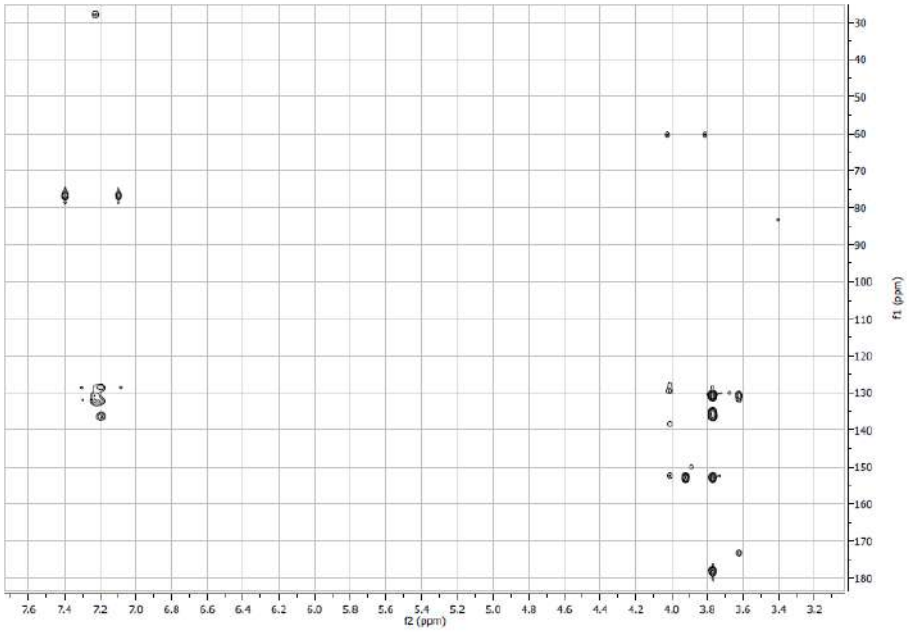

HRESIMS spectrum of compound **75**

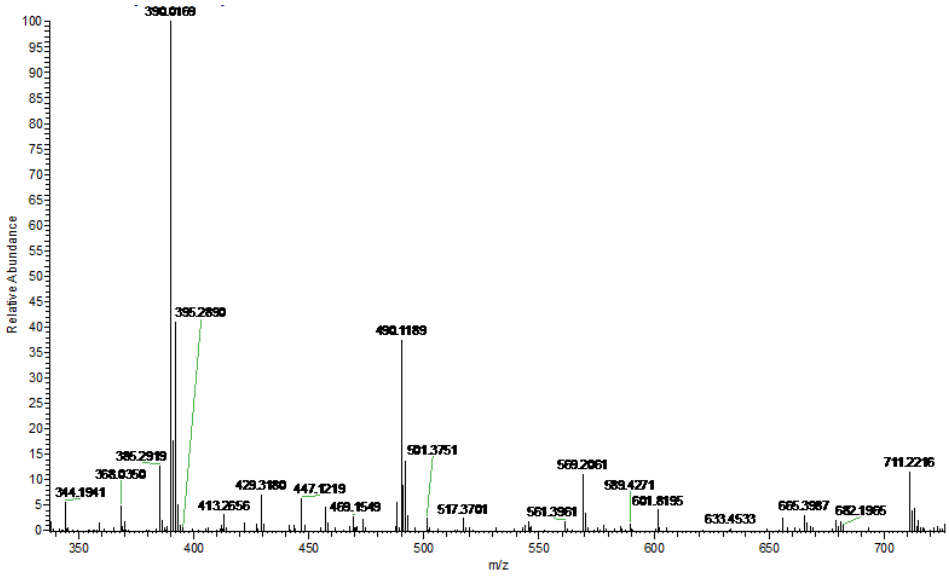

^{1}H NMR of compound **76** in $CDCl_3$

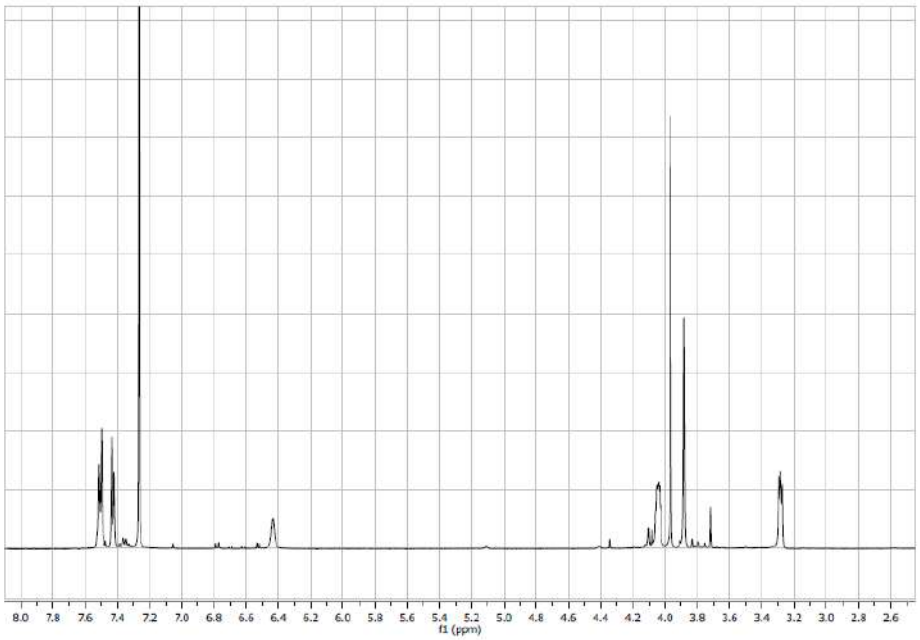

HMBC spectrum of compound **76** in $CDCl_3$

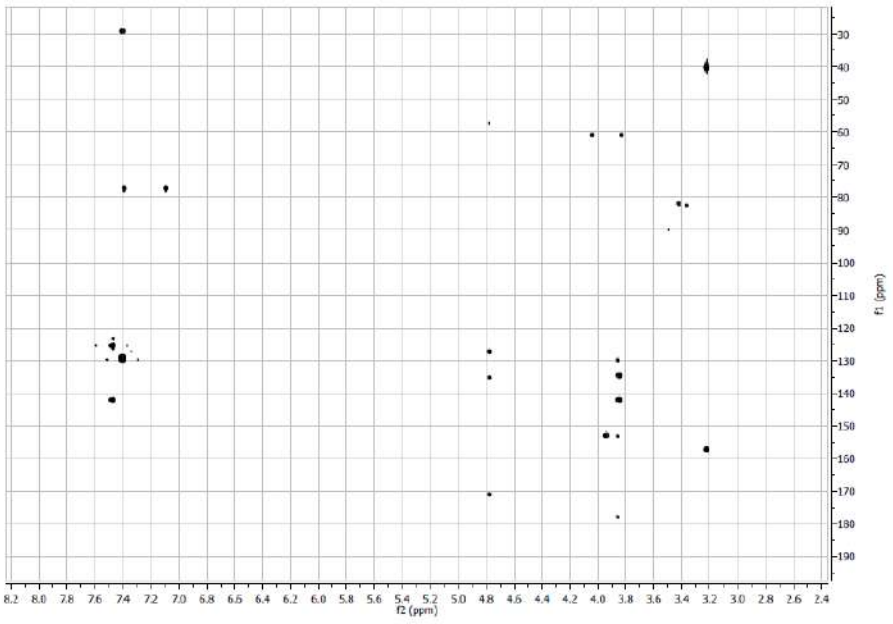

HRESIMS spectrum of compound **76**

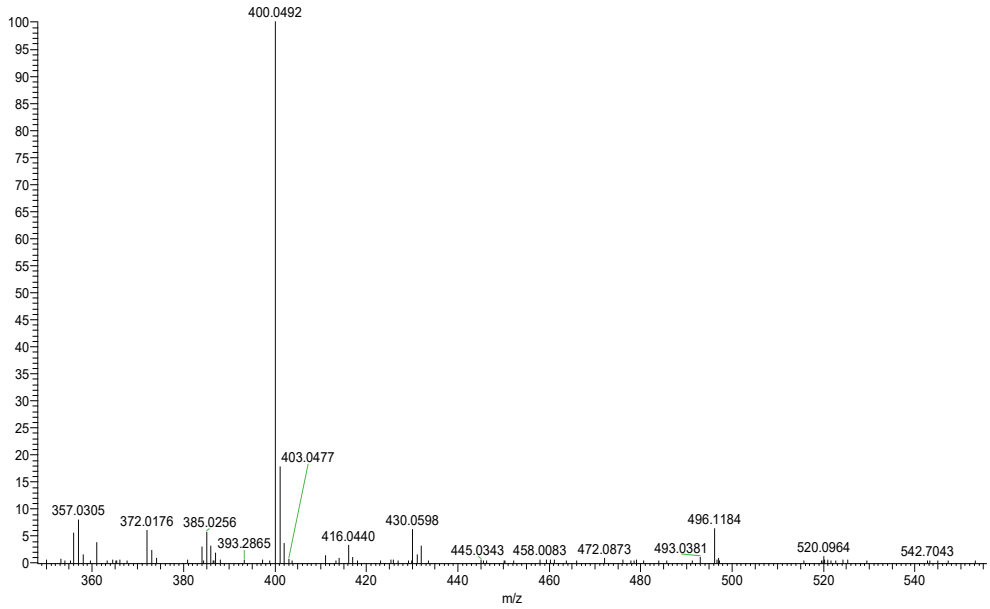

^{1}H NMR of compound **77** in $CDCl_3$

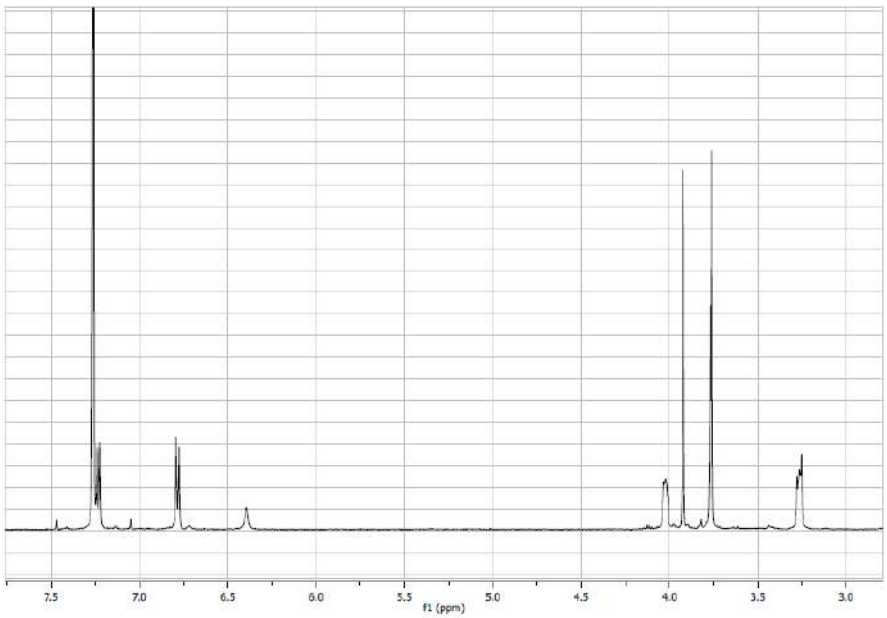

^{1}H NMR of compound **77** in $CDCl_3$

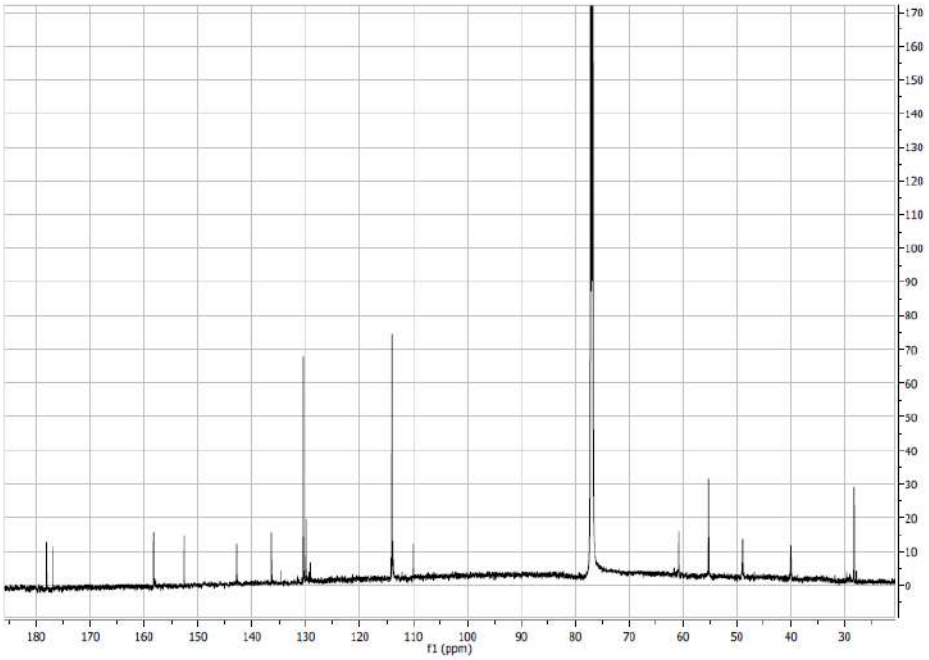

HRESIMS spectrum of compound **77**

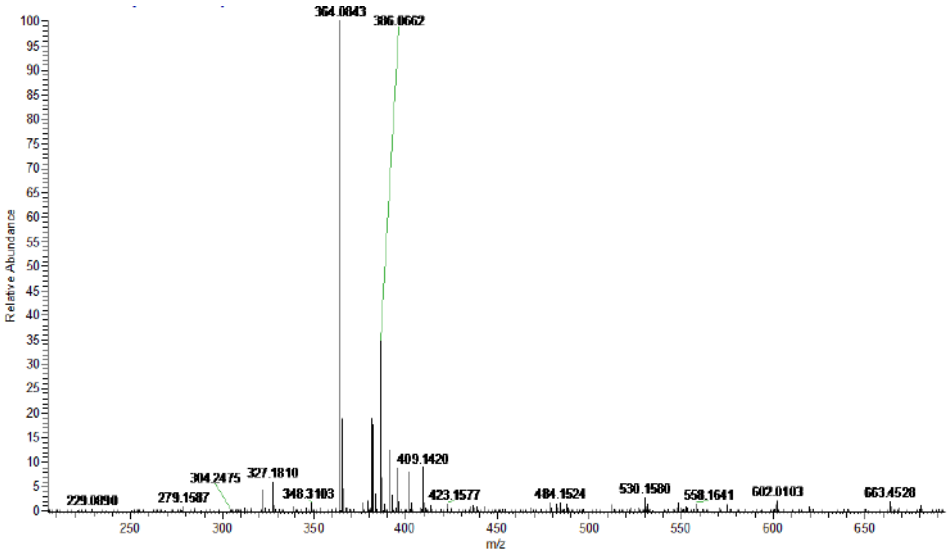

^{1}H NMR of compound **78** in $CDCl_3$

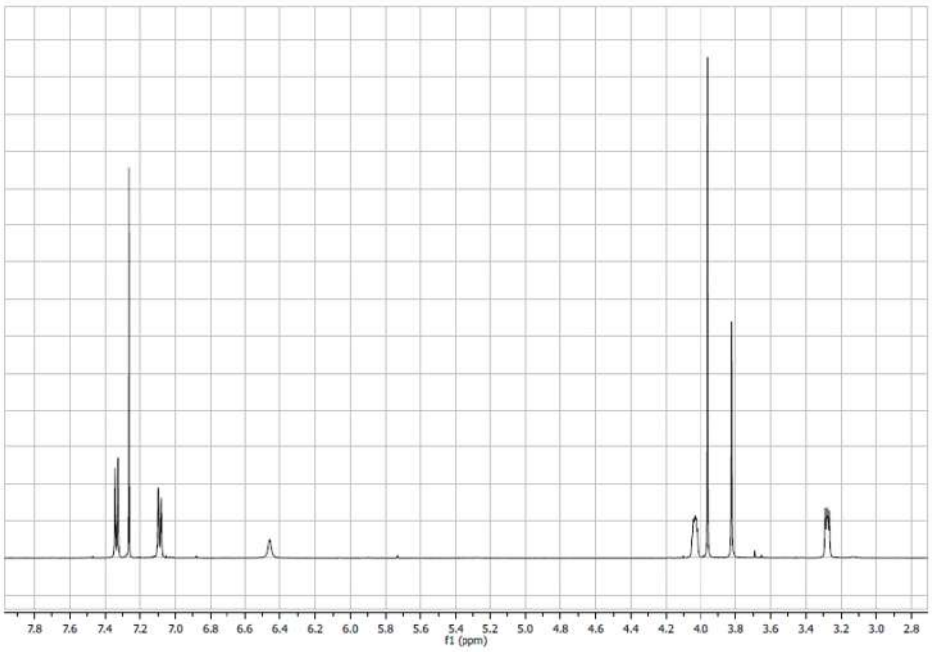

^{13}C NMR of compound **78** in $CDCl_3$

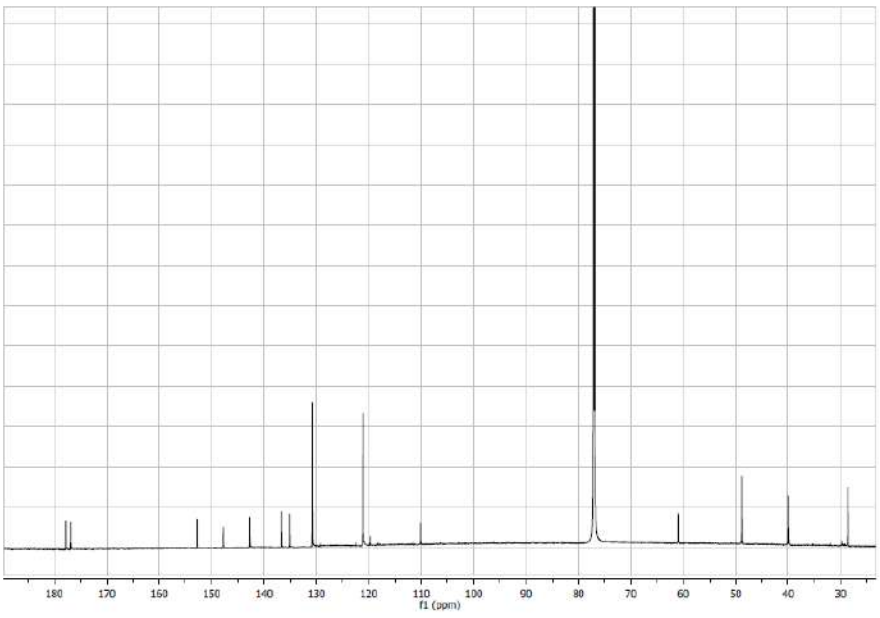

HRESIMS spectrum of compound **78** in $CDCl_3$

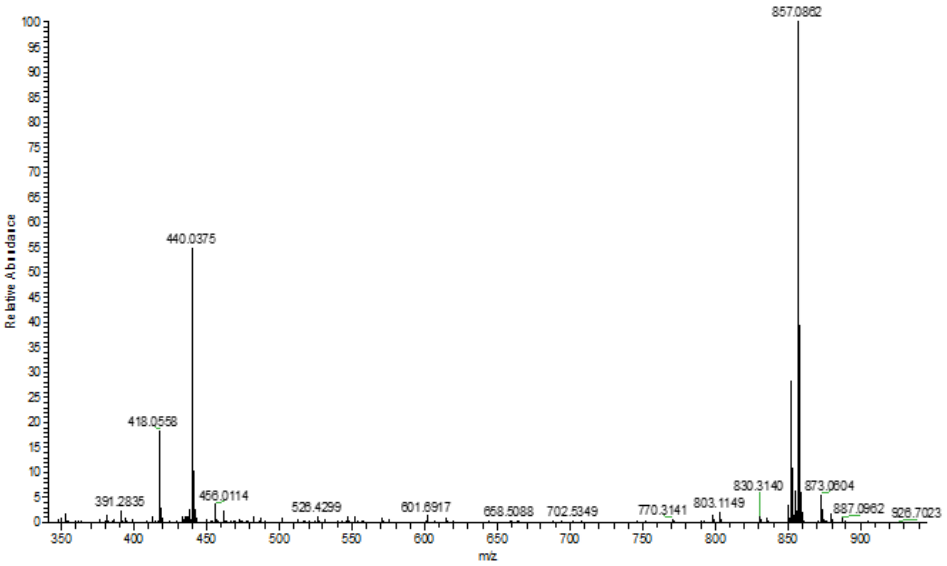

^1H NMR of compound **79** in $CDCl_3$

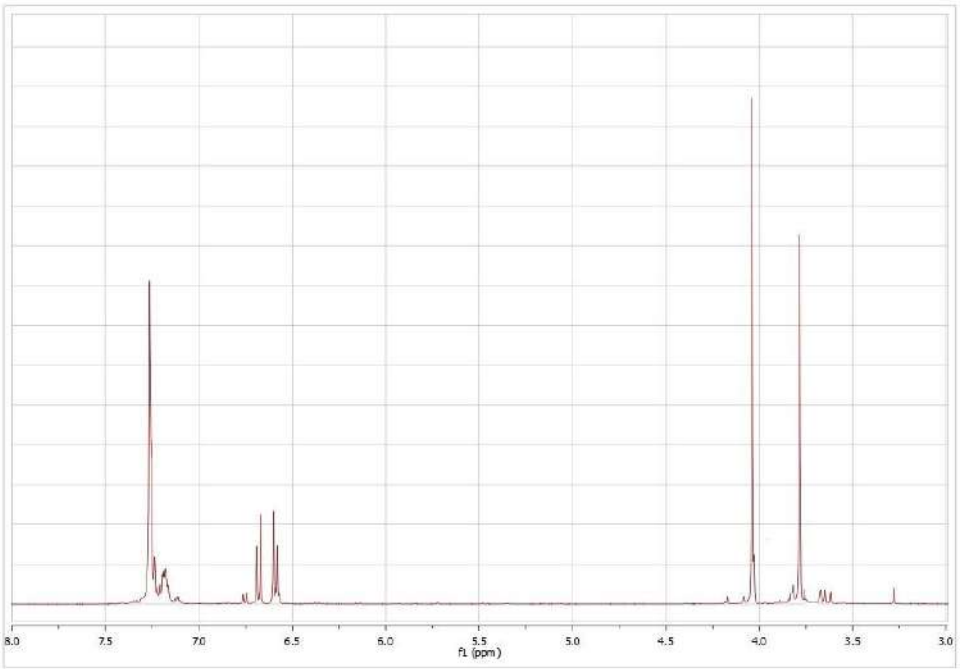

HRESIMS spectrum of compound **79**

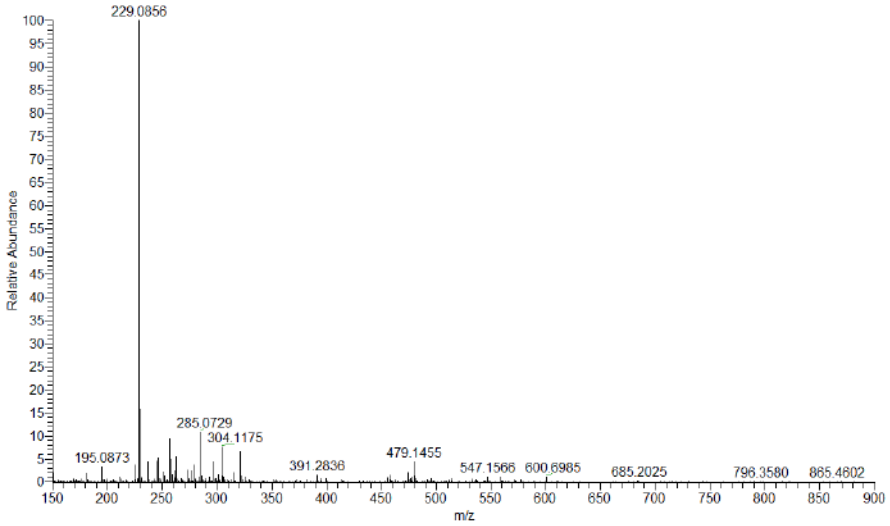

^{1}H NMR of compound **81-R$_2$** in $CDCl_3$

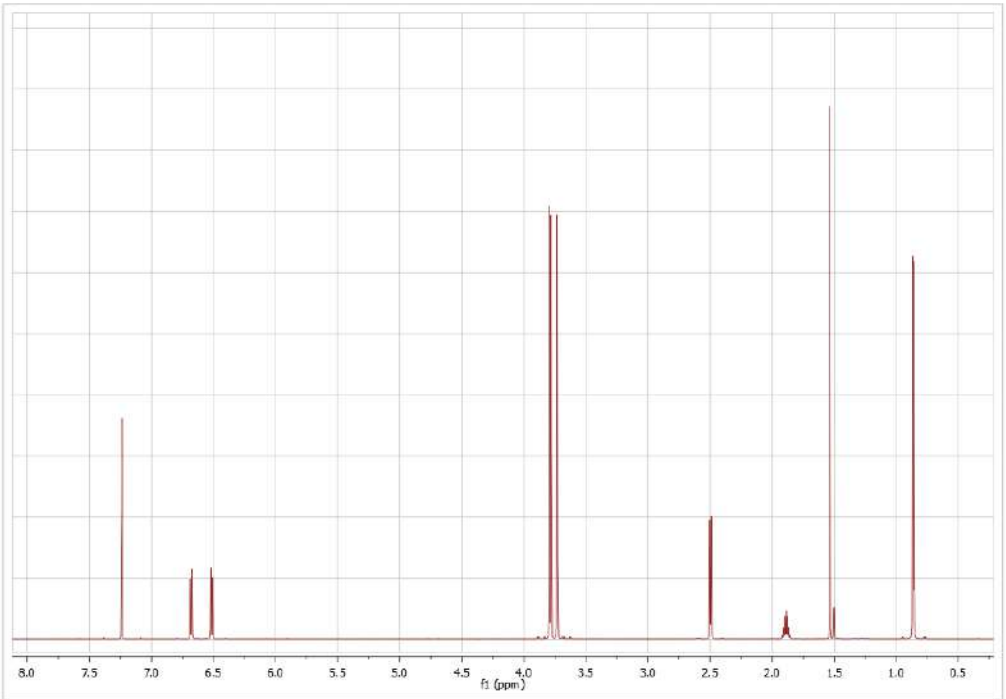

HRESIMS spectrum of compound **81-R_2**

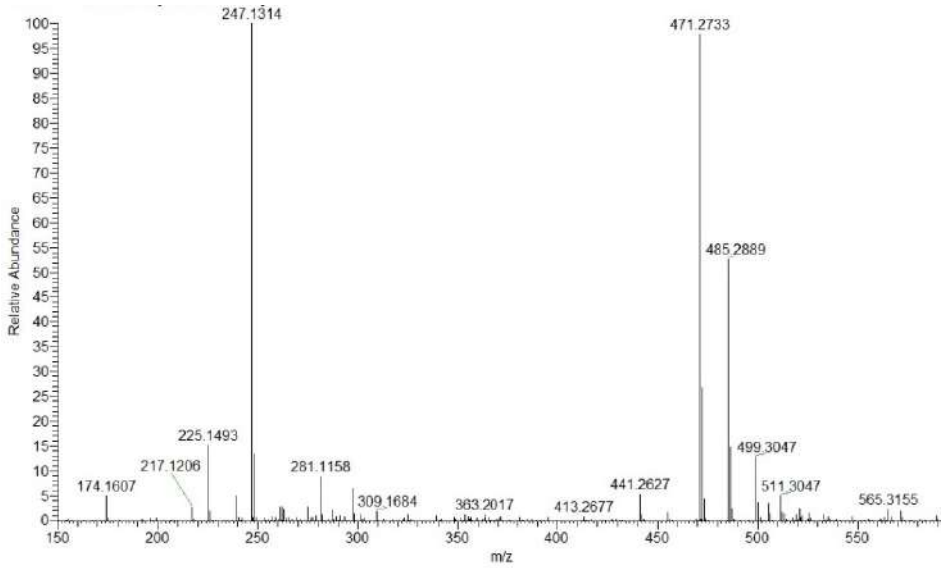

^{1}H NMR of compound **81-R_3** in $CDCl_3$

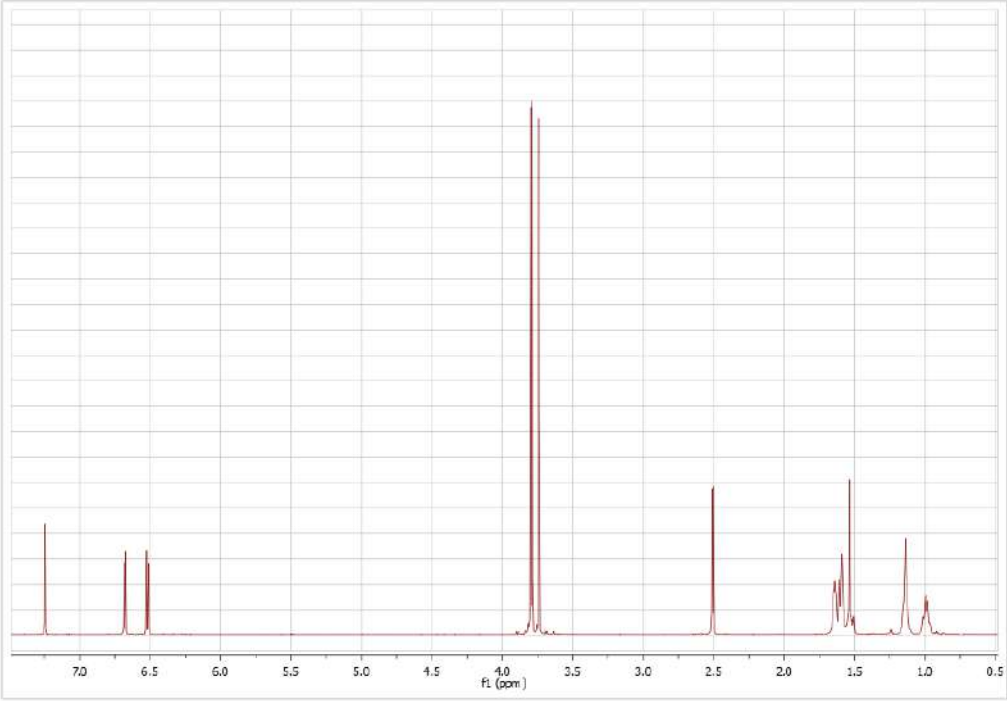

HRESIMS spectrum of compound **81-R_3**

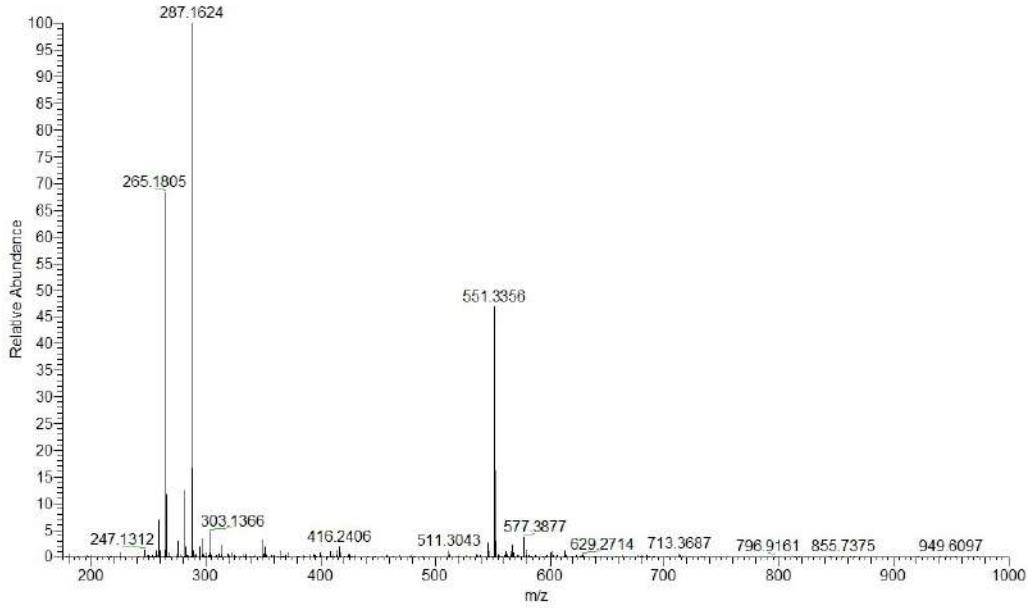

^{1}H NMR of compound **82-R_2** in $CDCl_3$

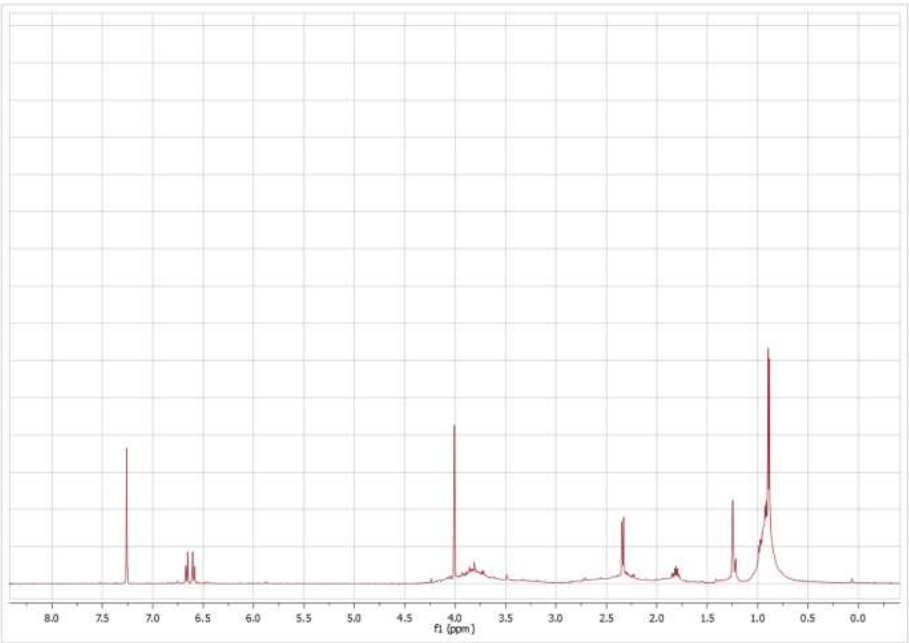

HRESIMS spectrum of compound **82-R_2**

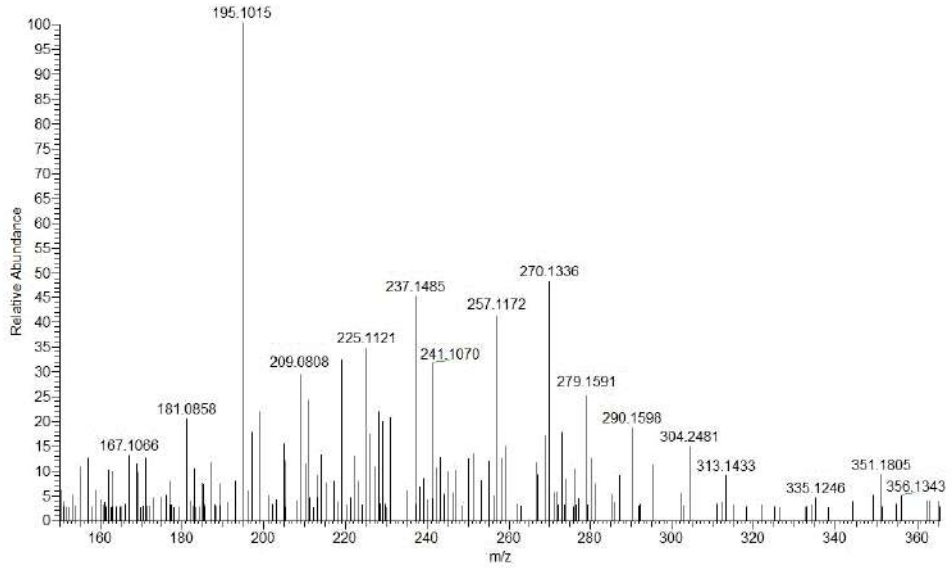

^{1}H NMR of compound **82-R_3** in $CDCl_3$

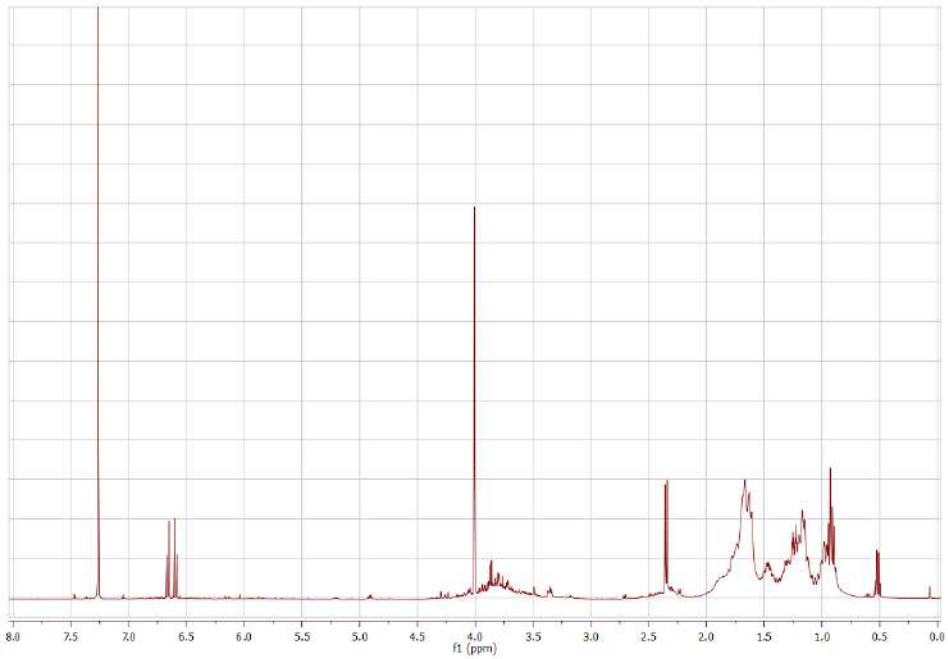

HRESIMS spectrum of compound **82-R$_3$**

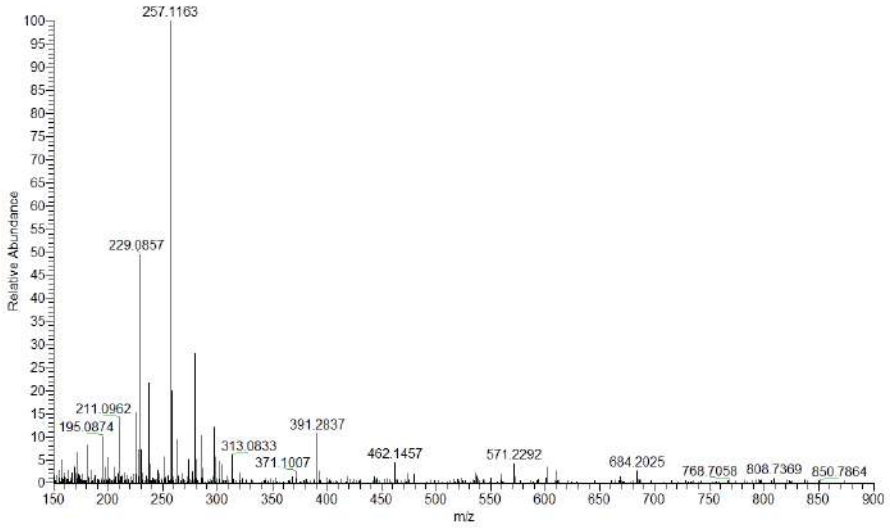

^{1}H NMR of compound **83-R$_4$** in $CDCl_3$

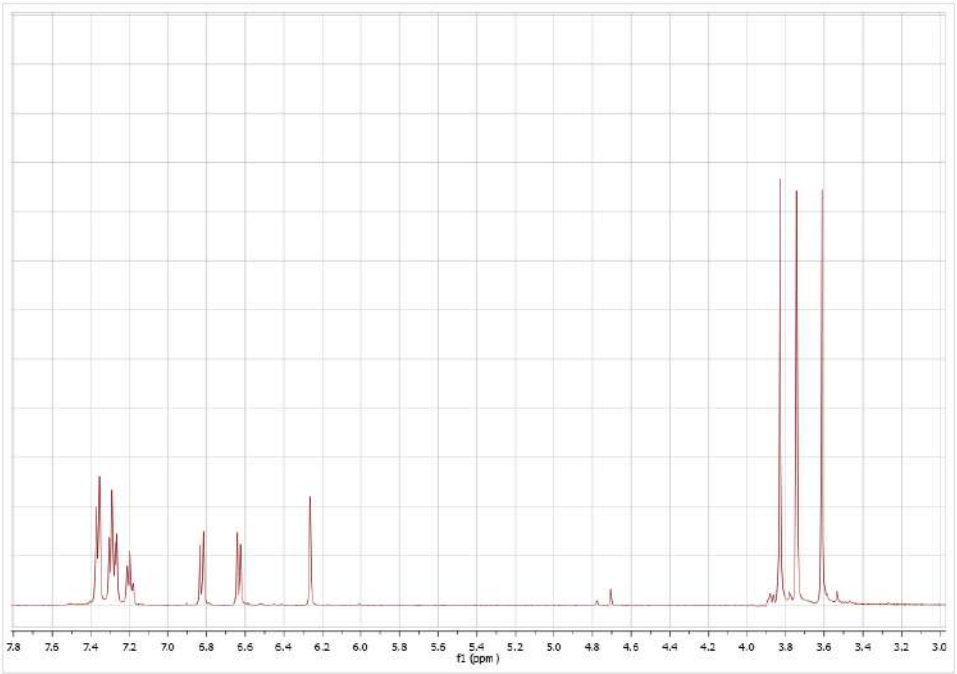

HRESIMS spectrum of compound **83-R$_4$**

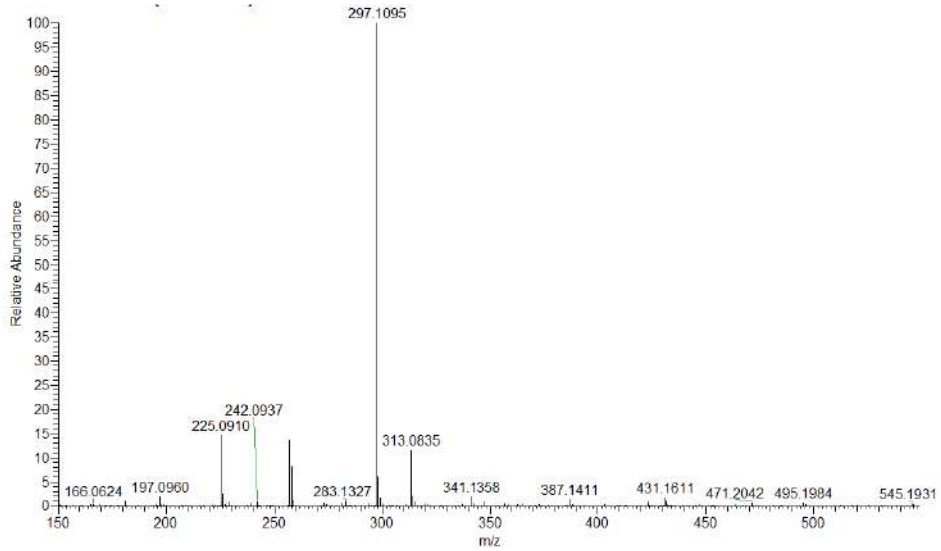

^{1}H-NMR of **83-R$_5$** in $CDCl_3$

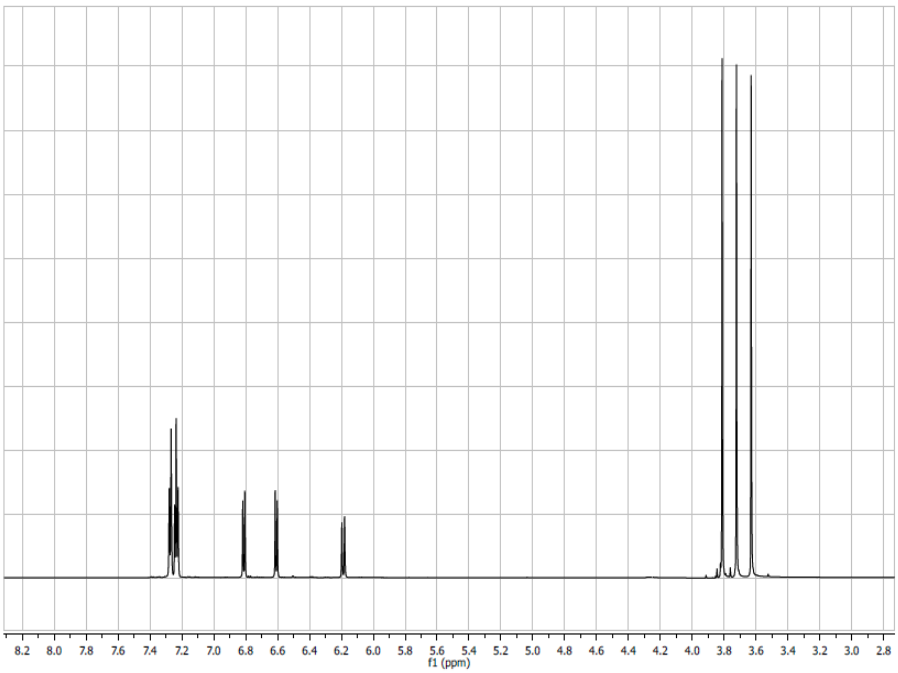

^{13}C-NMR of **83-R$_5$** in $CDCl_3$

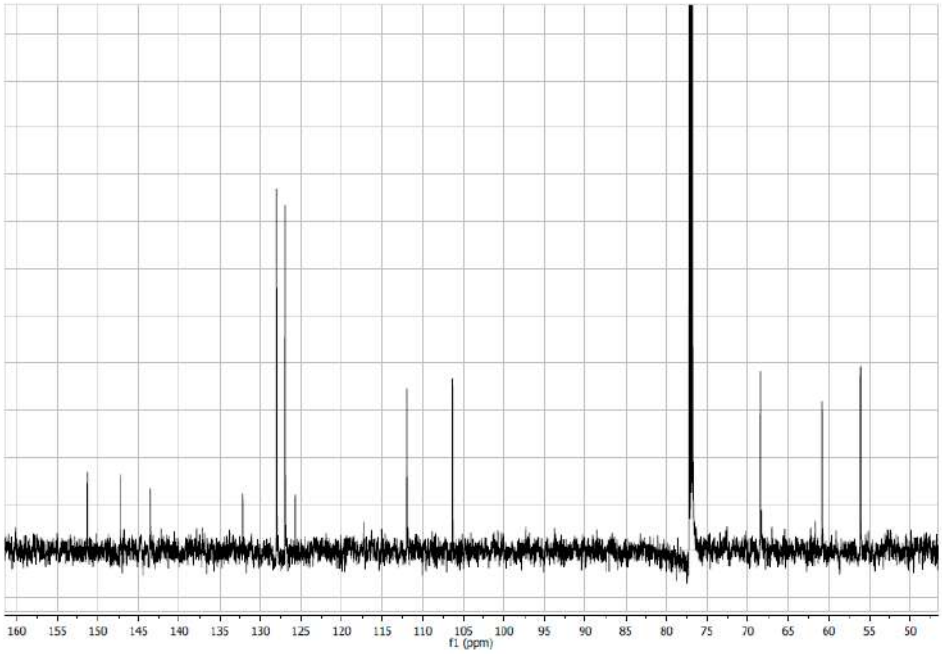

^{1}H-NMR of **83-R$_6$** in $CDCl_3$

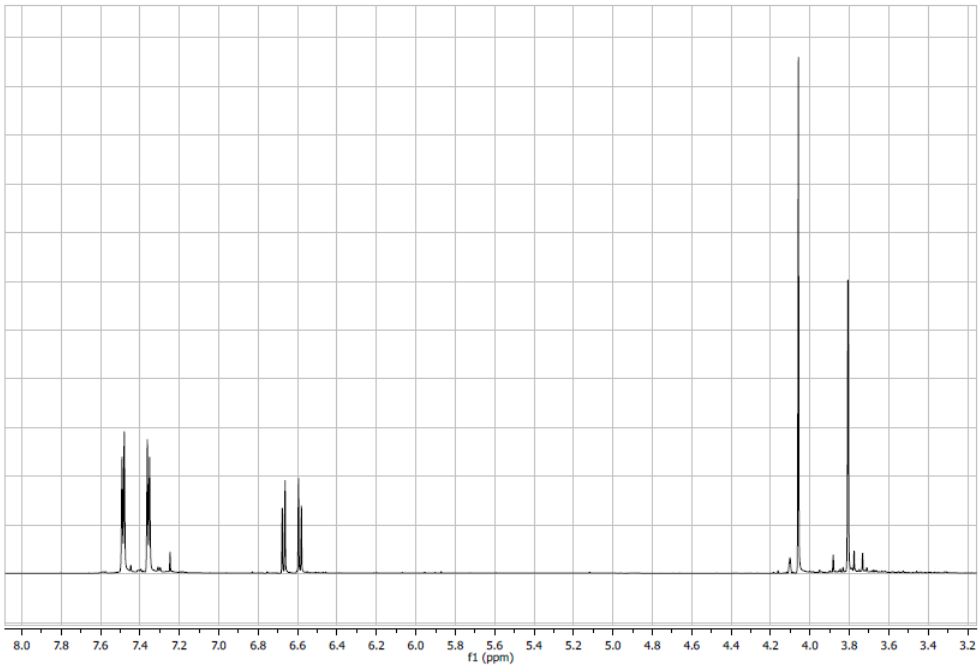

^{13}C-NMR of **83-R$_6$** in $CDCl_3$

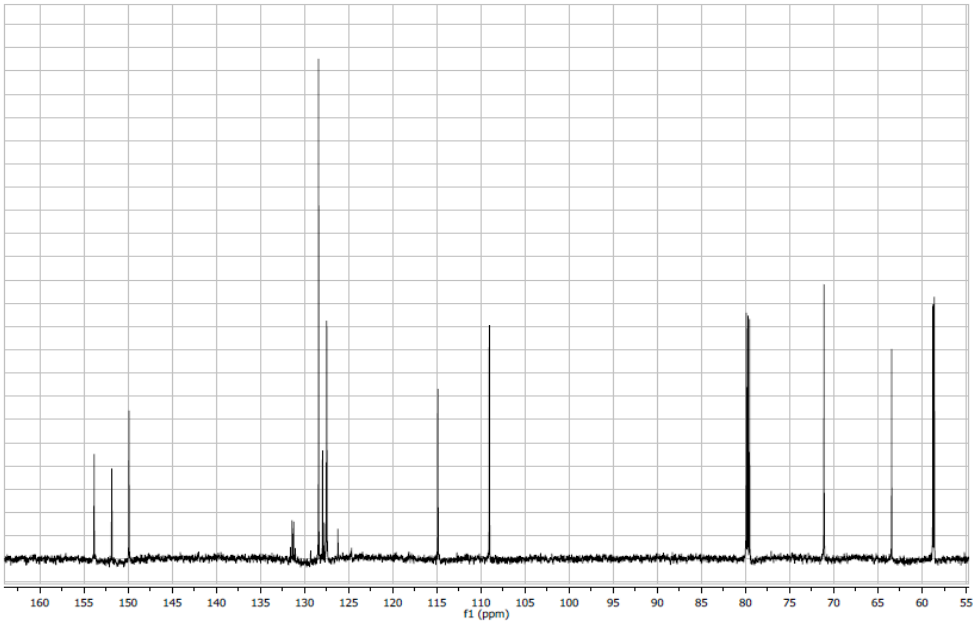

^{1}H-NMR of **83-R$_7$** in $CDCl_3$

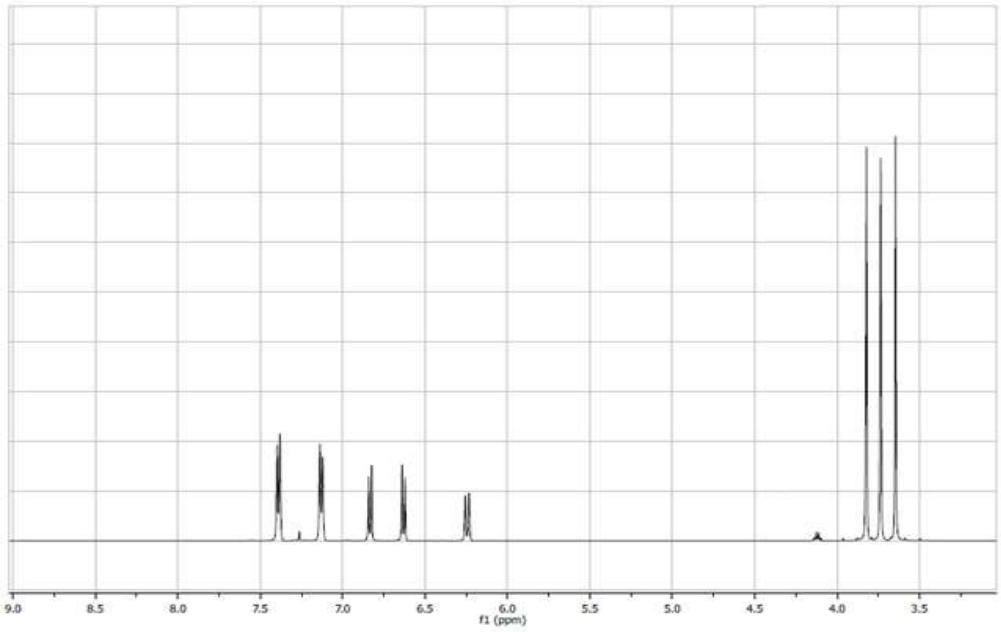

^{13}C-NMR of **83**-**R$_7$** in $CDCl_3$

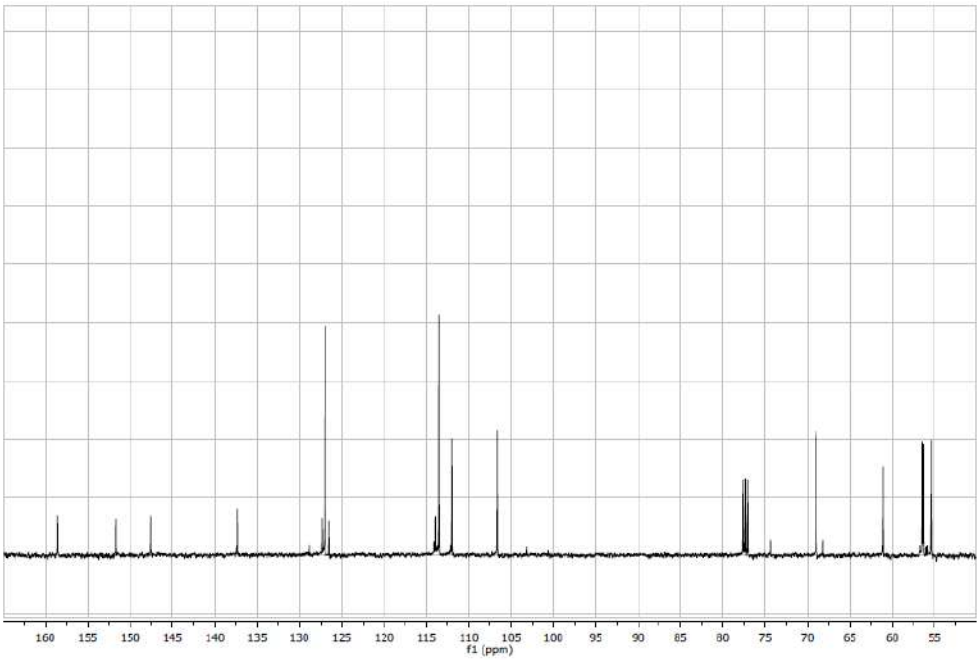

^{1}H-NMR of **83**-**R$_8$** in $CDCl_3$

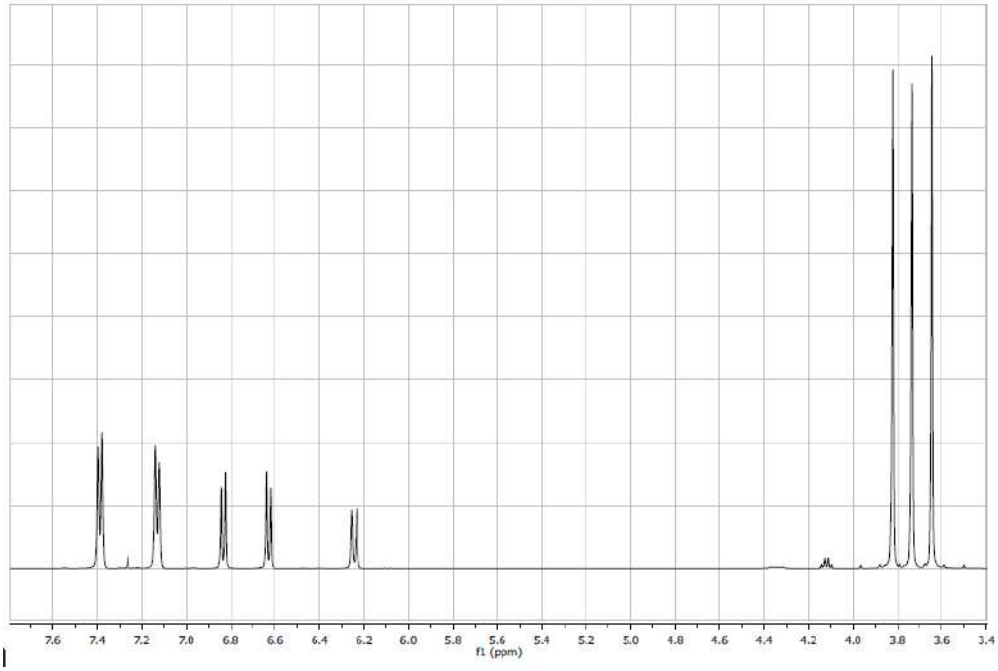

^{1}H NMR of compound **84-R$_4$** in $CDCl_3$

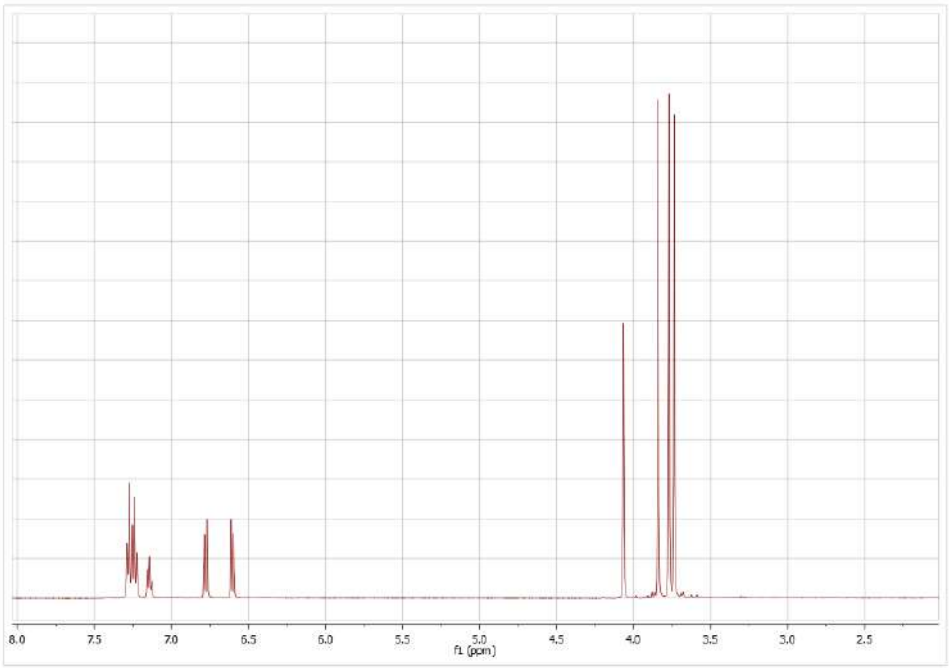

HRESIMS spectrum of compound **84-R$_4$**

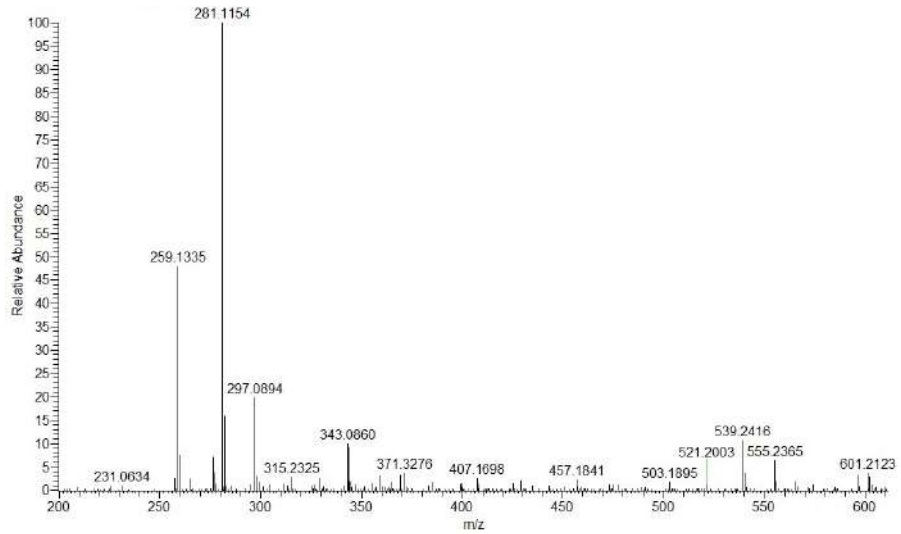

^{1}H NMR of compound **84-R$_5$** in $CDCl_3$

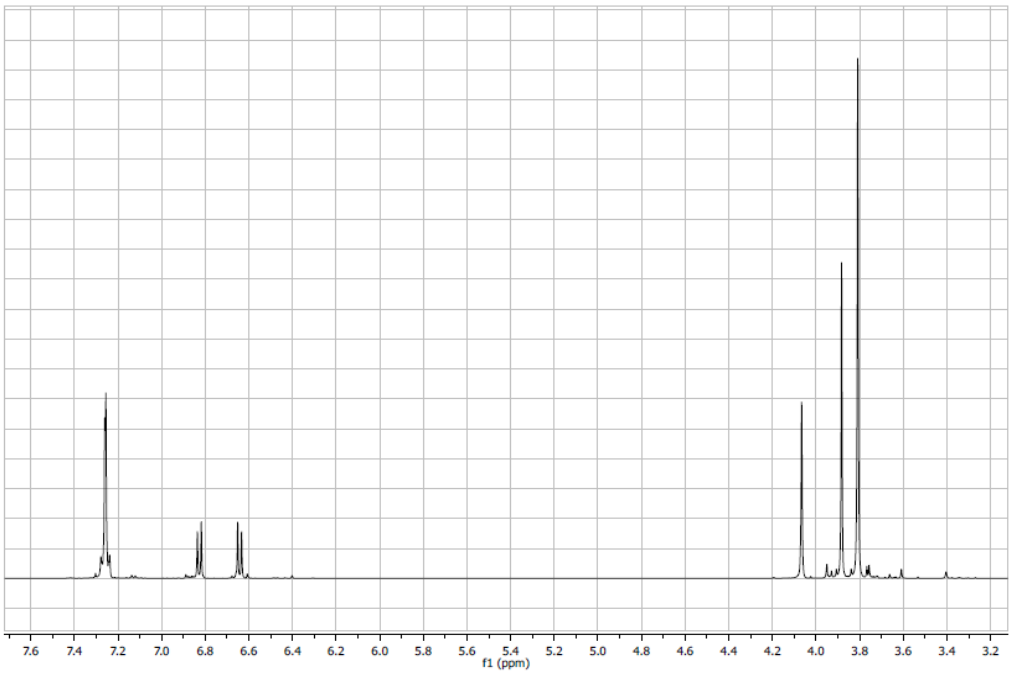

^{13}C NMR of compound **84-R$_5$** in $CDCl_3$

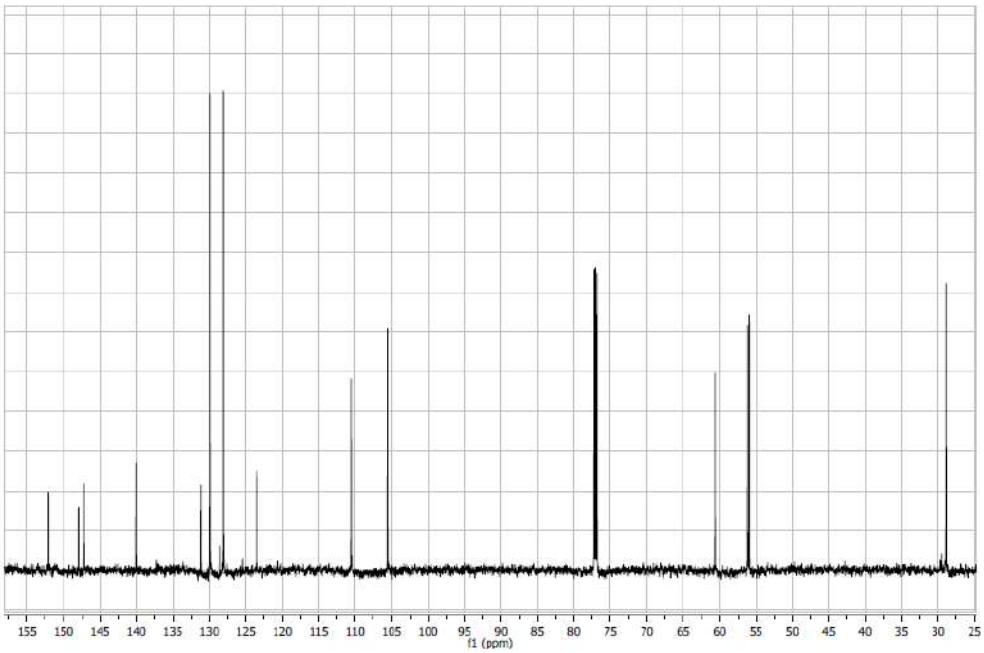

^{1}H NMR of compound **84-R$_6$** in $CDCl_3$

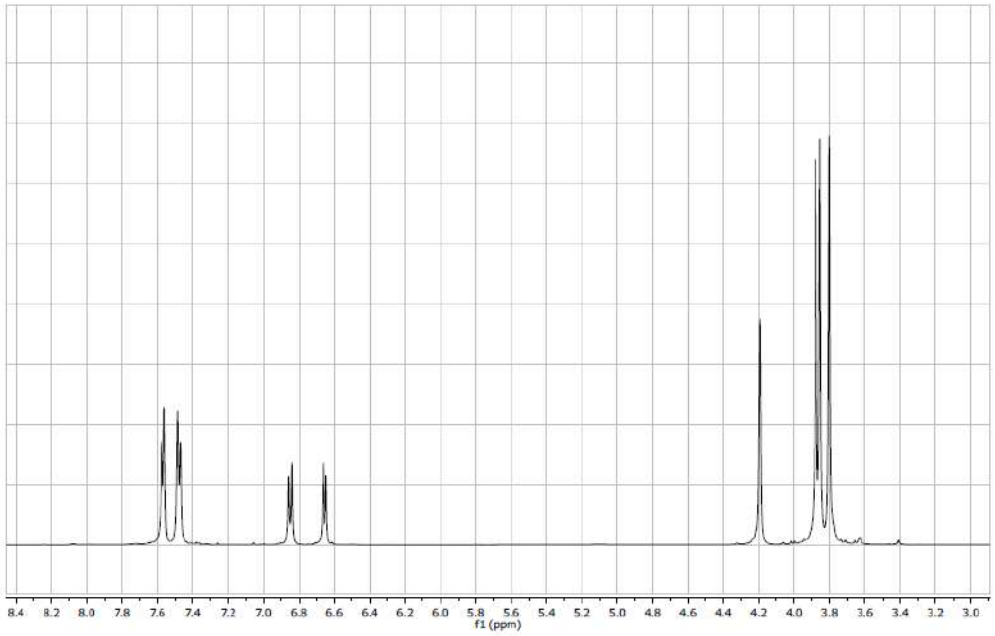

^{13}C NMR of compound **84-R$_6$** in $CDCl_3$

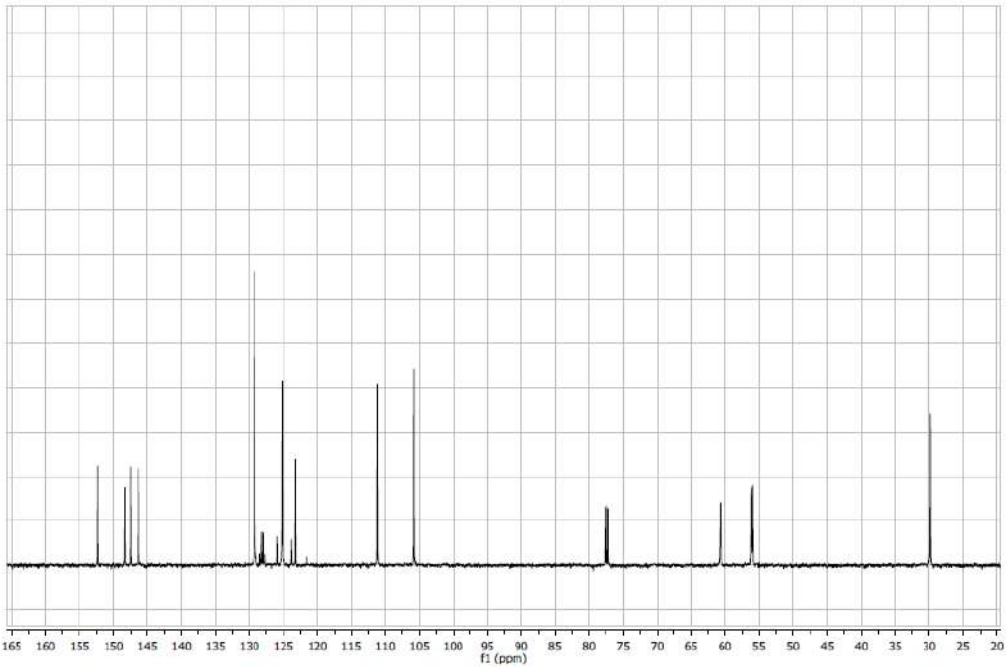

^{1}H NMR of compound **84-R$_7$** in $CDCl_3$

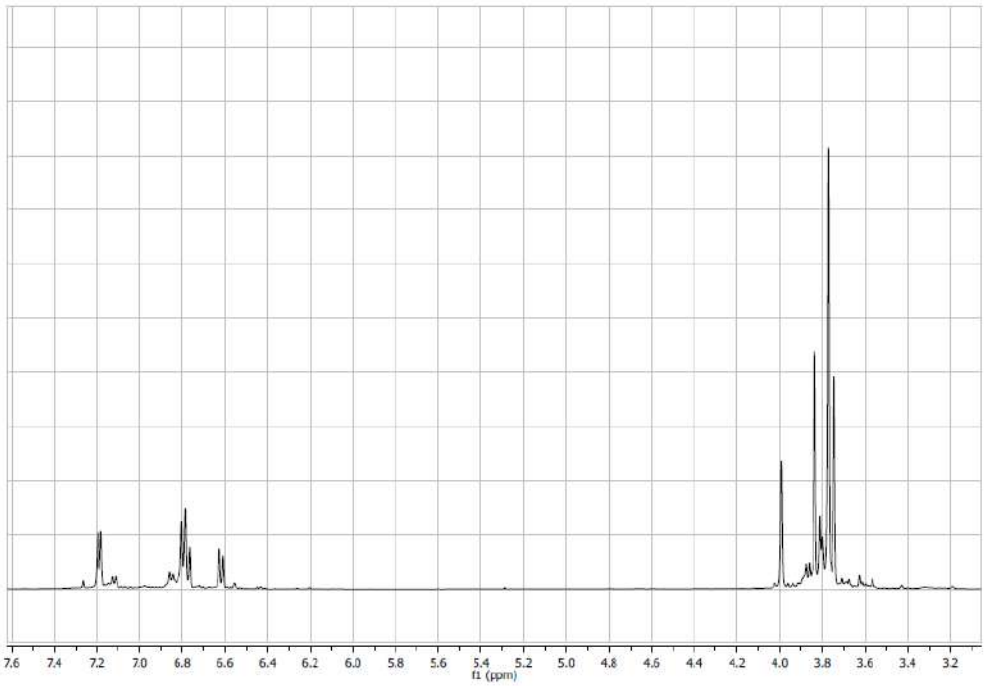

^{13}C NMR of compound **84-R$_7$** in $CDCl_3$

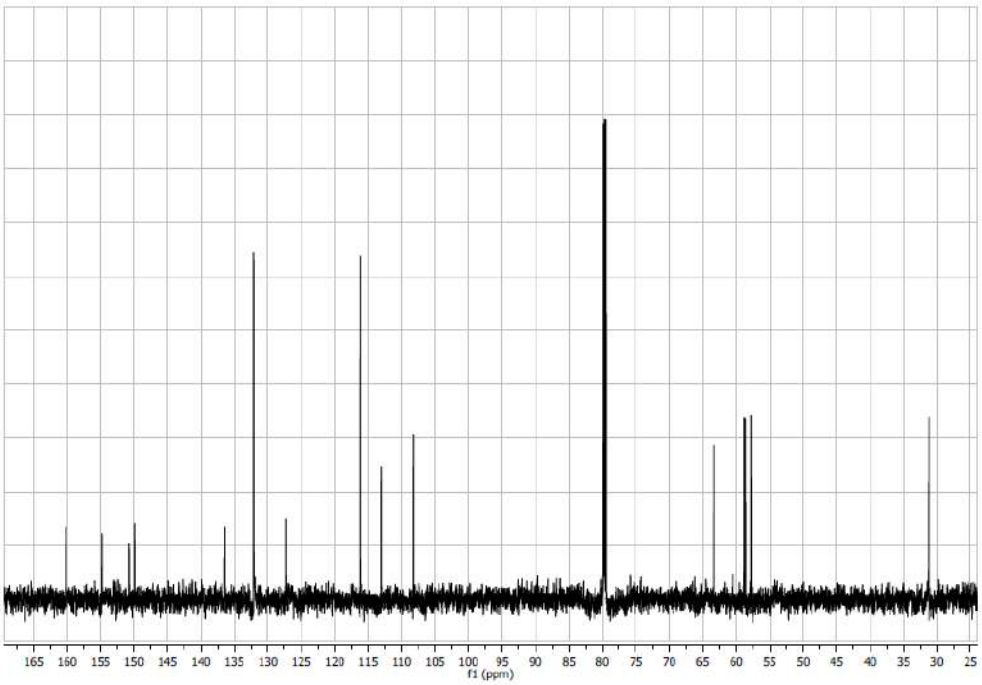

^{1}H NMR of compound **84-R$_8$** in $CDCl_3$

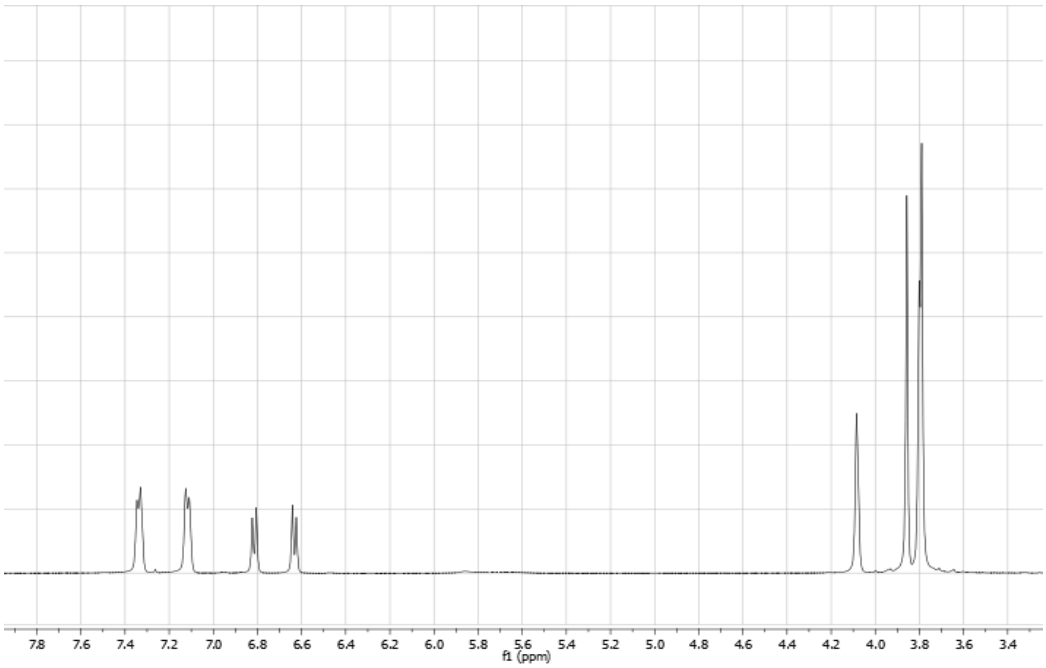

^{13}C NMR of compound **84-R$_8$** in $CDCl_3$

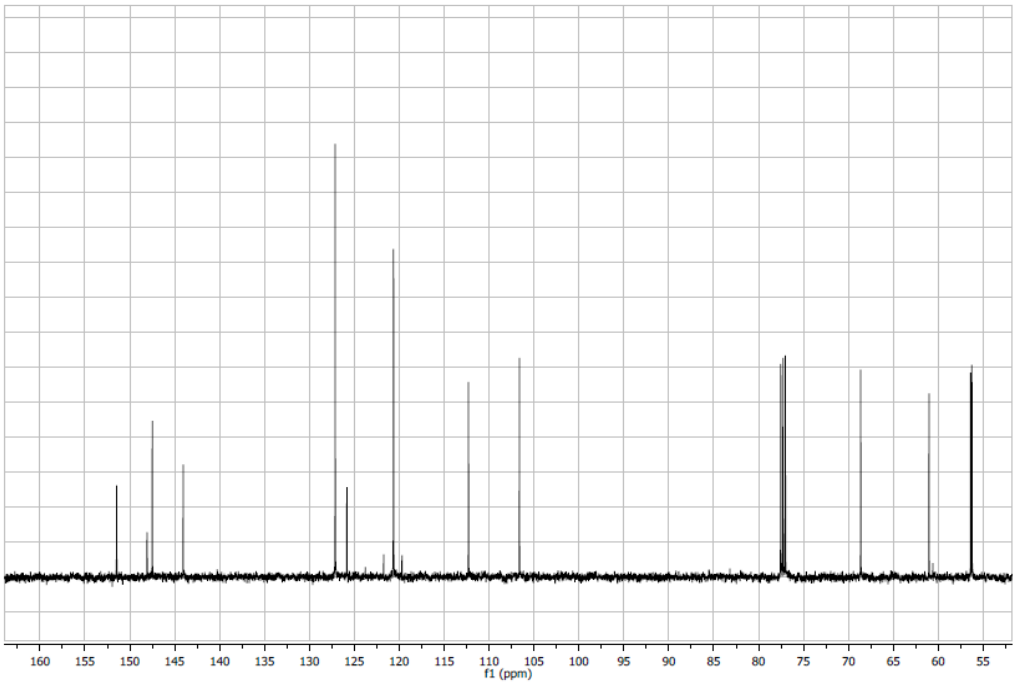

^{1}H NMR of compound **85-R$_5$** in $CDCl_3$

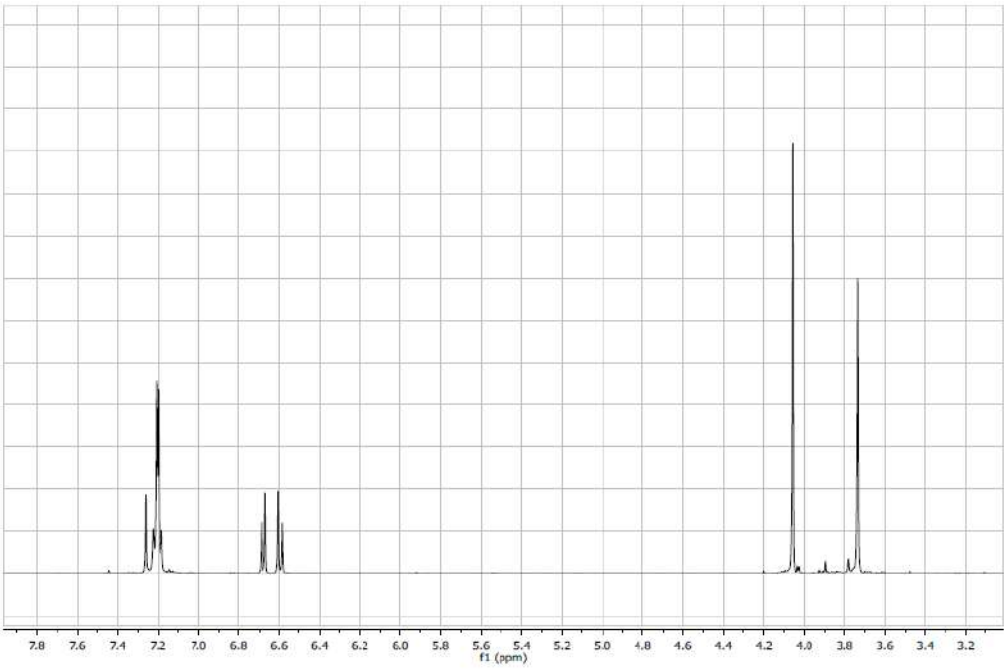

^{13}C NMR of compound **85-R$_5$** in $CDCl_3$

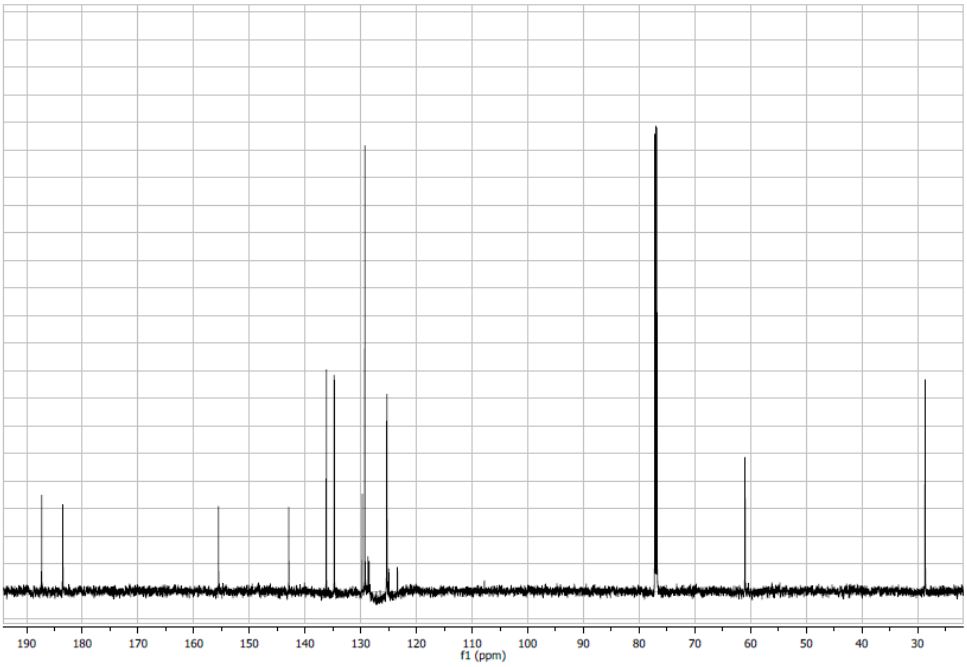

^{1}H NMR of compound **85-R$_6$** in $CDCl_3$

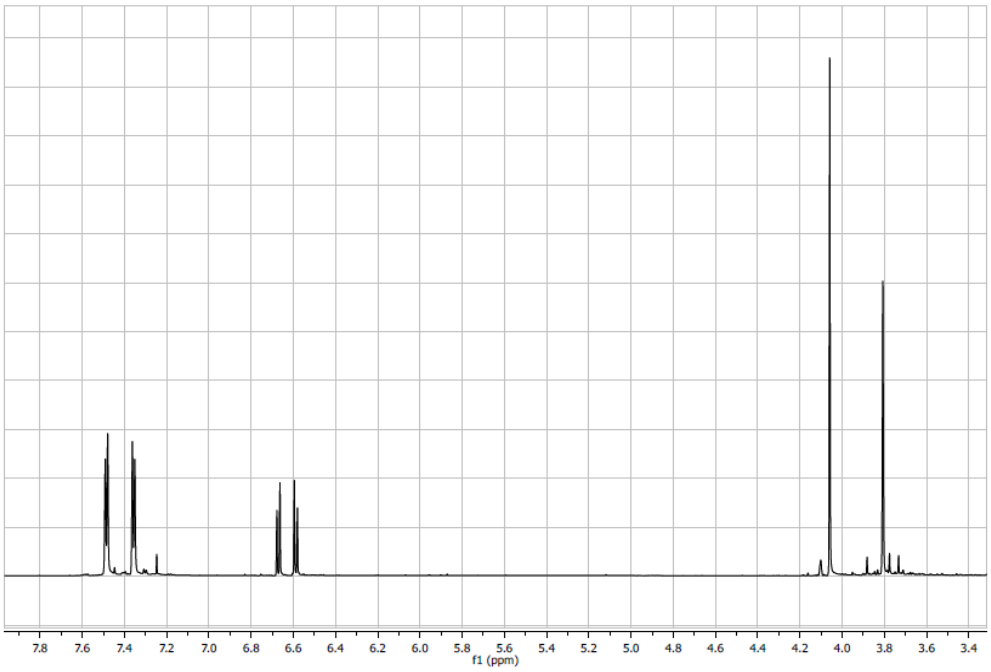

^{13}C NMR of compound **85-R$_6$** in $CDCl_3$

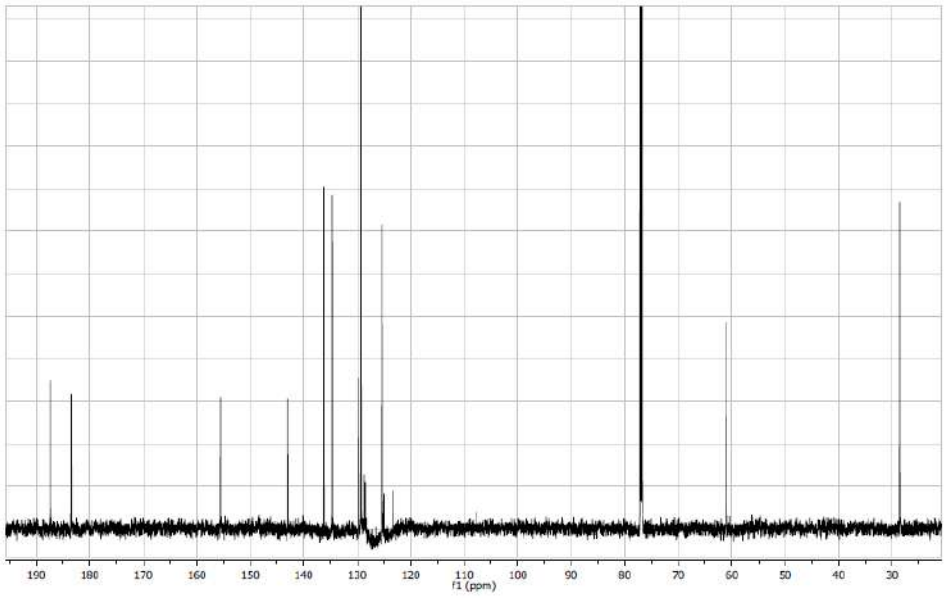

^{1}H NMR of compound **85-R$_7$** in $CDCl_3$

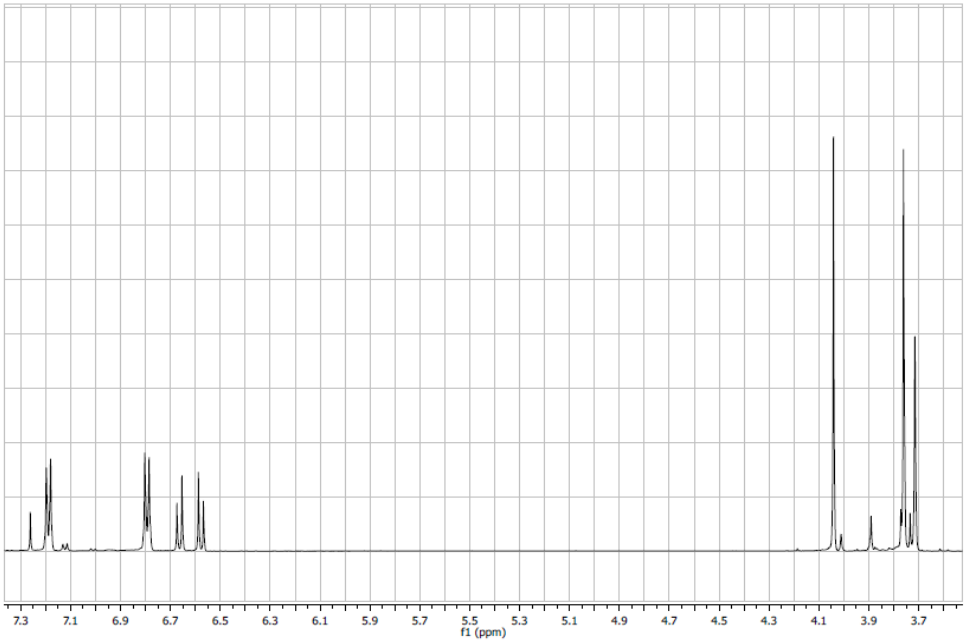

^{13}C NMR of compound **85-R$_7$** in $CDCl_3$

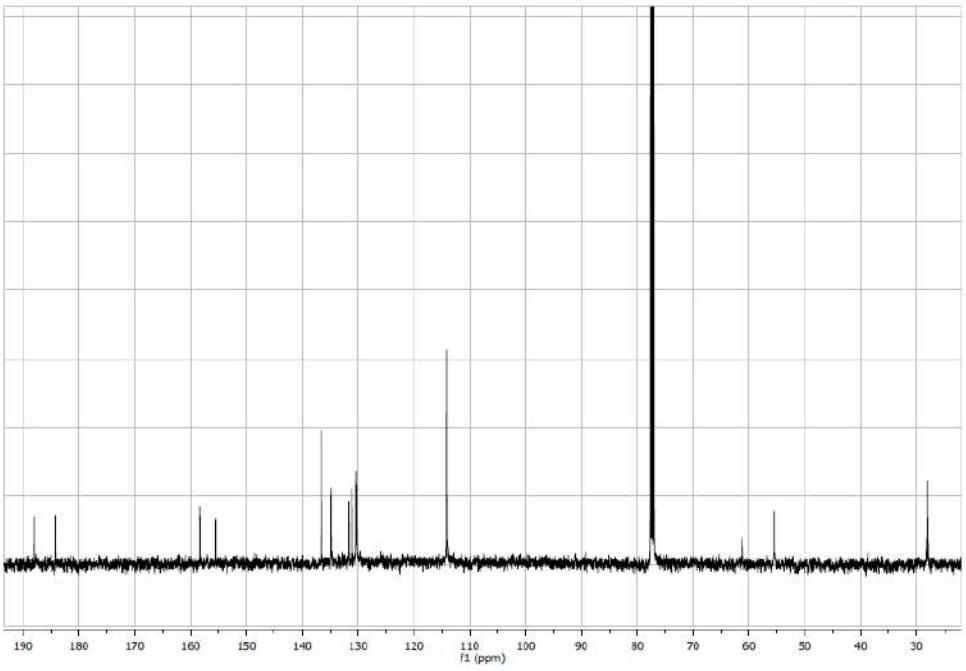

^{1}H NMR of compound **85-R$_8$** in $CDCl_3$

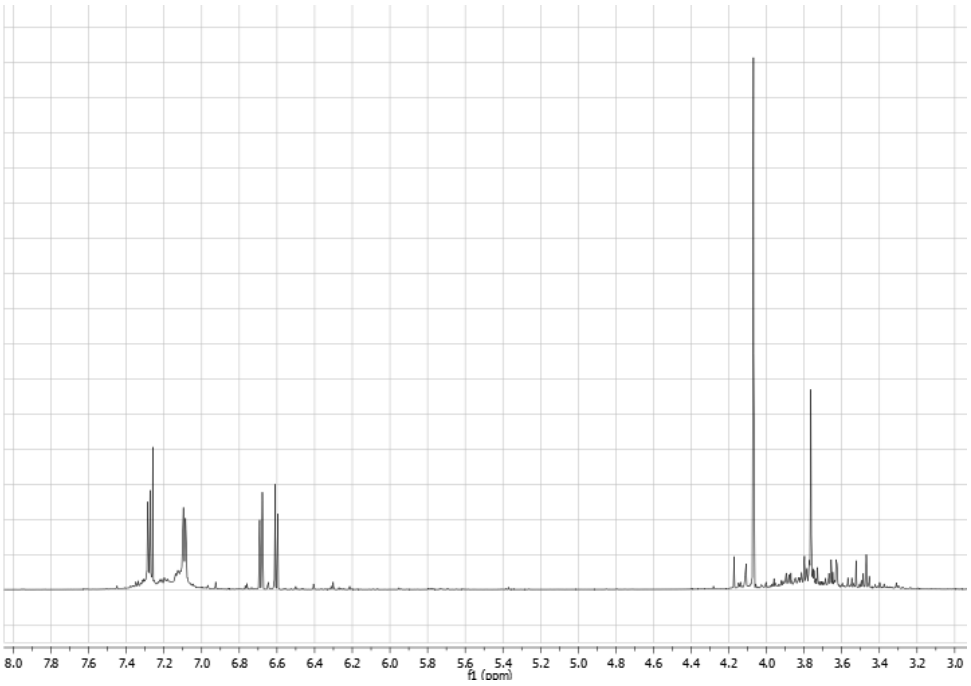

^{13}C NMR of compound **85-R$_8$** in $CDCl_3$

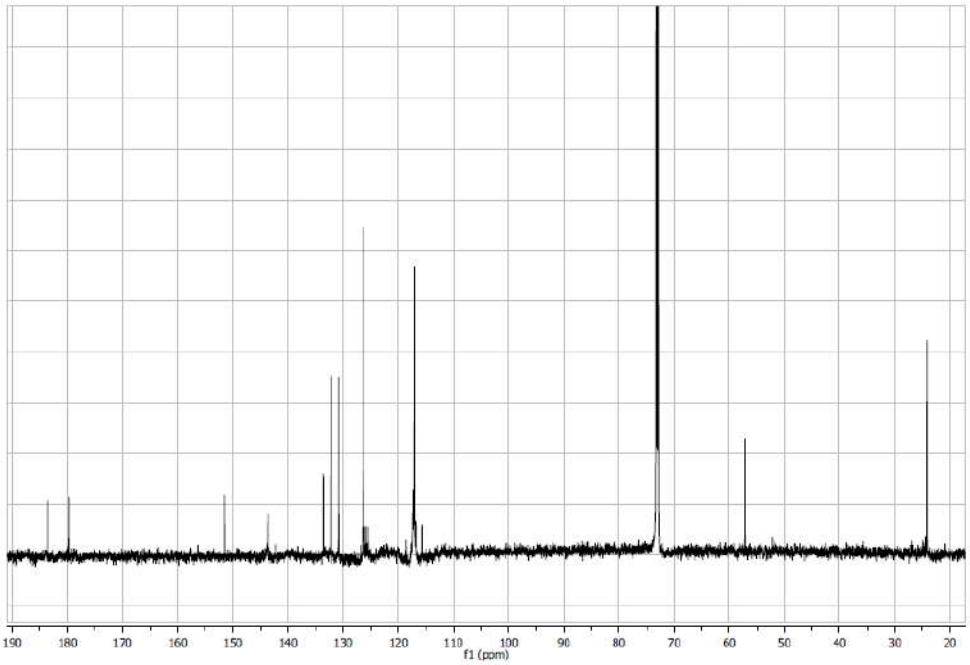

^{1}H NMR spectrum of compound **87** in $CDCl_3$

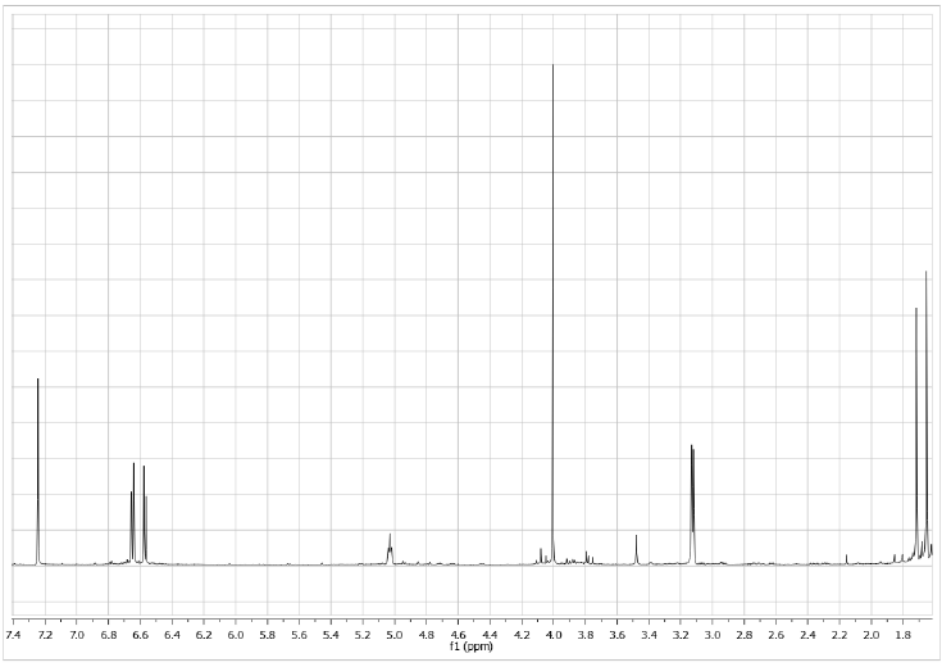

^{13}C NMR spectrum of compound **87** in $CDCl_3$

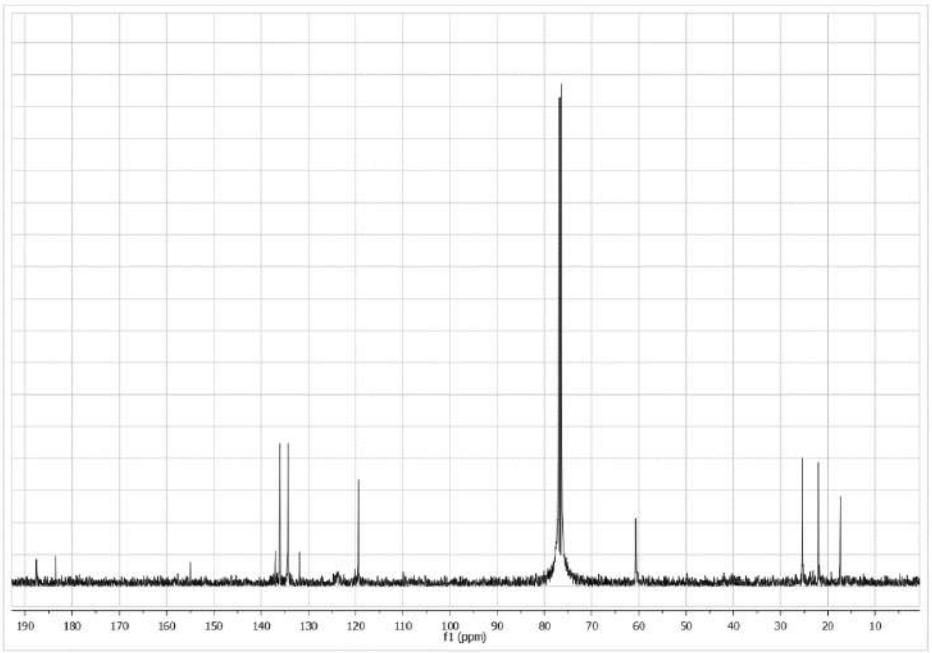

HRESIMS spectrum of compound **87**

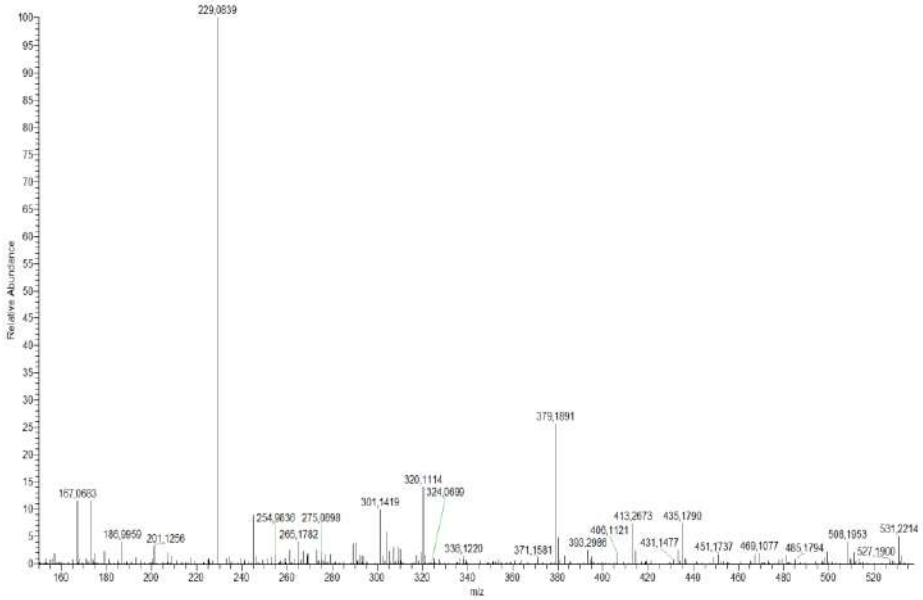

^{1}H NMR spectrum of compound **88** in $CDCl_3$

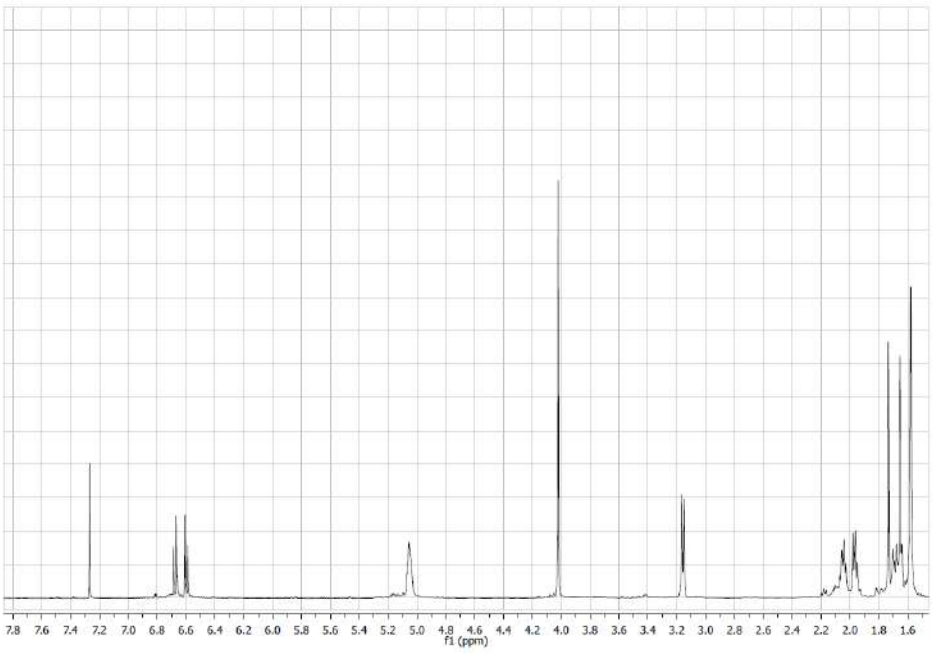

^{13}C NMR spectrum of compound **88** in $CDCl_3$

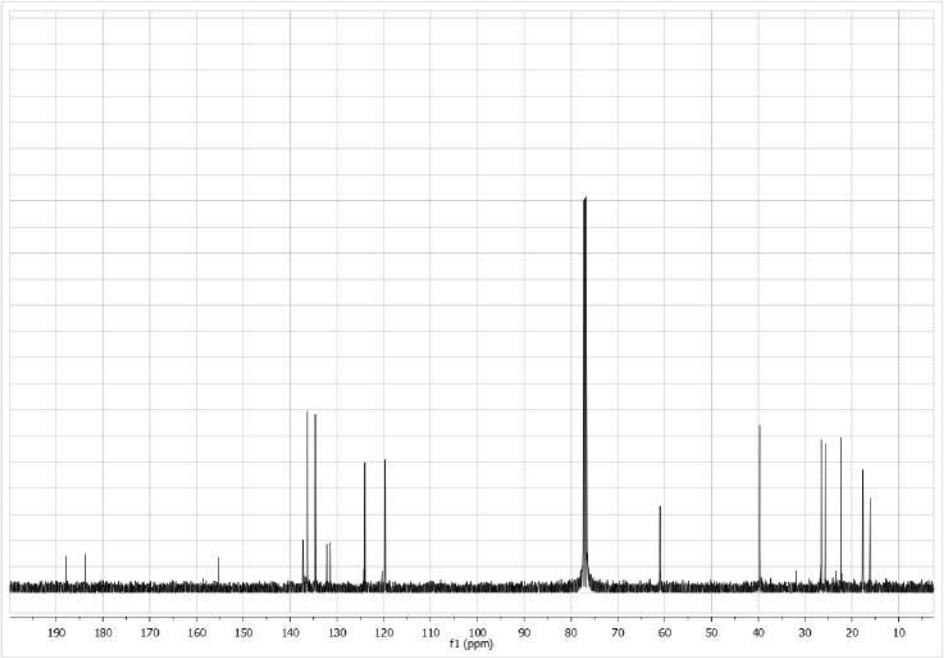

HRESIMS spectrum of compound **88**

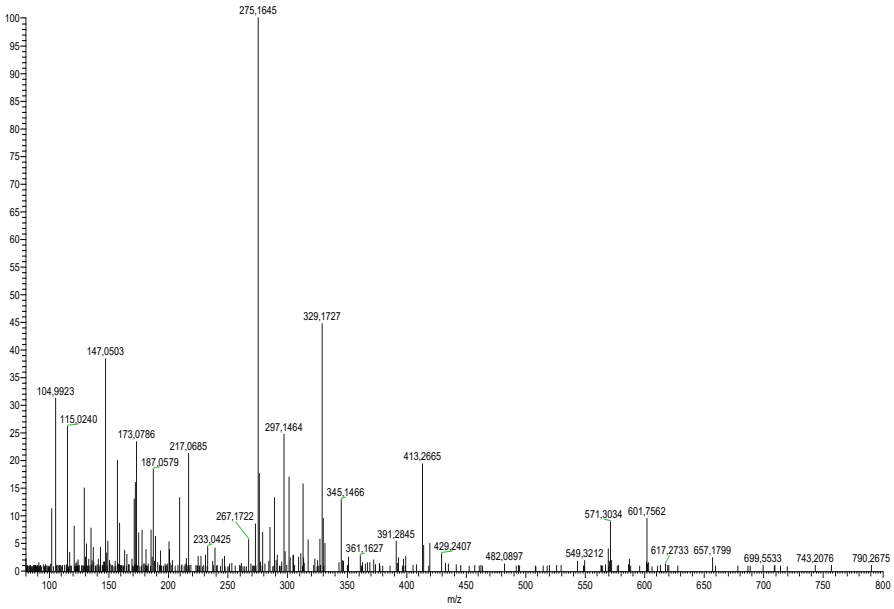

^{1}H NMR spectrum of compound **89** in $CDCl_3$

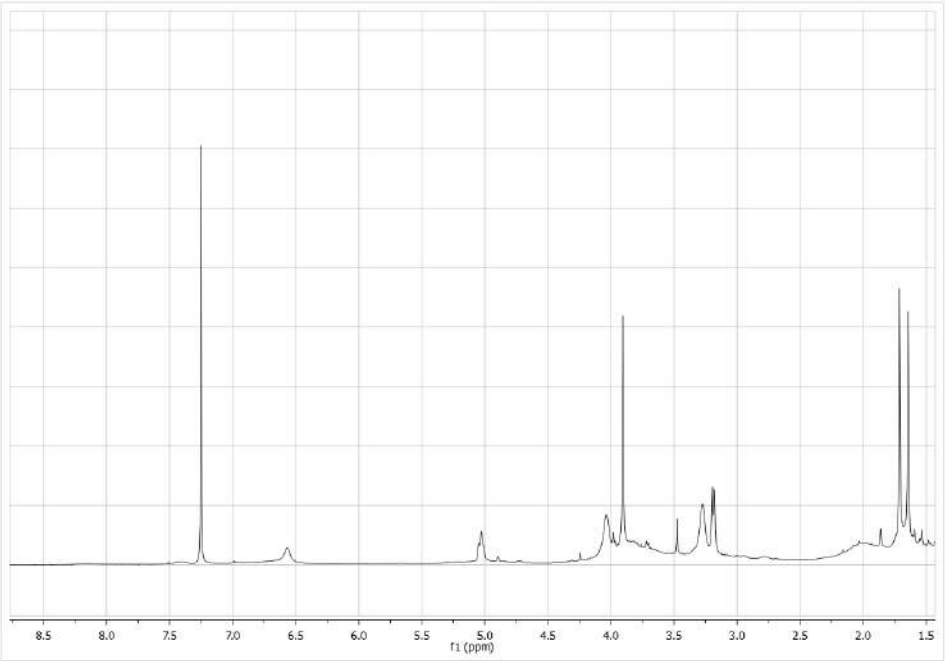

^{13}C NMR spectrum of compound **89** in $CDCl_3$

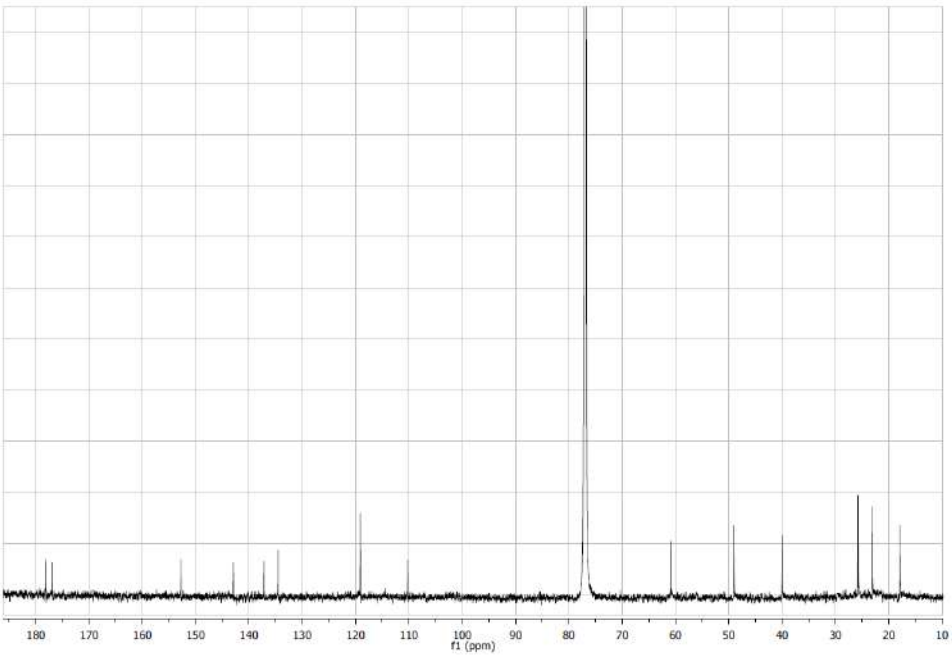

HMBC spectrum of compound **89** in $CDCl_3$

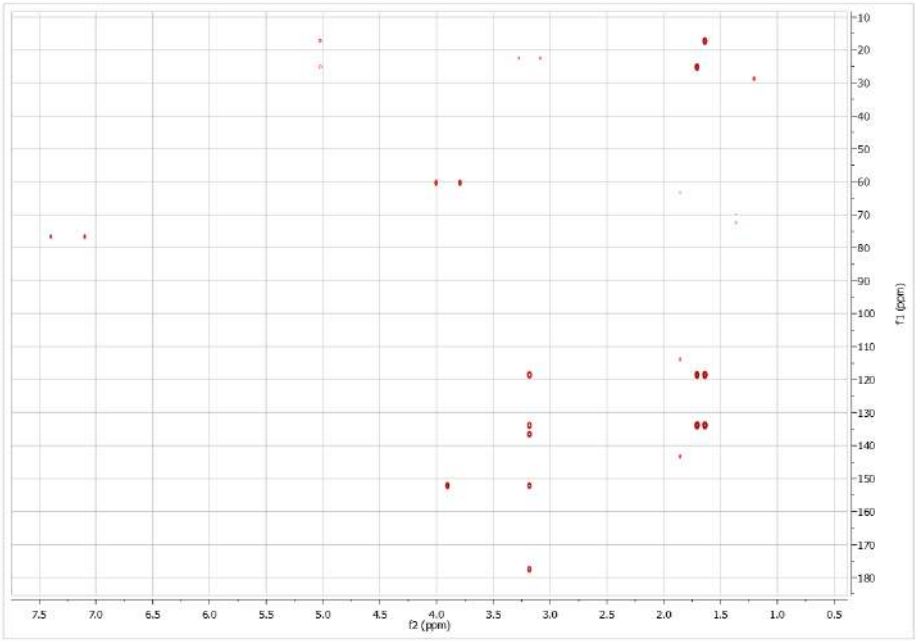

HRESIMS spectrum of compound **89**

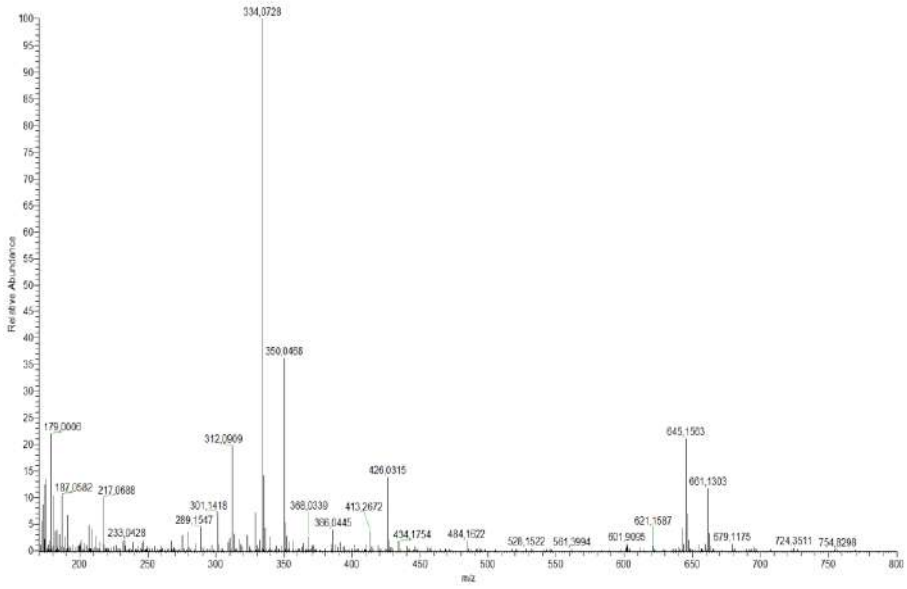

^{1}H NMR spectrum of compound **90** in $CDCl_3$

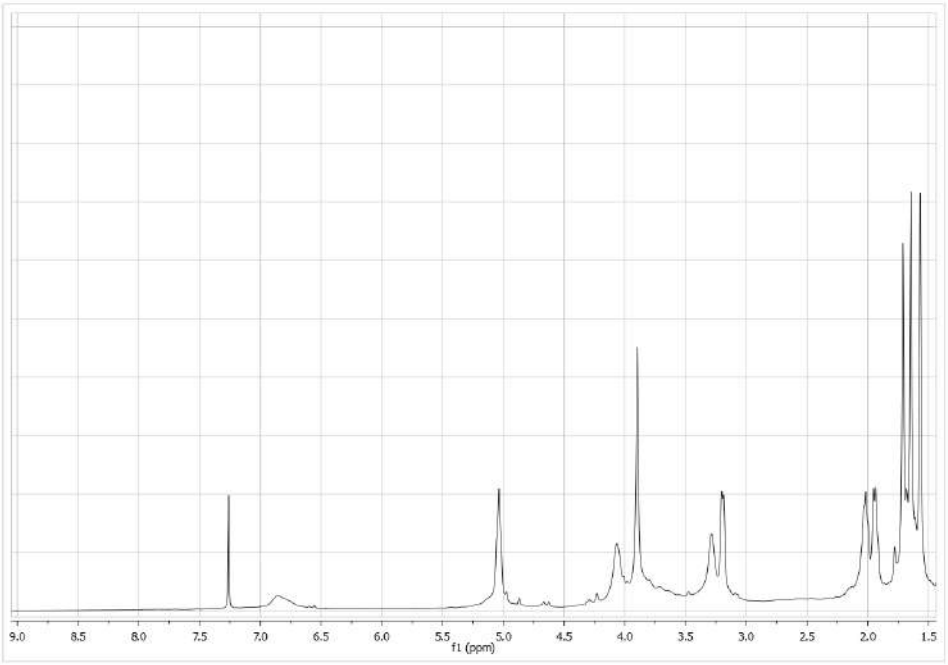

^{13}C NMR spectrum of compound **90** in $CDCl_3$

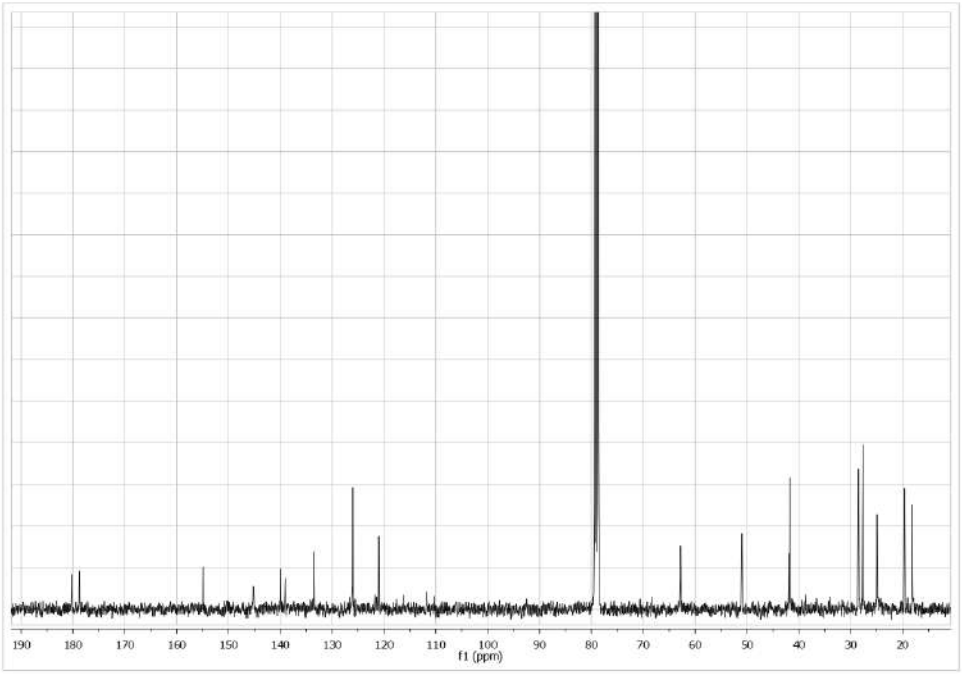

HMBC spectrum of compound **90** in $CDCl_3$

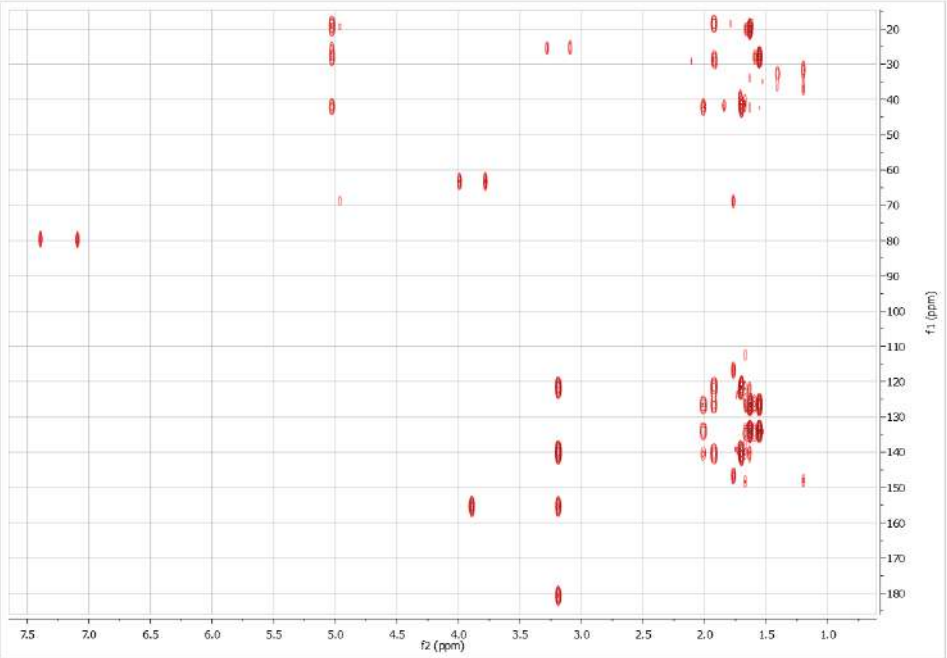

HRESIMS spectrum of compound **90**

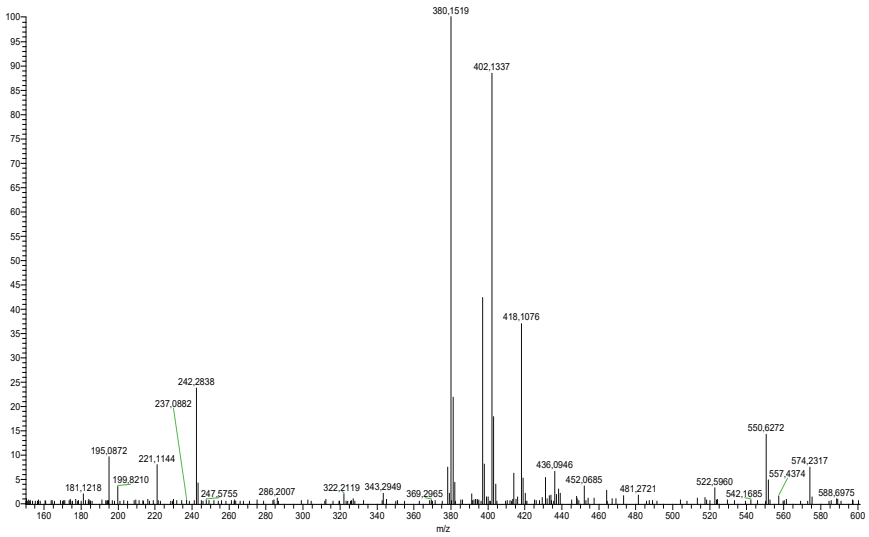

^{1}H NMR spectrum of compound **91-R$_1$** in $CDCl_3$

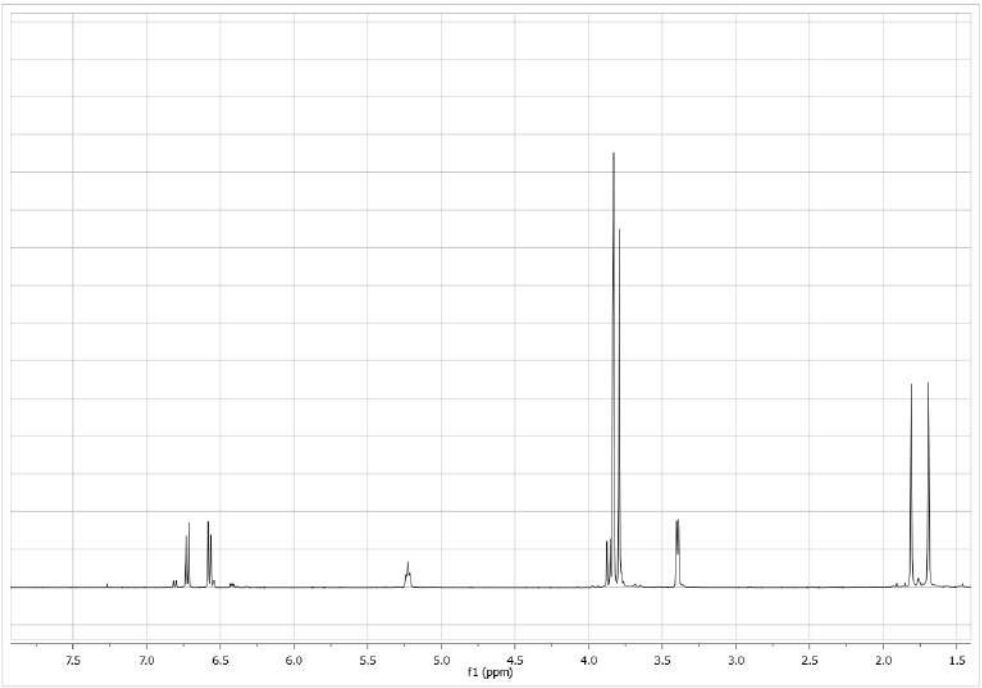

^{13}C NMR spectrum of compound **91-R$_1$** in $CDCl_3$

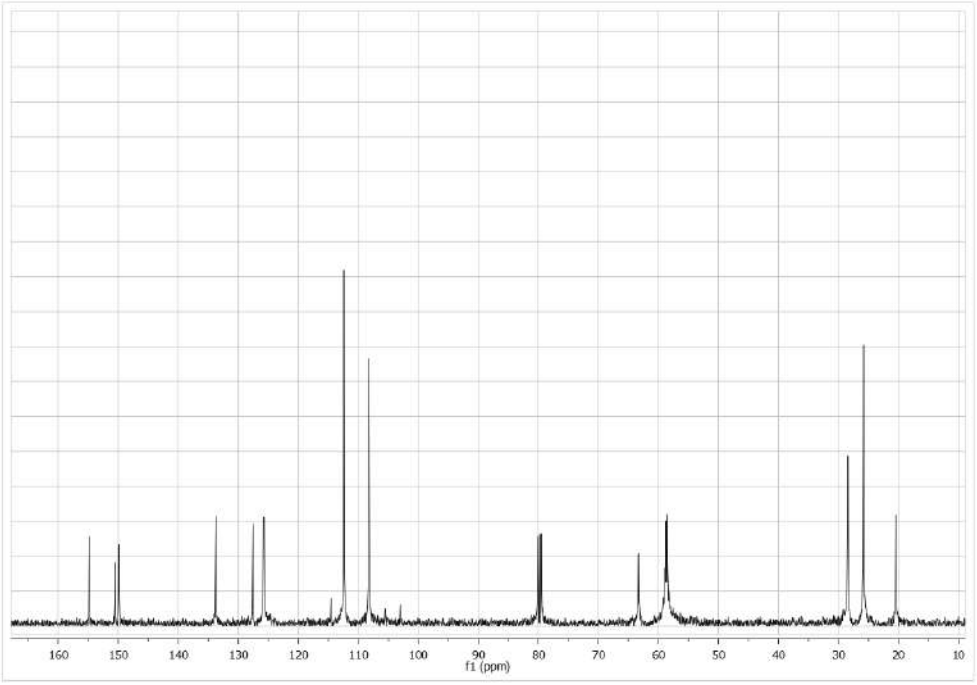

HRESIMS spectrum of compound **91-R$_1$**

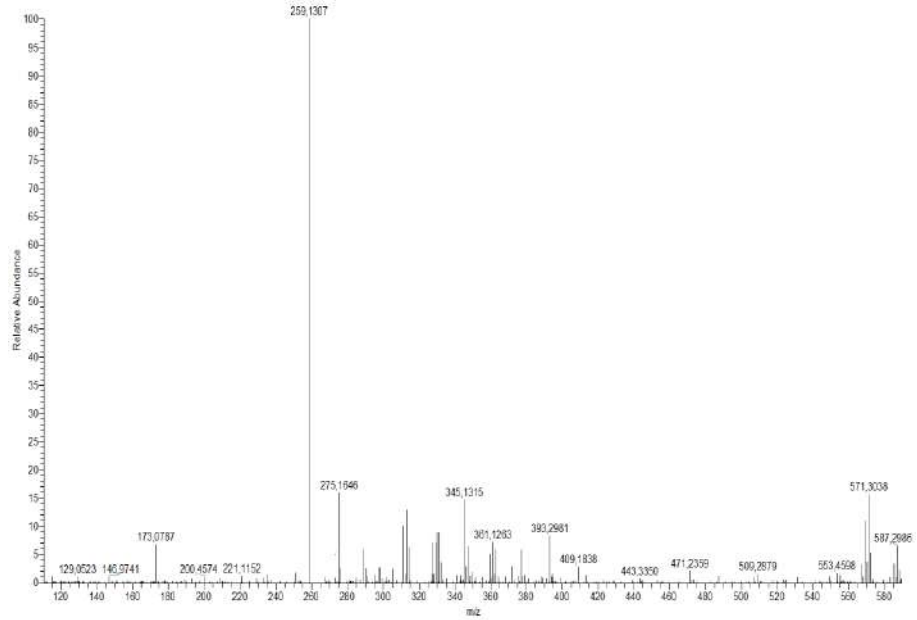

^{1}H NMR spectrum of compound **91-R$_2$** in $CDCl_3$

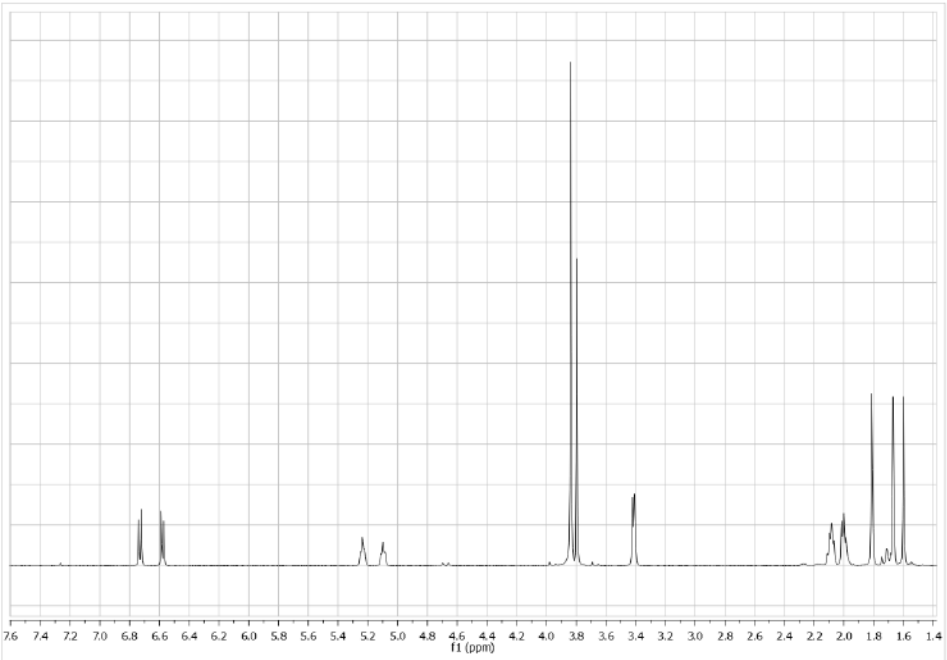

^{13}C NMR spectrum of compound **91-R_2** in $CDCl_3$

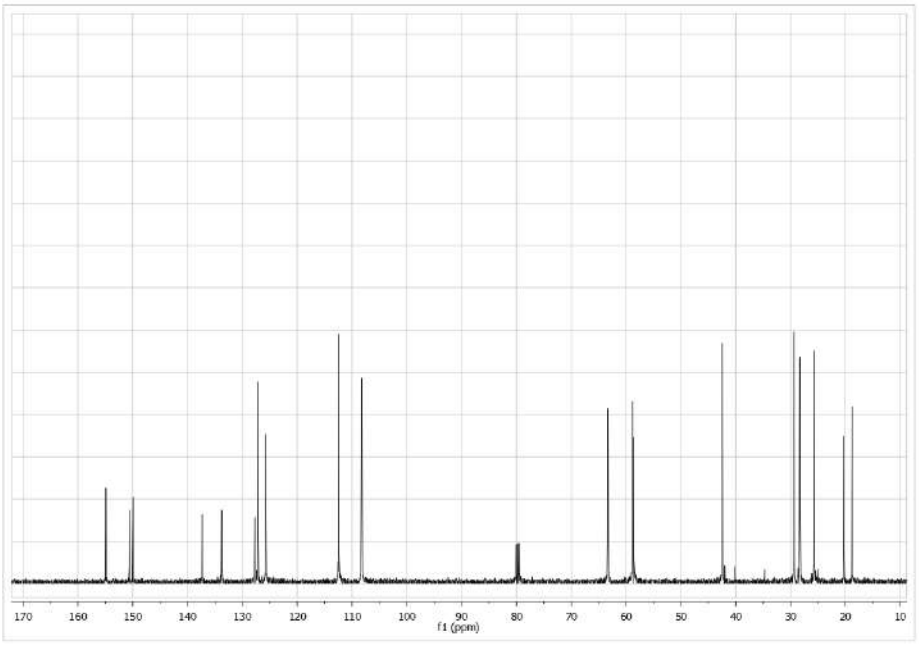

HRESIMS spectrum of compound **92-R_2**

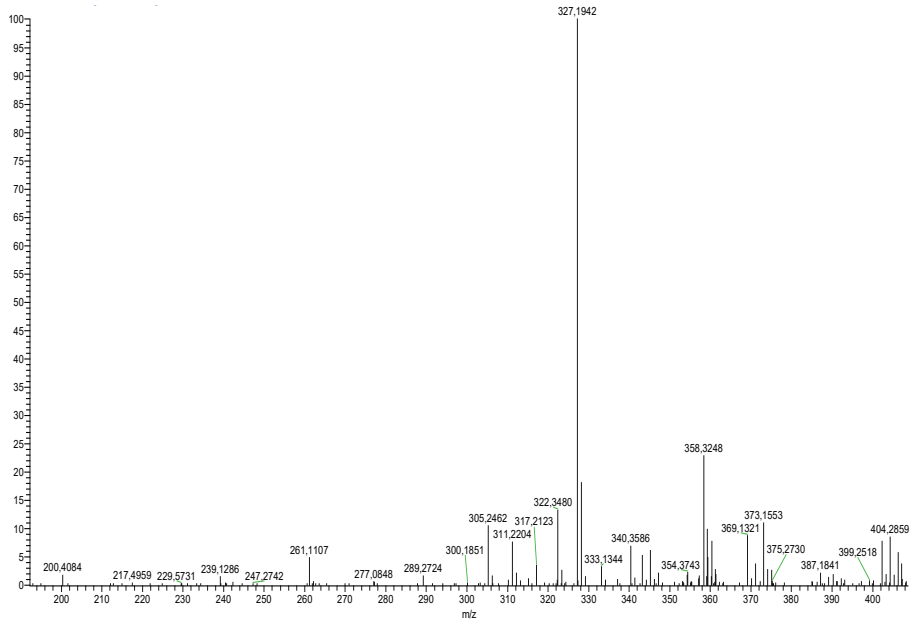

^{1}H NMR spectrum of compound **96** in $CDCl_3$

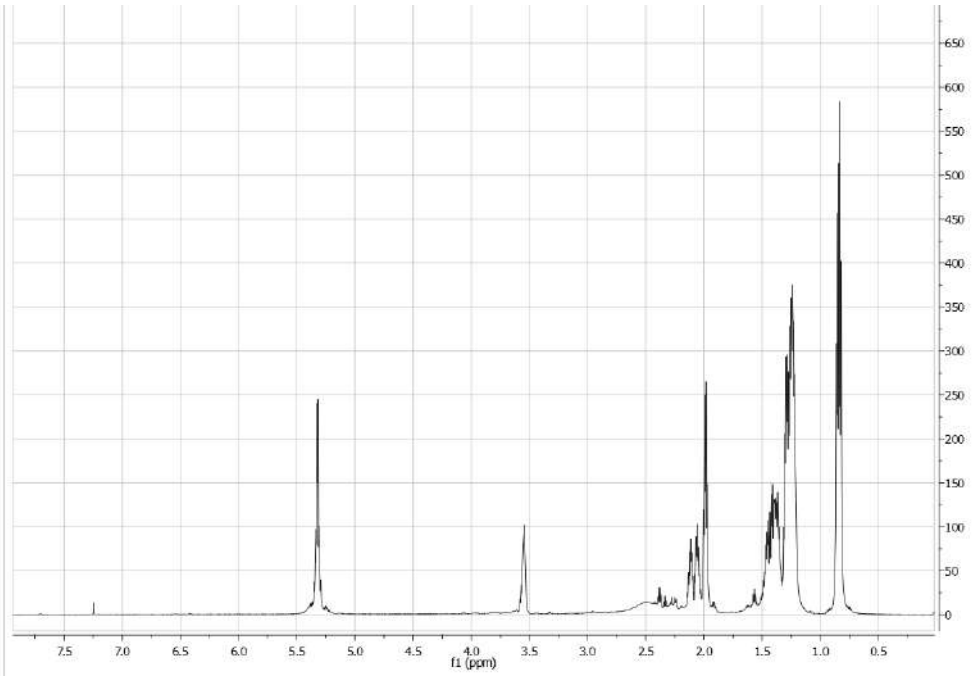

^{13}C NMR spectrum of compound **96** in $CDCl_3$

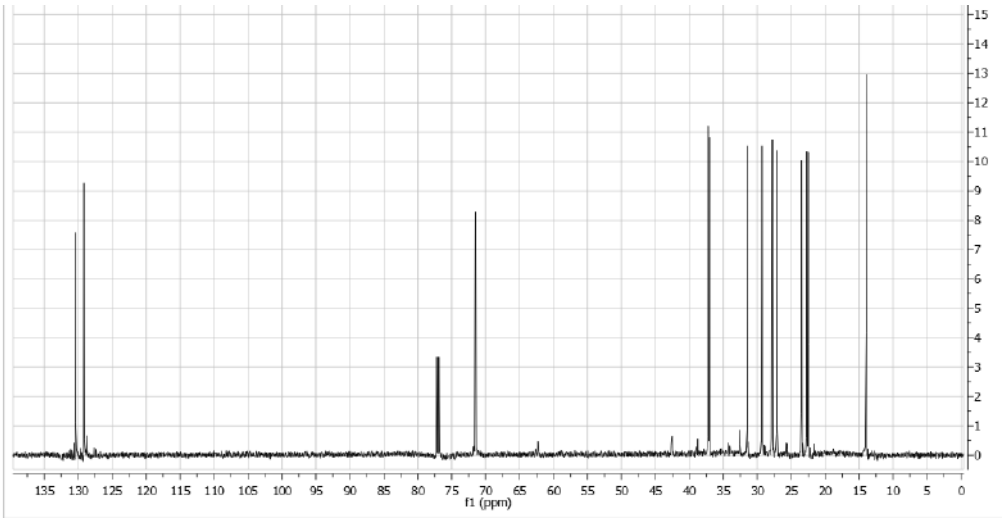

^{1}H NMR spectrum of compound ***rac*-97** in CD_3OD

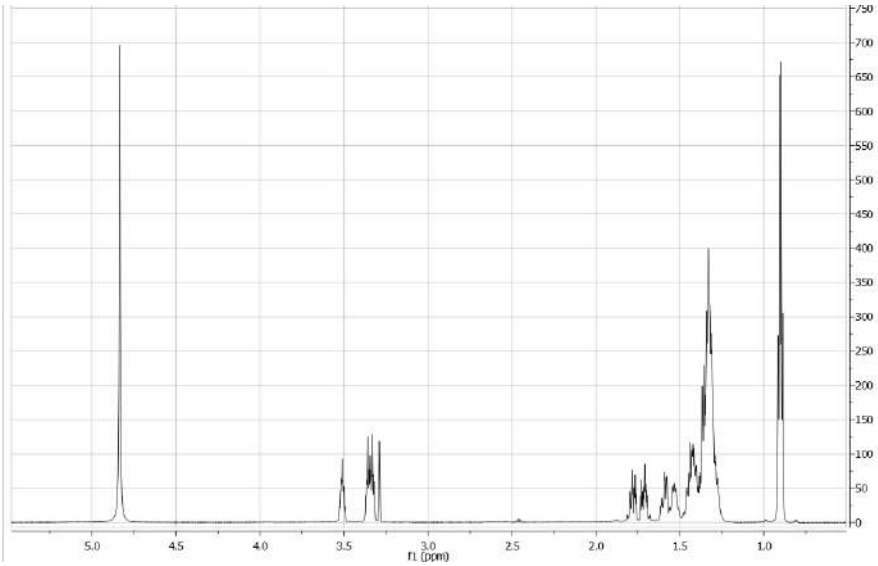

^{13}C NMR spectrum of compound ***rac*-97** in CD_3OD

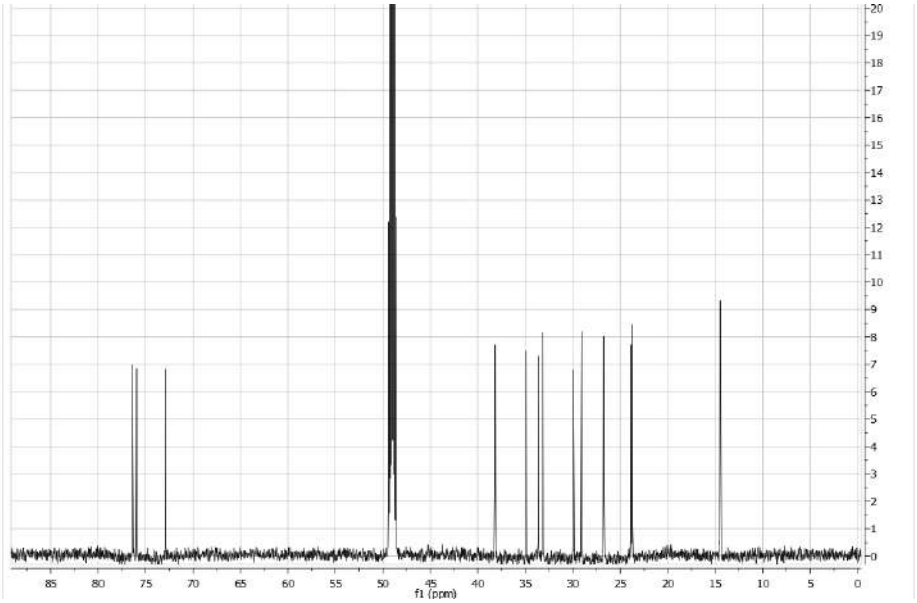

^{1}H NMR spectrum of compound ***rac*-98** in CD_3OD

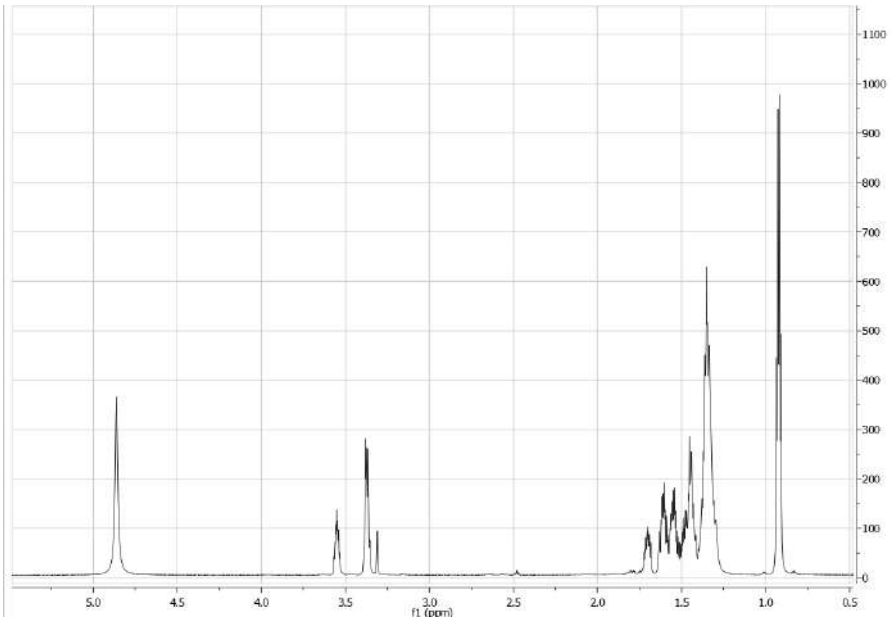

^{13}C NMR spectrum of compound ***rac*-98** in CD_3OD

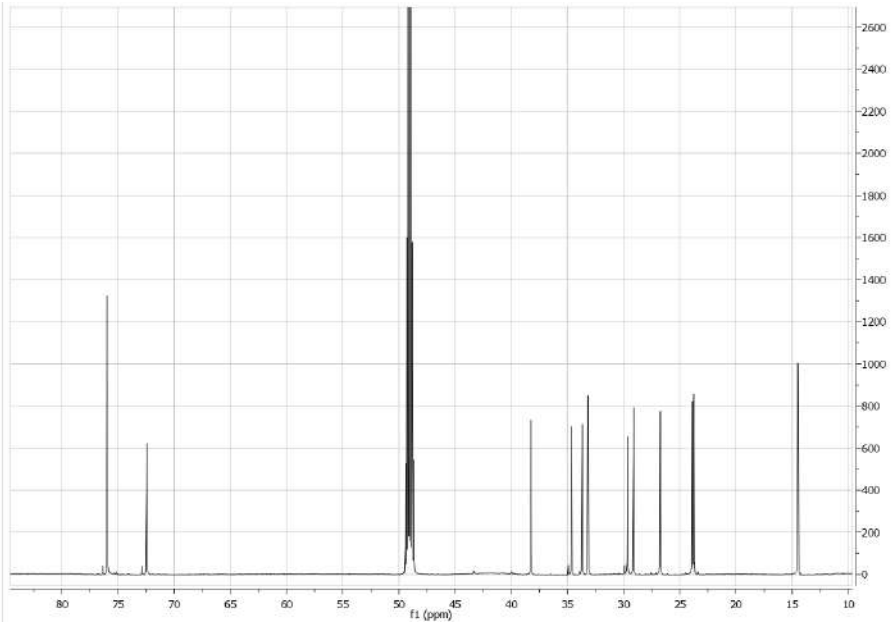

^{1}H NMR spectrum of compound **97a** in $CDCl_3$

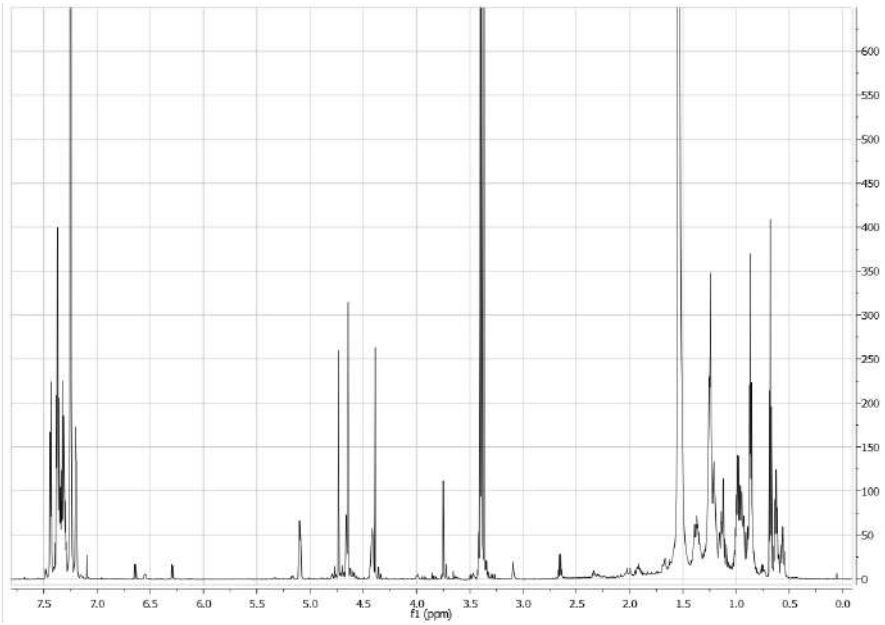

^{1}H NMR spectrum of compound **97b** in $CDCl_3$

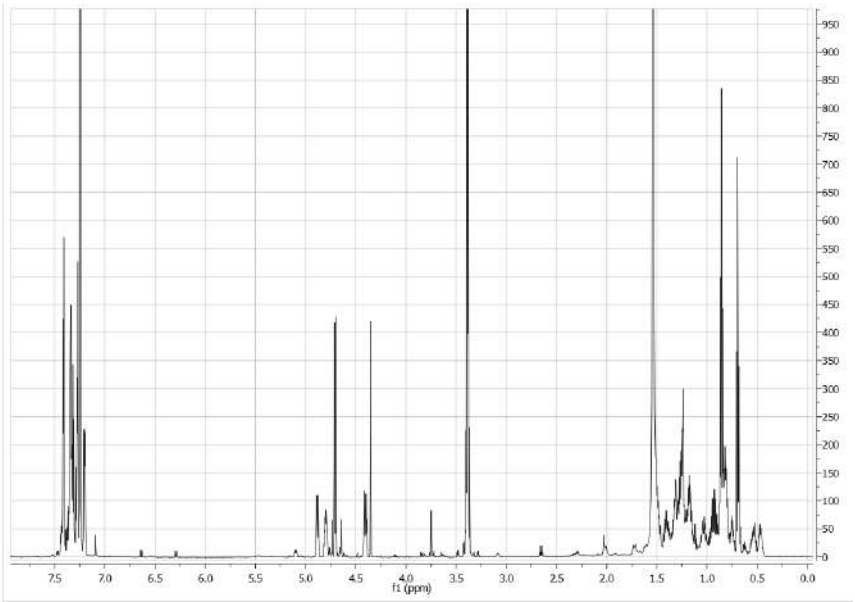

^{1}H NMR spectrum of compound **98a** in $CDCl_3$

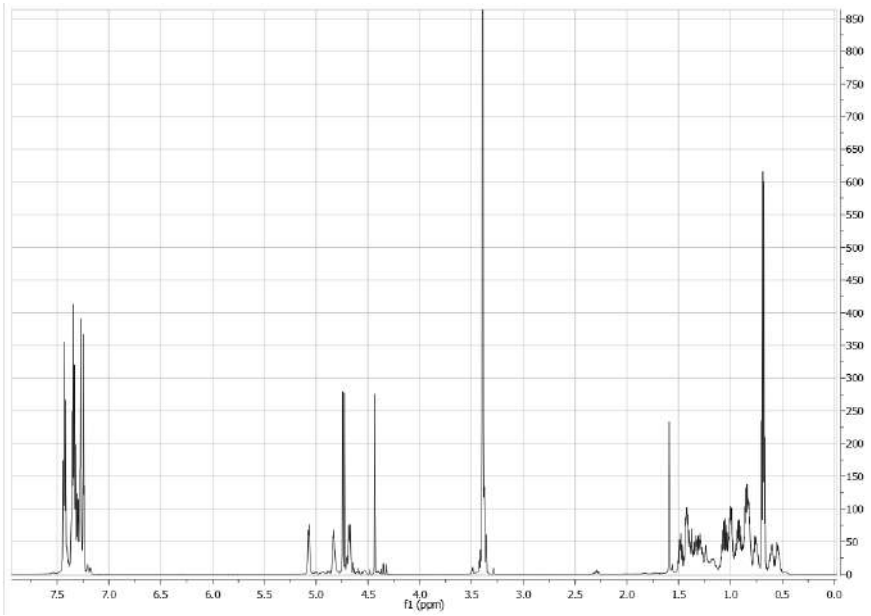

^{1}H NMR spectrum of compound **98b** in $CDCl_3$

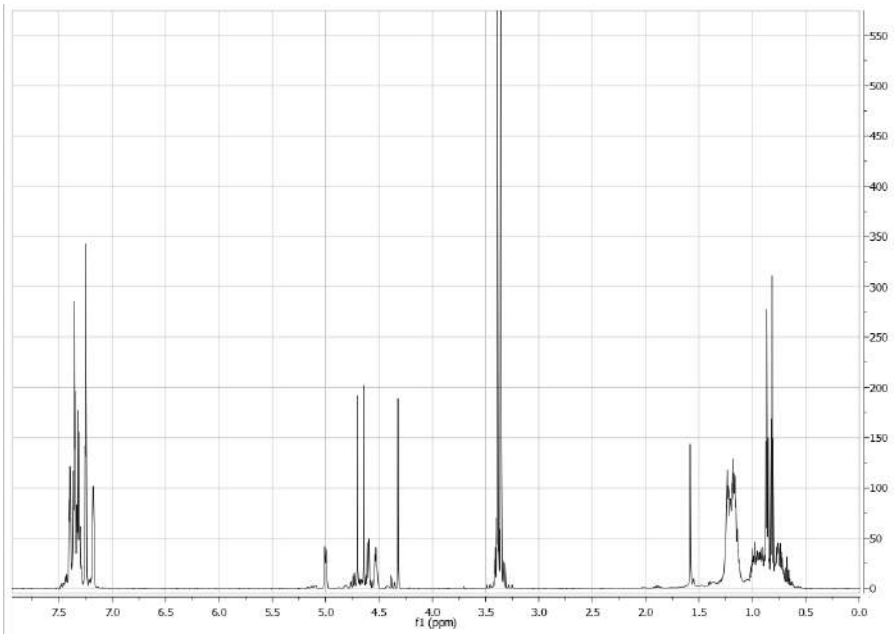

^{1}H NMR spectrum of compound **102** in $CDCl_3$

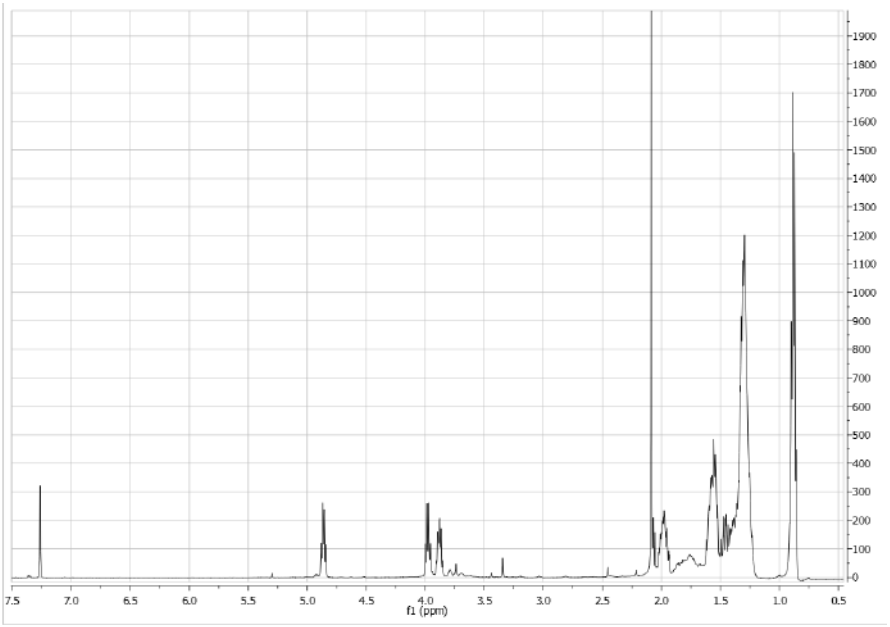

ROESY spectrum of compound **102** in $CDCl_3$

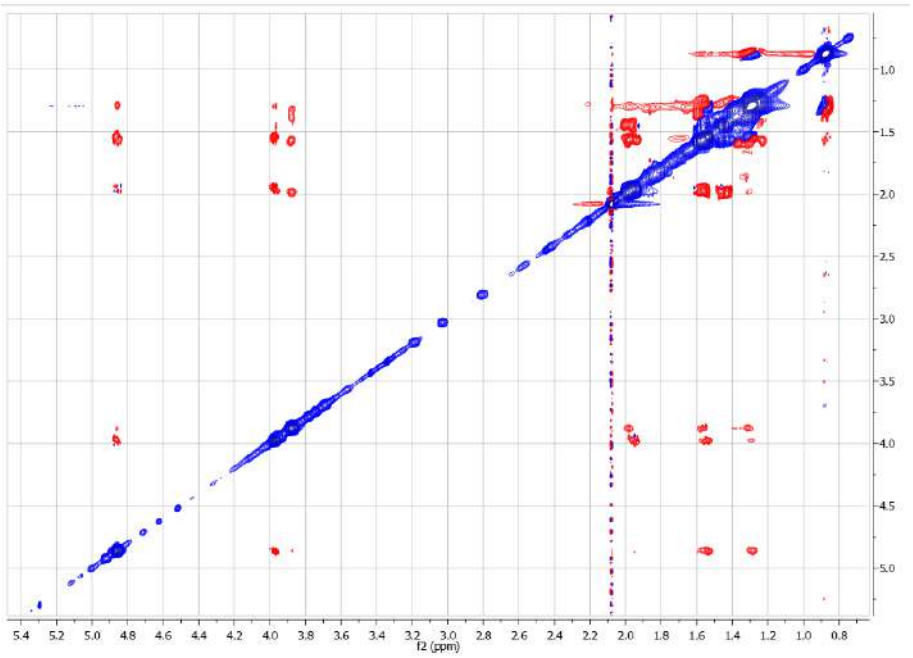

HSQC spectrum of compound **102** in $CDCl_3$

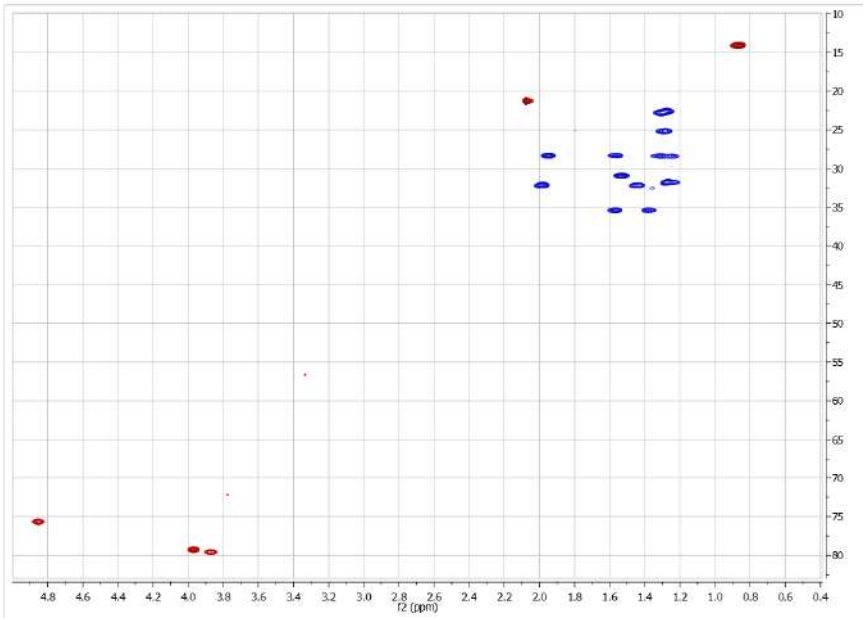

^1H NMR spectrum of compound **103** in $CDCl_3$

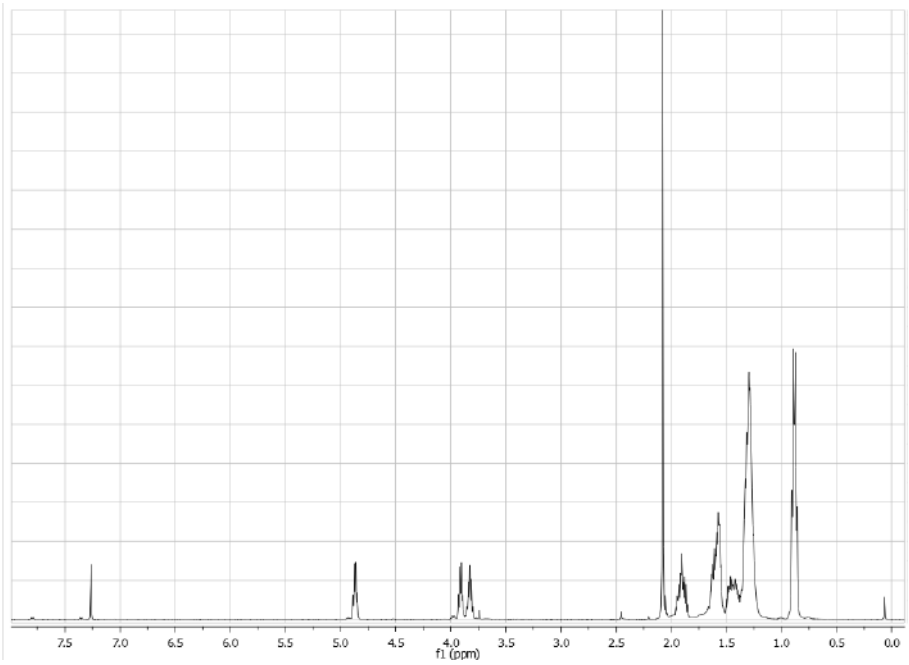

ROESY spectrum of compound **103** in $CDCl_3$

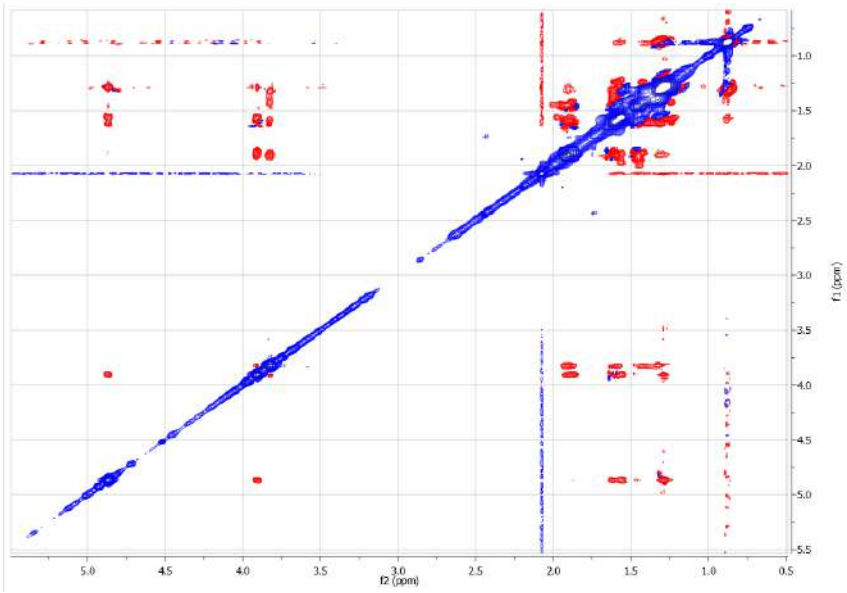

HSQC spectrum of compound **103** in $CDCl_3$

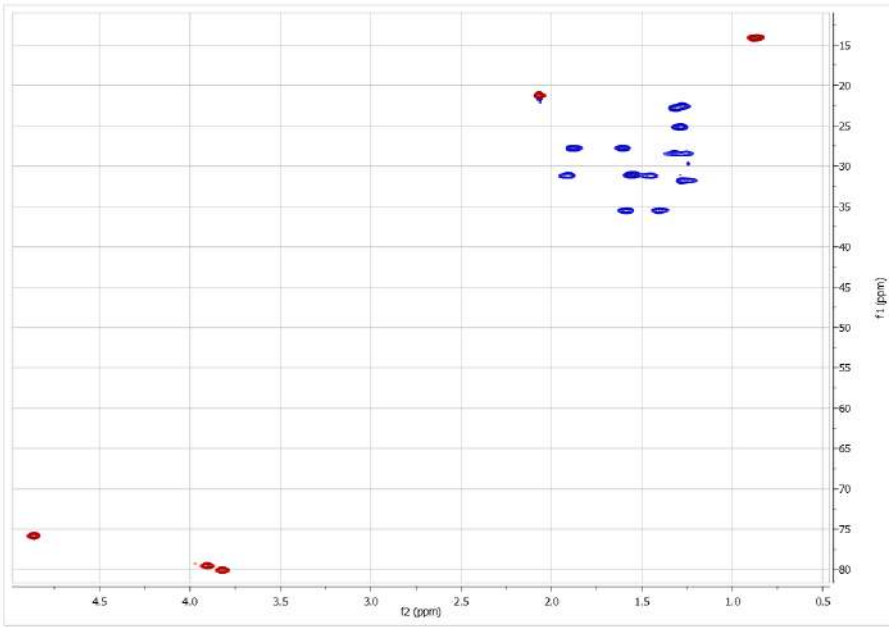

^{1}H NMR spectrum of compound **104** in CD_3OD

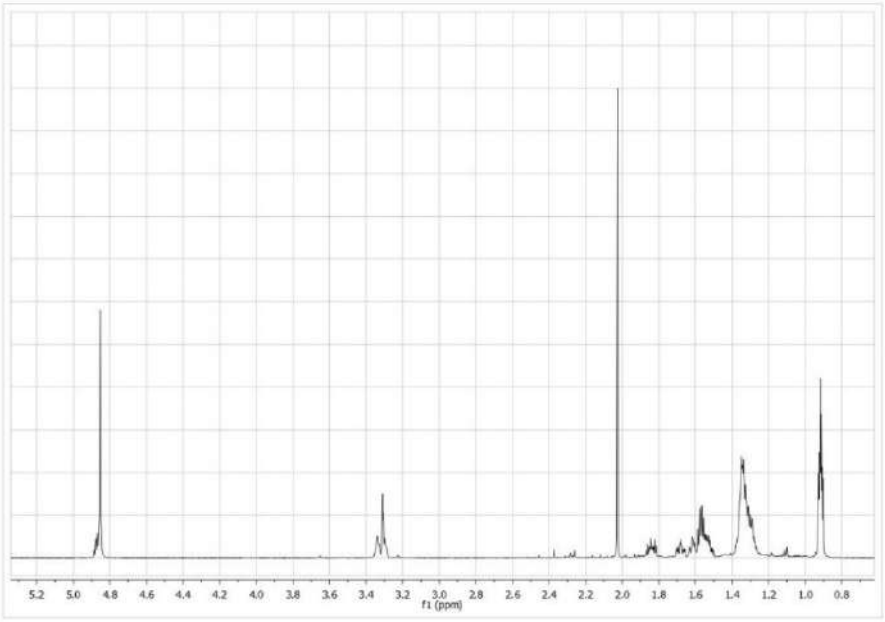

HSQC spectrum of compound **104** in CD_3OD

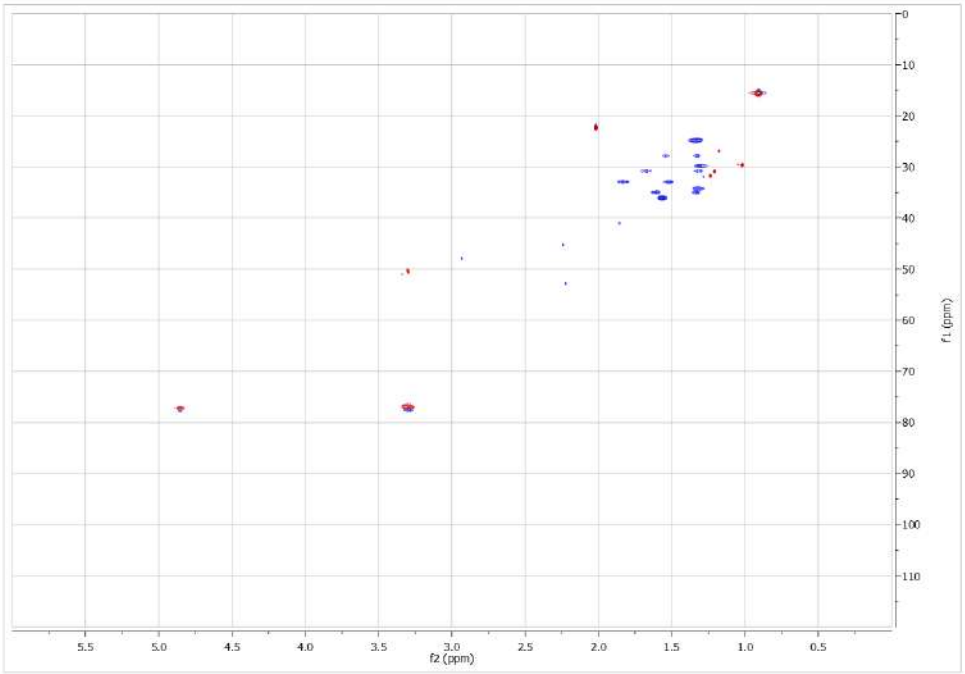

^{1}H NMR spectrum of compound **105** in CD_3OD

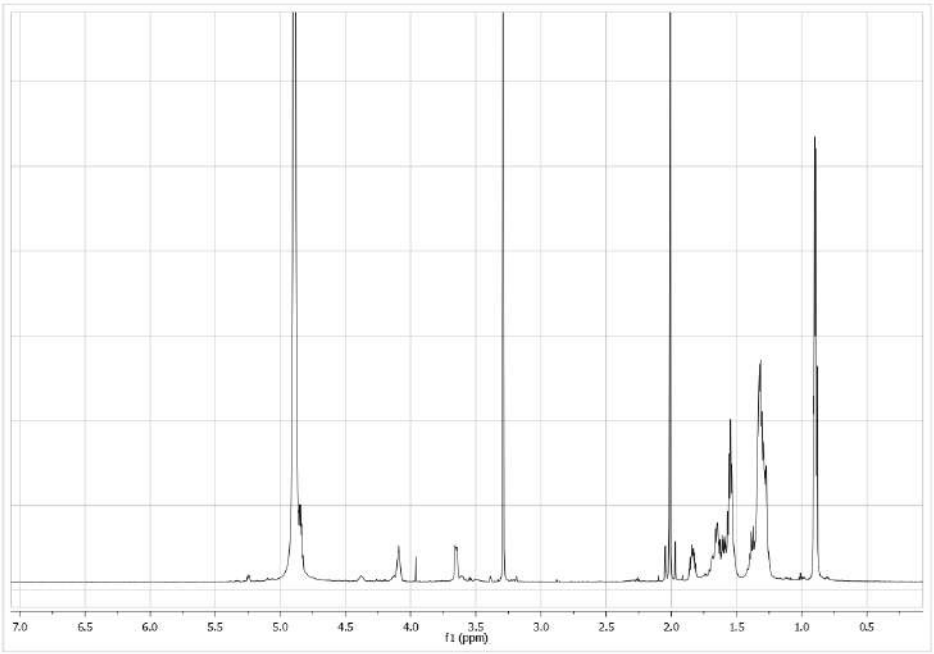

COSY spectrum of compound **105** in CD_3OD

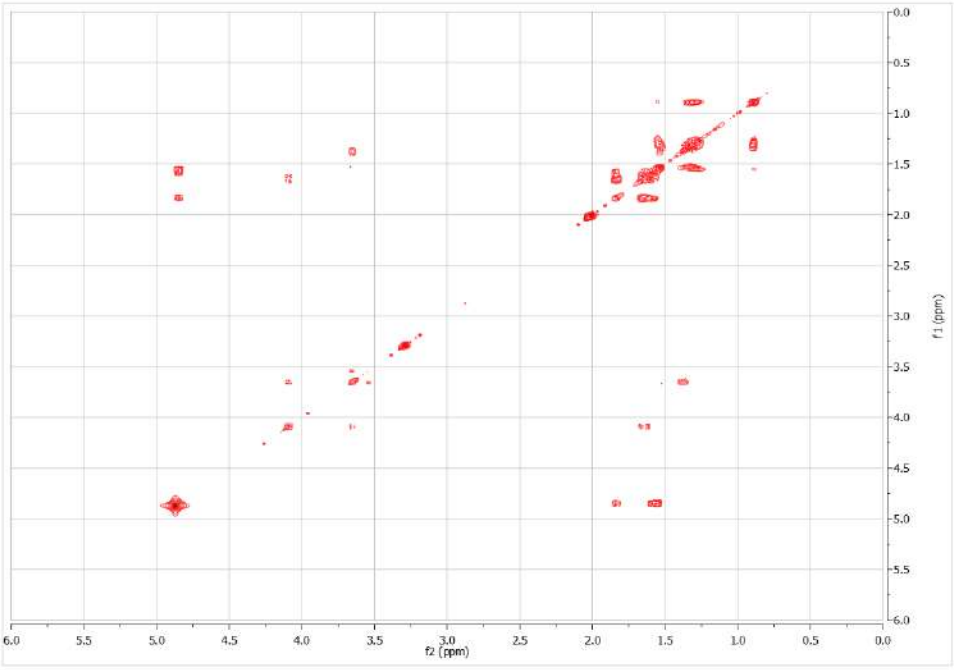

HSQC spectrum of compound **105** in CD_3OD

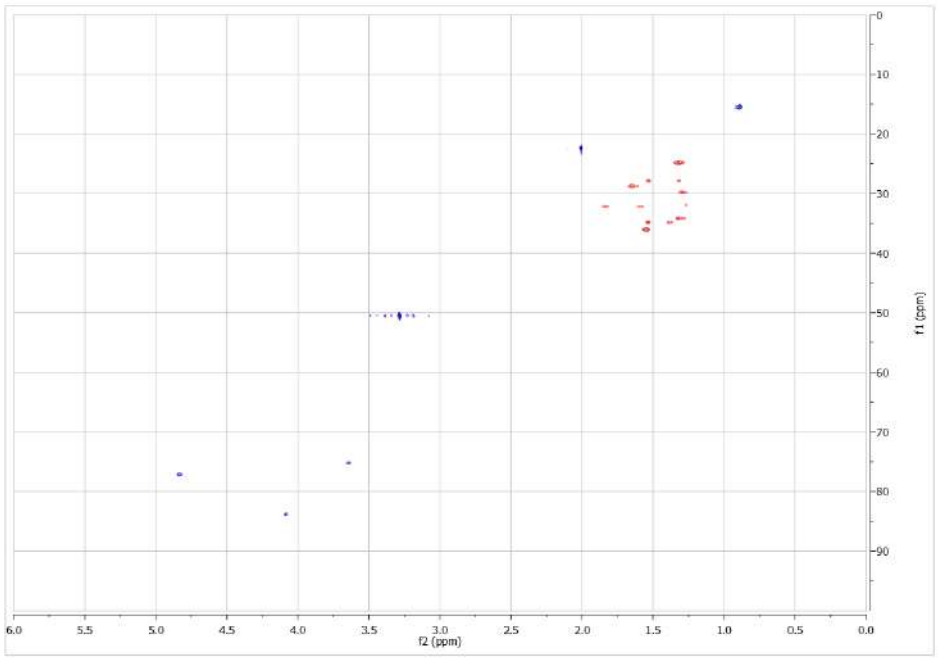

HRESIMS spectrum of compound **105**

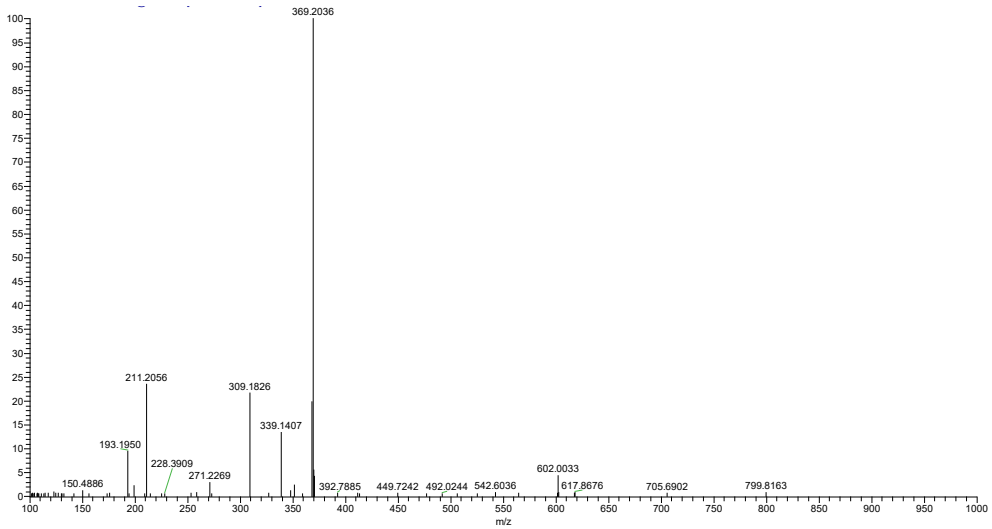

^{1}H NMR spectrum of compound **106** in CD_3OD

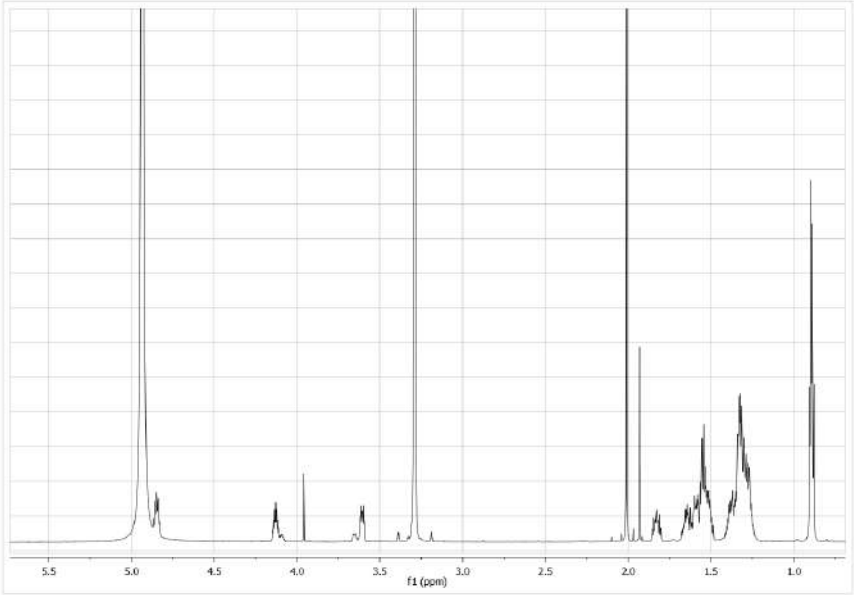

COSY spectrum of compound **106** in CD_3OD

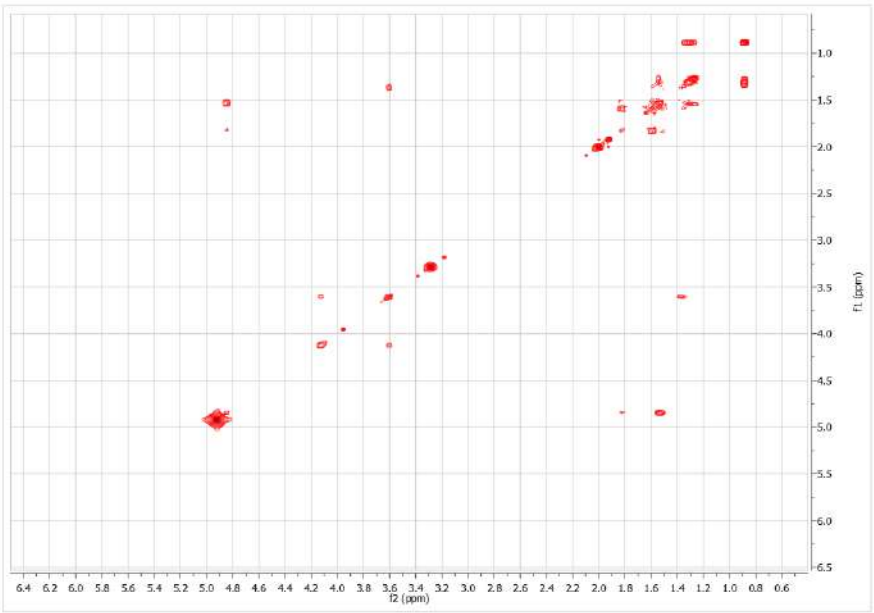

TOCSY spectrum of compound **106** in CD_3OD

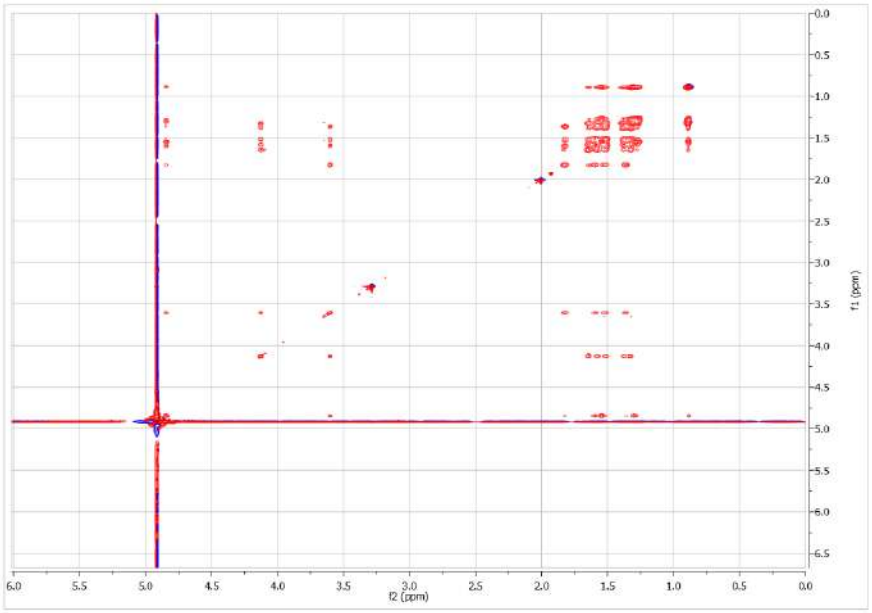

HRESIMS spectrum of compound **106**

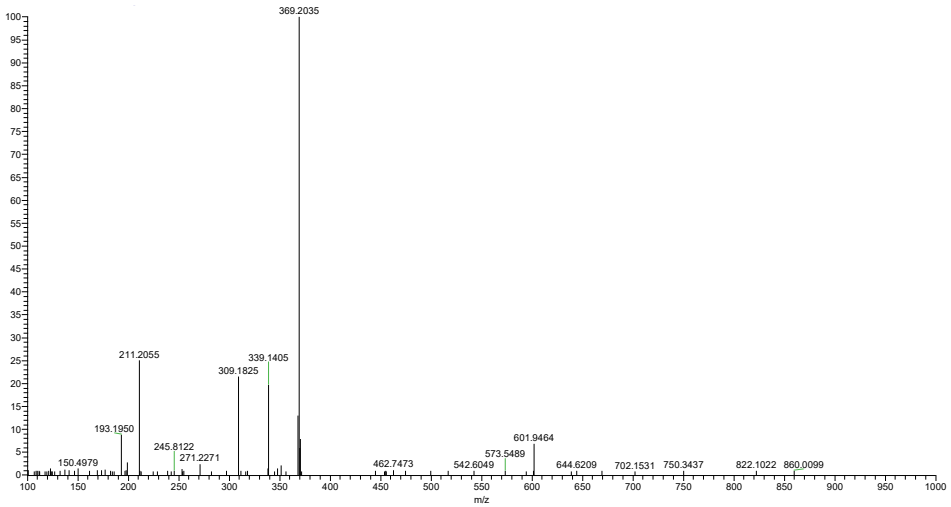

^{1}H NMR spectrum of compound **107** in CD_3OD

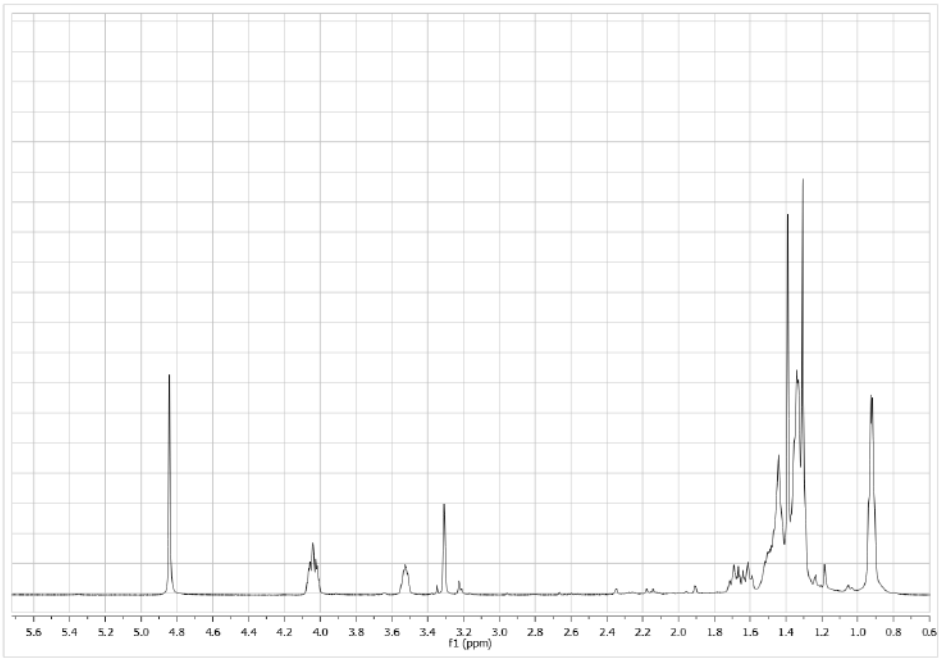

HSQC spectrum of compound **107** in CD_3OD

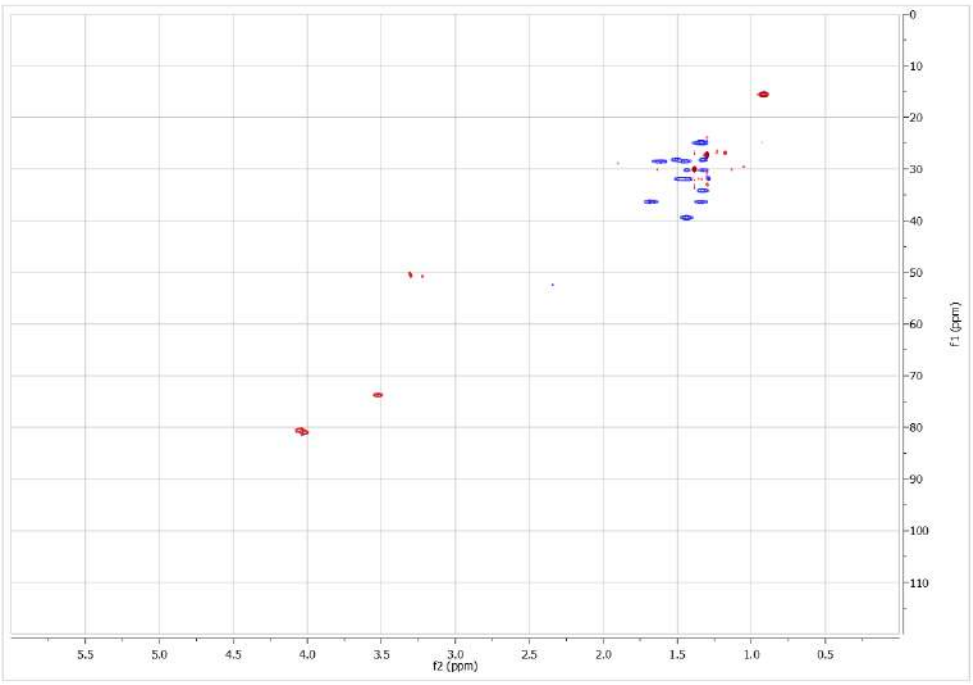

^{1}H NMR spectrum of compound **108** in CD_3OD

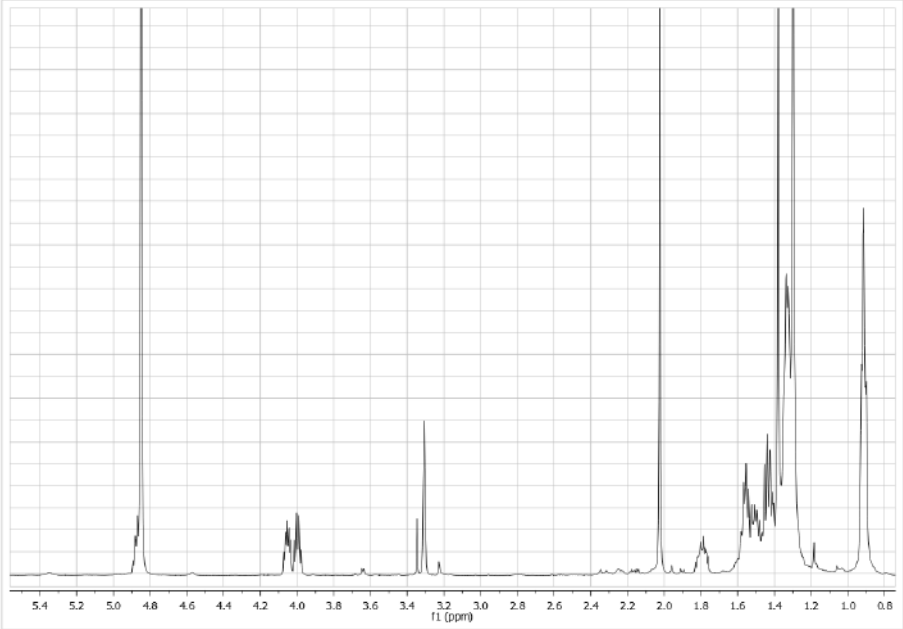

HSQC spectrum of compound **108** in CD_3OD

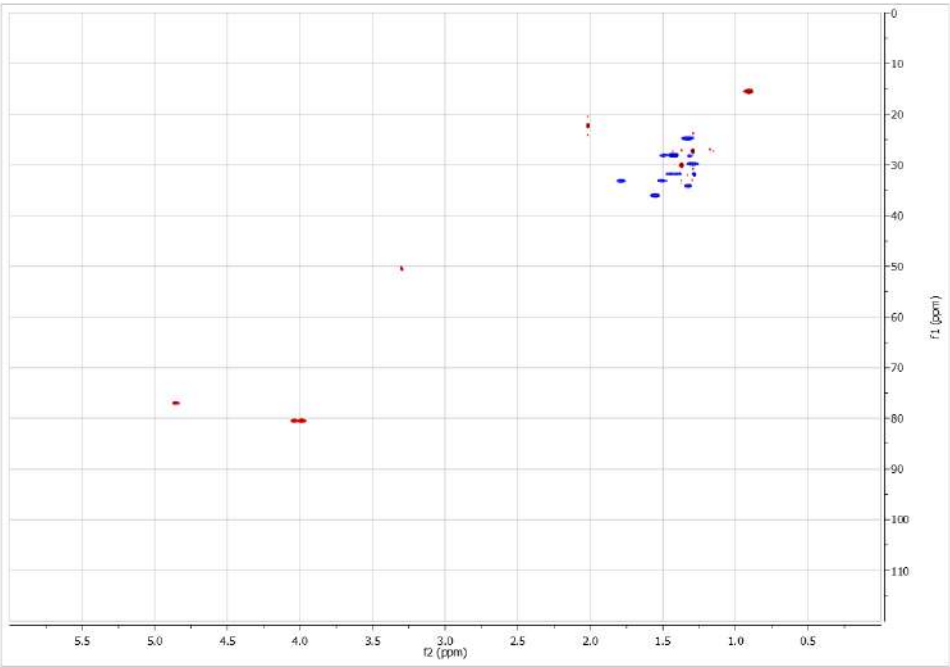

HRESIMS spectrum of compound **108**

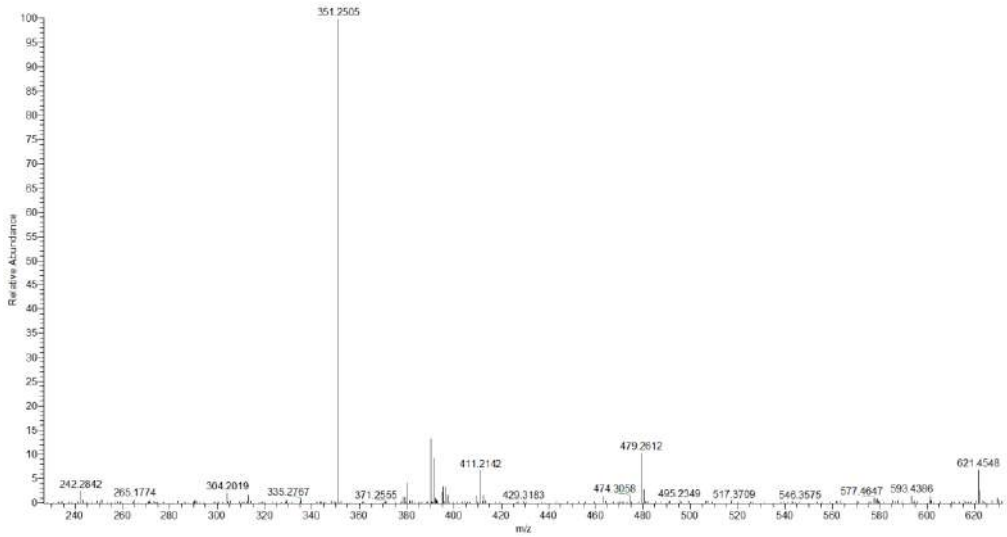

References

1. Bo, Y.; Dong-Mei, F.; Xian-Li, Z.; Feng, G. Natural products as important tyrosine kinase inhibitors. *Eur. Med. J. Chem.* **2019**, *182*, 111664.
2. Newman, D.J.; Cragg, G.M. Natural Products as Sources of New Drugs from 1981 to 2014. *J. Nat. Prod.* **2016**, *79*, 629-661.
3. Proksch, P.; Ebel, R. Alkaloids, biochemistry, ecology and medicinal applications. Plenum Press: New York, **1998**.
4. Pawlik, J.R. Marine invertebrate chemical defences. *Chem. Rev.* **1993**, *93*, 1911-1922.
5. Rosén, J.; Gottfries, J.; Muresan, S.; Backlund, A.; Oprea, T.I. Novel Chemical Space Exploration via Natural Products. *J. Med. Chem.* **2009**, *52*, 1953-1962.
6. Kennedy, J.P.; Williams, L.; Bridges, T.M.; Daniels, R.N.; Weaver, D.; Lindsley, C.W.J. Application of Combinatorial Chemistry Science on Modern Drug Discovery. *J. Comb. Chem.* **2008**, *10*, 345-354.
7. Harvey, A.L. Natural products as a screening resource. *Curr. Opin. Chem. Biol.* **2007**, *11*, 480-484.
8. Fabricant, D.S.; Farnsworth, N.R. The value of plants used in traditional medicine for drug discovery. *Environ. Health Perspect.* **2001**, *109*, 69-75.
9. Cragg, G.M.; Newman, D.J. Natural Products: A Continuing Source of Novel Drug Leads. *Biochim. Biophys. Acta* **2013**, *1830*, 3670-3695.
10. Raskin, I.; Ribnicky, D.M.; Komarnytsky, S.; Ilic, N.; Poulev, A.; Borisjuk, N.; Brinker, A.; Moreno, D.A.; Ripoll, C.; Yakoby, N.; O'Neal, J.M.; Cornwell, T.;

Pastor, I.; Fridlander, B. Plants and human health in the twenty-first century. *Trends Biotech.* **2002**, *20*, 522-531

11. Newman, D.J.; Cragg, G.M. Marine Natural Products and Related Compounds in Clinical and Advanced Preclinical Trials. *J. Nat. Prod.* **2004**, *67*, 1216-1238.
12. Michl, J.; Gladysz, J.A.; George, S.M. Marine natural products chemistry. *Chem. Rev.* **1993**, *93*, 1671.
13. Blunt, J.W.; Copp, B.R.; Munro, M.H.G.; Northcote, P.T.; Prinsep, M.R. Marine natural products. *Nat. Prod. Rep.* **2003**, *20*, 1-48.
14. Costantino, V.; Fattorusso, E.; Menna, M.; Taglialatela-Scafati, O. Chemical diversity of bioactive marine natural products: an illustrative case study. *Curr. Med. Chem.* **2004**, *11*, 1671-1692.
15. Hagadone, M.R.; Burreson, B.J.; Scheuer, P.J.; Finer, J. S.; Clardy, J. Defensive allomones of the nudibranch *Phyllidia varicosa* Lamarck, 1801. *Helv. Chim. Acta* **1979**, *62*, 2484-2494.
16. Burgoyne, D.L.; Dumdei, E.J.; Andersen, R.J. Acanthenes A to C: a chloro, isothiocyanate, formamide sesquiterpene triad isolated from the northeastern Pacific marine sponge Acanthella sp. and the dorid nudibranch *Cadlina luteomarginata*. *Tetrahedron* **1993**, *49*, 4503-4510.
17. Capon, R.J.; Skene, C.; Liu, E.H.; Lacey, E.; Gill, J.H.; Heiland, K.; Friedel, T. The Isolation and Synthesis of Novel Nematocidal Dithiocyanates from an Australian Marine Sponge, *Oceanapia* sp. *J. Org. Chem.* **2001**, *66*, 7765-7769.
18. He, H.Y.; Faulkner, D.J.; Shumsky, J.S.; Hong, K.; Clardy, J. A sesquiterpene thiocyanate and three sesquiterpene isothiocyanates from the sponge *Trachyopsis aplysinoides*. *J. Org. Chem.* **1989**, *54*, 2511-2514.

19. Liang, X.; Luo, D.; Luesch, H. Advances in exploring the therapeutic potential of marine natural products. *Pharmacol. Res.* **2019**, *147*, 104373-104391.
20. Aiello, A.; Fattorusso, E.; Luciano, P.; Mangoni, A.; Menna, M. Isolation and structure determination of aplidinones A-C from the Mediterranean ascidian *Aplidium conicum*: A successful regiochemistry assignment by quantum mechanical ^{13}C NMR chemical shift calculations. *Eur. J. Org. Chem.* **2005**, 5024-5030.
21. Gerwick, W.H.; Moore, B.S. Lessons from the Past and Charting the Future of Marine Natural Products Drug Discovery and Chemical Biology. *Chem. Biol.* **2012**, *19*, 85-98.
22. Wallace, M.S. Ziconotide: a new nonopioid intrathecal analgesic for the treatment of chronic pain. *Expert Rev. Neurother.* **2006**, *6*, 1423-1428.
23. Bulaj, G.; Buczek, O.; Goodsell, I.; Jiminez, E.C.; Kranski, J.; Nielsen, J.S.; Garrett, J.E.; Olivera, B.M. Efficient oxidative folding of conotoxins and the radiation of venomous cone snails. *Proc. Natl. Acad. Sci. USA* **2003**, *100*, 14562-14568.
24. McGivern, J.G. Ziconotide: a review of its pharmacology and use in the treatment of pain. *Neuropsychiatr. Dis. Treat.* **2007**, *3*, 69-85.
25. Sakai, R.; Rinehart, K.L.; Guan, Y.; Wang, A.H. Additional antitumor ecteinascidins from a Caribbean tunicate: crystal structures and activities *in vivo*. *Proc. Natl. Acad. Sci. USA* **1992**, *89*, 11456-11460.
26. Le, V.H.; Inai, M.; Williams, R.M.; Kan, T. Ecteinascidins. A review of the chemistry, biology and clinical utility of potent tetrahydroisoquinoline antitumor antibiotics. *Nat. Prod. Rep.* **2015**, *32*, 328-347.

27. Álvarez, A.S.; Pardal, E.; Sánchez-Nieto, D.; Navarro, M.; Caballero, M.D.; Mateos, M.V.; Martín, A. Plitidepsin: design, development, and potential place in therapy. *Drug Des. Dev. Ther.* **2017**, *11*, 253-264.
28. Cuevas, C.; Francesch, A. Development of Yondelis® (trabectedin, ET-743). A semisynthetic process solves the supply problem. *Nat. Prod. Rep.* **2009**, *26*, 322-337.
29. Hirata, Y.; Uemura, D. Halichondrins - antitumor polyether macrolides from a marine sponge. *Pure Appl. Chem.* **1986**, *58*, 701-710.
30. Pettit, G.R.; Herald, C.L.; Doubeck, D.L.; Herald, D.L.; Arnold, E.; Clardy, J. Isolation and structure of bryostatin 1. *J. Am. Chem. Soc.* **1982**, *104*, 6846-6848.
31. Piel, J. Metabolites from symbiotic bacteria. *Nat. Prod. Rep.* **2004**, *21*, 519-538.
32. Piel, J.; Butzke, D.; Fusetani, N.; Hui, D.; Platzer, M.; Wen, G.; Matsunaga, S. Exploring the Chemistry of Uncultivated Bacterial Symbionts: Antitumor Polyketides of the Pederin Family. *J. Nat. Prod.* **2005**, *68*, 472-479.
33. Bewley, C.A.; Faulkner, D.J. Lithistid Sponges: Star Performers or Hosts to the Stars. *Angew. Chem.* **1998**, *37*, 2162-2178.
34. Faulkner, D.J. Highlights of marine natural products chemistry (1972-1999). *Nat. Prod. Rep.* **2000**, *17*, 1-6.
35. Komaki, H.; Sakurai, K.; Hosoyama, A.; Kimura, A.; Igarashi, Y.; Tamura T. Diversity of nonribosomal peptide synthetase and polyketide synthase gene clusters among taxonomically close *Streptomyces* strains. *Sci. Rep.* **2018**, *8*, 6888.
36. Cane, D.E.; Walsh, C.T. The parallel and convergent universes of polyketide synthases and nonribosomal peptide synthetases. *Chem. Biol.* **1999**, *6*, 319-325.

37. Bewley, C.A.; Holland, N.D.; Faulkner, D.J. Two classes of metabolites from *Theonella swinhoei* are localized in distinct populations of bacterial symbionts. *Experientia* **1996**, 52, 716-722.
38. Mayer, A.M.S.; Hamann, M.T. Marine Pharmacology in 2000: Marine Compounds with Antibacterial, Anticoagulant, Antifungal, Anti-inflammatory, Antimalarial, Antiplatelet, Antituberculosis, and Antiviral Activities; Affecting the Cardiovascular, Immune, and Nervous Systems and Other Miscellaneous Mechanisms of Action. *Mar. Biotechnol.* **2004**, *6*, 37-52.
39. Mayer, A.M.S.; Hamann, M.T. Marine pharmacology in 2001-2002: Marine compounds with anthelmintic, antibacterial, anticoagulant, antidiabetic, antifungal, anti-inflammatory, antimalarial, antiplatelet, antiprotozoal, antituberculosis, and antiviral activities; affecting the cardiovascular, immune and nervous systems and other miscellaneous mechanisms of action. *Comp. Biochem. Physiol. C Toxicol. Pharmacol.* **2005**, *140*, 265-286.
40. Mayer, A.M.S.; Rodríguez, A.D.; Taglialatela-Scafati, O.; Fusetani, N. Marine pharmacology in 2012-2013: Marine compounds with antibacterial, antidiabetic, antifungal, anti-inflammatory, antiprotozoal, antituberculosis, and antiviral activities; affecting the immune and nervous systems, and other miscellaneous mechanisms of action. *Mar. Drugs* **2017**, 15, 273.
41. Fattorusso, E.; Taglialatela-Scafati, O. Marine Antimalarials. *Mar. Drugs*, **2009**, *7*, 130-152.
42. Viegas, F. P. D.; de Castro, A. T.; Castro, A. P.; Siqueira, R. W.; Espuri, P. F.; Coelho, L. F. L.; Marques, M. J.; Soares, M. G. In vitro schistosomicidal activity of the crude extract, fractions and Primin, the major active benzoquinone

constituent from the leaves of *Miconia willdenowii* (Melastomaceae). *S. Afr. J. Bot.* **2017**, *111*, 365-370.

43. Lira, M.L.F.; Lopes, R.; Gomes, A.P.; Barcellos, G.; Verícimo, M.; Osako, K.; Ortiz-Ramirez, F.A.; Ramos, C.J.B.; Cavalcanti, D.N.; Teixeira, V.L.; do Amaral, V. Anti-leishmanial activity of Brazilian green, brown, and red alga. *J. Appl. Phycol.* **2016**, *28*, 591-598.
44. El Sayed, K.A.; Bartyzel, P.; Shen, X.; Perry, T.L.; Zjawiony, J.K.; Hamann, M.T. Marine natural products as antituberculosis agents. *Tetrahedron* **2000**, *56*, 949-953.
45. WHO, https://www.who.int/neglected_diseases/diseases/en.
46. Cohen, J.P.; Silva, L.; Cohen, A.; Awatin, J.; Sturgeon, R. Progress Report on Neglected Tropical Disease Drug Donation Programs. *Clin. Ther.* **2016**, *38*, 1193-1204.
47. Hotez, P. J.; Pecoul, B.; Rijal, S.; Boehme, C.; Aksoy, S.; Malecela, M.; Tapia-Conyer, R.; Reeder, J. C. Eliminating the Neglected Tropical Diseases: Translational Science and New Technologies. *PLoS Negl. Trop. Dis.* **2016**, *10*, e0003895.
48. Siqueira, L. P.; Fontes, D.A.F.; Aguilera, C.S.B.; Timóteo, T.R.R.; Ângelos, M.A.; Silva, L.C.P.B.B.; Melo, C.G.; Rolim, L. A.; Silva, R.M.F.; Neto, P.J.R. Schistosomiasis: Drugs used and treatment strategies. *Acta Tropica* **2017**, *176*, 179-187.
49. Utzinger, J.; Raso, G.; Brooker, S.; de Savigny, D.; Tanner, M.; Ørnbjerg, N.; Singer, B.H.; N'Goran, E.K. Schistosomiasis and neglected tropical diseases: towards integrated and sustainable control and a word of caution. *Parasitology* **2009**, *136*, 1859-74.

50. Mbabazi, P.S.; Andan, O.; Fitzgerald, D.W.; Chitsulo, L.; Engels, D.; Downs, J.A. Examining the relationship between urogenital schistosomiasis and HIV infection. *PLoS Negl. Trop. Dis.* **2011**, *5,* e1396.

51. Keiser, J.; Utzinger, J. Antimalarials in the treatment of schistosomiasis. *Curr. Pharm. Des.* **2012**, *18*, 3531-3538.

52. Danso-Appiah, A.; De Vlas, S.J. Interpreting low praziquantel cure rates of Schistosoma mansoni infections in Senegal. *Trends Parasitol.* **2002**, *18*, 125-129.

53. Xiao, S.H.; Catto, B.A.; Webster, L.T. Effects of praziquantel on different developmental stages of *Schistosoma mansoni* in vitro and in vivo. *J. Infect. Dis.* **1985**, *151*, 1130-1137.

54. Lanfranchi, D. A.; Cesar-Rodo, E.; Bertrand, B.; Huang, H.; Day, L.; Johann, L. Elhabiri, M.; Becker, K.; Williams, D. L.; Davioud-Charvet, E. Synthesis and biological evaluation of 1,4-naphthoquinones and quinoline-5,8-diones as antimalarial and schistosomicidal agents. *Org. Biomol. Chem.* **2012**, *10*, 6375-6387.

55. Egan, T.J. Recent advances in understanding the mechanism of hemozoin (malaria pigment) formation. *J. Inorg. Biochem.* **2008**, *102*, 1288-1299.

56. Weissbuch, I.; Leiserowitz, L. Interplay Between Malaria, Crystalline Hemozoin Formation, and Antimalarial Drug Action and Design. *Chem. Rev.* **2008**, *108*, 4899-4914.

57. Corrêa Soares, J.B.; Maya-Monteiro, C.M.; Bittencourt-Cunha, P.R.; Atella, G.C.; Lara, F.A.; d'Avila, J.C.; Menezes, D.; Vannier-Santos, M.A.; Oliveira, P.L.; Egan, T.J.; Oliveira, M.F. Extracellular lipid droplets promote hemozoin crystallization in the gut of the blood fluke *Schistosoma mansoni*. *FEBS Lett.* **2007**, *581*, 1742-1750.

58. Casertano, M.; Imperatore, C.; Luciano, P.; Aiello, A.; Putra, M.Y.; Gimmelli, R.; Ruberti, G.; Menna, M. Chemical investigation of the Indonesian tunicate *Polycarpa aurata* and evaluation of the effects against *Schistosoma mansoni* of the novel alkaloids polyaurines A and B. *Mar. Drugs* **2019**, *17*, 278.
59. Abas, S.A.; Hossain, M.B.; van der Helm, D.; Schmitz, F.J.; Laney, M.; Cabuslay, R.; Schatzman, R.C. Alkaloids from the Tunicate *Polycarpa aurata* from Chuuk Atoll. *J. Org. Chem.* **1996**, *61*, 2709-2712.
60. Lindquist, N.; Fenical, W. Polycarpamines A-E, antifungal disulfides from the marine ascidian *Polycarpa auzata*. *Tetrahedron Lett.* **1990**, *31*, 2389-2392.
61. Wang, W.; Oda, T.; Fujita, A.; Mangindaan, R.E.P.; Nakazawa, T.; Ukai, K.; Kobayashi, H.; Namikoshi, M. Three new sulfur-containing alkaloids, polycarpaurines A, B, and C, from an Indonesian ascidian *Polycarpa aurata*. *Tetrahedron* **2007**, *63*, 409-412.
62. Pham, C.; Weber, H.; Hartmann, R.; Wray, V.; Lin, W.; Lai, D.; Proksch, P. New Cytotoxic 1,2,4-Thiadiazole Alkaloids from the Ascidian *Polycarpa aurata*. *Org. Lett*. **2013**, *15*, 2230-2233.
63. Popov, A.M.; Novikov, V.L.; Radchenko, O.S.; Elyakov, G.B. The cytotoxic and antitumor activities of the imidazole alkaloid polycarpin from the Ascidian *Polycarpa aurata* and its synthetic analogues. *Dokl. Biochem. Biophys.* **2002**, *385*, 213-218.
64. Fedorov, S.N.; Bode, A.M.; Stonik, V.A.; Gorshkova, I.A.; Schmid, P.C.; Radchenko, O.S.; Berdyshev, E.V.; Dong, Z. Marine alkaloid polycarpine and its synthetic derivative dimethylpolycarpine induce apoptosis in JB6 cells through p53-and caspase 3-dependent pathways. *Pharm. Res.* **2004**, *21*, 2307-2319.

65. Oda, T.; Lee, J.S.; Sato, Y.; Kabe, Y.; Sakamoto, S.; Handa, H.; Mangindaan, R.E.P.; Namikoshi, M. Inhibitory effect of *N*,*N*-Didesmethylgrossularine-1 on inflammatory cytokine production in lipopolysaccharide-stimulated RAW 264.7 cells. *Mar. Drugs* **2009**, *7,* 589-599.

66. Wessels, M.; König, G.M.; Wright, A.D. New 4-methoxybenzoyl derivatives from the ascidian *Polycarpa aurata*. *J. Nat. Prod.* **2001**, *64*, 1556-1558.

67. Oltz, E.M.; Bruening, R.C.; Smith, M.J.; Kustin, K.; Nakanishi, K. The tunichromes. A class of reducing blood pigments from sea squirts: isolation, structures, and vanadium chemistry. *J. Am. Chem. Soc.* **1988**, *110*, 6162-6172.

68. Sheikh, N. S. Synthetic endeavours towards oxasqualenoid natural products containing 2,5-disubstituted tetrahydrofurans - eurylene and teurilene. *Nat. Prod. Rep.* **2014**, *31*, 1088-1100.

69. Lorente, A.; Lamariano-Merketegi, J.; Albericio, F.; Alvarez, M. Tetrahydrofuran-Containing Macrolides: A Fascinating Gift from the Deep Sea. *Chem. Rev.* **2013**, *113*, 4567-4610.

70. Pilkington, L.I.; Barker, D. Synthesis and biology of 1,4-benzodioxane lignan natural products. *Nat. Prod. Rep.* **2015**, *32*, 1369-1388.

71. Davison, E.K.; Sperry, J. Natural Products with Heteroatom-Rich Ring Systems. *J. Nat. Prod.* **2017**, *80*, 11, 3060-3079.

72. Heitz, S.; Durgeat, M.; Guyot, M.; Brassy, C.; Bachet, B. New indolic derivative of 1,2,4-thiadiazole, isolated from a tunicate (*Dendrodoa grossular*). *Tetrahedron Lett*. **1980**, *21*, 1457-1458.

73. Chen, M.; Lin, S.; Li, L.; Zhu, C.; Wang, X.; Wang, Y.; Jiang, B.; Wang, S.; Li, Y.; Jiang, J.; Shi, J. Enantiomers of an Indole Alkaloid Containing Unusual

Dihydrothiopyran and 1,2,4-Thiadiazole Rings from the Root of *Isatis indigotica*. *Org. Lett.* **2012**, *14*, 5668-5671.

74. Yang, Z.; Huang, N.; Xu, B.; Huang, W.; Xie, T.; Cheng, F.; Zou, K. Cytotoxic 1,3-Thiazole and 1,2,4-Thiadiazole Alkaloids from *Penicillium oxalicum*: Structural Elucidation and Total Synthesis. *Molecules* **2016**, *21*, 232.
75. Pätzel, M.; Liebscher, J.; Andreae, S.; Schmitz, E. Ring Transformations of Semicyclic 1,3-Dicarbonyl Heteroanalogs; IV. Synthesis of 3-(ω-Aminoalkyl)-1,2,4-thiadiazoles by Ring Transformation Reaction of Semicyclic Thioacylamidines with 3,3-Pentamethyleneoxaziridine. *Synthesis* **1990**, *11*, 1071-1073.
76. Hogan, I.T.; Sainsbury, M. The synthesis of dendrodoine, 5-[3-(*N*,*N*-dimethylamino- 1,2,4-thiadiazolyl]-3-indolylmethanone, a metabolite of the marine tunicate *Dendrodoa grossularia*. *Tetrahedron* **1984**, *40*, 681-682.
77. Lalli, C.; Guidi, A.; Gennari, N.; Altamura, S.; Bresciani, A.; Ruberti, G. Development and validation of a luminescence-based, medium-throughput assay for drug screening in *Schistosoma mansoni*. *PLoS Negl. Trop. Dis.* **2015**, *9*, e0003484.
78. Guidi, A.; Lalli, C.; Perlas, E.; Bolasco, G.; Nibbio, M.; Monteagudo, E.; Bresciani, M.; Ruberti, G. Discovery and Characterization of novel anti-schistosomal properties of the anti-anginal drug, perhexiline and its impact on *Schistosoma mansoni* male and female reproductive systems. *PLoS Negl. Trop. Dis.* **2016**, *10*, e0004928.
79. Müller, W. E. G.; Maidhof, A.; Zahn, R. K.; Schröder, H. C.; Gašić, M. J.; Heidemann, D.; Bernd, A.; Kurelec, B.; Eich, E.; Seibert, G. Potent Antileukemic

Activity of the Novel Cytostatic Agent Avarone and Its Analogues in vitro and in vivo. *Cancer Res.* **1985**, *45*, 4822-4826.

80. Ferrándiz, M. L.; Sanz, M. J.; Bustos, G.; Payá, M.; Alcaraz, M. J.; De Rosa, S. Avarol and avarone, two new anti-inflammatory agents of marine origin. *Eur. J. Pharmacol.* **1994**, *253*, 75-82.
81. Seibert, G.; Raether, W.; Dogović, N.; Gašić, M. J.; Zahn, R. K.; Müller, W. E. G. Antibacterial and antifungal activity of avarone and avarol. *Zbl. Bakt. Hyg.* **1985**, *260A*, 379-386.
82. Loya, S.; Hizi, A. The inhibition of human immunodeficiency virus type 1 reverse transcriptase by avarol and avarone derivatives. *FEBS Lett.* **1990**, *269*, 131-134.
83. Belisario, M. A.; Maturo, M.; Pecce, R.; De Rosa, S.; Villani, G. R. Effect of avarol and avarone on in vitro-induced microsomal lipid peroxidation. *Toxicology* **1992**, *72*, 221-233.
84. Amigó, M.; Payá, M.; Braza-Boïls, A.; De Rosa, S.; Terencio, M. C. Avarol inhibits TNF-alpha generation and NF-kappaB activation in human cells and in animal models. *Life Sci.* **2008**, *82*, 256-264.
85. Tsoukatou, M.; Maréchal, J. P.; Hellio, C.; Novaković, I.; Tufegdzic, S.; Sladić, D.; Gašić, M. J.; Clare, A. S.; Vagias, C.; Roussis, V. Evaluation of activity of the sponge metabolites avarol and avarone and their synthetic derivatives against fouling micro- and macroorganisms. *Molecules* **2007**, *12*, 1022-1034.
86. Vilipic, J.; Novakovic, I.; Stanojkovic, T.; Matic, I.; Segan, D.; Kljajic, Z.; Sladic, D. Synthesis and biological activity of amino acid derivatives of avarone and its model compound. *Bioorg. Med. Chem.* **2015**, *23*, 6930-6942.

87. Bozic, T.; Novakovic, I.; Gasic, M. J.; Juranic, Z.; Stanojkovic, T.; Tufegdzic, S.; Kljajic, Z.; Sladic, D. Synthesis and biological activity of derivatives of the marine quinone avarone. *Eur. J. Med. Chem.* **2010**, *5*, 923-929.

88. De Giulio, A.; De Rosa, S.; Strazzullo, G.; Diliberto, L.; Obino, P.; Marongiu, M.E.; Pani, A.; La Colla, P. Synthesis and evaluation of cytostatic and antiviral activities of 3' and 4'-avarone derivatives. *Antiviral Chem. Chemother.* **1991**, *2*, 223-227.

89. Minale, L.; Riccio, R.; Sodano, G. Avarol, a novel sesquiterpenoid hydroquinone with a rearranged drimane skeleton from the sponge *Dysidea avara*. *Tetrahedron Lett.* **1974**, *38*, 3401-3404.

90. De Rosa, S.; Minale, L.; Riccio R.; Sodano, G. The absolute configuration of avarol, a rearranged sesquiterpenoid hydroquinone from a marine sponge. *J. Chem. Soc. Perkins Trans*. **1976**, *1*, 1408-1414.

91. Cozzolino, R.; De Giulio, A.; De Rosa, S.; Strazzullo, G.; Gašić, M. J.; Sladić, D.; Zlatović, M. Biological activities of avarol derivatives, 1. amino derivatives. *J. Nat. Prod.* **1990**, *53*, 699-702.

92. Bielitza, M.; Belorgey, D.; Ehrhardt, K.; Johann, L.; Lanfranchi, D. A.; Gallo, V.; Schwarzer, E.; Mohring, F.; Jortzik, E.; Williams, D. L.; Becker, K.; Arese, P.; Elhabiri, M.; Davioud-Charvet, E. Antimalarial NADPH-Consuming Redox-Cyclers As Superior Glucose-6-Phosphate Dehydrogenase Deficiency Copycats. *Antioxid. Redox Sign.* **2015**, *22*, 1337-1351.

93. Morin, C.; Besset, T.; Moutet, J.; Fayolle, M.; Brueckner, M.; Limosin, D.; Becker, K.; Davioud-Charvet, E. The aza-analogues of 1,4-naphthoquinones are potent substrates and inhibitors of plasmodial thioredoxin and glutathione reductases and

of human erythrocyte glutathione reductase. *Org. Biomol. Chem.* **2008**, *6*, 2731-2742.

94. Utzinger, J.; Xiao, S.H.; Tanner, M.; Keiser, J. Artemisinins for schistosomiasis and beyond. *Curr. Opin. Investig. Drugs* **2007**, *8*, 105-116.
95. Liu, R.; Dong, H.F.; Guo, Y.; Zhao, Q.P.; Jiang, M.S. Efficacy of praziquantel and artemisinin derivatives for the treatment and prevention of human schistosomiasis: a systematic review and meta-analysis. *Parasit. Vectors* **2011**, *4*, 201.
96. Keiser, J.; N'Guessan, N.A.; Adoubryn, K.D.; Silué, K.D.; Vounatsou, P.; Hatz, C.; Utzinger, J.; N'Goran, E.K. Efficacy and safety of mefloquine, artesunate, mefloquine-artesunate, and praziquantel against *Schistosoma haematobium*: randomized, exploratory open-label trial. *Clin. Infect. Dis.* **2010**, *50*, 1205-1213.
97. Alisky, J.M.; Chertkova, E.L.; Iczkowski, K.A. Drug interactions and pharmacogenetic reactions are the basis for chloroquine and mefloquine-induced psychosis. *Med. Hypotheses* **2006**, *67*, 1090-1094.
98. Mossallam, S.F.; Amer, E.I.; El-Faham, M.H. Efficacy of Synriam™, a new antimalarial combination of OZ277 and piperaquine, against different developmental stages of *Schistosoma mansoni*. *Acta Trop.* **2015***, 143*, 36-46.
99. Klonis, N.; Crespo-Ortiz, M.P.; Bottova, I.; Abu-Bakar, N.; Kenny, S.; Rosenthal, P.J.; Tilley, L. Artemisinin activity against *Plasmodium falciparum* requires hemoglobin uptake and digestion. *Proc. Natl. Acad. Sci. USA* **2011**, *108*, 11405-11410.
100. Correa Soares, J.B.R.; Menezes, D.; Vannier-Santos, M.A.; Ferreira-Pereira, A.; Almeida, G.T.; Zishiri, V.K.; Kuter, D.; Hunter, R.; Egan, T.J.; Oliveira, M.F. Interference with hemozoin formation represents an important mechanism of

schistosomicidal action of antimalarial quinoline methanols. *PLoS Negl. Trop. Dis.* **2009**, *3*, e477.

101. Davis, R. A.; Duffy, S.; Fletcher, S.; Avery, V.M.; Quinn, R.J. Thiaplakortones A-D: Antimalarial Thiazine Alkaloids from the Australian Marine Sponge *Plakortis lita*. *J. Org. Chem.* **2013**, *78,* 9608-9613.

102. Imperatore, C.; Cimino, P.; Cebrián-Torrejón, G.; Persico, M.; Aiello, A.; Senese, M.; Fattorusso, C.; Menna, M.; Doménech-Carbó, A. Insight into the Mechanism of Action of Marine Cytotoxic Thiazinoquinones. *Mar. Drugs* **2017**, *15*, 335.

103. Imperatore, C.; Persico, M.; Aiello, A.; Luciano, P.; Guiso, M.; Sanasi, M. F.; Taramelli, D.; Parapini, S.; Cebrián-Torrejón, G.; Doménech-Carbó, A.; Fattorusso, C.; Menna, M. Marine inspired antiplasmodial thiazinoquinones: synthesis, computational studies and electrochemical assays. *RSC Advances* **2015**, *5*, 70689-70702.

104. Imperatore, C.; Persico, M.; Senese, M.; Aiello, A.; Casertano, M.; Luciano, P.; Basilico, N., Parapini, S.; Paladino, A.; Fattorusso, C.; Menna, M. Exploring the antimalarial potential of the methoxy-thiazinoquinone scaffold: Identification of a new lead candidate. *Bioorg. Chem*. **2019**, *85*, 240–252.

105. Gimmelli, R.; Persico, M.; Imperatore, C.; Saccoccia, F.; Guidi, A.; Casertano, M.; Luciano, P.; Pietrantoni, A.; Bertuccini, L.; Paladino, A.; Papoff, G.; Menna, M.; Fattorusso, C.; Ruberti, G. Thiazinoquinones as New Promising Multistage Schistosomicidal Compounds Impacting *Schistosoma mansoni* and Egg Viability. *ACS Infect. Dis.* **2020**, *6*, 124-137.

106. Imperatore, C.; Gimmelli, R.; Persico, M.; Casertano, M.; Guidi, A.; Saccoccia, F.; Ruberti, G.; Luciano, P.; Aiello, A.; Parapini, S.; Avunduk, S.; Basilico, N.;

Fattorusso, C.; Menna, M. Investigating the Antiparasitic Potential of the Marine Sesquiterpene Avarone, Its Reduced Form Avarol, and the Novel Semisynthetic Thiazinoquinone Analogue Thiazoavarone. *Mar. Drugs* **2020**, *18*, 112.

107. Abdjul, D.B.; Yamazaki, H.; Takahashi, O.; Kirikoshi, R.; Ukai, K.; Namikoshi, M. Sesquiterpene Hydroquinones with Protein Tyrosine Phosphatase 1B Inhibitory Activities from a *Dysidea sp.* Marine Sponge Collected in Okinawa. *J. Nat. Prod.* **2016**, *79*, 1842-1847.
108. Iguchi, K.; Sahashi, A.; Kohno, J.; Yamada, Y. New sesquiterpenoid hydroquinone and quinones from the Okinawan Marine sponge (*Dysidea sp.*). *Chem. Pharm. Bull.* **1990**, *38*, 1121-1123.
109. Crispino, A.; De Giulio, D.; De Rosa, S.; Strazzullo, G. A new bioactive derivative of avarol from the marine sponge *Dysidea avara*. *J. Nat. Prod.* **1989**, *52*, 646-648.
110. Perez-Garcia, E.; Zubia, E.; Ortega, M. J.; Carballo, J. L. Merosesquiterpenes from Two Sponges of the Genus *Dysidea*. *J. Nat. Prod.* **2005**, *68*, 653-658.
111. Diaz-Marrero, A. R.; Austin, P.; Van Soest, R.; Matainaho, T.; Roskelley, C. D.; Roberge, M.; Andersen, R. J. Avinosol, a meroterpenoid-nucleoside conjugate with antiinvasion activity isolated from the marine sponge *Dysidea sp. Org. Lett.* **2006**, *8*, 3749-3752.
112. Faulkner, D.J. Marine natural products. *Nat. Prod. Rep.* **2002**, *19*, 1-48.
113. Blunt, J.W.; Copp, B.R.; Munro, M.H.G.; Northcote, P.T.; Prinsep, M.R. Marine natural products. *Nat. Prod. Rep.* **2005**, *22*, 15-61.
114. Ling, T.; Xiang, A.X.; Theodorakis, E.A. Enantioselective total synthesis of avarol and avarone. *Angew. Chem.* **1999**, *111*, 3089-3091.

115. Sakurai, J.; Oguchi, T.; Watanabe, K.; Abe, H.; Kanno, S.; Ishikawa, M.; Katoh, T. Highly Efficient Total Synthesis of the Marine Natural Products (+)-Avarone, (+)-Avarol, (-)-Neoavarone, (-)-Neoavarol and (+)-Aureol. *Chem. Eur. J.* **2008**, *14*, 829-837.

116. Sladić, D.; Gašić, M.J. Reactivity and Biological Activity of the Marine Sesquiterpene Hydroquinone Avarol and Related Compounds from Sponges of the Order Dictyoceratida. *Molecules* **2006**, *11*, 1-33.

117. Luibrand, R.T.; Erdman, T.R.; Vollmer, J.J.; Scheur, P.J.; Finer, J.; Clardy, J.C. Ilimaquinone, a sesquiterpenoid quinone from a marine sponge. *Tetrahedron* **1979**, *35*, 609-612.

118. Capon, R.J.; McLeod, J.K. Revision of the absolute stereochemistry of ilimaquinone. *J. Org. Chem.* **1987**, *52*, 5059-5060.

119. Kazlauskas, R.; Murphy, R.T.; Warren, R.G.; Wells, R.J.; Blount, J.F. New quinones from a dictyoceratid sponge. *Aust. J. Chem.* **1978**, *31*, 2685-2697.

120. Capon, R.J. The acid-catalyzed rearrangement and absolute stereochemistry of isospongiaquinone. *J. Nat. Prod.* **1990**, *53*, 753-756.

121. Kobayashi, J.; Madono, T.; Shigemori, H. Nakijiquinones C and D, new sesquiterpenoid quinones with a hydroxy amino acid residue from a marine sponge inhibiting c-erbB-2 kinase. *Tetrahedron* **1995**, *51*, 10867-10874.

122. de Guzman, F.; Cop, B.R.; Mayne, C.L.; Concepcion, G.P.; Mangalindan, G.C.; Barrows, L.R.; Ireland, C.M. Bolinaquinone: A Novel Cytotoxic Sesquiterpene Hydroxyquinone from a Philippine *Dysidea* Sponge. *J. Org. Chem.* **1998**, *63*, 8042-8044.

123. Božić, T.; Sladić, D.; Zlatović, M.; Novaković, I.; Trifunović, S.; Gašić, M.J. Regioselectivity of conjugate additions to monoalkyl-1,4-benzoquinones. *J. Serb. Chem. Soc.* **2002**, *67*, 547-551.

124. Butterworth, A.S.; Skinner-Adams, T.S.; Gardiner, D.L.; Trenholme, K.R. *Plasmodium falciparum* gametocytes: with a view to a kill. *Parasitology* **2013**, *140*, 1718-1734.

125. Pérez-Pertejo, Y.; Escudero-Martínez, J. M.; Reguera, R. M.; Balaña-Fouce, R.; García, P. A.; Jambrina, P. G.; San Feliciano, A.; Castro, M.Á. Antileishmanial activity of terpenylquinones on *Leishmania infantum* and their effects on *Leishmania* topoisomerase IB. *Int. J. Parasitol. Drugs Drug Resist.* **2019**, *11*, 70-79.

126. Katsuno, K.; Burrows, J.N.; Duncan, K.; van Huijsduijnen, R.H.; Kaneko, T.; Kita, K.; Slingsby, B.T. Hit and lead criteria in drug discovery for infectious diseases of the developing world. *Nat. Rev. Drug Discov.* **2015**, *14*, 751-758.

127. Skelly, P. J.; Shoemaker, C. B. Induction cues for tegument formation during the transformation of *Schistosoma mansoni* cercariae. *Int. J. Parasitol.* **2000**, *30*, 625-631.

128. Jurberg, A. D.; Gonçalves, T.; Costa, T. A.; de Mattos, A. C. A.; Pascarelli, B. M.; de Manso, P. P. A.; Ribeiro-Alves, M.; Pelajo-Machado, M.; Peralta, J. M.; Coelho, P. M. Z.; Lenzi, H. L. The embryonic development of *Schistosoma mansoni* eggs: proposal for a new staging system. *Dev. Genes Evol.* **2009**, *219*, 219-234.

129. Ewig, C. S.; Berry, R.; Dinur, U.; Hill, J. R.; Hwang, M. J.; Li, H.; Liang, C.; Maple, J.; Peng, Z.; Stockfisch, T. P.; Thacher, T. S.; Yan, L.; Ni, X.; Hagler, A.T.

Derivation of class II force fields. VIII. Derivation of a general quantum mechanical force field for organic compounds. *J. Comput. Chem*. **2001**, *22*, 1782-1800.

130. Cossi, M.; Rega, N.; Scalmani, G.; Barone V. Energies, structures, and electronic properties of molecules in solution with the C-PCM solvation model. *J. Comp. Chem*. **2003**, 24, 669-681.

131. Makler, M.T.; Ries, J.M.; Williams, J.A.; Bancro, J.E.; Piper, R.C.; Gibbins, B.L.; Hinrichs, D.J. Parasite lactate dehydrogenase as an assay for *Plasmodium falciparum* drug sensitivity. *Am. J. Trop. Med. Hyg.* 1993, 48, 739-741.

132. Fletcher, R. Practical Methods of Optimization, 1st ed.; John Wiley & Sons Ltd.: New York, NY, USA, **1980**; Volume 1, pp. 1-128, ISBN 978-0471277118.

133. Frisch, M.J.; *et al*. Gaussian 09, **2009**, revision A.1. Gaussian Inc. Wallingford.

134. Reed, E.; Weinstock, R. B., Weinhold, F. Natural population analysis. *J. Chem. Phys.* **1985**, *83*, 735-746.

135. Li, J.; Fisher, C. L.; Chen, J. L.; Bashford, D.; Noodleman, L. Calculation of redox potentials and pK_a values of hydrated transition metal cations by a combined density functional and continuum dielectric theory. *Inorg. Chem.* **1996**, *35*, 4694-4702.

136. Moens, J.; Geerlings, P.; Roos, G. A conceptual DFT approach for the evaluation and interpretation of redox potentials. *Chem. Eur. J*. **2007***, 13*, 8174 -8184.

137. Aiello, A.; Fattorusso, E.; Luciano, P.; Menna, M.; Calzado, M.A.; Muñoz, E.; Bonadies, F.; Guiso, M.; Sanasi, M.F.; Cocco, G.; Nicoletti, R. Synthesis of structurally simplified analogues of aplidinone A, a pro-apoptotic marine thiazinoquinone. *Bioorg. Med. Chem*. **2010**, *18*, 719-727.

138. Laurent, D.; Jullian, V.; Parenty, A.; Knibiehler, M.; Dorin, D.; Schmitt, S.; Lozach, O.; Lebouvier, N.; Frostin, M.; Alby, F.; Maurel, S.; Doerig, C.; Meijer,

L.; Sauvain, M. Antimalarial potential of xestoquinone, a protein kinase inhibitor isolated from a Vanuatu marine sponge *Xestospongia sp*. *Bioorg. Med. Chem.* **2006**, *14*, 4477-4482.

139. Longeon, A.; Copp, B.R.; Rou´e, M.; Dubois, J.; Valentin, A.; Petek, S.; Debitus C.; Bourguet-Kondracki, M. New bioactive halenaquinone derivatives from South Pacific marine sponges of the genus *Xestospongia*. *Bioorg. Med. Chem.* **2010**, *18*, 6006-6011.
140. Saunders, D.L.; Chaorattanakawee, S.; Gosi, P.; Lanteri, C.; Somethy, S.; Kuntawunginn, W.; Ittiverakul, M.; Chann, S.; Gregory, C.; Chuor, C.M.; Prom, S.; Spring, M.D.; Lon, C. Atovaquone-proguanil remains a potential stopgap therapy for multidrug-resistant *Plasmodium falciparum* in areas along the Thai-Cambodian border. *Antimicrob. Agents Chemother.* **2016**, *60*, 1896-1898.
141. Imperatore, C.; Della Sala, G.; Casertano, M.; Luciano, P.; Aiello. A.; Laurenzana, I.; Piccoli, P.; Menna, M. *In Vitro* Antiproliferative Evaluation of Synthetic Meroterpenes Inspired by Marine Natural Products. *Mar. Drugs* **2019**, *17*, 684.
142. Waterlot, C.; Couturier, D.; De Backer, M.; Rigo, B. A study of hydrogenation of benzhydrols in the presence of catalytic amount of triflic acid. *Can. J. Chem.* **2000**, *78*, 1242-1246.
143. Mayr, H.; Dogan, B. Selectivities in ionic reductions of alcohols and ketones with triethylsilane/trifluoroacetic acid. *Tetrahedron Lett.* **1997**, *38*, 1013-1016.
144. Lipinski, C.A.; Lombardo, F.; Dominy, B.W.; Feeney, P.J. Experimental and computational approaches to estimate solubility and permeability in drug discovery and development settings. *Adv. Drug Deliv. Rev.* **2001**, *46*, 3-26.

145. Sonawane, D.P.; Persico, M.; Corbett, Y.; Chianese, G.; Di Dato, A.; Fattorusso, C.; Taglialatela-Scafati, O.; Taramelli, D.; Trombini, C.; Dhavale, D.D.; Quintavalla, A.; Lombardo, M. New antimalarial 3-methoxy-1,2-dioxanes: optimization of cellular pharmacokinetics and pharmacodynamics properties by incorporation of amino and *N*-heterocyclic moieties at C4. *RSC Adv.* **2015**, *5*, 72995-73010.

146. Kirk, K. Membrane transport in the malaria-infected erythrocyte. *Physiol. Rev.* **2001**, *81*, 495-537.

147. Angelucci, F.; Basso, A.; Bellelli, A.; Brunori, M.; Pica Mattoccia, L.; Valle, C. The anti-schistosomal drug praziquantel is an adenosine antagonist. *Parasitology* **2007**, *134*, 1215-1221.

148. Menna, M.; Imperatore, C.; D'Aniello, F.; Aiello, A. Meroterpenes from Marine Invertebrates: Structures, Occurrence, and Ecological Implications. *Mar. Drugs* **2013**, *11*, 1602-1643.

149. Gordaliza, M. Cytotoxic Terpene Quinones from Marine Sponges. *Mar. Drugs* **2010**, *8*, 2849-2870.

150. García, P. A.; Hernández Á. P.; San Feliciano, A.; Castro, M. Á. Bioactive Prenyl- and Terpenyl-Quinones/Hydroquinones of Marine Origin. *Mar. Drugs* **2018**, *16*, 292.

151. Zubia, E.; Ortega, M. J.; Salva, J. Natural Products Chemistry in Marine Ascidians of the Genus *Aplidium*. *Mini-Rev. Org. Chem.* **2005**, *2*, 389-399.

152. Fedorov, S.N.; Radchenko, O.S.; Shubina, L.K.; Balaneva, N.N.; Bode, A.M.; Stonik, V.A.; Dong, Z. Evaluation of cancer-preventive activity and structure-

activity relationships of 3-demethylubiquinone Q2, isolated from the ascidian *Aplidium glabrum*, and its synthetic analogs. *Pharm. Res.* **2006**, *23*, 70-81.

153. Della Sala, G.; Agriesti, F.; Mazzoccoli, C.; Tataranni, T.; Costantino, V.; Piccoli C. Clogging the Ubiquitin-Proteasome Machinery with Marine Natural Products: Last Decade Update. *Mar Drugs*. **2018**, *16*, 467.

154. Teta, R.; Della Sala, G.; Esposito, G.; Via, C.W.; Mazzoccoli, C.; Piccoli, C.; Bertin, M.J.; Costantino, V.; Mangoni, A. A joint molecular networking study of a *Smenospongia* sponge and a cyanobacterial bloom revealed new antiproliferative chlorinated polyketides. *Org. Chem. Front.* **2019**, *6*, 1762-1774.

155. Superchi, S.; Scafato, P.; Górecki, M.; Pescitelli, G. Absolute Configuration Determination by Quantum Mechanical Calculation of Chiroptical Spectra: Basics and Applications to Fungal Metabolites. *Curr. Med. Chem.* **2018**, *25*, 287-320.

156. Finefield, J.M.; Sherman, D.H.; Kreitman, M.; Williams, R.M. Enantiomeric natural products: occurrence and biogenesis. *Angew. Chem. Int.* **2012**, *51*, 4802-4836.

157. Molinski, T. F. NMR of natural products at the 'nanomole-scale'. *Nat. Prod. Rep.* **2010**, *27*, 321-329.

158. Halabalaki, M.; Vougogiannopoulou, K.; Mikros E.; Skaltsounis, A. L. Recent advances and new strategies in the NMR-based identification of natural products. *Curr. Opin. Biotechnol.* **2014**, *25*, 1-7.

159. Menna, M.; Imperatore, C.; Mangoni, A.; Della Sala, G.; Taglialatela-Scafati, O. Challenges in the configuration assignment of natural products. A case-selective perspective. *Nat. Prod. Rep.* **2019**, *36*, 476-489.

160. Imperatore, C.; Luciano, P.; Aiello, A.; Vitalone, R.; Irace, C., Santamaria, R.; Li, J.; Guo, Y.; Menna, M. Structure and Configuration of Phosphoeleganin, a Protein Tyrosine Phosphatase 1B Inhibitor from the Mediterranean Ascidian *Sidnyum elegans*. *J. Nat. Prod.* **2016**, *79*, 1144-1148.

161. Luciano, P.; Imperatore, C.; Senese, M.; Aiello, A.; Casertano, M.; Guo, Y.; Menna, M. Assignment of the Absolute Configuration of Phosphoeleganin via Synthesis of Model Compounds. *J. Nat. Prod.* **2017**, *80*, 2118-2123.

162. Kobayashi, Y.; Tan, C.-H.; Kishi, Y. Toward Creation of a Universal NMR Database for Stereochemical Assignment: Complete Structure of the Desertomycin/Oasomycin Class of Natural Products. *J. Am. Chem. Soc.* **2001**, *123*, 2076-2078.

163. Higashibayashi, S.; Kishi, Y. Assignment of the relative and absolute configurations of acyclic secondary 1,2-diols. *Tetrahedron* **2004**, *60*, 11977-11982.

164. Matsumori, N.; Kaneno, D.; Murata, M.; Nakamura, H.; Tachibana, K. Stereochemical Determination of Acyclic Structures Based on Carbon-Proton Spin-Coupling Constants. A Method of Configuration Analysis for Natural Products. *J. Org. Chem*. **1999**, *64*, 866-876.

165. Nath, N.; Schmidt, M.; Gil, R.R.; Williamson, R.T.; Martin, G.E.; Navarro-Vazquez, A.; Griesinger, C.; Liu, Y. Determination of Relative Configuration from Residual Chemical Shift Anisotropy. *J. Am. Chem. Soc.* **2016**, *138*, 9548-9556.

166. Tantillo, D. J. Walking in the woods with quantum chemistry-applications of quantum chemical calculations in natural products research. *Nat. Prod. Rep.* **2013**, *30*, 1079-1086.

167. Grimblat, N.; Sarotti, A. M. Computational Chemistry to the Rescue: Modern Toolboxes for the Assignment of Complex Molecules by GIAO NMR Calculations. *Chem. Eur. J*. **2016**, *22*, 12246-12261.

168. Freire, F.; Manuel, J.; Quiñoá, E.; Riguera, R. Determining the absolute stereochemistry of secondary/secondary diols by ^{1}H NMR: basis and applications. *J. Org. Chem.* **2005**, *70*, 3778-3790.

169. Seco, J.M.; Quiñoá, E.; Riguera, R. Assignment of the absolute configuration of polyfunctional compounds by NMR using chiral derivatizing agents. *Chem. Rev.* **2012**, *112*, 4603-4641.

170. Seco, J.M.; Riguera, R. Methods for the Assignment of Absolute Stereochemistry of Bioactive Compounds. *eMagRes.* **2015**, *4*, 1-30.

171. Zheng, T.; Narayan, R.S.; Schomaker, J.M.; Borhan, B. One-Pot Regio- and Stereoselective Cyclization of 1,2,*n*-Triols. *J. Am. Chem. Soc.* **2005**, *127*, 6946-6947.

172. Haftchenary, S.; Ball, D.P.; Aubry, I.; Landry, M.; Shahani, V.M.; Fletcher, S.; Page, B.D.G.; Jouk, A.O.; Tremblay, M.L.; Gunning, P.T. Identification of a potent salicylic acid-based inhibitor of tyrosine phosphatase PTP1B. *Med. Chem. Comm.* **2013**, *4*, 987-992.

173. Kennedy, B.P.; Ramachandran, C. Protein tyrosine phosphatase-1B in diabetes. *Biochem*. *Pharmacol*. **2000**, *60*, 877-883.

174. Östman, A.; Hellberg, C.; Böhmer, F.D. Protein-tyrosine phosphatases and cancer. *Nat. Rev. Cancer* **2006**, *6*, 307-320.

175. Muise, A.M.; Walters, T.; Wine, E.; Griffiths, A.M.; Turner, D.; Duerr, R.H.; Regueiro, M.D.; Ngan, B. Y.; Xu, W.; Sherman, P.M.; Silverberg, M.S.; Rotin, D.

Protein-tyrosine phosphatase sigma is associated with ulcerative colitis. *Curr. Biol.* **2007**, *17*, 1212-1218.

176. Combs, A. P. Recent advances in the discovery of competitive protein tyrosine phosphatase 1B inhibitors for the treatment of diabetes, obesity, and cancer. *J. Med. Chem.* **2010**, *53*, 2333-2344.

177. Haftchenary, S.; Jouk, A.O.; Aubry, I.; Lewis,A.M.; Landry, M.; Ball, D.P.; Shouksmith, A.E.; Collins, C.V.; Tremblay, M.L.; Gunning, P.T. Identification of Bidentate Salicylic Acid Inhibitors of PTP1B. *ACS Med. Chem. Lett.* **2015**, *6*, 982-986.

178. Johnson, T.O.; Ermolieff, J.; Jirousek, M.R. Protein tyrosine phosphatase 1B inhibitors for diabetes. *Nat. Rev. Drug Discovery* **2002**, *1*, 696-709.

179. Dueymes, C.; Pirat, C.; Pascal, R. Facile synthesis of simple mono-alkyl phosphates from phosphoric acid and alcohols. *Tetrahedron Lett.* **2008**, *49*, 5300-5301.

180. Lira, L.M.; Vasilev, D.; Pilli, R.A.; Wessjohann, L.A. One-pot synthesis of organophosphate monoesters from alcohols. *Tetrahedron Lett.* **2013**, *54*, 1690-1692.

181. Perry, R.H.; Cooks, R.G.; Noll, R.J. Orbitrap mass spectrometry: instrumentation, ion motion and applications. *Mass Spectrom. Rev.* **2008**, *27*, 66-669.